Investigating the role of yeast Glutathione peroxidase 3 and related proteins in mitochondria and peroxisomes

Amelia Victoria Mordas MSci (Hons)

A thesis submitted to the University of Glasgow for the degree of Doctor of Philosophy (PhD) in Molecular and Cellular Biology

Institute of Molecular, Cell and Systems Biology

College of Medical, Veterinary and Life Sciences

University of Glasgow

Abstract

In *Saccharomyces cerevisiae*, Gpx3 is a H_2O_2 sensor that resides in the cytosol, the mitochondrial intermembrane space (IMS) and the peroxisomal matrix. Upstream translation from a non-AUG codon after exposure to H_2O_2 results in production of an N-terminally extended form, N18Gpx3, that targets the protein to mitochondria in a more efficient manner. Whilst the major role of Gpx3 in the cytosol is known, notably its interaction with (and activation of) the transcription factor Yap1, the role/s of Gpx3 and N18Gpx3 in the mitochondrial IMS and peroxisomal matrix are yet to be fully determined. Previous work published by our lab and collaborators identified the oxidoreductase Mia40 as an interactor of Gpx3; however, others were anticipated. Here, we identified two new putative IMS interactors of Gpx3: Cytochrome *c* (Cyt*c*) and Cytochrome b2 (Cytb2). Cyt*c* is an abundant electron carrier in the IMS that plays a role in both respiration and the mitochondrial IMS assembly (MIA) oxidative folding pathway, and in mammals Cyt*c* is also involved in triggering apoptosis. In contrast, little is known about Cytb2. We focused our attention on the potential Gpx3-Cyt*c* interaction and found that by mutating Cys64 of Gpx3, a highly conserved cysteine residue with no known function, its interaction with Cyt*c* was affected. As both Mia40 and Cyt*c* are components of the MIA pathway, we hypothesise that Gpx3 plays a role in oxidative folding and may be a regulator of this pathway under oxidative stress. Next, we uncovered six small proteins with no previous mitochondrial associations and went on to investigate one in particular, Ypl107w, an uncharacterised protein containing a highly conserved oxidoreductase-like domain (OXLD) that, despite being present in thousands of proteins across hundreds of species, has an unknown function. We confirmed its targeting and localisation to the mitochondrial matrix and hypothesise, based on bioinformatics and BN-PAGE data, that Ypl107w has many interactors and may be involved in mitochondrial assembly. There may also be a link between Ypl107w, Gpx3 and Cyt*c* as *ypl107w*Δ mitochondria have lower amounts of both Gpx3 and Cyt*c*. Finally, we confirmed the presence of Gpx3 in peroxisomes and discovered a shorter version of Mia40 along with Trx1 and Trx2 also residing in peroxisomes. We hypothesise that the targeting of these proteins occurs by previously unrecognised peroxisomal targeting signals, and that the MIA pathway may operate in both mitochondria and peroxisomes. Altogether, the work presented in this thesis adds to our knowledge of yeast Gpx3 in regards to its compartment-specific roles.

Table of contents

Abstract..... 2

Table of contents..... 3

List of Figures..... 8

List of Tables..... 12

Acknowledgements..... 13

Author's declaration..... 14

Abbreviations..... 15

1. Introduction..... 20

1.1. Mitochondria..... 21

1.2. Mitochondrial biogenesis..... 21

1.2.1. Mitochondrial structure..... 22

1.2.2 Outer membrane protein translocation..... 23

1.2.3. Inner membrane and matrix protein import..... 26

1.2.4. Intermembrane space protein import..... 30

1.3. Conservation and evolution of protein import pathways..... 37

1.3.1. The MIA pathway across eukaryotes..... 39

1.3.1.1 The *Arabidopsis* MIA pathway..... 39

1.3.1.2. Parasitic MIA pathways..... 40

1.4. Intermembrane space proteins..... 43

1.5. Redox regulation of protein disulphide bond formation..... 44

1.6. Glutathione peroxidases in yeast..... 47

1.6.1. Cytosolic Gpx3..... 48

1.6.2. Mitochondrial Gpx3..... 50

1.6.3. Peroxisomal Gpx3..... 51

1.7. Peroxisomes..... 52

1.7.1. Peroxisome protein targeting and import..... 52

1.7.2. Mitochondria-peroxisome links..... 53

1.8. Protein targeting and import in disease..... 54

1.9. Aims..... 55

2. Materials and methods..... 56

2.1. Materials..... 57

2.1.1. Plasmids..... 58

2.1.2. Primers..... 58

2.1.3. Antibodies..... 58

2.1.4. Bacterial strains and media for bacterial growth..... 58

2.1.5. Yeast strains and media for yeast growth..... 60

2.1.6. Solutions and buffers..... 61

2.2. Methods..... 63

2.2.1. Molecular biology assays..... 63

2.2.1.1. Yeast genomic DNA extraction..... 63

2.2.1.2. PCR..... 63

2.2.1.3. Cloning..... 64

2.2.1.4. Plasmid DNA purification and sequencing..... 65

2.2.1.5. Mutagenesis..... 65

2.2.1.6. Protein expression and purification..... 66

2.2.1.7. ÄKTA FPLC..... 69

2.2.1.8. Radiolabelled protein production..... 70

2.2.1.9. Tricine SDS-PAGE, western blotting and autoradiography..... 70

2.2.1.10. Silver staining..... 71

2.2.2. *In organello* assays..... 72

2.2.2.1. Isolation of yeast mitochondria and peroxisomes..... 72

2.2.2.2. Mitochondrial import assay..... 72

2.2.2.3. Mitochondrial localisation assay..... 74

2.2.2.4. Pulldown assay using His-tagged proteins..... 75

2.2.2.5. Complex immunoprecipitations..... 76

2.2.2.6. BN-PAGE..... 77

2.2.3. *In vitro* assays..... 78

2.2.3.1. *In vitro* binding assay using Ni-NTA beads..... 78

2.2.3.2. *In vitro* protein-protein interaction assay..... 78

2.2.4. *In vivo* assays..... 79

2.2.4.1. Yeast growth, drop tests and sensitivity assays..... 79

2.2.4.2. Immunofluorescence assay..... 80

2.2.5. Mass spectrometry..... 81

2.2.6. Circular dichroism..... 81

2.2.7. Electron Microscopy..... 81

3. Identifying mitochondrial protein interactors of Gpx3..... 83

3.1. Introduction..... 84

3.2. Aims..... 86

3.3. Results..... 87

3.3.1. Purification of Gpx3 and N18Gpx3 proteins..... 87

3.3.2. Mitochondrial import of Gpx3 and N18Gpx3..... 93

3.3.3. *In organello* affinity pulldown assays to identify Gpx3 interactors..... 95

3.3.4. Mass spectrometry analysis of Gpx3 pulldown eluates..... 102

3.3.5. Investigating the potential interaction between Gpx3 and Cyt*c*.. 107

3.3.5.1. *In vitro* binding assays using His-tagged Gpx3 proteins... 107

3.3.5.2. Reciprocal *in vitro* binding assays using Cyt*c*His..... 110

3.3.5.3. *In vitro* interaction assays between Gpx3 and Cyt*c*..... 112

3.3.5.4. Immunoprecipitations to detect Gpx3-Cyt*c in vivo*..... 120

3.3.6. Alternative tags..... 121

3.3.6.1. Gpx3-TAP..... 121

3.3.6.2. Gpx3-V5..... 122

3.3.7. Import of Ybr124w and Ypl107w..... 124

3.4. Discussion..... 127

4. Ypl107w: a putative oxidoreductase of unknown function..... 132

4.1. Introduction..... 133

4.2 Aims..... 135

4.3. Results..... 136

4.3.1. Bioinformatics analysis of Ypl107w and its homologs..... 136

4.3.2. Import and localisation of Ypl107w..... 144

4.3.3. BN-PAGE analysis..... 148

4.3.4. Growth assays and drop tests..... 150

4.3.5. Hydrogen peroxide and diamide sensitivity assays..... 153

4.3.6. Steady-state protein levels in *ypl107wΔ* mitochondria..... 156

4.4. Discussion..... 159

5. Investigating Gpx3 in peroxisomes..... 164

5.1. Introduction..... 165

5.2. Aims..... 167

5.3. Results..... 168

5.3.1. Isolation of mitochondria and peroxisomes confirms the presence of Gpx3 in both organelles..... 168

5.3.2. Sequence analysis of mitochondrial proteins found in peroxisomal fractions..... 172

5.3.3. 'Peroxisomal' Mia40..... 175

5.3.4. *In vitro* binding assays to investigate peroxisomal Gpx3 interactors..... 180

5.3.5. Electron microscopy to visualise *S. cerevisiae* organelles..... 183

5.3.6. Import and localisation of Pex11 in mitochondria..... 185

5.3.7. Import of N17Pex11 – does an N17 extension exist?..... 188

5.4. Discussion..... 190

6. General discussion..... 193

6.1. Mitochondrial interactors of Gpx3..... 194

6.2. Missing mitochondrial proteins?..... 195

6.3. A new mitochondrial matrix protein – Ypl107w..... 196

6.4. Does the MIA pathway exist in yeast peroxisomes?..... 199

6.5. Conclusion…..... 201

7. Appendices…..... 202

7.1. Appendix 1 – Gpx3 purifications…..... 203

7.2. Appendix 2 - Ypl107w and hOXLD-1 bioinformatics..... 207

7.3. Appendix 3 - *ypl107wΔ* mitochondria..... 212

7.4. Appendix 4 - Supplementary materials and methods..... 213

7.5. Appendix 5 – Characterisation of *Toxoplasma gondii* Erv3..... 216

References…… 227

List of Figures

Figure 1.1. Structure of a mitochondrion..... 23

Figure 1.2. Mitochondrial outer membrane import pathways..... 26

Figure 1.3. Mitochondrial matrix protein import pathway..... **29**

Figure 1.4. Mitochondrial inner membrane and matrix import pathways..... 30

Figure 1.5. The MIA oxidative folding pathway..... 33

Figure 1.6. Mia40 recognition and oxidation of substrates..... 35

Figure 1.7. The six major eukaryotic groups..... 38

Figure 1.8. Schematic representation of Erv homologs..... 41

Figure 1.9. H_2O_2-induced activation of Yap1 by Gpx3 and Ybp1..... 48

Figure 1.10. Localisation of Gpx3 in *S. cerevisiae* cells..... 51

Figure 2.1. Mr standard curve for ÄKTA protein standards..... 70

Figure 3.1. Expression and purification of His-tagged Gpx3 proteins..... 88

Figure 3.2. Expression and purification of His-tagged N18Gpx3 and N18M20L proteins..... 90

Figure 3.3. Thiol redox state of purified Gpx3 and N18Gpx3 proteins..... 91

Figure 3.4. Schematic of all Gpx3 proteins purified..... 92

Figure 3.5. Import of purified Gpx3His and N18M20LGpx3His..... 93

Figure 3.6. Import of radiolabelled Gpx3 and N18M20LGpx3..... 94

Figure 3.7. Illustration of the pulldown assay..... 95

Figure 3.8. Illustration of how Gpx3C82AHis traps mixed disulphide intermediates..... 97

Figure 3.9. Gpx3His pulldown assay – first attempt..... 98

Figure 3.10. Optimisation of Gpx3His pulldown conditions..... 100

Figure 3.11. Solubilisation of mitochondrial proteins to isolate intermembrane space proteins..... 105

Figure 3.12. Illustration of the *in vitro* binding assay..... 107

Figure 3.13. *In vitro* binding assays to detect Gpx3 interactors..... 109

Figure 3.14. Purification of Cyt*c*His and *in vitro* binding assay to detect Cyt*c* interactors..... 111

Figure 3.15. Gpx3 interaction with Cyt*c* *in vitro*..... 113

Figure 3.16. Confirmation of a mixed intermediate between Gpx3-Cyt*c* *in vitro*..... 114

Figure 3.17. Reduction of Cyt*c* *in vitro*..... 115

Figure 3.18. *S. cerevisiae* Gpx3 multiple sequence alignment..... 116

Figure 3.19. Gpx3 single cysteine mutant interactions with Cyt*c* *in vitro*..... 117

Figure 3.20. CD spectra of Gpx3 cysteine mutants..... 119

Figure 3.21. Mitochondria isolated from a Gpx3-TAP yeast strain..... 122

Figure 3.22. Import of radiolabelled Ybr124w and Ypl107w..... 126

Figure 4.1. *S. cerevisiae* Ypl107w multiple sequence alignment..... 137

Figure 4.2. Graphical representation of the oxidoreductase-like family across species..... 138

Figure 4.3. Profile HMM for oxidoreductase-like protein family..... 138

Figure 4.4. Secondary structure prediction for Ypl107w and hOXLD-1..... 139

Figure 4.5. Small ligand binding-site prediction for Ypl107w..... 140

Figure 4.6. Import of radiolabelled Ypl107w and Su9-DHFR..... 145

Figure 4.7. Radiolabelled Ypl107w localisation after mitochondrial import..... 146

Figure 4.8. Import of radiolabelled *N26*ΔYpl107w and Ypl107w..... 147

Figure 4.9. BN-PAGE analysis of Ypl107w after radiolabelled import..... 149

Figure 4.10. Growth of *ypl107wΔ* vs wild-type yeast..... 150

Figure 4.11. Yeast drop tests in fermentable vs non-fermentable media..... 151

Figure 4.12. Colour of wild-type vs *ypl107wΔ* yeast grown on non-fermentable media..... 152

Figure 4.13. H_2O_2 sensitivity assay – plates..... 153

Figure 4.14. H_2O_2 sensitivity assay – diameters..... 154

Figure 4.15. Diamide sensitivity assay..... 155

Figure 4.16. Comparison of protein levels in wild-type BY4741 vs *ypl107wΔ* mitochondria..... 157

Figure 4.17. Quantification of protein levels in wild-type BY4741 vs *ypl107wΔ* mitochondria..... 158

Figure 5.1. Isolation of mitochondria and peroxisomes..... 168

Figure 5.2. Yeast Gpx3 localises to both mitochondria and peroxisomes..... 169

Figure 5.3. PTS1 and PTS2 consensus motifs..... 172

Figure 5.4. Detection of yeast Mia40 in mitochondria vs peroxisomes..... 175

Figure 5.5. Mia40 amino acid sequence in *S. cerevisiae* vs *A. thaliana*..... 176

Figure 5.6. Isolation of mitochondria and peroxisomes from *gpx3Δ* and galMia40 yeast..... 178

Figure 5.7. *In vitro* binding assays to detect peroxisomal interactors of Gpx3 cysteine mutants..... 180

Figure 5.8. Further *in vitro* binding assays to detect peroxisomal interactors of Gpx3..... 181

Figure 5.9. Wild-type yeast cells visualised by transmission electron microscopy..... 183

Figure 5.10. Import of radiolabelled Pex11 and Su9-DHFR..... 185

Figure 5.11. Radiolabelled Pex11 localisation after mitochondrial import..... 187

Figure 5.12. Alignment of the N18 upstream of Gpx3 with the putative N17 upstream of Pex11..... 188

Figure 5.13. Radiolabelled import of Pex11 vs N18Pex11 in mitochondria.... 189

Figure 7.1. Purification of Gpx3His – ÄKTA peaks..... 203

Figure 7.2. Purification of Gpx3C36SHis – ÄKTA peaks..... 204

Figure 7.3. Purification of Gpx3C64SHis – ÄKTA peaks..... 205

Figure 7.4. Purification of Gpx3C82AHis – ÄKTA peaks..... 206

Figure 7.5. Steady-state protein levels in wild-type BY4741 vs *ypl107wΔ* mitochondria..... 212

Figure 7.6. Confocal microscopy to detect localisation of TgErv3 and ScErv1 in *T. gondii* mitochondria..... 217

Figure 7.7. Purification of GST-TgErv3 219

Figure 7.8. Purification of GST 220

Figure 7.9. Purification of GST-TgErv3 from inclusion bodies – ÄKTA peaks 221

Figure 7.10. Purification of GST-TgErv3 from inclusion bodies – Fractions from ÄKTA peaks 222

Figure 7.11. Purification of GST-TgErv3 from the soluble fraction – ÄKTA peaks..... 224

Figure 7.12. Purification of GST-TgErv3 from the soluble fraction – Fractions from ÄKTA peaks (-DTT) 225

Figure 7.13. GST alone – ÄKTA peaks 226

List of Tables

Table 2.1. List of plasmids..... 57

Table 2.2. List of bacterial strains..... 59

Table 2.3. List of yeast strains..... 60

Table 2.4. List of individual protein expression conditions..... 66

Table 2.5. List of ÄKTA protein standards..... 69

Table 2.6. Treatment conditions for proteins prior to their mitochondrial import..... 73

Table 3.1. Pulldown assay optimisation conditions..... 99

Table 3.2. Final conditions after pulldown optimisation..... 101

Table 3.3. Hits identified by mass spectrometry..... 103

Table 3.4. Potential mitochondrial proteins based on mass spectrometry analysis of mitochondria isolated from *S. cerevisiae*..... 124

Table 4.1. *YPL107W* genetic interactors associated with mitochondria..... 141

Table 4.2. Gene Ontology search for *YPL107W* genetic interactors..... 142

Table 4.3. hOXLD-1 physical interactors associated with mitochondria..... 143

Table 5.1. Predicting peroxisomal targeting signals based on consensus PTS1 and PTS2 motifs..... 173

Table 7.1. Genes with similar expression patterns to *YPL107W*..... 207

Table 7.2. GO Term Finder search of 38 mitochondrial hOXLD-1 interactors 209

Table 7.3 List of primers..... 213

Table 7.4. List of antibodies..... 215

Acknowledgements

I would like to start by thanking the BBSRC and the College of MVLS at the University of Glasgow for providing the funding to undertake my PhD at a University (and city) that has well and truly been my home for the last nine years. My warmest and sincerest thanks go to Professor Kostas Tokatlidis for his continuous guidance throughout my PhD and for allowing me the opportunity to explore many side-line scientific curiosities for which I am ever grateful. I would also like to thank everyone who has been a part of the Tokatlidis lab between 2014-2018 for their daily support, and also the Bulleid lab for providing technical advice and last-minute reagents. I would also like to thank the Glasgow Polyomics facility for carrying out the mass spectrometry, Dr Sharon Kelly for her assistance with circular dichroism, and Margaret Mullin for help with electron microscopy. Finally, my deepest thanks go to all my family and friends who were always there to provide emotional support and for their non-judgemental understanding during the roughest times, with special thanks to my Mum and Dad, Dr Chloe Stoyle and Tom Herriot. Furthermore, I would like to credit my two non-human supporters, Luna and Mia, for providing much needed 'cat therapy' at the end of every day.

Three weeks before my original submission deadline, I was admitted to hospital after experiencing seizures. I had developed a life-threatening infection that required surgical removal of a brain abscess, alongside a whole host of other drugs. Extraordinary thanks must therefore go to the fantastic staff at the Queen Elizabeth University Hospital in Glasgow for saving my life. Ironically, immediately prior to this I commented on how I was unsure how much more stress my body could take. The reason why I developed such a severe infection is unknown but the words 'don't burn yourself out' have an eerie ring.

Whilst this PhD thesis marks the ending of an emotionally turbulent four and a bit years, small eureka moments were enough to keep my passion for science alive alongside incredibly supportive supervisors, fellow academics, family, and friends (including those of the furry kind). My gratitude will always remain.

Author's declaration

I declare that, except where explicit reference is made to the contribution of others, that this thesis is the result of my own work and has not been submitted for any other degree at the University of Glasgow or any other institution.

Abbreviations

AMS ..... 4-acetamido-4'-maleimidylstilbene-2,2'-disulfonic acid

ATP ..... Adenosine triphosphate

β-me ..... β-mercaptoethanol

BN ..... Blue native

BSA ..... Bovine serum albumin

CBP ..... Calmodulin-binding peptide

CCCP ..... Carbonyl cyanide m-chlorophenyl hydrazone

CD ..... Circular dichroism

CE ..... Carbonate extraction

CH ..... Coiled helix

CL ..... Cardiolipin

Co-IP ..... Complex immunoprecipitation

COX ..... Cytochrome *c* oxidase

CPC ..... Cysteine proline cysteine

DDM ..... n-Dodecyl β-D-maltoside

DHFR ..... Dehydrofolate reductase

$DiSC_3(_5)$ ..... 3, 3' - dipropylthiadicarbocyanine iodide

DMSO ..... Dimethyl sulfoxide

DNA ..... Deoxyribonucleic acid

DTT ..... Dithiothreitol

EDTA ..... Ethylenediaminetetraacetic acid

EGTA ..... Ethylene glycol-bis(β-aminoethyl ether)-N,N,N',N'-tetraacetic acid

E/EL ..... Elution

Ellip ..... Molar ellipticity

ER ..... Endoplasmic reticulum

ERMES ..... Endoplasmic reticulum – mitochondria encounter structure

FAD ..... Flavin adenine dinucleotide

FASP ..... Filter-aided sample preparation

Fe/S ..... Iron-sulphur

FPLC ..... Fast protein lipid chromatography

Fth ..... Flowthrough

GSH ..... Reduced glutathione

GSSG ..... Oxidised glutathione

HEPES ..... 4-(2-hydroxyethyl)piperazine-1-ethanesulfonic acid

His ..... 6 x Histidine tag

HT ..... High tension

IgG ..... Immunoglobulin G

IM ..... Inner membrane

IMI ..... Imidazole

IMP ..... Inner membrane protease

IMS ..... Intermembrane space

IPTG ..... Isopropyl β-D-1-thiogalactopyranoside

ITC ..... Isothermal titration calorimetry

ITS/MISS ..... Intermembrane space targeting signal/mitochondrial intermembrane space sorting signal

KISS ..... Kinetoplastid-specific second domain

LB ..... Luria-Bertani

LC-MS ..... Liquid chromatography-mass spectrometry

MIA ..... Mitochondrial intermembrane space assembly

MICOS ..... Mitochondrial contact site and cristae organising system

MIM ..... Mitochondrial import

Mito ..... Mitochondria

MP ..... Mitoplast

MPP ..... Matrix processing peptidase

Mr ..... Molecular weight (Da)

mtDNA ..... Mitochondrial DNA

MTS ..... Mitochondrial targeting signal

MW ..... Molecular weight (kDa)

NADP ..... Reduced nicotinamide adenine dinucleotide

NADPH ..... Reduced nicotinamide adenine dinucleotide phosphate

NES ..... Nuclear export signal

Ni-NTA ..... Nickel-nitriloacetic acid

OM ..... Outer membrane

ox ..... Oxidised

OXA ..... Oxidase assembly translocase

OXLD ..... Oxidoreductase-like domain

OXPHOS ..... Oxidative phosphorylation

P ..... Pellet

pA ..... Protein A beads

PAGE ..... Polyacrylamide gel electrophoresis

PAM ..... Presequence translocase-associated motor

PCR ..... Polymerase chain reaction

PDI ..... Protein disulphide isomerase

Perox ..... Peroxisomes

PFA ..... Paraformaldehyde

PK ..... Proteinase K

PM ..... Peroxisomal membrane

PMSF ..... Phenylmethylsulfonyl fluoride

POL ..... Polarised light

PTS1 ..... Peroxisome targeting signal 1

PTS2 ..... Peroxisome targeting signal 2

PVDF ..... Polyvinylidene fluoride

red ..... reduced

RNA ..... Ribonucleic acid

RNAi ..... Ribonucleic acid interference

ROS ..... Reactive oxygen species

RT ..... Room temperature

S ..... Supernatant

SAM ..... Sorting and assembly machinery

SB ..... Sample buffer

SBTI ..... Soybean trypsin inhibitor

SDS ..... Sodium dodecyl sulphate

TAP ..... Tandem affinity purification

TCA ..... Tricarboxylic acid

TEM ..... Transmission electron microscope

TEV ..... Tobacco etch virus

TIM ..... Translocase of the inner membrane

TOM ..... Translocase of the outer membrane

tRNA ..... Transfer RNA

Tx Triton-X-100

UV ..... Ultraviolet

W ..... Wash

WT ..... Wild-type

w/v ..... weight/volume

YPD ..... Yeast extract, peptone, dextrose (glucose)

YPG ..... Yeast extract, peptone, galactose

YPGly ..... Yeast extract, peptone, glycerol

YPL ..... Yeast extract, peptone, lactic acid

$\Delta\Psi$ ..... Inner mitochondrial membrane potential

Chapter 1

Introduction

1. Introduction

1.1. Mitochondria

In the final decade of the nineteenth century, the first account of mitochondria was documented by a German pathologist, Richard Altmann, who originally referred to them as "bioblasts" (Altmann, 1890). Altmann believed that these organelles were self-governing living organisms present within cells which were capable of performing cellular functions. Eight years later they were renamed mitochondria (Benda, 1898). After more than a century's research, mitochondria are now widely accepted to have arisen as a result of an endosymbiotic event whereby a proteobacterium entered a eukaryotic cell sparking a series of evolutionary steps which led to their progressive integration (Roger et al., 2017). They are also now known to be involved in a multitude of intra- and extra-cellular functions (Spinelli and Haigis, 2018). One very well-known and important function is mitochondrial respiration, a series of metabolic reactions which generates adenosine triphosphate (ATP) at the final step of oxidative phosphorylation (OXPHOS); this ATP is then used to drive many diverse cellular processes (Smeitink et al., 2001). Other functions include calcium homeostasis, synaptic homeostasis, apoptosis, production of reactive oxygen species (ROS), cell signalling, and iron-sulphur (Fe/S) cluster biogenesis, but this is by no means an exhaustive list (Joza et al., 2001; Finkel, 2012; Kallergi et al., 2014; Lill et al., 2014; Picard et al., 2015; Pathak and Trebak, 2018).

The most fundamental milestones in mitochondrial research underpinning what we know today were made in the mid 20th century. In 1937, Krebs and Johnson discovered the tricarboxylic acid (TCA) cycle (also known as the Kreb's or citric acid cycle) that was later found to occur within mitochondrial isolates (Kennedy and Lehninger, 1947; Schneider, 1948). Then in 1953, the first electron microscope images of mitochondria revealed their classic rod-like structure comprising two lipid bilayers: a smooth outer membrane and a transverse, irregular inner membrane (Sjöstrand, 1953; Palay and Palade, 1955). Ten years on, mitochondria were found to contain their own circular DNA (mtDNA) which was entirely separate from the cells nuclear genome; however, the mtDNA itself only encodes

~15% of all mitochondrial respiratory complex subunits – 13 in humans and 8 in yeast (Nass and Nass, 1963; Clayton and Vinograd, 1967; Chacinska et al., 2009). Furthermore, to carry out their extensive range of functions mitochondria require approximately 1000-1500 proteins depending on the organism, of which 99% are encoded by the nuclear genome and are synthesised on cytosolic ribosomes (Chacinska et al., 2009). Of course, this then raised many important questions regarding the targeting and import of these proteins into mitochondria.

1.2. Mitochondrial biogenesis

As the majority of mitochondrial proteins are translated in the cytosol, they must be correctly targeted, imported, sorted and folded into their specific mitochondrial subcompartment. The next sections describe the structure of mitochondria and discuss the many sophisticated protein import pathways that govern these crucial events. As *S. cerevisiae* has been the most commonly used model organism to identify mitochondrial protein import pathways, the following sections refer to *S. cerevisiae* unless otherwise stated. Although, the pathways are generally well conserved from yeast to mammals.

1.2.1. Mitochondrial structure

Four mitochondrial subcompartments exist: the outer membrane (OM), the inner membrane (IM) which form folds known as cristae, and two enclosed aqueous subcompartments, one entirely sealed by the IM, known as the matrix, and the other sealed by both the OM and the IM, known as the intermembrane space (IMS) (**Figure 1.1**). Although the OM and IM are both phospholipid bilayers, they differ from each other in terms of both phospholipid and protein content which reflect their distinct functions. The OM contains small channels, including the major voltage-anion dependent channel (VDAC, also known as porin), that permit the diffusion of small molecules up to 5000 Da in size (Becker and Wagner, 2018). Whereas the IM has a much tighter structure that consists of three times more cardiolipin (CL) than the OM and is impermeable to small molecules (Houtkooper and Vaz, 2008). Proteins of the OM are largely involved in the entry of all

mitochondrial proteins from the cytosol as well as fusion/fission events. Whereas the IM plays a major role in respiration as it harbours all of the respiratory chain complexes whilst also containing some protein import machineries - the final entry gates to the matrix (Wiedemen and Pfanner, 2017). Matrix proteins are largely involved in Fe/S cluster biogenesis and cellular respiration (Lill, 2009; Lill et al., 2014). Finally, IMS proteins play important roles in redox regulation, oxidative folding and apoptosis (Joza et al., 2001; Vögtle et al., 2012; Kritsiligkou et al., 2017). The ratio of mitochondrial proteins across the OM, IMS, IM and matrix is roughly 1:4:1:4, with fourfold more proteins present in the IMS and the matrix in comparison to the OM and IM (Calvo et al., 2017; Morgenstern et al., 2017).

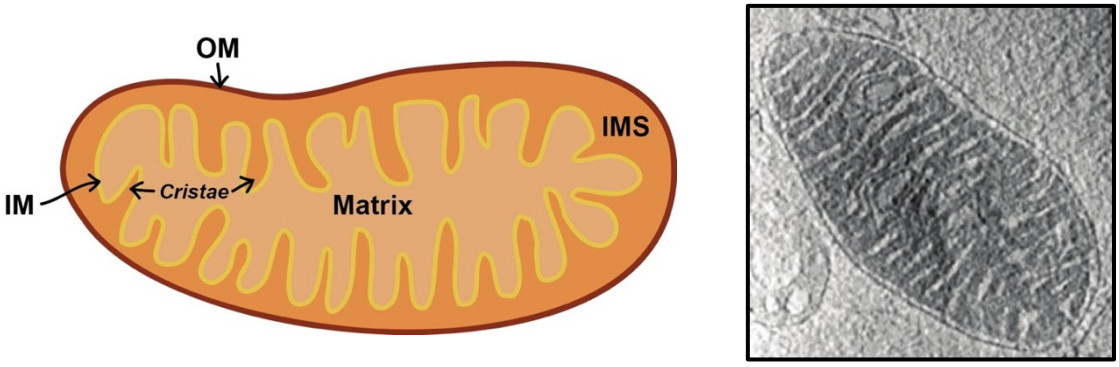

Figure 1.1. Structure of a mitochondrion. OM – outer membrane; IM – inner membrane; IMS – intermembrane space. The matrix is enclosed by the IM; the IMS by the OM and IM. The panel on the right is a cryo-electron tomography image of a mouse heart mitochondrion taken from Brandt et al. (2017).

1.2.2. Outer membrane protein translocation

All precursors arrive at the OM and must translocate through in order to reach any one of the mitochondrial subcompartments. Up until recently, only one OM protein import channel had been characterised – the translocase of the outer membrane (TOM) – which is thought to act as the main entry gate (Neupert and Herrmann, 2007; Dudek et al., 2013). However, new OM channels are being discovered; one of which has already been shown to be capable of importing proteins - the MIM channel (Krüger et al., 2017;

Checchetto and Szabo 2018). Regardless of which channel precursors enter, specific chaperones are first required to keep precursors in an import-competent state, i.e. by preventing misfolding and aggregation, and to carry them to the OM where they will be in close proximity to OM receptors (Komiya et al. 1997, Chacinska and Rehling, 2004). At this stage, the OM receptors recognise some of the mitochondrial targeting signals (MTSs) present within precursor proteins that begin to dictate which pathways they will use in order to reach their final destination (Mossmann et al., 2012; Melin et al., 2014). Two thirds of mitochondrial proteins contain classical N-terminal α-helical signals that are usually cleaved upon import (Vögtle et al., 2009), but there are many others, including internal signals, that will be discussed throughout **Section 1.2**.

The TOM complex

Seven subunits make up the TOM complex: three receptors – Tom20, Tom22 and Tom70 that interact with incoming precursors on the cytosolic side; the main pore forming subunit Tom40; and three non-essential smaller subunits (Tom5, Tom6 and Tom7) that also make up the main pore-forming core (Dietmeier et al., 1997; Dekker et al., 1998; Hill et al., 1998; Sherman et al., 2005; Neupert and Herrmann 2007; Shiota et al., 2015). Although Tom20 and Tom70 exhibit their own preference for substrates, they are both anchored to the OM via their N-terminal regions, with hydrophilic domains exposed to the cytosol that are responsible for recognising precursors. Their main difference lies in how they recognise their precursors as the cytosol-exposed domain of Tom20 contains a groove that binds hydrophobic residues within MTSs, whereas Tom70 recognises internal targeting signals (Abe et al., 2000; Chan et al., 2006). Tom22 is entirely different in the sense that it has two domains exposed either side of the OM – a cytosol-exposed, negatively charged N-terminal domain, and an IMS-exposed, negatively charged C-terminal domain (van Wilpe et al., 1999). Upon entering the TOM complex, proteins are then sorted based on their final destination.

The SAM complex

For β-barrel proteins that are for insertion into the OM, the SAM complex (the Sorting and Assembly Machinery) is required (Neupert and Herrmann, 2007). Precursors move from TOM to SAM via the Tim9/Tim10 chaperone complex (Höhr et al., 2015). Three subunits make up the SAM complex: the essential main subunit Sam50 with its C-terminal β-barrel domain embedded in the OM and an IMS-exposed N-terminal hydrophilic domain; and two entirely cytosol-exposed hydrophilic subunits, Sam35 and Sam37, of which only Sam35 is essential (Wiedemann et al., 2003; Chan and Lithgow, 2008). Unlike the majority of precursors, OM proteins that follow the SAM pathway do not contain N-terminal presequences. Instead, they harbour internal hydrophobic β-hairpin motifs that are recognised by Tom20 upon entry to mitochondria (Jores et al., 2016).

The MIM complex

For α-helical proteins that are to be inserted into the OM, the newly discovered mitochondrial import (MIM) complex is required (Checchetto and Szabo, 2018). Two subunits make up the MIM complex: Mim1 and Mim2. Mim1, a small 13 kDa OM protein, was found to promote the import of these proteins (Becker et al., 2008; Becker et al., 2011; Papic et al., 2011), and was later shown to form a channel with a predicted α-helical structure (Krüger et al., 2017). Mim1 also has a cytosol-exposed N-terminal domain and an IMS-exposed C-terminal domain (Popov-Celeketić et al., 2008). This is in contrast to the TOM and SAM complexes which both have β-barrel structures (Hill et al., 1998; Neupert and Herrmann, 2007). Mim2 has been shown to physically interact with Mim1, and its absence causes defects in the TOM complex, import of OM proteins, and mitochondrial morphology (Dimmer et al., 2012), but the actual mechanism of the MIM pathway is still unknown. Furthermore, it is unlikely that all of the OM pathways have yet been discovered as there are more recently identified channels that have yet to be characterised, such as Ayr1 (Krüger et al., 2017). A summary of all the known OM import channels is shown in **Figure 1.2**.

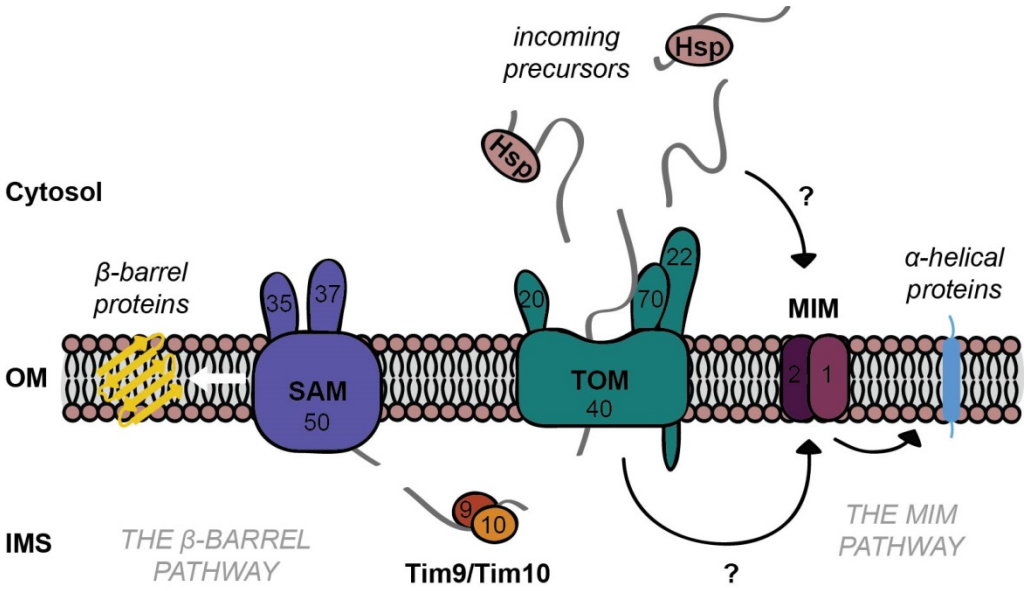

Figure 1.2. Mitochondrial outer membrane import pathways. β-barrel OM precursors enter the TOM complex via Hsp chaperones then travel to the SAM complex via the chaperone complex Tim9/Tim10 (the β-barrel pathway). Arrows with question marks are present next to the MIM pathway that inserts α-helical proteins as the exact mechanism has yet to be elucidated. OM – outer membrane; IMS – intermembrane space; Hsp – Heat-shock proteins 70 or 90. *See **Section 1.2.2** for detailed descriptions.*

1.2.3. Matrix and inner membrane protein import

Upon entry into the IMS, proteins that are destined to the matrix follow the matrix pathway that takes precursors through the TIM23 complex assisted by PAM, the presequence translocase-associated motor. Those that are destined to the IM follow one of two pathways: the stop-transfer pathway or the carrier pathway that utilise the two translocases of the inner membrane, TIM22 and TIM23, respectively (Neupert and Herrmann, 2007). Another IM complex exists, OXA, the oxidase assembly translocase, which is involved in exporting mitochondrial encoded proteins from the matrix to the IM (Wiedemen and Pfanner, 2017). OXA has also been implicated in the import of nuclear encoded IM proteins (Stiller et al., 2014), but this is still debated and will not be discussed here. This section discusses the roles of the TIM23, TIM22, and PAM complexes in the import of matrix and/or IM proteins.

The TIM23 complex

The TIM23 complex comprises its main pore-forming channel, TIM23 that comprises two subunits, Tim23 and Tim17; Tim50; Tim21; and its motor, the presequence-associated motor (PAM) which comprises three subunits – Tim44, Tim14 and Tim16 (Backes and Herrmann, 2017). Both Tim23 and Tim17 have IMS-exposed N-terminal domains but with slight differences; Tim23's has a coiled-coil domain that is involved in substrate binding and dimerisation and can stretch across to the OM (Bauer et al., 1996; Donzeau et al., 2000), whereas Tim17's is shorter and contains conserved negatively charged residues and is involved in gating of the channel (Meier et al., 2005; Martinez-Caballero et al., 2007). Tim50 exposes a large domain to the IMS where it interacts with precursors in the IMS bringing them closer to the main pore of the channel (Geissler et al., 2002; Yamamoto et al., 2002), and is involved in controlling the gating of the channel (Mokranjac et al., 2009; Schulz et al., 2011; Bajaj et al., 2014). Lastly, Tim21 has been shown to interact with the IMS-exposed domain of Tom22, one of the TOM channel receptors, and is only required for the import of IM embedded proteins (Chacinska et al., 2005; Mokranjac et al., 2005). To drive proteins into the IM through the TIM23 complex, membrane potential $\Delta\Psi$ is required; but for the complete import of precursors through to the matrix, the ATP-powered PAM motor is additionally required. The Tim17 subunit of TIM23 is involved in switching between TIM23 and TIM23-PAM, and has regions that directly bind to PAM (Chacinska et al., 2005; Demishtein- Zohary et al., 2017).

The PAM motor

PAM comprises five subunits: the main component Tim44 that harbours a binding site for the matrix localised mitochondrial Hsp70 chaperone, mtHsp70 (also known as Ssc1); two DnaJ-like proteins – Tim14 and Tim16 – that regulate mtHsp70 binding to precursors; and two mtHsp70 co-chaperones - Mge1 and Mdj1 (Backes and Herrmann, 2017). Tim44 also has a hydrophobic binding site that binds precursors upon their entry to the matrix (Josyula et al., 2006). Precursors are then pulled through via the mtHsp70 chaperone, Ssc1, upon hydrolysis of Ssc1's N-terminal ATPase domain (Kang et al., 1990; Voos et al., 1993; Liu et al., 2001). Mge1, a nucleotide release factor, facilitates ADP release from Ssc1 after substrates enter the matrix which are then correctly folded by a complex consisting

of Ssc1/Mdj1/Mge1 (Horst et al., 1997). However, despite this knowledge the full mechanistic details of how PAM functions is still to be fully uncovered, and many models exist for how mtHsp70 pulls precursors through (Backes and Herrmann, 2017; Craig, 2018). Once precursors enter the matrix, their mitochondrial presequences are usually, but not always, cleaved by MPP (the matrix processing peptidase) (Braun and Schmitz, 1997). Precursors that laterally enter the IM after entering the TIM23 complex are also cleaved by MPP if their N-terminal presequences are exposed. The matrix import pathway is depicted in **Figure 1.3**.

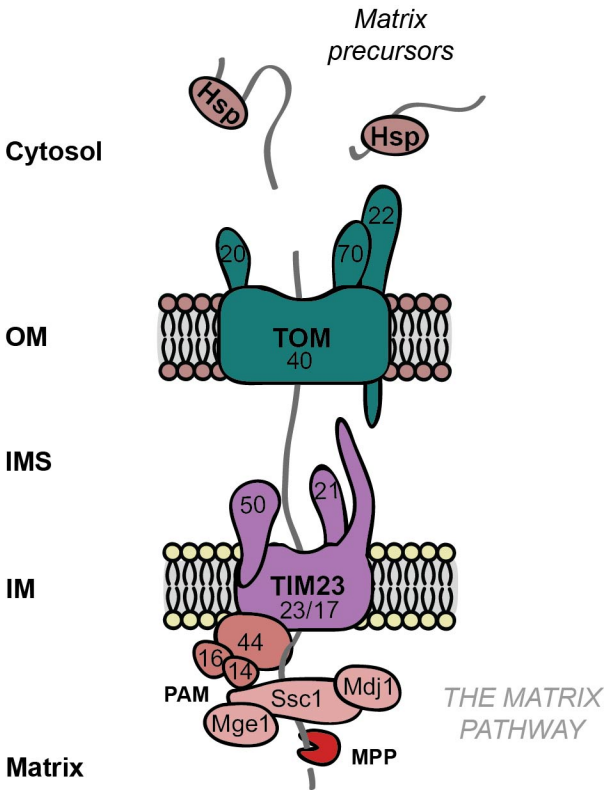

Figure 1.3. Mitochondrial matrix protein import pathway. Matrix precursors follow the matrix pathway whereby precursors cross the OM and are pulled through the TIM23-PAM complex. Ssc1 represents the major mitochondrial Hsp70 which, along with its co-chaperones (Mdj1 and Mge1), helps to refold proteins as they enter the matrix. Some N-terminal mitochondrial targeting presequences are cleaved by MPP upon entry/exposure to the matrix. OM – outer membrane; IMS – intermembrane space; IM – inner membrane; Hsp – heat-shock proteins 70 or 90. *See **Section 1.2.3** for detailed descriptions.*

The TIM22 complex

Three subunits make up the TIM22 complex: Tim22, which forms the main core; and two accessory subunits - one essential, Tim18, and the other non-essential, Tim54 (Sirrenberg et al., 1996; Kerscher et al., 1997; Kovermann et al., 2002). An additional subunit, Tim29, exists but is specific to metazoan TIM22 complexes (Callegari et al., 2016; Kang et al., 2016). Akin to the TOM and SAM complexes, chaperone proteins are also required to bring precursors to the TIM22 complex whilst preventing them from aggregation – these are the small TIMs of the IMS, including Tim8, Tim9, Tim10, Tim12 and Tim13 (Kovermann et al., 2002; Truscott et al., 2002; Koehler, 2004; Vergnolle et al., 2005; Webb et al., 2016). The small TIMs contain CX_3C motifs that form hetero-oligomeric protein complexes that recognise and bind to hydrophobic regions on precursors. After precursors are 'carried' to the TIM22 complex, they are inserted into the IM, thus this pathway is known as the carrier pathway. IM insertion via the TIM22 complex requires the mitochondrial inner membrane potential (denoted $\Delta\Psi$) (Dyall et al., 2003). **Figure 1.4** summarises the import pathways for IM targeted proteins.

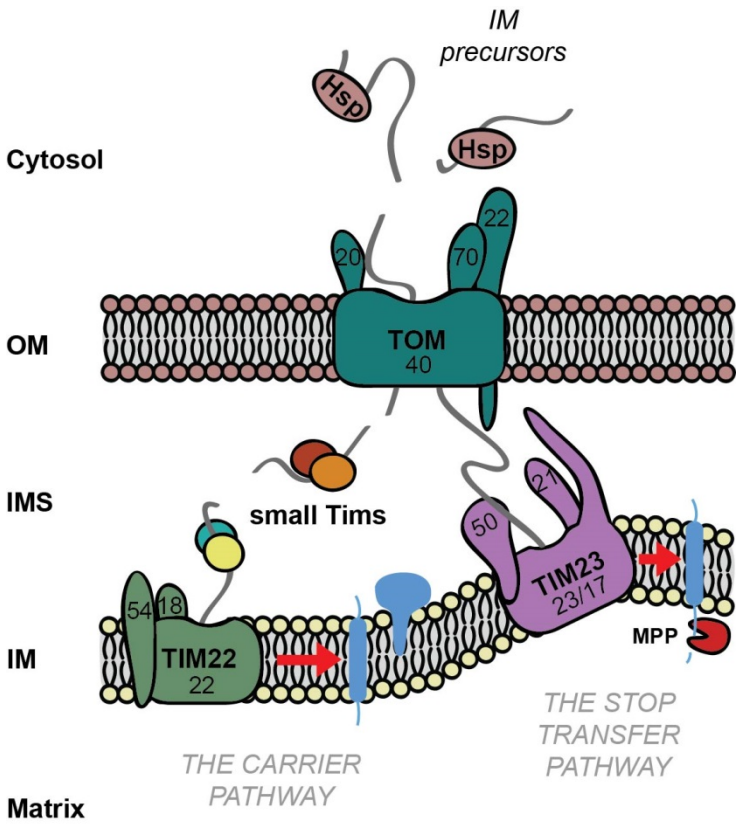

Figure 1.4. Mitochondrial inner membrane protein import pathways. IM precursors can follow one of two pathways: the carrier pathway whereby precursors cross the OM and are carried to the TIM22 complex via hetero-oligomeric small Tim complexes, and then laterally inserted into the IM; or by the stop transfer pathway whereby precursors cross the OM and are pulled through the TIM23 complex followed by lateral insertion in the IM. OM – outer membrane; IMS – intermembrane space; IM – inner membrane; Hsp – heat-shock proteins 70 or 90. *See **Section 1.2.3** for detailed descriptions.*

1.2.4. Intermembrane space protein import

IMS proteins can follow one of four known import pathways: (i) a variation of the TIM23 stop-transfer pathway whereby precursors are released into the IMS from the IM; (ii) a direct 'non-conservative' import pathway into the IMS after entry via the TOM channel; (iii) a co-factor driven import pathway into the IMS by co-factor binding after entry via TOM; and (iv), an oxidative folding import pathway mediated by Mia40 in the IMS (Glick et al., 1992; Steiner et al., 1995; Mordas and Tokatlidis, 2015; Manganas et al., 2017).

The IMS stop-transfer pathway

IMS precursors containing bipartite presequences (N-terminal MTSs followed by a hydrophobic region), such as Cytochrome *c* (Cyt *c*, isoform 1) and Cytochrome b2 (Cyb2), are imported via the stop-transfer pathway (Glick et al., 1992), similar to the one described in **Section 1.2.3**. The difference being that after entering the TIM23 channel their hydrophobic sequences cause an arrest that then allows an IMS protease (IMP or Pcp1), to cleave off their presequences, releasing precursors into the IMS (Nunnari et al., 1993; Esser et al., 2002; McQuibban et al., 2003).

The direct import pathway

Unlike the IMS stop-transfer pathway, the direct import pathway is a one-step route that does not require the IM; example proteins include the two Cyt*c* heme lyases, CCHL and CC1HL (Steiner et al., 1995). Precursors are recognised by two TOM receptors – Tom20 and Tom22 – and enter the IMS through the TOM channel (Mayer et al., 1995; Künkele et al., 1998; Kiekert et al., 1999). As the IM is not needed in this pathway, neither $\Delta\Psi$ nor ATP is required; nor are any Hsp chaperones (Steiner et al., 1995). A conserved internal targeting signal within CC1HL was found to be necessary for its targeting and import (Diekert et al., 1999).

The co-factor import pathway

The co-factor import pathway was uncovered when determining the import of an apoprotein, apocytochrome *c*, which like the direct import pathway, does not involve the IM (Diekert et al., 2001). However, instead of precursor recognition by the TOM receptors, Tom40 itself was required for substrate interaction, followed by an interaction with the IMS heme lyase CCHL that then covalently attaches its heme group creating a fully folded Cyt*c*. No targeting signals have been found within apocytochrome *c*.

The MIA pathway

The MIA oxidative folding pathway differs from all other import pathways as it is the only one that results in the covalent modification of precursors; this being the introduction of disulphide bonds (Mordas and Tokatlidis, 2015). IMS precursors following this pathway contain internal, non-cleavable targeting signals, known as either ITS or MISS, that are usually nine amino acids in length which are recognised by the redox-regulated IMS receptor Mia40 (Milenkovic et al., 2009; Sideris et al., 2009). Cysteine motifs are also present, either upstream or downstream of the ITS/MISS. Typically, these are twin cysteine motifs of either CX_3C or CX_9C, such as those found in the small TIMs and members of the cytochrome *c* oxidase (COX) family that all share a coiled coil-helix1-coiled coil-helix2 (CHCH) fold (Chacinska et al., 2004; Allen et al., 2005; Mesecke et al., 2005; Rissler et al., 2005). However, the repertoire of cysteine motifs has expanded in recent years as new precursors following this pathway are uncovered, such as Atp23 and Ccs1 (Reddehase et al., 2009; Weckbecker et al., 2012).

Precursors enter the IMS using the TOM channel in a reduced and unfolded state where Mia40 then recognises them (Lu et al., 2004; Chacinska et al., 2004). In yeast, Mia40 is anchored to the IM after its import through TIM23, and has a large IMS-exposed C-terminal region (Chatzi et al., 2013). Upon substrate binding, Mia40 introduces disulphide bonds within precursors via a series of electron transfer reactions upon their entry into the IMS (**Figure 1.5**). The IMS sulfhydryl oxidase Erv1 functions as a recycler of Mia40 as it binds to and accepts electrons from Mia40 in its reduced state, i.e. after Mia40 has accepted electrons from incoming precursors as a result of disulphide bond formation (Allen et al., 2005; Mesecke et al., 2005; Rissler et al., 2005). Erv1 then passes electrons to Cyt*c*, and Cyt*c* then shuttles electrons to COX/Complex IV of the respiratory chain (Ang and Lu, 2009), and molecular oxygen becomes the final electron acceptor (Bihlmaier et al., 2007; Dabir et al., 2007). Alternatively, Erv1 can pass electrons directly to molecular oxygen, or Cytochrome *c* peroxidase (Ccp) in yeast. Hydrogen peroxide, H_2O_2, is produced as a by-product of electron transfer to molecular oxygen; whereas H_2O is the final by-product of electron transfer after Cyt*c* has transferred electrons to the respiratory chain (Farrell and Thorpe, 2005). In humans, MIA40/CHCHD4 is a 16 kDa soluble protein

(Hofmann et al., 2005) that has been shown to interact with apoptosis-inducing factor, AIF, a protein also involved in respiratory chain complex biogenesis (Hangen et al., 2015).

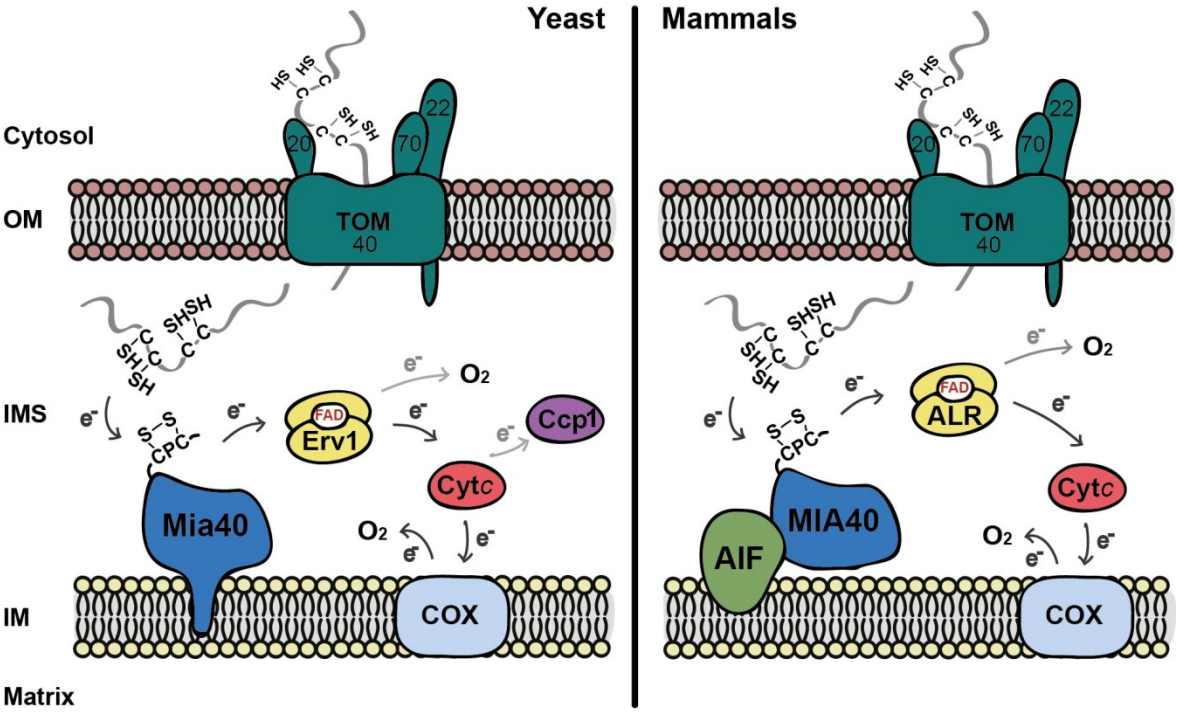

Figure 1.5. The MIA oxidative folding pathway. Electron transfer across the MIA pathway in yeast vs mammalian cells. IMS precursors cross the OM via the TOM channel in a reduced and unfolded state, and are recognised by Mia40. Electron flow begins from the reduced precursor to the redox active CPC of Mia40/MIA40, on to the N-terminal domain of one Erv1/ALR subunit, then to the C-terminal FAD core domain of the second Erv1/ALR subunit, then to Cyt*c*, and finally to either COX which then donates electrons to O_2, or Ccp1 (in yeast). *Figure adapted from Mordas and Tokatlidis (2015).*

Site-specific hydrophobic interactions, occurring within milliseconds upon precursor entry to the IMS, are involved in substrate recognition of precursors by Mia40 between precursor ITS/MISSs and the CPC site of Mia40 (Milenkovic et al., 2009; Sideris et al., 2009; Banci et al., 2010;). These interactions facilitate a two-step event resulting in initial precursor disulphide bond formation, and typically occurs at the first "docking" cysteine within the N-terminal CX_nC motif following a nucleophilic attack from the second cysteine of Mia40's CPC motif (**Figure 1.6A**); a process which is coupled to Mia40-induced folding

of the first coiled-helix (CH). A second nucleophilic attack then occurs at the second "resolving" cysteine within the CX_nC motif from the first "docking" cysteine, followed by substrate release leaving Mia40's CPC motif in a reduced state. At this stage substrates containing twin CX_nC motifs still require a second S-S but the mechanism is unknown.

Three hypothesis currently exist for the formation of the second disulphide bond. The first hypothesis, **Figure 1.6B(i)**, proposes that an oxidant such as molecular oxygen, glutathione or another unknown oxidant, catalyses oxidation of the second disulphide bond, whilst the first folded CH induces folding of the second CH – both without the need for Mia40 (Sideris et al., 2007; Banci et al., 2010; Bien et al., 2010; Fraga et al., 2014). The second possibility, **Figure 1.6B(ii)**, suggests that another oxidised Mia40 in close proximity to the partially oxidised precursor allows for a second round of oxidation. However, an experiment whereby Cox19 was presented to an excess of oxidised Mia40, long-lived mixed disulphide intermediates were present alongside completely oxidised Cox19, which suggests that this is not an efficient mechanism (Bien et al., 2010). The third hypothesis, **Figure 1.6B(iii)**, proposes that Mia40, Erv1 and the substrate form a ternary complex which allows Mia40 to introduce more than one disulphide bond before the substrate is released; evidence for this complex has been observed *in vivo* and *in organello* but how exactly electrons are shuttled through is yet to be explained (Stojanovski et al., 2008; Bottinger et al., 2012). More recent evidence suggests a fourth possibility, not shown in **Figure 1.6B**, that implies Mia40 can catalyse up to three disulphide bonds by utilising all three of its cysteine pairs as they can all become completely reduced, a scenario which has been seen both *in vivo* and *in vitro* (Neal et al., 2015).

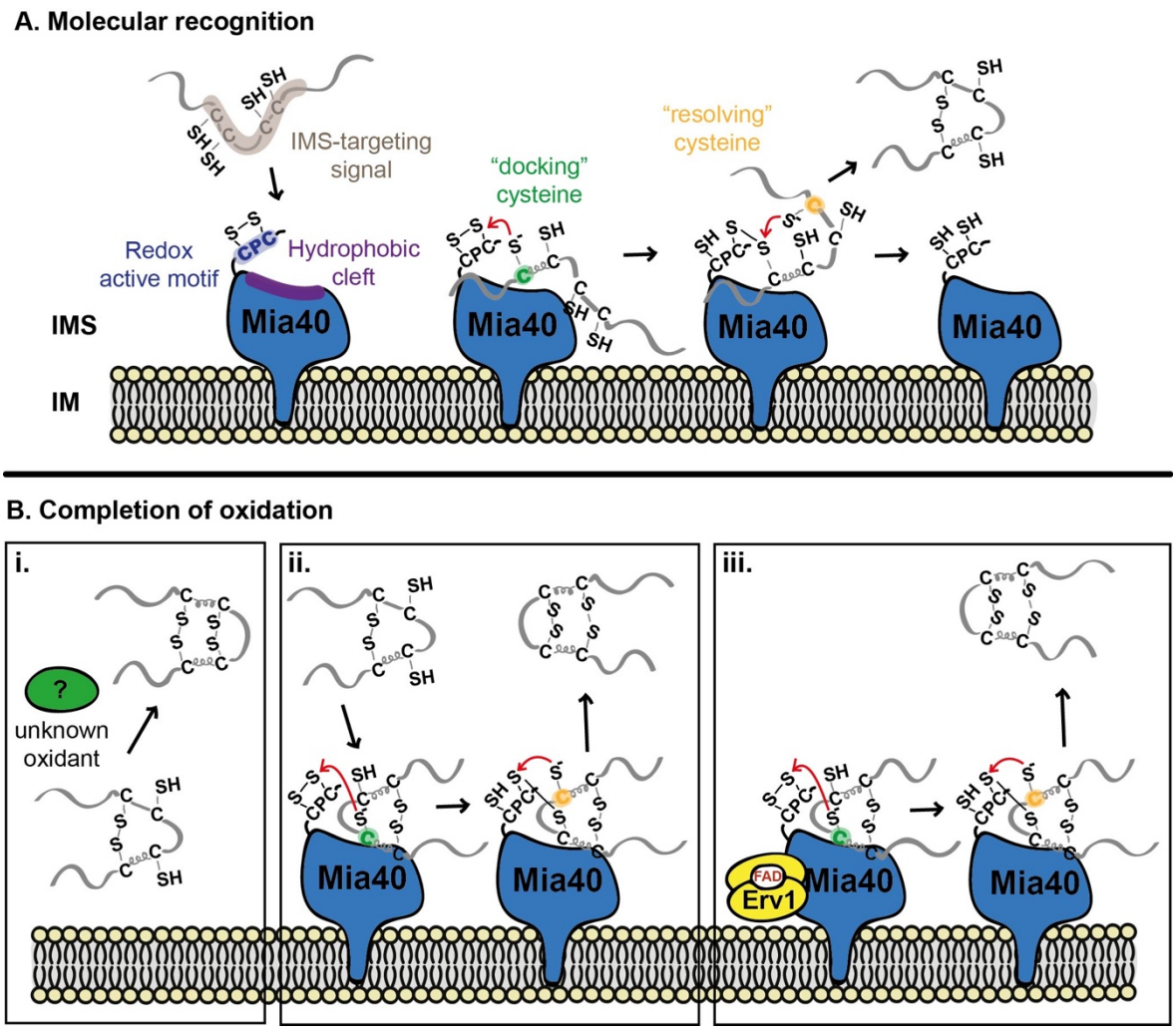

Figure 1.6. Mia40 recognition and oxidation of substrates. (**A**) Molecular recognition of substrates containing classical ITS/MISS and twin CX_3C or CX_9C motifs. Hydrophobic interactions allow precursors with ITS/MISS to "slide" onto Mia40's hydrophobic binding cleft. Once in place, the redox active CPC motif of Mia40 then forms an intermolecular interaction with the first substrate cysteine motif via its docking cysteine. Substrates are released when the resolving cysteine forms an S-S with the docking cysteine. (**B**) Three possible mechanisms for completion of substrate oxidation: (i) an unknown oxidant induces formation of the second disulphide bond, coupled to substrate release; (ii) substrates "slide" onto a nearby oxidised Mia40 which triggers the same reaction; or (iii) sequential reactions take place at the same site as part of a ternary complex involving Mia40, Erv1 and substrate, whereby Erv1 cyclically reoxidises Mia40. *Figure adapted from Mordas and Tokatlidis (2015).*

Whilst these hypotheses may explain how two disulphide bonds can be introduced into substrates with classical twin CX_nC motifs, it has yet to be uncovered how Mia40 catalyses the folding and oxidation of substrates with more complex cysteine motifs, such as the copper chaperone Ccs1 with a $CX_2CX_6CX_{36}CX_nC$ motif (Reddehase et al., 2009) amongst others (see Mordas and Tokatlidis 2015). Furthermore, the import of proteins by Mia40 can also occur as an oxidation-independent event, implying that Mia40 is not just a foldase but a holdase as well, as substrates could still be imported when the CPC of Mia40 was mutated (Baker et al., 2012; Weckbecker et al., 2012; Wrobel et al., 2013; Peleh et al., 2016; Ramesh et al., 2016). In addition, some Mia40 substrates can still be imported when their cysteine residues are mutated, for example: Atp23 – an IM-associated IMS protease with five cysteine pairs. An Atp23 mutant with all 10 of its cysteines abolished can still be imported in a process dependent on Mia40; the critical feature being the hydrophobic binding cleft of Mia40 (Weckbecker et al., 2012). Other proteins that rely on the holdase function of Mia40 are Tim22, Mrp10, and hCHCHD3; notably none of which are IMS resident proteins (Darshi et al., 2012; Wrobel et al., 2013; Longen et al., 2014). Thus, it is now accepted that Mia40 has a distinct chaperone-like role for both IMS and non-IMS proteins.

Looking at the recycler of Mia40 in more detail, Erv1 is a soluble sulfhydryl oxidase that binds to its redox-cofactor flavin adenine dinucleotide (FAD) and, like Mia40, contains three conserved cysteine pairs (Ang and Lu, 2009). Its C-terminal cysteine pair (C159/C176) acts as a structural disulphide when oxidised, but upon Erv1 import to the IMS it is recognised by Mia40 which introduces this disulphide bond (Terziyska et al., 2007; Kallergi et al., 2012). Once folded in the IMS, its N-terminal cysteine pair (C30/C33), known as its shuttle disulphide, is directly responsible for interacting with and accepting electrons from Mia40's CPC motif, thus reoxidising Mia40 (Bien et al., 2010; Lionaki et al., 2010; Banci et al., 2011). These electrons are then shuttled to Erv1's middle cysteine pair (C130/133), before being transferred to bound FAD which then passes electrons to either Cyt*c* or molecular oxygen - as shown in **Figure 1.5**.

Similar to the prokaryotic oxidative folding of periplasmic proteins, the eukaryotic MIA pathway can also function under both aerobic and anaerobic conditions. Whilst all of the Erv1 electron acceptors described above function aerobically, until very recently no electron acceptors had been identified that could function anaerobically. In 2017, the IMS-localised fumarate reductase Osm1 was found to complete the oxidation of substrates in reconstitution assays with reduced Tim13, Mia40 and Erv1, and with an efficiency comparable to Cyt*c* (Neal et al., 2017). In addition, yeast mutants lacking Osm1 exhibit decreased import of Mia40 substrates and an upregulation of Cyt*c* expression. As Osm1 has the ability to transfer electrons from fumarate to succinate without the need for molecular oxygen (Muratsubaki and Enomoto, 1998), Osm1 is both an aerobic and anaerobic electron acceptor of Erv1. However, the exact physiological conditions needed to specify electron flow to a particular electron acceptor are not known, but it is plausible that oxygen levels and respiratory chain activity might dictate the decision.

To conclude **Section 1.2**, although the separate mitochondrial import pathways have been discussed, it is becoming more apparent that these pathways do not always act as independent units. New evidence is emerging regarding the role of mitochondrial membrane contact sites (Horvath et al., 2014), and the import of proteins, such as the OM protein Om45, that require both the TOM channel and TIM23 thus combining the use of two import pathways (Song et al., 2014; Wenz et al. 2014).

1.3. Conservation and evolution of protein import pathways

Eukaryotes can be split into numerous major groups: **Opisthokonts**, including metazoa and fungi; **Archaeplastida**, including plants and green/red algae; **Excavata**, including kinetoplastid parasites and trichomonads and *Giardia*; **Chromalveolata**, including apicomplexan parasites and dinoflagellates; and two others – **Rhizaria** and **Amoebozoa** (**Figure 1.7**) (Adl et al., 2005). The majority of studies on mitochondrial protein import have been carried out in two Opisthokonts, yeast and humans, which share many of the same characteristics due to their close evolutionary lineage. However, as mitochondrial endosymbiosis is thought to have occurred as a one-time only event at the very beginning

of eukaryotic life (Lang et al., 1999), it is therefore not surprising that many features of mitochondrial protein import have been conserved across these groups (Lister et al., 2005; Kutik et al., 2009).

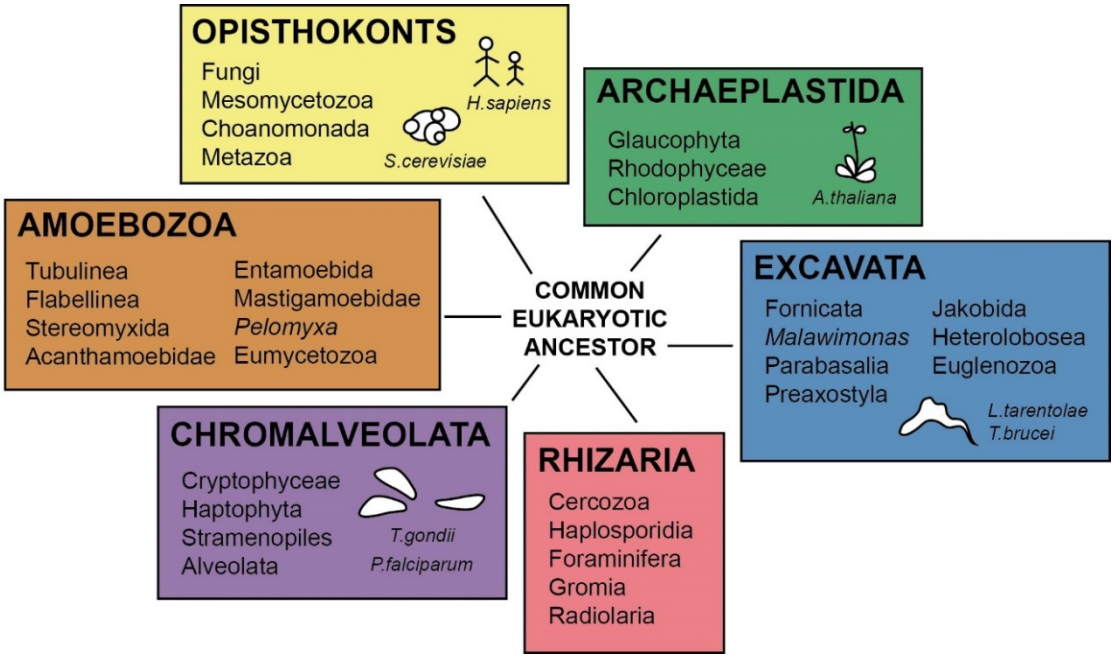

Figure 1.7. The six major eukaryotic groups. Eukaryotes are currently split into six major groups that all diverged from a common eukaryotic ancestor. These include: Opisthokonts, Archaeplastida, Excavata, Chromalveolata, Rhizaria and Amoebozoa (Adl et al., 2005).

A combination of *in silico* analyses and functional complementation assays indicates that three classes of mitochondrial protein import components exist: (i) those derived from the original proteobacterium, (ii) 'de novo' components that arose during the early days of the eukaryotic endosymbiont, and (iii) those that arose after eukaryotes diverged and are thus specific to lineages. For example, whilst the pore-forming subunits of protein import translocases remain well conserved, some additional smaller subunits such as the receptors are not. Despite this, the majority of the known mitochondrial protein import pathways and precursor targeting signals are largely functionally conserved, and thus are a great example of convergent evolution (Murcha et al., 2007; Eckers et al., 2012; Mani et al., 2015; Backes and Herrmann, 2017). However, the story is somewhat different for the MIA oxidative folding pathway.

1.3.1. The MIA pathway across eukaryotes

The small TIMs of the IMS, which are all substrates of the MIA pathway, are found across all eukaryotic lineages as they share conserved sequence motifs with distinct features (Gentle et al., 2007). This suggests they were present in at least the last common ancestor before the eukaryotic divide. However, the number of small TIMs present within and across different eukaryotic lineages does differ, ranging from 1-5. For example, the apicomplexan *Plasmodium* has four distinct TIMs (Tim8, Tim9, Tim10 and Tim13), whereas the closely related apicomplexans *Theileria* and *Cryptosporidium* have either Tim9, Tim10 and a Tim8-Tim13 hybrid, or a Tim8-Tim13 hybrid only. Thus, the small TIMs have evolved differently even within individual eukaryotic groups. Despite this, because all eukaryotes have at least some of the small TIMs present in Opisthokonts, it can be inferred that they must all have an oxidative protein import pathway capable of bringing these proteins into the IMS that was present at the beginning of the eukaryotic divide. In addition, a systematic analysis of proteins containing a twin CX_9C motif, identified proteins that are conserved across animals, fungi and plants.

Both Mia40 and Erv1 are present in plants such as *Arabidopsis* from the Archaeplastida group, along with classical IMS substrate proteins. Whereas although Mia40 substrates have been identified during *in silico* analyses across all groups, intriguingly it appears that kinetoplastid and apicomplexan parasites from both the Excavata and Chromalveolata groups respectively, do not have a Mia40 homolog (Allen et al., 2008). However, Erv1 homologs are present as they are universally found in all eukaryotes, but their domain organisations do vary widely (Eckers et al., 2013). The next three sections discuss what is currently known about Archaeplastida, Excavata, and Chromalveolata IMS oxidative protein folding in relation to the well-studied yeast and human pathways.

1.3.1.1. The *Arabidopsis* MIA pathway

Research on the model organism *Arabidopsis thaliana* has revealed differences in the way that the two core components of the MIA pathway function in plants. Unlike Mia40 and

Erv1 in yeast which are both essential, only AtErv1 is essential in *A. thaliana* (Carrie et al., 2010). Data gathered using *A. thaliana* lacking Mia40 (*Δmia40*) implies that Mia40 does not play an essential role in the import of the small TIMs as no defects were found in the carrier pathway. Instead, Erv1 was upregulated in this mutant, which suggests that Erv1 might function alone in the import of IMS proteins. Interestingly, AtMia40 localises to both mitochondria and peroxisomes - a cellular compartment that typically does not harbour any mitochondrial protein import components. Furthermore, these organelles exhibited a reduction in protein abundance when isolated from *Δmia40* plants, as well as a decreased ability to import both mitochondrial and peroxisomal proteins. Finally, AtErv1 could not complement a yeast Erv1 mutant thus suggesting that both AtErv1 and AtMia40 have novel functions in plants.

A recent study by Peleh et al. (2017) focused on characterising AtErv1 and confirmed the previous finding that AtErv1 could not complement yeast Erv1, as it was unable to reoxidise yeast Mia40 and actually resulted in a dominant-negative effect on Mia40. However, it could directly interact with IMS precursors and facilitate their import and oxidative folding, thus confirming the likelihood that Erv1 can act alone when importing IMS proteins in plants. The authors therefore suggest that the evolution of the MIA pathway began from a system that contained Erv1 *without* Mia40, as had previously been hypothesised by Allen et al. (2008), and that Mia40 evolved to add substrate specificity. Although it is still possible that Mia40 once existed but became lost during the evolution of certain eukaryotic lineages as its function was obsolete.

1.3.1.2. Parasitic MIA pathways

Parasitic protists are believed to be more representative of 'primitive' eukaryotes and fall under two classification groups: Excavata and Chromalveolata, including the non-related kinetoplastid and apicomplexan parasites, respectively. A comparison of Erv homologs across both kinetoplastid and apicomplexan parasites revealed that, although they all share the conserved FAD-binding domain, there are some potentially significant differences (Eckers et al., 2013). Firstly, they lack the N-terminal cysteine-containing

domain of yErv1 responsible for its import in yeast, as well as lacking the final alpha-helical structure (α5), and harbour a variety of cysteine motifs. Despite this, structural predictions suggest they more than likely adopt the same Erv1/ALR fold seen in yeast and humans (Eckers et al., 2013). This fold is crucial for FAD-binding and homo-dimerisation of Erv. The bioinformatics analysis also revealed an additional C-terminal domain that is specific only to kinetoplastids; this domain has been coined 'KISS' for kinetoplastid-specific second domain. Akin to AtErv1, a representative Erv homolog from each group (LtErv from the kinetoplastid *Leishmania tarentolae*, and PfErv from the apicomplexan *Plasmodium falciparum*) could not functionally replace yeast Erv1. Schematic representations of parasitic Erv homologs that have been identified in organisms from both the kinetoplastid and apicomplexan groups, along with yErv1 and AtErv1, is shown in **Figure 1.8**. From now on, studies that have explored kinetoplastid and apicomplexan mitochondrial protein import will be discussed separately.

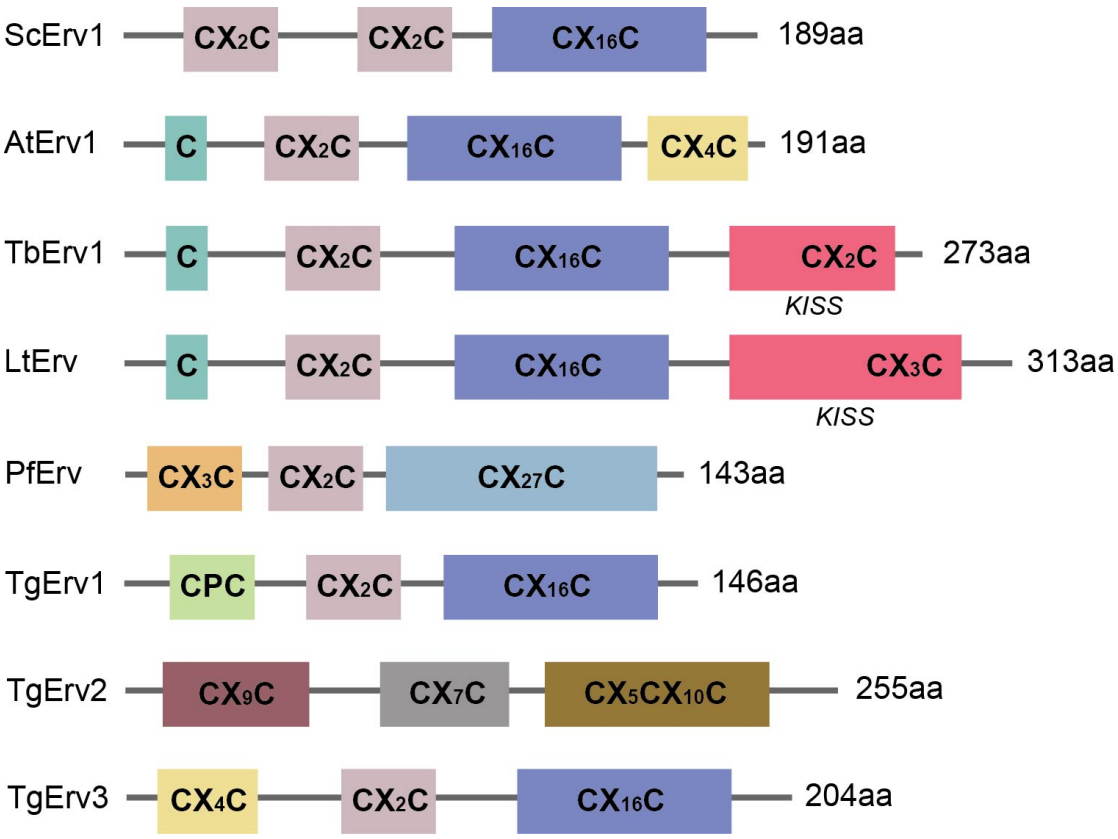

Figure 1.8. Schematic representation of Erv homologs. *S. cerevisiae* Erv1, *A. thaliana* Erv1, *T. brucei* Erv1, *L. tarentolae* Erv, *P. falciparum* Erv, and *T. gondii* Erv1, Erv2 and Erv3 (Eckers et al., 2013).

Kinetoplastid parasites

Two model organisms for kinetoplastid parasites are currently used for mitochondrial protein import studies: *Leishmania tarentolae*, a parasite that can cause Leishmaniasis; and *Trypanosoma brucei*, the parasite responsible for causing African trypanosomiasis. LtErv, TbErv1 and another Erv homolog from another *Leishmania* parasite, *L. infantum*, LiErv can all be successfully imported into yeast mitochondria (Basu et al., 2013; Eckers et al., 2013; Specht et al., 2018). TbErv1 has also been implicated in the import of IMS proteins based on its TbErv1 RNAi knockdown in *T. brucei* that causes both mitochondrial morphology defects (Haindrich et al., 2017), and the downregulation of candidate IMS substrates with twin CX_nC motifs (Peikert et al., 2017). However, no TbErv1 IMS interactors have been identified despite mass spectrometry efforts, suggesting that it acts alone in the IMS and may only be involved in transiently interacting with precursors.

From a biochemical perspective, kinetic analyses using recombinant proteins indicate that LtErv has the ability to reduce Cyt*c* (Eckers et al., 2013), and TbErv1 can reduce Cyt*c* and molecular oxygen simultaneously (Eckers et al., 2013; Basu et al., 2013). As mentioned previously, LtErv cannot complement yeast cells lacking Erv1; however, a recent study has shown that a single cysteine mutant, $LtErv^{C17S}$, can (Specht et al., 2018). Furthermore, chimeras between the N-terminal arm of yeast Erv1 and various truncated LtErvs could also functionally rescue Erv1 mutant yeast. Although it is not yet known why these versions of LtErv can compensate for yErv1, it does suggest there is some degree of flexibility between the kinetoplastid and yeast systems, but they definitely both have their stark differences. The evidence gathered so far is certainly suggestive of kinetoplastid parasites employing an Erv-only oxidative folding pathway. However, a very recent paper by Kaurov et al. (2018) has suggested that one essential component of the MICOS complex (mitochondrial contact site and cristae organising system) in *T. brucei*, TbMic20, has thioredoxin-like activities and is involved in the import of IMS proteins.

Apicomplexan parasites

Two model organisms are commonly used to study apicomplexan parasites: *Plasmodium falciparum*, responsible for transmitting malaria; and *Toxoplasma gondii*, responsible for causing toxoplasmosis. In comparison to kinetoplastid parasites, no published literature exists on their Erv homologs other than *in silico* analysis of their mitochondrial protein import systems (Eckers et al., 2013). A side project to this PhD was to investigate the three *T. gondii* Erv homologs: TgErv1, TgErv2 and TgErv3. Some of these data are shown in **Appendix 5, Figures 7.6-7.13.**

1.4. Intermembrane space proteins

The importance of oxidative protein folding in the IMS is apparent across eukaryotic groups when considering that most IMS proteins contain disulphide bonds that are critical for their function (Haque et al., 2012; Backes and Herrmann, 2017; Habich et al., 2018). Most of these proteins harbour conserved cysteine residues (around 82%, at least in mammalian mitochondria) that are involved in a variety of functions within the IMS, such as: substrate binding, oxidative folding itself, protein homo- and hetero-dimerisation, detoxification of H_2O_2, and the transfer of metal ions (Habich et al., 2018). Aside from cysteine residue function, IMS proteins can be categorised into four groups depending on their broader role (metabolism, morphology, signalling, and logistics). Around 50-150 proteins are currently known; ~50 in yeast and ~150 in humans. Although it should be noted that for roughly 20% of IMS proteins, their functions have yet to be determined, and new proteins are continuously being added to the mitochondrial IMS proteome (Vögtle et al., 2012; Morgenstern et al., 2017). For example, the addition of Gpx3, Trx1 and Trr1 to the yeast IMS proteome in 2012 raised questions regarding the significance of these redox proteins within such a highly redox-active subcompartment.

1.5. Redox regulation of protein disulphide bond formation

The oxidative folding of proteins is compartmentalised in cells due to the reducing nature of the cytosol, and occurs within the endoplasmic reticulum (ER), the mitochondrial IMS, and the bacterial periplasm (Kojer and Riemer, 2014). All three compartments utilise similar oxidative folding pathways whereby electrons flow from substrates to thiol oxidoreductases, to thiol oxidases and then finally to electron acceptors. In mitochondria, protein oxidation occurs specifically in the IMS, as like the cytosol, the mitochondrial matrix must maintain a reducing environment in order to carry out protein translation. The importance of disulphide bonds in the correct folding, stability and function of many proteins means it is no surprise that cells must tightly regulate this process, especially within environments where both oxidising and reducing pathways exist. It is also critical for cells to prevent irreversible protein oxidation, such as the hyperoxidation of cysteine residues, under conditions whereby the levels of reactive oxygen species (ROS) exceeds the antioxidant capacity of cells; a situation known as either oxidative stress or oxidative distress (Sies et al., 2017). Therefore, cells have evolved a wide range of strategies, both non-enzymatic and enzymatic, to protect themselves against the damaging effects of excessive oxidation and to reverse the formation of non-native disulphide bonds. Non-enzymatic defences include small molecules such as Glutathione (GSH) and ascorbic acid; whereas enzymatic defences which are believed to be responsible for the majority of antioxidant activity include catalases, peroxiredoxins and the two disulphide reductive systems - the Glutaredoxin and Thioredoxin systems (Morano et al., 2012).

In the bacterial periplasm, oxidative protein folding is achieved by the oxidoreductase DsbA that, upon substrate oxidation, becomes re-oxidised by the thiol oxidase DsbB that then passes electrons on to the respiratory chain (Kojer and Riemer, 2014). To remove non-native disulphides, the oxidoreductase DsbC is required in its reduced state (Missiakas et al., 1995; Rietsch et al., 1996). DsbC is kept reduced by the plasma membrane protein DsbD that receives electrons from the cytosolic Thioredoxin A (TrxA) and shuttles them across the membrane via three redox-active domains (Stewart et al., 1999; Collet et al., 2002; Rozhkova et al., 2004). The NADPH-dependent cytosolic Thioredoxin reductase (TrxB) then reduces TrxA. Thus, oxidative protein folding in the

bacterial periplasm is linked to the reducing Thioredoxin pathway. The oligomeric states of the oxidoreductases that participate in these pathways ensure that they are kinetically separated; DsbD cannot reduce DsbA in its monomeric state, and DsbB cannot oxidise DsbC in its dimeric state (Goldstone et al., 2001; Rozhkova and Glockshuber, 2008).

The situation in the ER is similar with respect to the use of reduced oxidoreductases in isomerising non-native disulphide bonds, but more complex as both the oxidising and isomerising/reducing pathways use the same oxidoreductases (Oka and Bulleid, 2013; Bulleid and van Lith, 2014). In the ER, protein disulphide isomerases (PDIs) are responsible for introducing disulphide bonds into substrates *and* removing non-native disulphides. Separate domains within PDIs are responsible for either the oxidation or reduction of disulphide bonds (Appenzeller-Herzog and Ellgaard, 2008; Oka and Bulleid, 2013). Like DsbA and Mia40, oxidised PDIs introduce disulphide bonds to substrates and electrons are then passed on to a thiol oxidase, in this case Ero1, which then transfers electrons to molecular oxygen, with H_2O_2 produced as a by-product (Gross et al., 2006; Baker et al., 2008). In addition, a complex feedback mechanism exists to regulate the activity of Ero1 when the pool of oxidised Ero1 becomes too high (Appenzeller-Herzog et al., 2008; Baker et al., 2008). This mechanism involves the introduction of 'regulatory' disulphide bonds in Ero1 that block its activity; this process is reversible upon changing redox conditions. In order to reduce non-native disulphides in substrates, PDI must first be reduced by reduced Glutathione (GSH); reduced PDI can then accept electrons from non-native disulphides. As a result, oxidised Glutathione (GSSG) accumulates in the ER (Chakravarthi et al., 2006). However, little is currently understood about how the ER balances GSH/GSSG levels and its transport across the ER.

In the IMS, the oxidoreductase Mia40 introduces disulphide bonds into substrates (as described in detail in **Section 1.2.4**), but the mechanism for removal of non-native disulphide bonds has not yet been characterised, and Mia40 has not been shown to exhibit *in vivo* isomerase activity. In 2010, GSH was proposed to play a proofreading role based on the finding that its addition to an *in vitro* reconstitution system alongside oxidised Mia40 and reduced Cox19 resulted in accelerated Cox19 oxidation with fewer

long-lived intermediates (Bien et al., 2010). Though a direct role of GSH could not be established in this particular setup as the intermediates that were present could not be characterised. However, since then evidence has shown that the redox state of Mia40 is affected by GSH levels *in vivo* as GSH was shown to partially reduce Mia40 (Kojer et al., 2012). The potential role of semi-reduced Mia40 in regulating disulphide bond formation in the IMS has yet to be determined. On the other hand, an *in vitro* study has suggested that Mia40 itself can act directly and concurrently as both an oxidase and an isomerase as Mia40 was shown to reduce Cox17 in a reconstituted system (Koch and Schmid, 2014a, b), although its efficiency in doing so was relatively poor in comparison to both DsbA and PDI. Despite all this, the role of Mia40 and/or GSH in the removal of non-native disulphide bonds remains unclear; perhaps a separate reductive pathway exists.

Interestingly, the components from two cytosolic reductive systems (the Thioredoxin and Glutaredoxin systems) have also been found in the IMS (Vögtle et al., 2012; Kojer et al., 2015; Manganas, 2017, PhD thesis, University of Glasgow), and a study has shown that Glutaredoxin 2 (Grx2) levels in the IMS can influence the redox state of Mia40, shifting Mia40 to its reduced state which then indirectly affects IMS protein import. Furthermore, the presence of Thioredoxin in the IMS has also been shown to affect Mia40 oxidation levels (Mauricio Cárdenas-Rodriquez, 2019, PhD Thesis, University of Glasgow). In addition to the likelihood that two reductive systems operate within the IMS that may both play roles in fine-tuning oxidative protein folding, the well-characterised cytosolic H_2O_2 transducer, Glutathione peroxidase 3 (Gpx3), was also found in the IMS (Vögtle et al., 2012) and has been shown to interact with Mia40 (Kritsiligkou et al., 2017). Until Gpx3, no H_2O_2 sensor had been discovered in the IMS. Therefore, determining how the MIA import pathway is regulated under different redox conditions, i.e. oxidative vs reductive stress, is an important topic to address. As this PhD continued to investigate the role of Gpx3 in the yeast IMS, the following section will discuss Gpx3 in detail, including its well-characterised role in cytosolic H_2O_2 signalling.

1.6. Glutathione peroxidases in yeast

Gpx3 is one of three Glutathione peroxidases (Gpx1, Gpx2 and Gpx3/Hyr1/Orp1) in *S. cerevisiae* that play multiple roles in defending cells against oxidative stress, such as by reducing phospholipid hydroperoxides and quenching reactive oxygen species (Inoue et al., 1999; Avery and Avery, 2001). All three are classified as atypical 2-Cys peroxiredoxins (Ohdate et al., 2010) and are all present within the cytosol of the cell; however, they each have their individual associations with various mitochondrial subcompartments and with peroxisomes. Gpx1 is associated with the cytosolic-side of the outer membrane (OM) and the peroxisomal matrix (Ukai et al., 2011; Ohdate and Inoue, 2012). Gpx2 is also associated with the cytosolic-side of the OM, and the matrix-side of the inner mitochondrial membrane (IM) (Ukai et al., 2011). Gpx3 is found within the mitochondrial intermembrane space (IMS) and the peroxisomal matrix (Ohdate and Inoue, 2012; Vögtle et al., 2012; Kritsiligkou et al., 2017). Although all three Gpxs exhibit peroxidase activity, their differing localisations within yeast cells suggest that each have their own niche roles in redox regulation.

The peroxidase activity of yeast Gpx3 is considered to be the most important of the three, based on evidence that a yeast strain harbouring a single deletion of *GPX3* (*gpx3Δ*) is hypersensitive to peroxides, and is more detrimental to yeast cells than *gpx1Δ* or *gpx2Δ* single mutants under oxidative stress (Inoue et al., 1999). In contrast to Gpx1 and Gpx2, and despite its name, Gpx3 utilises Thioredoxin as its reducing substrate (Delaunay et al., 2002; Maiorino et al., 2007). The reaction that Gpx3 catalyses is: Gpx3(-SH) + H_2O_2 → Gpx3(-SOH) + $2H_2O$; the sulphenylated form of Gpx3 can then form transient conjugates with other proteins via intermolecular disulphides, or, form an intramolecular disulphide bond Gpx3 (S-S). The oxidised form of Gpx3(S-S) is then reduced by Thioredoxin. Thus, Gpx3 can already be distinguished from the other Glutathione peroxidases. Gpx3 may therefore utilise the IMS pool of Trx1 as its reducing substrate. A similar mechanism to reduce Gpx2 on the OM might be employed by the cytosolic pool of Trx1, as the active domain of Gpx2 is exposed to the cytosol. Gpx3 further differentiates itself from the others as it acts as a transducer of H_2O_2 signals in the cytosol (Delaunay et al., 2002).

1.6.1. Cytosolic Gpx3

In the cytosol, Gpx3 transduces H_2O_2 signals via the activation of the yeast AP-1-like transcription activator 1, Yap1, by multi-step disulphide bond formation – see **Figure 1.9** (Delaunay et al., 2002; Ma et al., 2007; Okazaki et al., 2007). Under H_2O_2 exposure, the Cys36 residue of Gpx3 becomes sulphenylated and forms either an intermolecular disulphide bond with the Cys598 residue of Yap1, or, an intramolecular disulphide bond with another of its cysteine residues, Cys82 (Delaunay et al., 2002). The former scenario causes a Yap1 conformational change whereby the nuclear export signal (NES) of Yap1 becomes blocked due to the formation of an intramolecular disulphide bond within Yap1 between Cys303 and Cys598 thus allowing the nuclear accumulation of Yap1 and subsequent activation of its target genes (Wood et al., 2004). Under reducing conditions, the intramolecular disulphide bond in Yap1 is reversed, the NES unblocked, and Yap1 exported back to the cytosol (Wood et al., 2004). Another protein, Yap1-binding protein 1 (Ybp1), is also required for inducing the nuclear accumulation of Yap1 under H_2O_2 stress by forming a noncovalent ternary complex with Yap1 and Gpx3, that brings these proteins into close proximity and inhibits Gpx3 from forming an intramolecular disulphide bond (Veal et al., 2003; Gulshan et al., 2011; Patterson et al., 2013; Bersweiler et al., 2017). Thus, Ybp1 promotes Yap1 activation via Gpx3 and is consequently a rate-limiting factor.

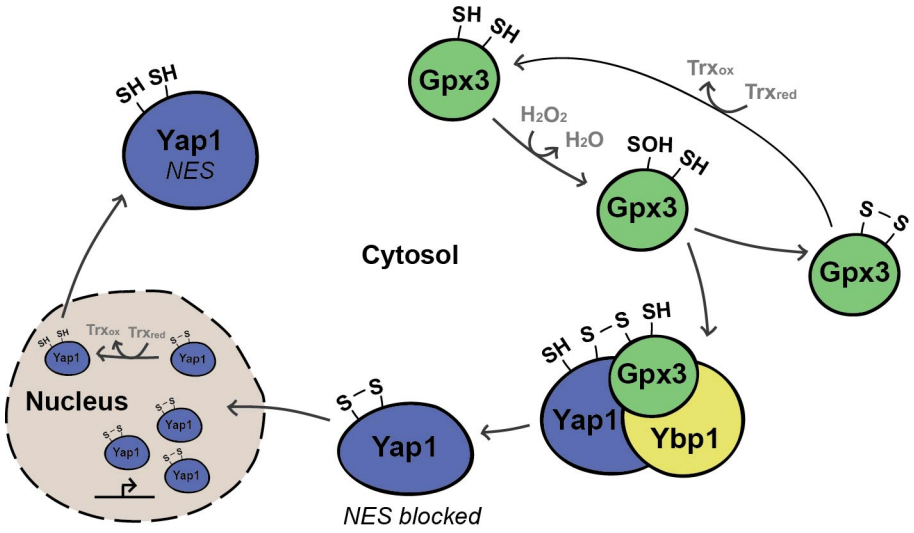

Figure 1.9. H_2O_2-induced activation of Yap1 by Gpx3 and Ybp1. Upon exposure to H_2O_2, Cys36 of Gpx3 becomes sulphenylated (-SOH) which can then form either a mixed disulphide bond with Yap1 via C598 of Yap1, or an intramolecular disulphide bond with C82 of Gpx3. The mixed disulphide formed between Gpx3 and Yap1 induces a further disulphide bond between

C303 and C598 of Yap1 which causes a protein conformational change in Yap1, blocking its nuclear export signal (NES). This leads to the nuclear accumulation of Yap1 and activation of >70 stress response genes. Ybp1 acts as a scaffold protein and forms a ternary complex between Gpx3, Yap1 and Ybp1 which promotes the formation of an intermolecular disulphide bond between Gpx3 and Yap1. NOTE: This diagram represents a wild-type BY4741 *S. cerevisiae* strain; wild-type W303 *S. cerevisiae* possess a *ybp1* mutation therefore the peroxiredoxin Tsa1 replaces Gpx3 (Okazaki et al., 2005). *See **Section 1.6.1** for a detailed description.*

Around 70 genes are known to be activated by Yap1 as a result of H_2O_2 exposure, many of which are involved in mounting a response to oxidative stress, such as *TRX2* (Ouyang et al., 2011; Veal et al., 2003; Kho et al., 2008). A study by Kho and colleagues in 2008 identified around 30 Gpx3-dependent proteins in response to H_2O_2 using a combination of proteomic and bioinformatics analyses (Kho et al., 2008). As expected, these included proteins involved in cell defence and survival. Interestingly, they also identified 17 proteins that respond to Gpx3 that are indifferent to H_2O_2 conditions which suggests a functional role of Gpx3 in scenarios other than just Yap1 activation as the 17 proteins include those involved in metabolism and protein fate (Kho et al., 2008). In another study, Lee et al. (2008) investigated the yeast Gpx3 interactome by immunoprecipitation using Myc-tagged Gpx3 proteins and crude yeast proteins extracted after the addition of H_2O_2, followed by mass spectrometry. Their analysis highlighted 11 interactors, including some already known to interact with Gpx3 (Yap1, Peptide methionine sulfoxide reductase and Glutamine synthetase) and others that were newly identified (Glutaredoxin 2, Protein disulphide isomerase 1, and SSY protein 3 among others) (Lee et al., 2008). Some of these proteins, like the genes identified by Kho et al. (2008), are involved in metabolism, transcription, and protein folding.

In 2012, Gerashchenko and colleagues carried out yeast mRNA ribosomal profiling along with deep sequencing to identify differentially translated proteins (from non-AUG codons) during H_2O_2 stress; one of these proteins was Gpx3 with a predicted N-terminal extension (Gerashchenko et al., 2012). The role of this extension is not yet fully understood; however, evidence suggests that it facilitates the import of Gpx3 into the mitochondrial IMS and allows it to associate more tightly with the IM (Kritsiligkou et al., 2017).

1.6.2. Mitochondrial Gpx3

Mitochondria are a major source of cellular ROS, particularly H_2O_2, as H_2O_2 is produced from the dismutation of superoxide anion radicals by superoxide dismutases, and as a by-product of NADPH oxidases, the respiratory chain and the MIA pathway (see **Section 1.2.4**) (Allen et al., 2005; Murphy, 2009; Sies et al., 2017). Although H_2O_2 can cause oxidative damage, it is also an important signalling molecule (Veal and Day, 2011). Therefore, H_2O_2 levels must be under tight control, particularly in the mitochondrial IMS and the ER. In the ER, H_2O_2 that is produced by Ero1 is quenched by peroxiredoxin IV (PrxIV) along with GPX7 and GPX8 (Tavender et al., 2010; Zito et al., 2010). As Gpx3 is the only known Gpx in the yeast IMS, it is likely that Gpx3 plays a role in H_2O_2 detoxification and signalling, akin to its role in the cytosol (Delaunay et al., 2002).

The presence of Gpx3 and its N-terminal extended version of around 18 amino acids (denoted N18Gpx3) have been confirmed within the IMS using a combination of import and localisation assays along with confocal microscopy (Kritsiligkou et al., 2017). Furthermore, experiments using *gpx3Δ* yeast have shown that these cells exhibit defects in mitochondrial morphology and inner membrane potential. Whilst Gpx3 does not rely on the MIA pathway for its import into the IMS, it has been shown to interact with and re-oxidise Mia40, thus implicating Gpx3 in mitochondrial oxidative protein folding.

Based on the previous evidence for multiple interactors and functional roles of Gpx3 in the cytosol, one aim of this PhD was to elucidate additional mitochondrial interactors of Gpx3 and N18Gpx3 in the IMS. It should be noted that the study by Lee et al. (2008) could not determine which cellular compartment the additional Gpx3 protein interactions occurred in as whole yeast cell extracts were used; only four of them were mitochondrial, none of which are solely localised within the IMS (see **Chapter 3**, **Section 3.1**). By identifying IMS-specific interactors of Gpx3, all of Gpx3s potential functional role/s in mitochondria can be uncovered.

1.6.3. Peroxisomal Gpx3

As mentioned previously, Gpx3 was also found to localise within the peroxisomal matrix, another cellular organelle that plays a role in metabolism and redox regulation (Ohdate and Inoue, 2012). No literature exists regarding the potential role(s) of Gpx3 within peroxisomes; however, it is likely that Gpx3 plays a role in detoxifying and transducing H_2O_2 signals in yet another important organelle. To summarise this section, an illustration of where Gpx3 is known to reside within *S. cerevisiae* cells is shown in **Figure 1.10**.

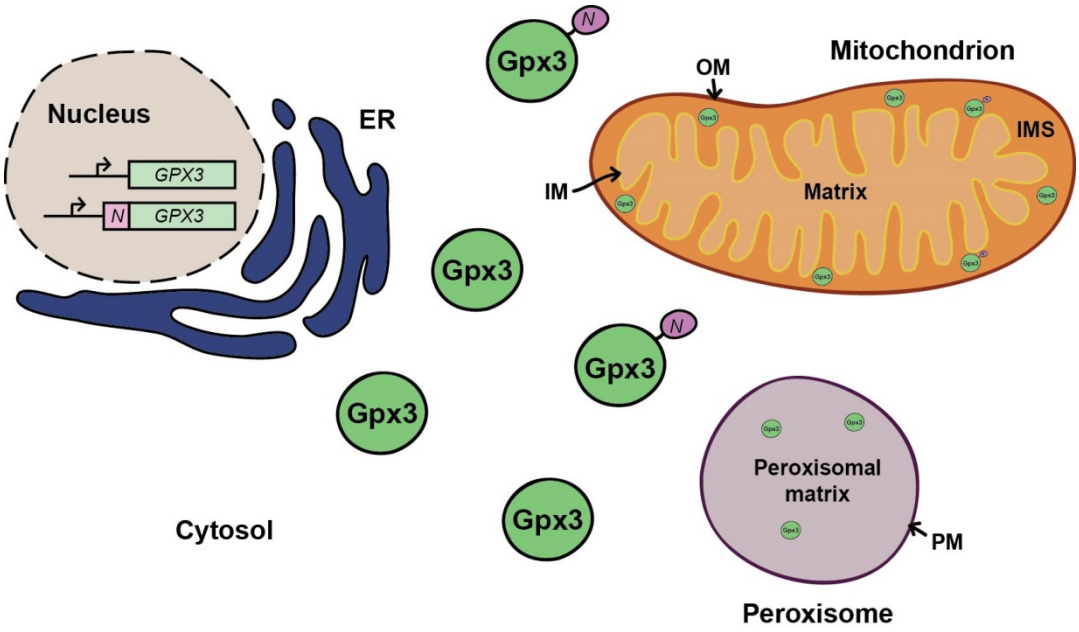

Figure 1.10. Localisation of Gpx3 in *S. cerevisiae* cells. Gpx3 resides in several cellular compartments including the cytosol, the mitochondrial IMS and the peroxisomal matrix. Upstream translation from a non-AUG codon in *GPX3* results in the production of an N-terminally extended Gpx3 of around 18 amino acids, N18Gpx3. Both Gpx3 and N18Gpx3 are imported into the IMS, but the N18 provides a more efficient import and results in a stronger association with the IM. It is not known which version of Gpx3 is imported into the peroxisomal matrix. ER – endoplasmic reticulum; OM – outer membrane; IM – inner membrane; IMS – intermembrane space; Matrix – mitochondrial matrix; PM – perixosomal membrane.

1.7. Peroxisomes

Peroxisomes are universal, essential organelles characterised by a single lipid-bilayer membrane that encapsulates a matrix full of proteins involved in oxidative metabolism. When peroxisomes were first isolated in the 1960s, their main functions were thought to be fatty acid β-oxidation and H_2O_2 degradation (De Duve and Baudhuin, 1966). However, recent research has uncovered their involvement in many metabolic pathways, and that their functions vary across eukaryotic groups *and* between different tissues, cell types and changing environmental conditions (Erdmann 2016; Reumann and Bartel, 2016; Waterham et al., 2016). It has also become apparent that they are both physically and metabolically linked with other cellular organelles, including the ER and mitochondria, and share some of the same proteins. Unlike mitochondria, they do not contain any of their own DNA and thus solely rely on nuclear-encoded proteins that are imported into peroxisomes in order to carry out their metabolic functions. Whilst mitochondria also import the vast majority of their proteins from the cytosol, the major protein targeting and import mechanisms exploited by peroxisomes are very different (Baker et al., 2016; Sibirny 2016; Schwerter et al., 2017).

1.7.1. Peroxisome protein targeting and import

Two types of targeting signals are so far known to exist: peroxisomal-targeting signal 1 (PTS1), short peptide sequences located at the extreme C-terminus, and peroxisomal-targeting signal 2 (PTS2), N-terminal sequences of which some share structural similarities, i.e. amphipathic alpha-helices, with mitochondrial presequences (Aitchison et al., 1991; Osumi et al., 1992; Brocard and Hartig, 2006; Kunze et al., 2011; Pan et al., 2013; Kunze and Berger, 2015). Whilst many variations of these targeting signals exist there are general consensuses for both PTS1 and PTS2 signals that can be used to identify potential peroxisomal proteins using various algorithms (refer to **Chapter 5**, **Figure 5.3**). Moving on from targeting signals, peroxisomal protein import machineries are comprised mainly of PEX (peroxin) proteins and are unusual for many reasons: (i) they can import folded proteins *and* oligomeric proteins (Glover et al., 1994; McNew et al., 1994), (ii) the same receptor can recognise a range of targeting signals with various affinities, (iii) the whole

process is cyclical and involves the docking of cargo proteins onto receptors, and (iv) protein import is coupled with protein export, the latter of which is ATP-dependent (Brown et al., 2014; Baker et al., 2016). As peroxisome protein import by peroxins is incredibly complex, a detailed description is unfortunately outside the scope of this introduction (refer to excellent reviews by Baker et al., 2016; Sibirny 2016; and Schwerter et al., 2017). Though what is interesting is that components of the MIA pathway exist in *A. thaliana* peroxisomes and are involved in the import of some plant peroxisomal matrix proteins (Carrie et al., 2010) - see previous **Section 1.3.1.1**.

The identification of bona fide peroxisomal proteins is hindered for various reasons, such as: contamination of other organelles when isolating peroxisomes and carrying out proteomic analyses; low levels of some proteins; dually-localised proteins; changes in protein content depending on physiological conditions; and the inability to predict proteins that do not contain PTS1 or PTS2 canonical signals. While new technological methods are being developed to assist in establishing the true peroxisomal proteome, until then bottom-up approaches are useful in detecting previously unidentified proteins, many of which are dually-localised. As this PhD project uncovered a number of mitochondrial proteins co-localising with peroxisomes in yeast, such as Gpx3 and Mia40, the following section briefly lists some inter-organelle connections currently unravelling between mitochondria and peroxisomes.

1.7.2. Mitochondria-peroxisome links

Although it is well known that peroxisomes are non-autonomous organelles that rely on highly interconnected metabolic networks with other organelles such as mitochondria (see Wanders et al., 2016), many questions remain with regards to the targeting of dually-localised proteins and their precise roles in other aspects of organelle interplay. Aside from their cooperation with mitochondria in metabolic pathways such as β-fatty acid oxidation, shared proteins are also known to be involved in eliciting responses including (i) organelle division, (ii) redox regulation, (iii) antiviral signalling, and (iv) vesicular trafficking. For a recent review of mitochondria-peroxisome connections, see Costello et al. (2018).

1.8. Protein targeting and import in disease

Diseases associated with mitochondrial protein targeting and import

Dysfunctional mitochondria are implicated in a number of human diseases, including two well-known neurodegenerative diseases - Alzheimer's and Parkinson's, but whether they play a direct or indirect role has yet to be established (Schapira, 2012; Mossman et al., 2014). However, there are a handful of rare diseases caused by known mutations within nuclear genes encoding mitochondrial proteins (Pfanner, Warscheid & Wiedemann, 2019). These mutations can affect mitochondrial targeting signals (MTSs) within precursors, the function of individual protein import components, and the processing and folding of mitochondrial proteins upon their import. On the other hand, there are mutations that can introduce MTSs in non-mitochondrial proteins (including peroxisomal proteins) which results in their mistargeting. Excellent examples of the above are highlighted in a recent review by Pfanner, Warscheid & Wiedemann (2019).

Connections with peroxisomes

Mutations within many of the *PEX* genes that play important roles in the biogenesis of peroxisomes are known to cause disorders such as Zellweger syndrome (Fujiki, Yagita & Matsuzaki, 2012). In addition to this, gene mutations can generate MTSs in peroxisomal proteins, for example, human EHHADH, which instead directs EHHADH to mitochondria causing renal Fanconi syndrome (Klootwijk et al., 2014). To conclude, thoroughly understanding organellar targeting signals and complex protein import machines across both mitochondria and peroxisomes will be of upmost importance in the development of novel therapeutic strategies to combat a multitude of human diseases.

1.8. Aims

Chapter 3 *– Investigating the role of Gpx3 in the mitochondrial IMS*

The initial aim of this PhD project was to identify Gpx3 and N18Gpx3 interactors in the yeast mitochondrial IMS, and determine whether they interact with different proteins. By determining mitochondrial-specific interactors, our aim was to elucidate the function/s of both Gpx3 and N18Gpx3 in the IMS. Our hypothesis was that Gpx3 is required in the defence against oxidative stress within the IMS, and that it also has additional roles akin to the multiple roles suggested for the cytosolic pool of Gpx3. Possible roles include general H_2O_2 detoxification to prevent oxidative damage to proteins, preventing lipid peroxidation at the IM, and transduction of H_2O_2 signals via various interaction partners.

Chapter 4 *– Investigating the role of Gpx3 in peroxisomes*

Based on the fact that Gpx3 was also found to localise within the peroxisomal matrix (Ohdate and Inoue, 2012), an additional aim was to investigate Gpx3 in peroxisomes. After confirming its dual-localisation to both organelles, we began to search for putative peroxisomal interaction partners. During this work, serendipitous findings led us to explore (i) the potential localisation of a shorter, soluble version of Mia40 in peroxisomes that may interact with Gpx3 and Trx1, and (ii) the potential localisation of an N-terminally extended version of Pex11 in mitochondria.

Chapter 5 *– Ypl107w: a putative oxidoreductase of unknown function*

The mass spectrometry data in **Chapter 3** uncovered Ypl107w as a previously unidentified mitochondrial protein with no known functions despite having a highly conserved oxidoreductase-like domain (OXLD). This warranted further consideration which began with us performing a thorough bioinformatics analysis of Ypl107w and its homologs whilst confirming its mitochondrial localisation. Although Ypl107w was found to localise to the mitochondrial matrix, we continued to carry out proteomics and phenotypic analyses in order to help elucidate its potential function.

Chapter 2

Materials and methods

2. Materials and methods

2.1. Materials

2.1.1. Plasmids

Table 2.1. List of plasmids.

Plasmids			
Gene	**Plasmid**	**Source**	**Use**
GPX3	pET-24/*GPX3*	(Kritsiligou et al., 2017)	Protein purification
	pET-24/*N18GPX3*	This study	Protein purification
	pET-24/*N18M20LGPX3*	This study	Protein purification
	pET-24/*GPX3C36S*	This study	Protein purification
	pET-24/*GPX3C64S*	This study	Protein purification
	pET-24/*GPX3C82A*	(Kritsiligou et al., 2017)	Protein purification
	pSP64/*GPX3*	(Kritsiligou et al., 2017)	Radiolabelled expression
	pSP64/*N18GPX3*	(Kritsiligou et al., 2017)	Radiolabelled expression
	pSP64/*N18M20LGPX3*	(Kritsiligou et al., 2017)	Radiolabelled expression
CYC1	pET-24/*CYC1*	This study	Protein purification
	pSP64/*CYC1*	This study	Radiolabelled expression
YBR124W	pSP64/*YBR124W*	This study	Radiolabelled expression
	pSP64/*YBR124W3Met*	This study	Radiolabelled expression
YPL107W	pSP64/*YPL107W*	This study	Radiolabelled expression
	pSP64/*N26ΔYPL107W*	This study	Radiolabelled expression
	pET-24/*YPL107W*	This study	Protein purification
PEX11	pSP64/*PEX11*	This study	Radiolabelled expression
	pSP64/*N17PEX11*	This study	Radiolabelled expression
SU9-DHFR	pSP65/*SU9-DHFR*	(Pfanner et al., 1987)	Radiolabelled expression
ERV1	pTUB8/*MYC-ScERV1*	Sheiner lab	Parasite transfection
TgERV1	pGEX-4T-1/*TgERV1*	Tokatlidis lab	Protein purification
	pTUB8/*MYC-TgERV1*	Sheiner lab	Parasite transfection
TgERV2	pGEX-4T-1/*TgERV2*	Tokatlidis lab	Protein purification
	pTUB8/*MYC-TgERV2*	Sheiner lab	Parasite transfection
TgERV3	pGEX-4T-1/*TgERV3*	Tokatlidis lab	Protein purification
	pTUB8/*MYC-TgERV3*	Sheiner lab	Parasite transfection

A list of all plasmids used in this study and where they were obtained from. Plasmids that were created for this study were made following the protocol described in **Section 2.2.1.3.**

2.1.2. Primers

All primers used in this thesis are listed in **Appendices**, **Table 7.3**.

2.1.3. Antibodies

All antibodies used in this thesis are listed in **Appendices**, **Table 7.4**.

2.1.4. Bacterial strains and media for bacterial growth

All *Escherichia coli* strains used in this study are listed in **Table 2.2**; DH5α cells were used to propagate plasmids ready for plasmid DNA extraction whereas DE3 cells with various genotypes were used to express plasmids by induction of T7 polymerase with Isopropyl β-D-1-thiogalactopyranoside (IPTG) ready for protein purification. *E. coli* were grown in either liquid Luria-Bertani (LB) medium (1% (w/v) bacto-tryptone, 0.5% (w/v) yeast extract and 1% (w/v) NaCl) or on solid LB plates containing 2% (w/v) agar. All media preparations were autoclaved at 121°C for 15 minutes. Media for bacterial growth also contained antibiotics where required: 25 μg/ml chloramphenicol or 12.5 μg/ml tetracycline for selection of pLysS and ORI cells, 100 μg/ml ampicillin for transformation and propagation of pSP64 vectors, and 30 μg/ml kanamycin for pET-24 vectors.

Table 2.2. List of bacterial strains.

Bacterial strains				
Strain	**Name**	**Genotype**	**Source**	**Use**
DH5α	DH5α	F– ϕ80*lac*ZΔM15 Δ(*lac*ZYA-*arg*F)U169 *rec*A1 *end*A1 *hsd*R17(r_K^-, m_K^+) *pho*A *sup*E44 λ– *thi*-1 *gyr*A96 *rel*A1	Life Tech	Plasmid propagation
BL21 (DE3)	DE3	*E. coli* B F^- *dcm ompT hsdS*(r_B^- m_B^-) *gal* λ(DE3)	Stratagene	Plasmid expression
BL21 (DE3) PLysS	PLysS	*E. coli* B F^- *dcm ompT hsdS*(r_B^- m_B^-) *gal* λ(DE3) BB [pLysS Cam^r]	Stratagene	Plasmid expression
Origami™ 2 (DE3)	ORI	*Δ(ara-leu)7697 ΔlacX74 ΔphoA Pvu*II *phoR araD139 ahpC galE galK rpsL* F'[lac^+ $lacI^q$ *pro*] (DE3) *gor522*::Tn*10 trxB* pLysS [Cam^R, Str^R,Tet^R]	Novagen	Plasmid expression
BL21-CodonPlus™ (DE3)	C+	*E. coli* B F^- *ompT hsdS*(r_B^- m_B^-) *dcm*$^+$ Tet^r *gal* λ(DE3) *endA* Hte [*argU ileY leuW* Cam^r]	Stratagene	Plasmid expression

A list of all bacterial strains used in this study, names used throughout this thesis, where they were obtained from and what they were used for.

2.1.5. Yeast strains and media for yeast growth

All *Saccharomyces cerevisiae* strains used in this study are listed in **Table 2.3**. Yeast were grown at 30°C in rich media containing 1% (w/v) yeast extract, 2% (w/v) peptone, plus a carbon source: 2% (w/v) glucose (for YPD), 2% (w/v) galactose (for YPG), 2% (w/v) lactic acid (for YPL), 3% (w/v) glycerol (for YPGly) or 0.12% (w/v) oleic acid (for YPOle). Solid plates also contained 2% (w/v) agar. All media preparations were autoclaved at 121°C for 15 minutes. Media for yeast growth also contained antibiotics where required, such as G418 at 200 µg/ml.

Table 2.3. List of yeast strains.

Yeast strains			
Name	**Genotype**	**Description**	**Source**
D273-10B	*MATα mal*	wild-type strain used for mitochondrial studies, constructed in the Sherman lab	(Sherman, 1964)
BY4741	*MATa, his3Δ1, leu2Δ0, met15Δ0, ura3Δ0*	wild-type strain derived from S288C	(Brachmann et al., 1998)
***gpx3Δ* (BY4741)**	*MATa, his3Δ1, leu2Δ0, met15Δ0, ura3Δ0, gpx3Δ0*	strain deleted for the endogenous *GPX3* gene	Dharmacon – GE healthcare
***ypl107wΔ* (BY4741)**	*MATa, his3Δ1, leu2Δ0, met15Δ0, ura3Δ0, ypl107wΔ0*	strain deleted for the endogenous *YPL107W* gene	Dharmacon – GE healthcare
W303	*MATα ,ura3-52, leu2-3, 112, trp1-1, ade2-1, his3-11, 15, can1-100*	wild-type strain derived from S288C, constructed by R Rothstein	Gifted by Prof. C. Grant
***trr1Δ* (W303)**	*MATa ura3–52 leu2–3, 112 trp1–1 ade2–1 his3–11, 15, can1–100, trr1::HIS3*	strain deleted for the endogenous *TRR1* gene	Gifted by Prof. C. Grant
***trx1/2Δ* (W303)**	*MATa ura3–52 leu2–3, 112 trp1–1 ade2–1 his3–11, 15, can1–10, trx1::TRP1, trx2::URA3*	strain deleted for the endogenous *TRX1* and *TRX2* genes	Gifted by Prof. C. Grant
FT5	*MATα, ura3-52, trp1-Δ63, his3-Δ200, leu2::PET56*	wild-type strain	(Tzamarias and Struhl, 1994)
galMia40 (FT5)	*MATα, ura3-52, trp1-Δ63, his3-Δ200, leu2::PET56 kanMX- GAL1-10-MIA40*	conditional knock-out strain in FT5 background, *MIA40* under the control of the *GAL1-10* promoter	(Banci et al., 2009)

A list of all yeast strains used in this study, their genotypes, a brief description and either the company where they were obtained from or the first publication in which a strain was described.

2.1.6. Solutions and buffers

ACA750: 750 mM aminocaproic acid, 50 mM Bis-Tris, 0.5 mM EDTA, adjusted to pH 7.0 with HCl

Binding buffer: 150 mM NaCl, 50 mM Tris-HCl pH 8.0, 1 mM DTT

Blocking buffer: 1 X PBS, 0.2% (v/v) Triton-X-100, 2% (w/v) BSA

BN acrylamide solution: 48% acrylamide, 1.5% bisacrylamide

BN gel buffer: 100 mM Bis-Tris-HCl pH 7.0, 1 M 6-aminocaproic acid

Breaking buffer (isotonic buffer): 600 mM sorbitol, 20 mM HEPES-KOH pH 7.4

Buffer A: 150 mM NaCl, 50 mM Tris-HCl pH 8.0, 10% (w/v) glycerol

Buffer B: 8 M urea, 50 mM Tris-HCl pH 8.0, 50 mM NaCl

Coomassie buffer (for Tricine gels): 30% (v/v) methanol, 10% (v/v) acetic acid, 0.2% (w/v) Coomassie Brilliant Blue R-250

Coomassie buffer (for BN-PAGE gels): 50% (v/v) methanol, 7% (v/v) acetic acid, 0.05% (w/v) Coomassie Brilliant Blue R-250

Denaturing/reducing buffer: 8 M urea, 20 mM DTT, 50 mM HEPES-KOH pH 7.4, (plus 5 mM EDTA for Gpx3 proteins)

Destaining buffer (for BN-PAGE gels): 50% (v/v) methanol, 7% (v/v) acetic acid

Destaining buffer (for Tricine gels): 15% (v/v) methanol, 10% (v/v) acetic acid

Elution buffer: 50 mM Tris-HCl pH 8.0, 10 mM reduced glutathione

ETS buffer: 3 mM EDTA, 50 mM Tris-HCl pH 8.0, 3% (w/v) SDS

Equilibration buffer (for Ni-NTA beads): 50 mM Tris-HCl pH 7.4, 150 mM NaCl, 10 mM imidazole, 1 mM PMSF

Import buffer: 600 mM sorbitol, 2 mM KH_2PO_4, 50 mM KCl, 50 mM HEPES-KOH pH 7.4, 10 mM $MgCl_2$, 2.5 mM Na_2EDTA pH 7, 5 mM L-methionine, 1 mg/ml fatty acid free BSA

IP buffer: 50 mM NaCl, 50 mM Tris-HCl pH 7.4, 5 mM EDTA, 2 mM PMSF

Lysis buffer (for *in vitro* binding assays): 50 mM Tris-HCl pH 7.4, 150 mM NaCl, 1mM PMSF and either 1% (w/v) DDM or 0.1% (v/v) Trixton-X-100

Lysis buffer (for yeast genomic DNA extraction): 2% (v/v) Triton-X-100, 1% (w/v) SDS, 100 mM NaCl, 10mM Tris-HCl pH 8.0, 1 mM EDTA

Mitoplasting buffer: 20 mM HEPES-KOH pH 7.4, 1 mM DTT

Native buffer: 50 mM HEPES-KOH pH 7.4

PBS: 10 mM PO_4^{3-}, 137 mM NaCl, and 2.7 mM KCl

Reducing buffer: 20 mM DTT, 50 mM HEPES-KOH pH 7.4

Renaturing buffer: 150 mM NaCl, 50 mM Tris-HCl pH 8.0, 1 mM DTT, 10 µM FAD

Solubilisation buffer (for creating IMS fractions): 50 mM Tris-HCl pH 7.4, 150 mM NaCl, 10% (w/v) glycerol, 2 mM PMSF

Solubilisation buffer (for *in vitro* binding assays): 50 mM Tris-HCl pH 7.4, 150 mM NaCl, 2 mM PMSF

Solubilisation buffer (for pulldown assays): 10 mM Tris-HCl pH 7.4, 50 mM NaCl, 2 mM PMSF

TAE: 40 mM Tris-HCl pH 8.0, 20 mM acetic acid, 1 mM EDTA

TBST: 150 mM NaCl, 100 mM Tris-HCl pH 7.4, 0.01% (v/v) Tween 20

Tricine gel buffer: 3 M Tris, 0.3% (w/v) SDS, adjusted to pH to 8.45 with HCl

Ponceau buffer: 10% (v/v) acetic acid, 0.1% (w/v) Ponceau S

1-5% milk: 1-5% (w/v) skimmed milk powder, TBST

5x cathode buffer: 250 mM Tricine, 75 mM Bis-Tris, adjusted to pH 7.0 with HCl

5% serva blue solution: ACA750, 5% (w/v) Coomassie G250

6x anode buffer: 300 mM Bis-Tris, adjusted to pH 7.0 with HCl

6x Laemmli sample buffer (SB): 375 mM Tris-HCl pH 6.8, 40% (w/v) glycerol, 9% (w/v) SDS, 0.03% (w/v) bromophenol blue, -/+ 600 mM β-mercaptoethanol

2.2. Methods

2.2.1. Molecular biology assays

2.2.1.1. Yeast genomic DNA extraction

Yeast cells were pelleted from 15 ml of overnight culture by centrifugation at 3500g for 5 minutes at room temperature (RT) and the cell pellet washed in dH_2O and resuspended in lysis buffer. An equal volume of glass beads and phenol:chloroform:isoamyl alcohol (50%:49%:1%) was added and then vortexed for 4 minutes. dH_2O was added and pelleted by centrifugation at 15000g for 5 minutes, RT. The supernatant was then washed twice with 100% ethanol and pelleted by centrifugation at 15000g for 5 minutes, RT and resuspended in dH_2O and RNAase A (75 ng/µl) followed by incubation at 37°C. After 10 minutes, 150 mM ammonium acetate and 2x volume of 100% ethanol were added followed by centrifugation at 15000g for 5 minutes, RT for 2 minutes to pellet the DNA before a final resuspension in 50 µl dH_2O.

2.2.1.2. PCR

The primers listed in **Table 7.3** were used to amplify *S. cerevisiae* genes from either yeast genomic DNA or plasmid DNA using polymerase chain reaction (PCR). PCR amplifications were carried out using a Biometra® T3 Thermocycler. In general, the final concentrations of PCR reagents were: 1 X PCR buffer, 1 mM dNTPs (Invitrogen), 0.4 mM of each primer (Sigma), 1 ng/µl DNA, and 0.1 u/µl polymerase. For difficult to amplify regions or reactions with non-specific products, 1% (v/v) dimethyl sulfoxide (DMSO) and/or 2-5 mM $MgCl_2$ were added and the concentration of each primer altered to 0.2-0.8 mM. Different polymerases were used depending on whether the PCR amplicon was for use in subsequent clonings (Pfu polymerase – high fidelity) or whether it was for gene detection only (Taq polymerase – low fidelity). Thermocycling conditions used were: 95°C for 5 minutes; 35 cycles of 95°C for 2 minutes, 50-60°C for 2 minutes, 72°C for 2-8 minutes; and

a final extension at 72°C for 10 minutes. Annealing temperatures and extension times varied depending on primer melting points and size of amplicons.

PCR products were visualised by gel electrophoresis on 1% (w/v) agarose gels containing 1 X TAE buffer and 0.5 X SYBR®Safe DNA gel stain (Invitrogen), and run at 60 V in 1 X TAE buffer for 45-60 minutes. Fragment sizes were determined by comparison with a 1 kb DNA ladder (Promega). PCR products were cleaned up using either NucleoSpin® Gel and PCR Clean-Up (Macherey-Nagel) or QIAEX II beads (QIAGEN) following the manufacturer's protocols. DNA concentrations were measured using a NanoDrop Spectrophotomer ND-1000 (Thermo).

2.2.1.3. Cloning

For clonings, primers were designed with both 5' and 3' restriction enzyme sites (refer to **Table 7.3**) which were then digested alongside the vector of choice. Digestion reaction mixes for both inserts (PCR products) and vectors contained 1 X CutSmart™ buffer, 0.4 u/µl Restriction enzyme I, 0.4 u/µl Restriction enzyme II, and 10 ng/µl DNA in a total reaction volume of 50 µl and were incubated at 37°C for 3 hours. Ligations of digested vectors with genes of interest were carried out using 1 X Buffer for T4 DNA ligase with 1 mM ATP, 40 u/µl T4 DNA ligase, plus a ratio of either 1:1, 1:3, 1:5, 1:7, or 1:9 of vector:insert in a total reaction volume of 15 µl. Ligation reactions were incubated at 25°C for 1-3 hours. All restriction enzymes and ligase reagents were obtained from New England BioLabs®. Half of the ligated DNA reaction mix (7.5 µl) was added to 100 µl DH5α competent cells and kept on ice for 30 minutes followed by a heat shock at 42°C for 45 seconds, then 2 minutes on ice. 900 µl LB were added and incubated at 37°C for 1 hour and the cells were pelleted by centrifugation at 4000g for 5 minutes. The pellet was resuspended in 200 µl LB before plating on LB + 30 µg/ml kanamycin or LB + 100 µg/ml ampicillin depending on vector resistance, and plates were left to grow at 37°C overnight. Positive colonies were then selected by checking for the presence of the gene of interest by using both colony PCR and digestion tests.

Colony PCRs were carried out using *E. coli* DNA (obtained by suspending individual colonies in 50 µl dH_2O) as a template. The conditions were otherwise as described in **Section 2.2.1.2**. Digestion tests were carried out after plasmid DNA purification (see **Section 2.2.1.4**) in digestion reaction mixes as described in this section.

2.2.1.4. Plasmid DNA purification and sequencing

Plasmid DNA was isolated using a QIAprep® Spin Miniprep Kit (QIAGEN) as per the manufacturer's protocol. Samples were sent to GATC Biotech for Sanger sequencing on ABI 3730xl platforms, and sequences were checked and aligned using CLC Genomics Workbench 7.

2.2.1.5. Mutagenesis

Primers were designed specifically for mutagenesis PCR (see **Table 7.3**) to introduce point mutations in the DNA sequences of our genes of interest which would result in amino acid residue changes. Plasmids containing the genes we wished to mutate were used as template DNA, and the high fidelity Accuzyme DNA polymerase (Bioline) was used to limit the likelihood of other mutations arising. Reaction conditions were as described in Section 2.2.1.2. with the following exceptions: 0.5 µM each primer and a minimum extension time of 8 minutes at 72°C. PCR products were then treated with 1 µl *Dpn*I (10 u/µl) per 50 µl reaction volume and incubated at 37°C for 1 hour to digest all non-mutated parental plasmid DNA. After *Dpn*I digestion, PCR products were transformed into DH5α *E. coli* as described in **Section 2.2.1.3**. Positive colonies were confirmed by colony PCR and digestion tests also as described in **Section 2.2.1.3** followed by plasmid DNA purification and sequencing as described in **Section 2.2.1.4**.

2.2.1.6. Protein expression and purification

The expression of proteins from pET-24 and pGEX plasmids were tested in various *E. coli* cells (see **Table 2.4**) to first determine which cell type and individual colony produced the largest quantity of recombinant protein. The pET-24 plasmid introduces a C-terminal 6xHistidine (His) tag to proteins, whereas pGEX produces glutathione *S*-transferase (GST) fusion proteins. Plasmids were transformed into *E. coli* as described in **Section 2.2.1.3**, and then induced using IPTG -/+ FAD depending on the protein. **Table 2.4** lists all of the proteins expressed in this study and their final expression conditions. Individual colonies were grown overnight at 37°C in LB plus either 30 µg/ml kanamycin for pET-24 plasmids or 100 µg/ml ampicillin for pGEX plasmids. In the morning, a 1:50 dilution of each colony was made into fresh LB plus the required antibiotic and incubated at 37°C for 2-3 hours until their OD_{600nm} reached 0.4-0.8 (logarithmic growth phase). IPTG was then added, along with FAD for proteins requiring FAD as a redox co-factor, for 4-16 hours at 18-30°C.

Table 2.4. List of individual protein expression conditions

Protein expression conditions					
Protein	**Plasmid**	***E. coli***	**IPTG/FAD**	**Temp**	**Time**
Gpx3His	pET-24/*GPX3*	DE3	0.4 mM IPTG	37°C	4 h
Gpx3C36SHis	pET-24/*GPX3C36S*	DE3	0.4 mM IPTG	37°C	4 h
Gpx3C64SHis	pET-24/*GPX3C64S*	DE3	0.4 mM IPTG	37°C	4 h
Gpx3C82AHis	pET-24/*GPX3C82A*	DE3	0.4 mM IPTG	37°C	4 h
N18Gpx3His	pET-24/*N18GPX3*	DE3	0.4 mM IPTG	18°C	16 h
N18M20LGpx3His	pET-24/*N18M20LGPX3*	DE3	0.4 mM IPTG	18°C	16 h
N18M20LGpx3C82AHis	pET-24/*N18M20LGPX3C82A*	DE3	0.4 mM IPTG	18°C	16 h
CytcHis	pET-24/*CYC1*	DE3	0.4 mM IPTG	37°C	4 h
Ypl107wHis	pET-24/*YPL107W*	DE3	0.4 mM IPTG	18°C	16 h
GST	pGEX-4T-1 (empty)	pLysS	0.4 mM IPTG	37°C	4 h
GST-TgErv3	pGEX-4T-1/*TgERV3*	pLysS or C+	0.4 mM IPTG, 10 µM FAD	37°C	4 h

A list of all proteins, the plasmids they were expressed from, the cell type they were transformed into and the final expression conditions used after small-scale expression and solubility tests. h - hours

After expression, cells were harvested by centrifugation at 3500g for 15 minutes and cell pellets resuspended in buffer A plus 0.1 mg/ml lysozyme, 1 mM phenylmethylsulfonyl fluoride (PMSF) and left on ice for 5 minutes, followed by an incubation at 37°C for 10 minutes. To rupture the cells, lysates were freeze-thawed three times (15 minutes at -80°C, 10 minutes at 37°C) before being passed twice through a French Press machine at a stable pressure of 1000 psi. Unbroken cells were then removed by centrifugation at 3500g for 5 minutes at 4°C, and the supernatant subjected to another centrifugation at 21000g for 30 minutes at 4°C. The new supernatant containing soluble protein material was kept on ice and the pellet containing broken membranes and inclusion bodies was resuspended in buffer B and kept at RT. At this point, the solubility of the expressed protein was checked by SDS-PAGE and Coomassie staining to reveal which fraction the protein was in. If the protein was largely in the supernatant, then it was purified following protocol (i) or (ii) depending on whether it contained a His or GST tag; if it was insoluble, then it was purified from inclusion bodies following either protocol (iii) or (iv).

i. ***Soluble His-tagged proteins***. The soluble supernatant was loaded onto a column containing equilibrated Ni-NTA beads plus 10 mM imidazole. The flowthrough was drained and the beads washed with buffer A plus 15 mM imidazole (wash 1). Beads were then washed again but with 50 mM Tris-HCl pH 7.4, 50 mM NaCl, 10% glycerol, 25 mM imidazole (wash 2). His-tagged proteins were eluted in 50 mM Tris-HCl pH 7.4, 50 mM NaCl, 25% glycerol and 250 mM imidazole.

ii. Soluble GST-tagged proteins. Equilibrated Glutathione Sepharose 4B beads (equilibrated in binding buffer) were added to the soluble supernatant and incubate for at least 30 minutes at 4°C. The supernatant plus beads were then transferred to a column and the flowthrough drained. Beads were then washed three times in binding buffer (washes 1-3). GST-tagged proteins were eluted three times in elution buffer.

iii. ***Insoluble His-tagged proteins***. The pellet was resuspended in buffer B and 5 mM DTT added before homogenisation of the pellet and incubation at 30°C for 1 hour, followed by centrifugation at 21000g for 30 minutes at 4°C to remove aggregates. The

supernatant was kept and diluted with buffer B from 8 M urea to 6 M urea by adding buffer A. 10 mM imidazole was then added and the supernatant loaded onto a column with equilibrated Ni-NTA beads. The flowthrough was drained and the beads washed with buffer A, 6 M urea and 10 mM imidazole (wash 1). Beads were washed again but with buffer A, 4M urea and 10 mM imidazole (wash 2), followed by a third wash with buffer A, 2 M urea and 20 mM imidazole (wash 3). A final wash with buffer A and 20 mM imidazole (wash 4) was carried out before elution in buffer A and 200 mM imidazole.

iv. ***Insoluble GST-tagged proteins***. The pellet was resuspended in buffer B and 5 mM DTT added before homogenisation of the pellet and incubation at 30°C for 1 hour, followed by centrifugation at 21000g. The supernatant was kept and diluted 10 times with renaturing buffer then incubated at 4°C for 3-16 hours, followed by centrifugation at 21000g for 30 minutes at 4°C to remove aggregates. Equilibrated Glutathione Sepharose 4B beads were added to the supernatant (equilibrated in binding buffer) and incubated for at least 30 minutes at 4°C. The supernatant plus beads were then transferred to a column and the flowthrough drained. Beads were washed three times in binding buffer (washes 1-3) before three consecutive elutions in elution buffer.

Cleavage of GST

Thrombin was used to cleave GST from fusion proteins when required; this was done either during the purification process or after purification. Cleavage during purification happened at the elution stage; instead of releasing GST fusion proteins from Glutathione Sepharose beads with reduced glutathione, the protein of interest was released by the addition of Thrombin at 1u/100 µg estimated protein for 16 hours at 4°C. Whereas after purification, GST fusion proteins were exchanged into a buffer suitable for cleavage – PBS – followed by the addition of Thrombin at 1u/100 µg protein for 16 hours at 4°C. Cleaved GST was then removed by the addition of Glutathione Sepharose beads for 3 hours at 4°C with the flowthrough then containing the protein of interest without GST.

2.2.1.7. ÄKTA FPLC

After each purification, proteins were analysed for their purity, estimated molecular weight and oligomeric state using an ÄKTA Fast Protein Liquid Chromatography (FPLC) machine (GE Healthcare), with UNICORN 6.3 software. Proteins were exchanged into buffers suitable for use in the ÄKTA, and the ÄKTA was equilibrated in the same buffer – all buffers were degassed prior to use. All aggregated proteins were removed from protein samples prior to injection into the machine by centrifugation at 16000g for 5 minutes at 4°C. Each injected sample contained around 100 µg protein which was then passed through a Superdex 200 10/300 GL (GE Healthcare) gel filtration column to separate proteins and complexes based on molecular weight. Sample protein mixes of known molecular weights (**Table 2.5**) were also passed through the column to generate a standard curve and equation (**Figure 2.1**) which was then used to calculate the approximate molecular weights of proteins of interest.

Table 2.5. List of ÄKTA protein standards.

ÄKTA protein standards			
Protein	**Mr (Da)**	**Retention volume (ml) (V_E)**	**V_E/V_O**
Blue dextran	2000000	8.8 (=V_O)	1
Thyroglobulin	660000	9.7	1.1
Ferritin	440000	10.5	1.19
Aldolase	158000	12.6	1.43
Conalbumin	75000	13.9	1.58
Ovalbumin	44000	15.1	1.72
Carbonic anhydrase	29000	16.3	1.85
Ribonuclease A	13700	17.6	2
Aprotinin	6500	19.3	2.19

Analysis of protein standards using an ÄKTA FPLC with a Superdex 200 10/300 GL gel filtration column. V_E – retention volume in ml; V_O – void volume at which Blue dextran elutes. The V_E/V_O ratio is calculated for each sample protein and used to generate the standard curve and equation shown in **Figure 2.1**.

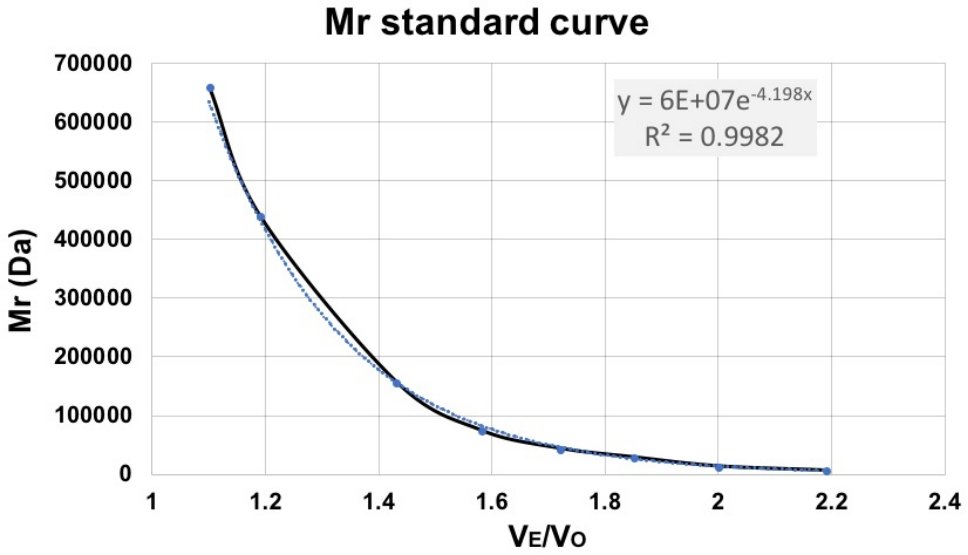

Figure 2.1. Mr standard curve for ÄKTA protein standards. Graph shows the standard curve and equation generated by analysed protein standards using a Superdex 200 10/300 GL gel filtration column. Protein samples of unknown molecular weight can be approximated using the equation shaded in grey. Mr (Da) – molecular weight in Daltons; V_E/V_O – retention volume in ml divided by the void volume calculated from Blue dextran (see **Table 2.5**). Blue dashed line represents Mr (Da); solid black line represents the exponential Mr (Da).

2.2.1.8. Radiolabelled protein production

^{35}S-methionine labelled precursor proteins were synthesised using a TNT® SP6 Quick Coupled Transcription/Translation System (Promega) following the manufacturer's protocol. Plasmids whereby gene expression is under the control of the SP6 polymerase promoter were used – pSP64 and pSP65. The radioactive reaction mixes were incubated at 30°C for 90 minutes shielded by foil, followed by centrifugation at 55000rpm in a TLA100 rotor for 15 minutes at 4°C to separate precursors from ribosomes.

2.2.1.9. Tris-Tricine SDS-PAGE, western blotting and autoradiography

Tris-Tricine SDS gels were prepared following the protocol by Schägger 2006, and all samples were resuspended in 2 X Laemmli sample buffer -/+ β-mercaptoethanol and

boiled at 95°C for 5 minutes prior to loading into wells. Gels were run at 60-180 V for 60-120 minutes and were then either soaked in Coomassie buffer for 5 minutes followed by destaining in destain buffer to detect proteins, or transferred onto nitrocellulose membranes using a Bio-Rad Semi-Dry Transfer System at a constant 25 V for 25 minutes. Prior to western blotting or autoradiography, membranes were soaked in Ponceau buffer for 2-3 minutes to stain the transferred proteins and check whether the transfer was successful. The Ponceau stain was then removed by soaking the membranes in dH_2O. For western blotting, membranes were blocked in a 5% milk solution at RT for at least one hour. After blocking, membranes were washed three times in TBST for 5 minutes before the addition of primary antibodies (diluted to working concentrations of 1:500-2000 in 1-5% milk – see **Table 7.4**) for 1-3 hours at RT or overnight at 4°C. Unbound primary antibodies were removed and membranes were washed three times in TBST for 5 minutes before the addition of secondary antibodies (diluted to 1:10000 in 1% milk for Horseradish Peroxidase (HRP)-labelled antibodies or dH_2O for fluorescently-labelled antibodies) for 1 hour at RT. Unbound secondary antibodies were removed and membranes were washed twice in TBST for 5 minutes before a final wash in dH_2O for 5-10 minutes. HRP-labelled antibodies were detected using X-ray films whilst fluorescently-labelled antibodies were detected using a LI-COR Odyssey CLx quantitative fluorescence imaging system. For autoradiography, membranes were placed into a cassette directly after removal of the Ponceau stain and left for 2-3 days before being visualised by a digital Phosphoimager (Fujifilm FLA-7000).

2.2.1.10. Silver staining

SDS-PAGE gels were fixed in 50% (v/v) methanol and 10% (v/v) acetic acid for 30 minutes at RT before being washed twice in dH_2O for 15 minutes per wash. Gels were then soaked in 0.005% (w/v) sodium thiosulfate for 30 minutes at RT before being transferred into cold 0.1% silver nitrate. After another 30 minutes, gels were washed in dH_2O for no more than 30 seconds before soaking in 0.036% (v/v) formaldehyde and 2% (w/v) sodium carbonate. After 1-2 minutes, the solution was then poured off and the gels were soaked in 50 mM EDTA for 15 minutes. *This protocol was kindly provided by Esther Nuebel.*

2.2.2. *In organello* assays

2.2.2.1. Isolation of yeast mitochondria and peroxisomes

Isolation of mitochondria only

Mitochondria were isolated and purified as described in Glick 1991 from wild-type D273-10B, wild-type BY4741, *gpx3Δ* and *ypl107wΔ* yeast. Cells were grown in liquid YPLac at 30°C to promote mitochondrial respiration and proliferation of mitochondria – this medium does not allow yeast to produce energy by glycolysis in the cytoplasm, thus the only cells that survive are those that have functional mitochondria (Turcotte et al., 2010). After isolation, mitochondria were stored at -80°C in breaking buffer plus 10 mg/ml fatty acid free BSA to stabilise the mitochondrial membranes. Mitochondrial protein concentration was measured by reading the absorbance at 280 nm using a UV spectrophotometer and the equation: mg/ml = A280/0.12 x 10.

Isolation of mitochondria and peroxisomes from the same yeast culture

Mitochondria and peroxisomes were isolated and purified following the protocol published in Current Protocols in Cell Biology, volume 1, 3.8.32 'Isolation of oleate-induced peroxisomes using sucrose step gradients' (Rieder and Emr, 2001) with the exception that Nycodenz step gradients were used instead of sucrose (as described in Ohdate and Inoue, 2012). Wild-type D273-10B, galMia40 and *gpx3Δ* yeast were grown in liquid YPOle media at 30°C to induce peroxisomal proliferation. After isolation, both mitochondria and peroxisomes were stored separately at -80°C in breaking buffer plus 10 mg/ml fatty acid free BSA.

2.2.2.2. Mitochondrial import assay

Purified recombinant His-tagged proteins or radiolabelled precursors were used in mitochondrial import assays. All His-tagged proteins, and radiolabelled proteins requiring

denaturing/reducing treatment before import, were precipitated in 2 volumes ammonium sulphate for 30 minutes on ice and pelleted by centrifugation at 25000g for 30 minutes at 4°C. Proteins were resuspended in either native buffer, reducing buffer or denaturing/reducing buffer and incubated for 30-90 minutes at 4-30°C (or ice for native buffer) depending on the protein (see **Table 2.6**). Afterwards, proteins were incubated with isolated mitochondria (following a rule of 6.25 µg His-tagged protein or 5 µl radiolabelled protein with 50 µg mitochondria) in an import reaction mix containing 1 X Import buffer plus 50% (w/v) mitochondria, 2 mM ATP and 2.5 mM NADH for 10-30 minutes at 30°C followed by centrifugation at 15000g for 5 minutes at 4°C. Mitochondria pellets were resuspended in Breaking buffer plus 0.1 mg/ml Trypsin and left on ice to digest unimported proteins. A control import reaction whereby 1% (v/v) Triton-X-100 was added at this stage was carried out for each assay to solubilise the mitochondrial membranes and allow the protease to destroy imported as well as unimported material. After 30 minutes, 1 mM SBTI was added and incubated on ice for a further 10 minutes to inhibit Trypsin. Mitochondria were then pelleted by centrifugation at 15000g for 5 minutes at 4°C, and resuspended in 2 X Laemmli sample buffer with β-me, then analysed by SDS-PAGE and visualised either by western blotting using anti-His or digital autoradiography using a Phosphoimager (Fujifilm FLA-7000) to detect His-tagged proteins and radiolabelled proteins, respectively.

Table 2.6. Treatment conditions for proteins prior to their mitochondrial import

Treatment conditions for mitochondrial import			
Protein	**Buffer**	**Temp**	**Time**
All Gpx3 proteins	Native buffer	Ice	n/a
	Denaturing and reducing buffer	30°C	90 minutes
Pex11 (radiolabelled)	Native buffer	Ice	n/a
CytcHis	Native buffer	Ice	n/a
Ybr124w-3Met	Native buffer	Ice	n/a
	Reducing buffer	30°C	30 minutes
	Denaturing and reducing buffer	30°C	60 minutes
Ypl107w	Native buffer	Ice	n/a
	Reducing buffer	Ice	30 minutes
	Denaturing and reducing buffer	Ice	30 minutes

2.2.2.3. Mitochondrial localisation assay

Radiolabelled proteins were produced and imported into mitochondria as described in **Sections 2.2.1.1 & 2.2.2.2** respectively. After treatment with Trypsin/SBTI to remove unimported material, the following protocols were used to determine which subcellular compartment the imported material resides in and whether it is likely a soluble, peripheral membrane or integral membrane protein.

Mitoplasting

To create mitoplasts (mitochondria without their outer membrane), mitochondria were resuspended in 1 X import buffer at a protein concentration of 5 mg/ml, and then diluted nine times in a hypotonic mitoplast buffer (-/+ 0.1 mg/ml Proteinase K (PK)) to a final concentration of 0.5 mg/ml and incubated on ice for 20 minutes, followed by the addition of 2 mM PMSF for 10 minutes to inactivate PK. Samples were then centrifuged at 16000g for 5 minutes at 4°C; supernatants contained soluble IMS proteins, whereas pellets contained mitoplasts along with fragments of the outer membrane.

Carbonate extraction

To separate soluble from membrane-bound proteins, 0.1 M ice-cold sodium carbonate was added to intact mitochondria after import at a final protein concentration of 0.5 mg/ml, and incubated on ice for 30 minutes. Samples were then centrifuged at 55000rpm using a TLA100 rotor for 30 minutes at 4°C; supernatants contained soluble mitochondrial proteins, whereas pellets contained membrane bound proteins.

Urea extraction

To extract peripherally associated membrane proteins, mitoplasting was carried out followed by extraction with urea. After mitoplasting, as described above, mitoplasts were resuspended in 1 x breaking buffer plus either 3 M urea or 5 M urea and incubated on ice for 30 minutes. Samples were then centrifuged at 55000rpm using a TLA100 rotor for 30

minutes at 4°C; supernatants contained peripheral-associated proteins, whereas pellets contained integral membrane proteins.

2.2.2.4. Pulldown assay using His-tagged proteins

His-tagged protein were imported into mitochondria as described in **Section 2.2.2.2**, followed by solubilisation of mitochondrial membranes using 1% n-Dodecyl β-D-maltoside (DDM) in solubilisation buffer for 30 minutes on ice. For pulldown experiments, 375 µg precursor protein and 3mg of isolated mitochondria were used. Solubilised mitochondrial membranes were pelleted by centrifugation at 16000g for 30 minutes. The supernatant containing the released mitochondrial proteins was kept. 10 mM imidazole was added to the supernatant before loading onto Ni-NTA beads which were equilibrated in solubilisation buffer plus 10 mM imidazole for five minutes at RT. The supernatant was left binding to the Ni-NTA beads for 30 minutes, 4°C, and rotating 360°. The beads were then centrifuged at 5000g for one minute and the flow through discarded. Wash buffer 1 (solubilisation buffer, 20 mM imidazole) was added to the beads for 10 minutes, 4°C, rotating 360°, and followed by centrifugation at 5000g for one minute. The flow through from wash 1 was discarded. Wash buffer 2 (solubilisation buffer, 40 mM imidazole) was added to the beads for 10 minutes, 4°C, rotating 360°. Finally, to elute the bound material, 300-400 mM imidazole in solubilisation buffer was added to the beads and left to rotate 360° at 4°C for 30 minutes. Beads were then centrifuged at 5000g for one minute and the eluates kept; 1/3 (equivalent to 800 µg mitochondria) was analysed by SDS-PAGE and western blotting, the remaining 2/3 was sent for mass spectrometry analysis. In case the elution buffer did not successfully elute all of the bound material, 2 X sample buffer plus β-me was added to the beads, vortexed, centrifuged at 16000g for five minutes, vortexed, boiled at 95°C for five minutes, and frozen at -20°C. See **Figure 3.7** for an illustration of the pulldown. The control for this experiment consisted of repeating the above protocol without the import of His-tagged proteins. Control eluates were also analysed by SDS-PAGE followed by western blotting and mass spectrometry.

2.2.2.5. Complex immunoprecipitations

Method I – endogenous protein Co-IP

Isolated wild-type mitochondria from D273-10B yeast were solubilised as described in **Section 2.2.2.4**. The supernatant containing soluble mitochondrial proteins was then split into multiple 1.5 mL tubes so that each tube contained 50 μg of solubilised material (at a concentration of 1 μg/μl), along with 1.2 mL IP buffer, plus either 4 μl undiluted anti-Gpx3, 4 μl undiluted anti-Cyt*c*, 4 μl undiluted pre-immune serum (PI) or nothing (extra control). Tubes were then rotated at 360° for two hours at 4°C. Afterwards, 30 μl of pre-equilibrated protein A beads were added to each tube and left rotating at 360° for a further hour at 4°C. Protein A beads were equilibrated in IP buffer with the addition of 3% BSA for 30 minutes shaking at RT, followed by a mild spin at 3000g for one minute before resuspension in fresh IP buffer. The tubes were then spun at 3000g for one minute and the supernatant removed. The beads were resuspended in 1.5 mL fresh IP buffer and spun again. To elute any bound material, the beads were resuspended in 20 μl 2 X sample buffer without β-me and then vortexed, boiled for five minutes, followed by a final vortex and spin at 16000g for 5 minutes at RT. The elutions step was repeated twice and the supernatants combined. Samples were then analysed by SDS-PAGE and visualised by western blotting using anti-Gpx3 or anti-Cyt*c*.

Method II – radiolabelled Co-IP

Radiolabelled Gpx3 and Cyt*c* were produced following the protocol described in **Section 2.2.1.8** and imported into isolated wild-type mitochondria from D273-10B yeast as described in **Section 2.2.2.2**. Mitochondria were then solubilised as described in Section **2.2.2.4**. After this, the Co-IP protocol was the same as that described above, apart from the visualisation which was carried out by digital autoradiography.

2.2.2.6. BN-PAGE

Gel and sample preparation

6-16% Bis-Tris gradient gels were made on the same day as use. Separate 6% and 16% Bis-Tris gel solutions were made fresh by adding the appropriate amount of BN acrylamide solution in 0.5 x BN gel buffer (plus 14.5% glycerol in the 16% solution) and mixed using a gradient mixer on a stir plate, followed by the addition of a stacking solution (4% Bis-Tris, 0.5 x BN gel buffer). For samples of 50-100 µg mitochondria, mitochondria were first washed in 1 x breaking buffer and centrifuged at 16000g for 5 minutes at 4°C. The supernatant was removed and mitochondrial pellets were resuspended in 45 µl ACA750, followed by the addition of 5 µl 10% (w/v) DDM which was freshly made in dH_2O from a powdered stock. Samples were incubated on ice for 5 minutes then centrifuged at 16000g for 10 minutes at 4°C. Supernatants were transferred to new tubes and 2.5 µl of 5% serva blue solution were added. Samples were kept on ice until loading.

Gel running and visualisation

Everything at this stage was carried out in a cold room at 4°C. The gel tank was prepared by filling the out chamber with 1 x anode buffer and the inner chamber with 1 x cathode buffer (plus 0.02% Coomassie G250 – dark blue). Samples were loaded into wells, along with a native protein marker (Amersham HMW Calibration Kit for Native Electrophoresis). Gels were run at 100 V (4-10 mA) for around 45 minutes, until the dye front had moved a third of the gel length down. The 1 x cathode buffer (dark blue) was then removed and replaced with 1 x cathode buffer (plus 0.002% Coomassie G250 – light blue), and gels were run at 250 V (15 mA) for a further 2-3 hours until the dye front was at the bottom of the gel. For Coomassie staining, gels were incubated in BN-PAGE Coomassie stain for 1-12 hours, followed by multiple washes in BN-PAGE destaining buffer. For digital autoradiography and western blotting, gels were soaked in 1 x cathode buffer and then transferred to Polyvinylidene fluoride (PVDF) membranes, which had been pre-soaked in 100% methanol then soaked in 1 x cathode buffer, using a Bio-Rad Semi-Dry Transfer System at a constant 25 V for 3 hours. After transfer, membranes were either visualised using a Phosphoimager (Fujifilm FLA-7000) or incubated with antibodies, as described in **Section 2.2.1.9**. *This BN-PAGE protocol was kindly provided by Andrew Mclean.*

2.2.3. *In vitro* assays

2.2.3.1. *In vitro* binding assay using Ni-NTA beads

Isolated mitochondria or peroxisomes were lysed in 1 ml solubilisation buffer for 30 minutes on ice followed by centrifugation at 16000g for 30 minutes at 4°C. His-tagged proteins were precipitated in 2 volumes saturated ammonium sulphate for 30 minutes on ice and pelleted by centrifugation for 30 minutes at 25000g at 4°C followed by resuspension in lysis buffer plus 10 mM imidazole. A 20 µg amount of His-tagged protein (0.02 µg/µl) was added to 20 µl equilibrated Ni-NTA beads for 30 minutes at 4°C, rotating at 360°. Beads were centrifuged at 3000g for 1 minute followed by the addition of 1 mg solubilised mitochondrial (or peroxisomal proteins) plus 10 mM imidazole for 60 minutes at 4°C, rotating 360°. Beads were centrifuged again at 3000g for 1 minute, then washed three times in 50 mM Tris-HCl pH 7.4, 150 mM NaCl, 10 mM imidazole, and 1 mM PMSF for 5-10 min per wash at 4°C, rotating 360°, followed by a final wash in 50 mM Tris-HCl pH 7.4, 150 mM NaCl, 20 mM imidazole, and 1mM PMSF. Beads were then incubated in 50 mM Tris-HCl pH 7.4, 150 mM NaCl and 300-400 mM imidazole for 30 minutes at 4°C, rotating 360°, followed by a final centrifugation to collect eluates containing His-tagged proteins and interaction partners. Samples were analysed by SDS-PAGE/western blotting.

2.2.3.2. *In vitro* protein-protein interaction assay

Proteins were precipitated in 2 volumes ammonium sulphate and resuspended in 50 mM Tris-HCl pH 8.0 before the addition of either 20 mM DTT or 200 µM H_2O_2 for 30 minutes at 30°C or RT, respectively. Per interaction, 50 µg of each protein were incubated together in 1 ml 50 mM Tris-HCl pH 8.0 for the desired amount of time at 30°C followed by TCA precipitation. TCA was added to a 10% final concentration for 20 minutes on ice then centrifuged at 16000g for 20 minutes at 4°C. Precipitates were then washed in 100% ice cold acetone, centrifuged again, air dried and resuspended in ETS buffer plus 15 mM AMS for 30 minutes at 30°C, followed by another 30 minutes at 37°C. 6 X Laemmli sample buffer (-βme) was added and samples were analysed by SDS-PAGE and western blotting.

2.2.4. *In vivo* assays

2.2.4.1. Yeast growth, drop tests and sensitivity assays

Liquid growth assays

Individual yeast colonies were grown overnight at 30°C in liquid YPD then diluted the next morning to an OD_{600nm} of 0.05 in each required media, i.e. liquid YPD, YPLac, YPGly or YPOle. Cells were then incubated at 30°C and cell density was measured (at OD_{600nm}) every 2 hours until 16 hours had been reached.

Drop tests

Individual yeast colonies were grown overnight at 30°C in liquid YPD then diluted the next morning to an OD_{600nm} of 0.1 in autoclaved dH_2O. Serial dilutions were then made to 0.01, 0.001 and 0.0001, and 2.5 µl from each were spotted onto YPD, YPLac and YPGly plates. Plates were then incubated for 48 hours at 30°C.

H_2O_2 sensitivity assay

Individual yeast colonies were grown overnight at 30°C in liquid YPD then diluted the next morning to an OD_{600nm} of 0.1 in autoclaved dH_2O and 400 µl spread onto individual YPD plates. Once dried, a 5 µl drop of 8.8 M H_2O_2 was spotted onto the centre of each plate. Plates were left to dry again and then incubated for 24 hours at 30°C. Diameters of the clear 'halo' zones were measured in mm using a ruler.

Diamide sensitivity assay

Individual yeast colonies were grown overnight at 30°C in liquid YPD then diluted the next morning to an OD_{600nm} of 0.1 in autoclaved dH_2O. Serial dilutions were then made to 0.01, 0.001 and 0.0001, and 2.5 µl from each were spotted onto YPD plates containing either 0, 2.0 or 2.5 mM diamide. Plates were then incubated for 72 hours at 30°C.

2.2.4.2. Immunofluorescence assay

Part I – parasite transient transfection

Plasmids suitable for expression in *T. gondii* were transfected into lysed *T. gondii* (host cells were human foreskin fibroblasts, which were obtained from ATCC (cat no. CRC1041)). Parasites were resuspended in cytomix (350 µl per transfection) and transferred to cuvettes suitable for electroporation. Plasmid DNA was then added at a concentration of 1 µg/µl (50 µg total DNA required per transfection). Cuvettes were then shock pulsed at 1700V and the parasites placed in petri dishes containing host cells and DMEM–Dulbecco's Modified Eagle Medium (GIBCO).

Part II – Immunofluorescence preparation

After 24-48 hours, when the parasites had lysed, all media was removed from the dishes and 3.7-4% (v/v) paraformaldehyde (PFA) was added for 20 minutes at RT. PFA was then removed and the dishes were washed three times with PBS before adding blocking buffer for 20 minutes at RT. Blocking buffer was then removed and primary antibodies (anti-myc at 1:1000 in blocking buffer) were added for 1 hour at RT. Primary antibodies were removed and the dishes washed three times in PBS for 5 minutes per wash before adding secondary antibodies (anti-mouse 680 (red) or 488 (green) at 1:500 in blocking buffer). After incubation in the dark for 45 minutes at RT, the secondary antibodies were removed and the dishes washed three times in PBS for 5 minutes. Glass slides were removed from the bottom of the dishes containing the host cells and parasites, and mounted on slides suitable for confocal microscopy using DAPI-fluoromount-G (Invitrogen).

Part III – Confocal microscopy

Slides were visualised using a DeltaVision microscope (RT deconvolution, Olympus Uplan/Apo) at 100x zoom using SoftWoRx 5.5 and analysed using ImageJ.

2.2.5. Mass spectrometry

Eluates were sent to the Glasgow Polyomics facility for mass spectrometry analysis. First, the eluates containing His-tagged proteins and their interacting proteins were digested with Trypsin using the filter-aided sample preparation (FASP) protocol. The digested peptides were then separated by RP-UPLC on C18, followed by analysis using a Bruker Amazon Speed ion trap (ESI-TRAP) to collect MS and MS/MS data. This data was then searched using the Mascot search engine against a *Saccharomyces* database (database: NCBInr 20150301, taxonomy: *S. cerevisiae*) with the following analysis criteria: fixed modifications (carbamidomethyl); variable modifications (oxidation); mass values (monoisotopic); protein mass (unrestricted); peptide mass tolerance (-/+ 0.4 Da); fragment mass tolerance (-/+ 0.4 Da); maximum missed cleavages (1); and MudPIT scoring with a significance threshold of $p<0.05$.

2.2.6. Circular dichroism

Circular dichroism measurements were obtained using a Jasco J-810 spectropolarimeter at 20°C and was carried out by Dr Sharon Kelly at the University of Glasgow. A 0.02cm pathlength quartz cuvette was used to measure far UV spectra between the 190 – 250 nm wavelength range. A 0.2cm pathlength quartz cuvette was used to measure near UV spectra between the 250 – 320 nm wavelength range. The scan rate was 10 nm/minute with 1 nm bandwidth and a two second response time. Three spectra were recorded from each sample and averaged, and all spectra were corrected for cell pathlength and protein concentration.

2.2.7. Electron microscopy

Individual yeast colonies were grown overnight at 30°C in liquid YPD then diluted the next morning to an OD_{600nm} of 0.05 in fresh liquid YPD. Once the cells reached an OD_{600nm} of 0.7-1.0, they were washed twice in PBS at 4°C and centrifuged at 3000g for 5 minutes. After this, the cells were fixed in 2% glutaraldehyde, 1 mM $CaCl_2$ and 0.1 M sodium cacodylate pH 7.2 for 30 minutes at 4°C followed by centrifugation at 3000g for 5 minutes

at RT. Cells were then washed three times in 0.1 M sodium cacodylate for 5 minutes per wash at RT, followed by centrifugation at 3000g for 5 minutes. Pelleted cells were resuspended in 50 mM Tris-HCl pH 7.4, 5 mM $MgCl_2$, 1.4 M sorbitol, 0.5% (v/v) 2-mercaptoethanol and 0.15 mg/ml Zymolyase 20T (AMS Biotechnology Europe) and incubated for 15 minutes at RT. After removal of the cell wall by Zymolyase, the cells were washed four times in 0.1 M sodium cacodylate buffer for 5 minutes at RT before a final centrifugation at 3000g for 5 minutes. At this point, the cells were handed over to Margaret Mullin at the Electron Microscopy Facility (University of Glasgow) who followed an electron microscopy protocol designed for the visualisation of yeast membrane structures published by Bauer et al. (2001). A transmission electron microscope (TEM) was used.

Chapter 3

Identifying mitochondrial protein interactors of yeast Gpx3

3. Identifying mitochondrial protein interactors of yeast Gpx3

3.1. Introduction

Gpx3 is a thiol peroxidase in *S. cerevisiae* with a well-established role as a major H_2O_2 sensor in the cytosol. The reaction that Gpx3 catalyses is: Gpx3(-SH) + H_2O_2 → Gpx3(-SOH) + $2H_2O$; the sulphenylated form of Gpx3 can then form transient conjugates with other proteins via intermolecular disulphides, or, form an intramolecular disulphide bond Gpx3 (S-S). The oxidised form of Gpx3(S-S) is then reduced by Thioredoxin. The most characterised partner of Gpx3 within the cytosol is the transcription factor Yap1, its interaction with Gpx3 results in its nuclear accumulation and subsequent activation of more than 70 stress response genes, as explained in Chapter 1, **Section 1.6** (Delaunay et al., 2002; Veal et al., 2003; Ma et al., 2007; Okazaki et al., 2007; Ouyang et al., 2011). However, additional functions are either known or hypothesised to exist based on interactome data using whole yeast cell extracts; these include roles in metabolism and protein homeostasis, some of which have been investigated in more detail (Kho et al., 2006; Lee et al., 2007; Lee et al., 2008; Tarassov et al., 2008; Lee et al., 2009; Lee et al., 2011).

The majority of Gpx3 interaction partners identified in these studies were predominantly cytosolic; only four exhibit mitochondrial localisation (Alo1, Grx2, Tfa1 and Tdh2) (Lee et al., 2008; Tarassov et al., 2008), though it cannot be inferred in which cellular compartment these interactions occur. At the time, it was thought that Gpx3 was solely cytosolic; it was not until 2012 that Gpx3 was found within an IMS fraction during a proteomics analysis by Vögtle et al. (2012) and later confirmed by Kritsiligkou et al. (2017). This raises the question as to what the role of Gpx3 is in the IMS – the smallest, but highly redox active, mitochondrial subcompartment.

Only two of the proteins previously identified are likely interactors of the IMS pool of Gpx3 based on their sub-mitochondrial localisation: Alo1 and Grx2. Alo1 is an integral outer membrane (OM) protein that catalyses the final step in dehydro-A-arabinono-1,4-lactone synthesis, an enantiomer of ascorbate that is protective against oxidative stress (Kenney et al., 1979). Glutaredoxin 2 (Grx2) is a glutathione-dependent disulphide oxidoreductase known to reside in the IMS in small amounts but it is largely found in the cytosol (Kojer et al., 2015). There is no current evidence to suggest the other two interactors of Gpx3, Tfa1 and Tdh2, localise to the IMS.

Work carried out in our lab previously and during the course of this PhD identified Mia40, an oxidoreductase that is a key player of the oxidative folding mitochondrial protein import machinery, as an interactor of Gpx3 (Kritsiligkou et al., 2017). In these studies, it was shown that one role of the IMS-localised Gpx3 is to maintain the redox state of Mia40 in the IMS, promoting efficient mitochondrial protein import via the Mia40 pathway. However, additional interaction partners are still thought to exist. It has also been shown that an N-terminally extended version of Gpx3 exists, denoted as N18Gpx3, which leads to more efficient targeting of Gpx3 to the IMS, and an increased affinity to mitochondrial membranes (Vögtle et al., 2012; Kritsiligkou et al., 2017; Tokatlidis, unpublished obs.). The work in this chapter has investigated such additional putative protein interactors of Gpx3 and also of N18Gpx3. Identifying these will help elucidate their roles within the IMS.

3.2. Aims

In this chapter, the aim was to identify protein partners of the H_2O_2 sensor Gpx3 and N18Gpx3 in the mitochondrial IMS in order to elucidate their function(s) in the IMS. Whilst much is known about the role of Gpx3 in the cytosol (see **Chapter 1**, **Section 1.6**), for example its interaction with Yap1, very little is understood about Gpx3 in the IMS. As an initial screening method, pulldowns from mitochondrial fractions were performed after import of His-tagged Gpx3/N18Gpx3 proteins and putative partners were identified by mass spectrometry. Cysteine trap mutant forms of Gpx3 and N18Gpx3 whereby the resolving cysteine was mutated to alanine (C82A) were also used in order to capture mixed disulphide intermediates and identify partner proteins that rely on intermolecular disulphide bonds. Once a list of putative proteins had been generated, *in vitro* binding assays were carried out to help confirm some of these partners. The interaction between Gpx3 and one such partner, Cytochrome *c* (Cyt*c*), was investigated further using *in vitro* interaction assays and immunoprecipitations.

Alternative approaches were also sought, including expression of an endogenously tagged Gpx3 in yeast (Gpx3-TAP) and the expression of yeast plasmids harbouring tagged versions of Gpx3 (Gpx3-V5). The aim was to confirm that these tagged versions were successfully expressed in yeast and that the tags did not affect their mitochondrial localisation. If confirmed, mitochondria would be isolated from these strains and pulldowns would be performed.

Finally, the mitochondrial import of two proteins with unknown localisation and function that were identified in the mass spectrometry data analysis was tested – Ybr124w and Ypl107w.

3.3. Results

3.3.1. Purification of Gpx3 and N18Gpx3 proteins

To begin, recombinant Gpx3 and N18Gpx3 proteins were expressed and purified from *E. coli* with a C-terminal 6xHistidine (His) tag for use in subsequent pulldown and *in vitro* binding assays. *GPX3* had previously been cloned by a former lab member into a pET-24 vector (Novagen) which includes a multiple cloning site followed by a sequence encoding a 6xHis tag (Chatzi, unpublished obs.). Here, the *N18GPX3* sequence was cloned in a similar manner and both constructs were sent for sequencing to ensure that no mutations had arisen during the cloning process, or within storage. Both the pET-24/*GPX3* and pET-24/*N18GPX3* plasmids contained the correct gene sequences with no mutations, deletions or insertions (sequencing data not shown). The plasmids were then transformed into BL21 (DE3) *E. coli* for bacterial expression and induced using IPTG. Proteins were purified by affinity chromatography using Ni-NTA columns, either from the soluble (supernatant) or insoluble (pellet containing inclusion bodies from which the protein was extracted after denaturation) fractions after cell disruption, depending on their solubility.

As Gpx3 had previously been expressed and purified a former lab member the optimal conditions were already determined and it was known to be an easily expressed, soluble protein (Chatzi, unpublished obs.). Following a pre-established protocol as described in **Chapter 2**, **Section 2.2.1.6**, a fresh stock of Gpx3 was purified for use in subsequent experiments (**Figure 3.1A**). In addition, single cysteine mutants of Gpx3 were purified using the same conditions after site-directed mutagenesis of the pET-24/*GPX3* plasmid to create pET-24/*GPX3C36S*, pET-24/*GPX3C64S*, and pET-24/*GPX3C82A* (**Figures 3.1B, 3.1C & 3.1D**). These proteins were purified further using an ÄKTA Fast Protein Liquid Chromatography (FPLC) machine (AKTA pure) to remove contaminants and to assess their oligomeric state (see **Appendices**, **Section 7.1**).

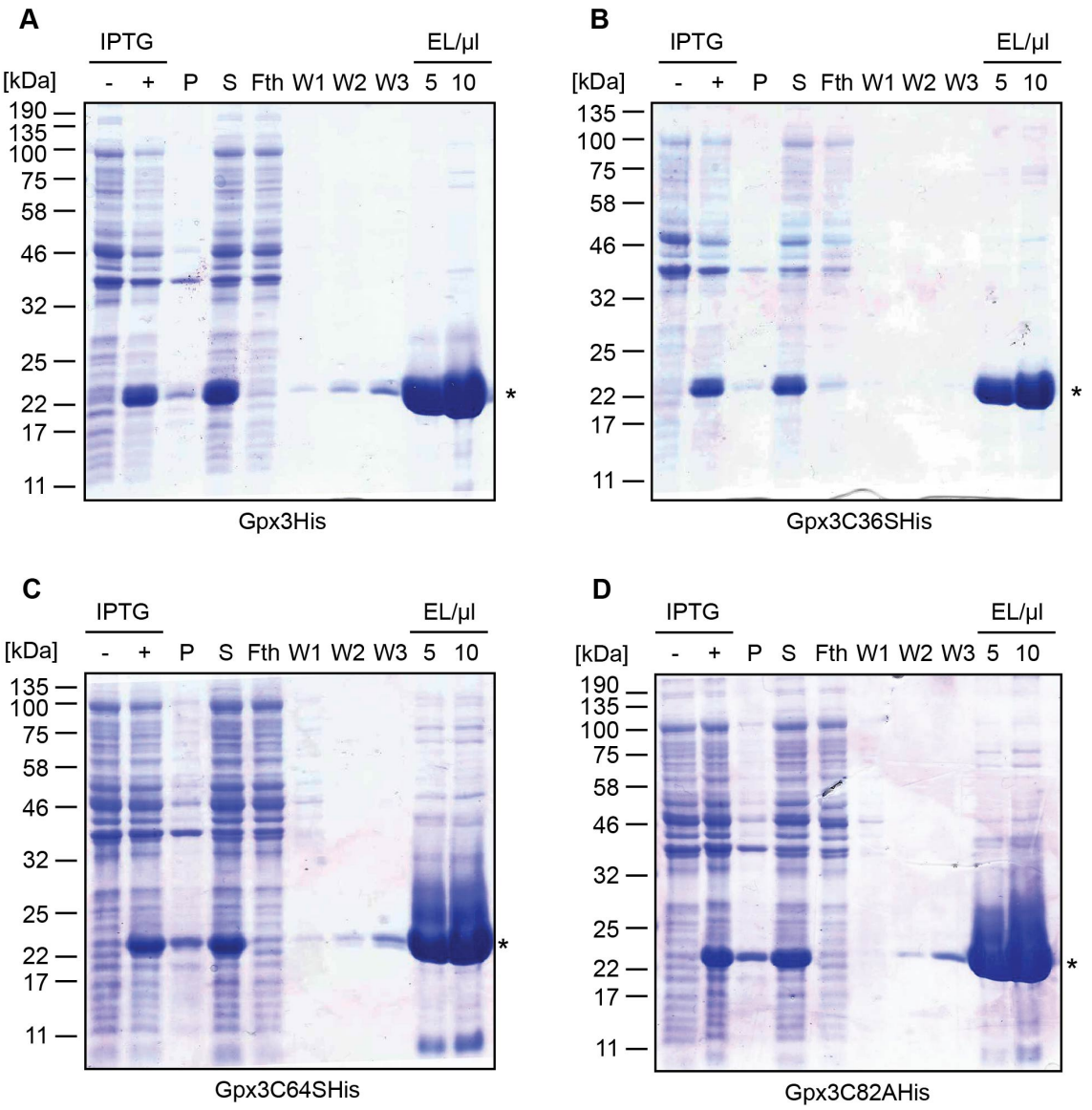

Figure 3.1. Expression and purification of His-tagged Gpx3 proteins. Purification of (**A**) Gpx3His, (**B**) Gpx3C32SHis, (**C**) Gpx3C64SHis, and (**D**) Gpx3C82AHis from the supernatant fraction of IPTG-induced DE3 *E. coli* cells (Coomassie stained SDS-PAGE gels; all samples loaded with β-me). –IPTG – no induction; +IPTG – induction/protein expression; P – pellet; S – supernatant; Fth – flow through; W1 – wash 1; W2 – wash 2; W3 – wash 3; EL – eluate. Asterisks indicate purified proteins of interest.

In parallel, the optimal conditions for expression of the extended N18Gpx3His protein were determined by transforming the pET-24/*N18GPX3* plasmid in DE3 *E. coli*, inducing with IPTG (0.1 - 1 mM IPTG), and incubating at different temperatures (18 - 37°C). There were no differences in expression levels when titrating IPTG and/or changing the

temperature as the N18Gpx3His protein expressed well under all conditions nor were there any differences in solubility (data not shown). Based on this, the expression conditions were kept the same as for Gpx3His, see **Table 2.4**, and the strongest expressing colony out of three was selected for the full purification process (**Figures 3.2A & 3.2B**). Interestingly, in comparison to Gpx3His the presence of the N18 extension resulted in a larger proportion of N18Gpx3His remaining in the insoluble fraction after solubilisation. Given that data from Kritsiligkou et al. (2017) suggests that the N18 tends to cause association of Gpx3 to the mitochondrial membrane, the recombinant N18Gpx3 proteins could be more 'sticky' and might have the ability to bind to bacterial membranes when cells are ruptured, thus causing their precipitation within inclusion bodies.

Another observable difference when comparing the expression and purification of Gpx3His to N18Gpx3His was that in the latter there were two bands with molecular weights both similar to the expected size of N18Gpx3His that were both induced and eluted at the final purification step (see asterisks in **Figures 3.2A & 3.2B**). This suggested that both versions must carry the C-terminal His tag - this was confirmed by western blotting using an antibody against the His tag itself (data not shown). Based on this, it was hypothesised that the two species were due to translation of both Gpx3His and N18Gpx3His from the pET-24/N18GPX3 plasmid, as it was possible that translation was occurring from both start methionines.

To test this, the pET-24/N18GPX3 plasmid was mutated via site-directed mutagenesis to change the normal start methionine of Gpx3 (M20) to an alanine, thus eliminating the possibility of expressing an unwanted translation product. When the mutated plasmid pET-24/N18M20LGPX3 was expressed in *E. coli*, one single species was observed and N18M20LGpx3His was purified; this time from insoluble inclusion bodies (**Figure 3.2D**) as attempts to purify the protein from the soluble fraction yielded nothing (**Figure 3.2C**). However, upon closer inspection, the purified N18M20LGpx3His protein still appears as a doublet (**Figure 3.2D, EL lane**). It is possible that the doublet in this case was only visible due to the low amount of protein in the elution as the two bands appear to be more similar in size than before.

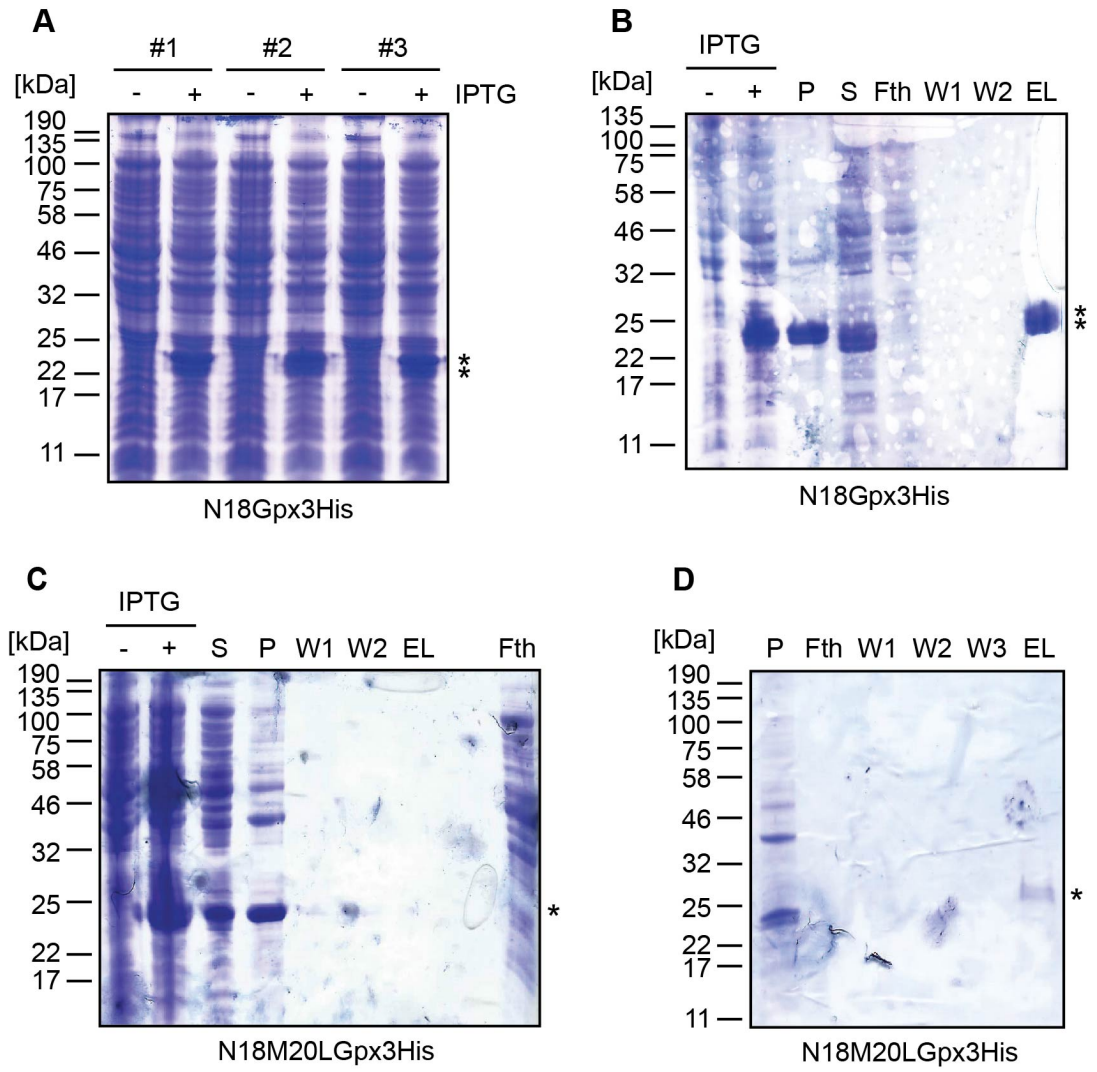

Figure 3.2. Expression and purification of His-tagged N18Gpx3 and N18Gpx3M20L proteins. **(A)** Induction of pET-24/N18GPX3 using 0.4 mM IPTG in three DE3 *E. coli* colonies labelled #1-3. Purification of (**B**) N18Gpx3His and (**C**) N18M20LGpx3His from the supernatant fractions of IPTG-induced DE3 *E. coli* cells. **(D)** Purification of N18M20LGpx3His from inclusion bodies (pellet fraction). –IPTG – no induction; +IPTG – induction/protein expression; P – pellet; S – supernatant; Fth – flow through; W1 – wash 1; W2 – wash 2; W3 – wash 3; EL – eluate. All images are Coomassie stained SDS-PAGE gels and all samples were loaded with β-me. Asterisks indicate purified proteins of interest.

An alternative explanation for the presence of two bands is that even though the M20L mutation eliminates the possibility of a second translation initiation product, there is still the potential for degradation of the N18 which is potentially cleaved due to its predicted unstructured nature. One further hypothesis is that the two bands are due to different

redox states of the purified proteins. To investigate how their redox state might affect their migration on SDS-PAGE gels, both the N18M20LGpx3His and Gpx3His purified proteins were treated with either a reducing or oxidising agent, DTT and H_2O_2 respectively, and compared to non-treated samples (**Figures 3.3A & 3.3B**). Gpx3C82AHis was used as a control as it lacks the ability to form an intra-molecular disulphide bond (**Figure 3.3B**). In addition, N18M20LGpx3His was treated with the alkylating agent AMS, 4'acetamido-4'-maleimidylstilbene-2,2'-disulphonic acid, which reacts with reduced thiols (-SH) and increases protein molecular weight by ~0.5 kDa for every –SH present. From these treatments, it was concluded that the doublets present when running N18M20LGpx3His and Gpx3His on SDS-PAGE gels are the result of a combination of reduced/oxidised species, despite the presence of the strong reducing agent β-me in previous gels (**Figures 3.1 & 3.2**).

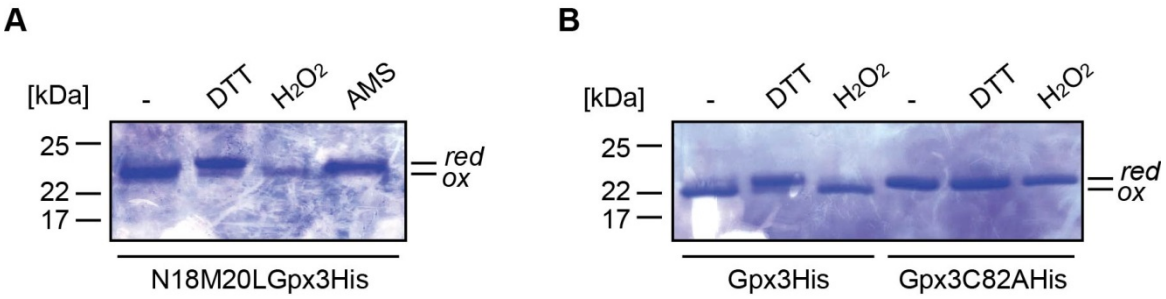

Figure 3.3. Thiol redox state of purified Gpx3 and N18Gpx3 proteins. Gel shift assays using AMS to investigate the thiol redox state of (**A**) purified N18M20LGpx3His and (**B**) purified Gpx3His and Gpx3C82AHis. (-) no treatment with DTT or H_2O_2; AMS – AMS addition to sample not treated with DTT or H_2O_2. Both images are Coomassie stained SDS-PAGE gels and all samples were loaded without β-me. 'red' – reduced thiol state; 'ox' – oxidised thiol state.

For the import experiments that followed, the redox state of the purified proteins was not an issue because all proteins were denatured and reduced prior to import. This treatment ensures that the proteins are completely import-competent. Post-import, the proteins are localised in the IMS where they can adopt their native folded structure. A depiction of all Gpx3/N18Gpx3 variant proteins purified can be seen in **Figure 3.4**.

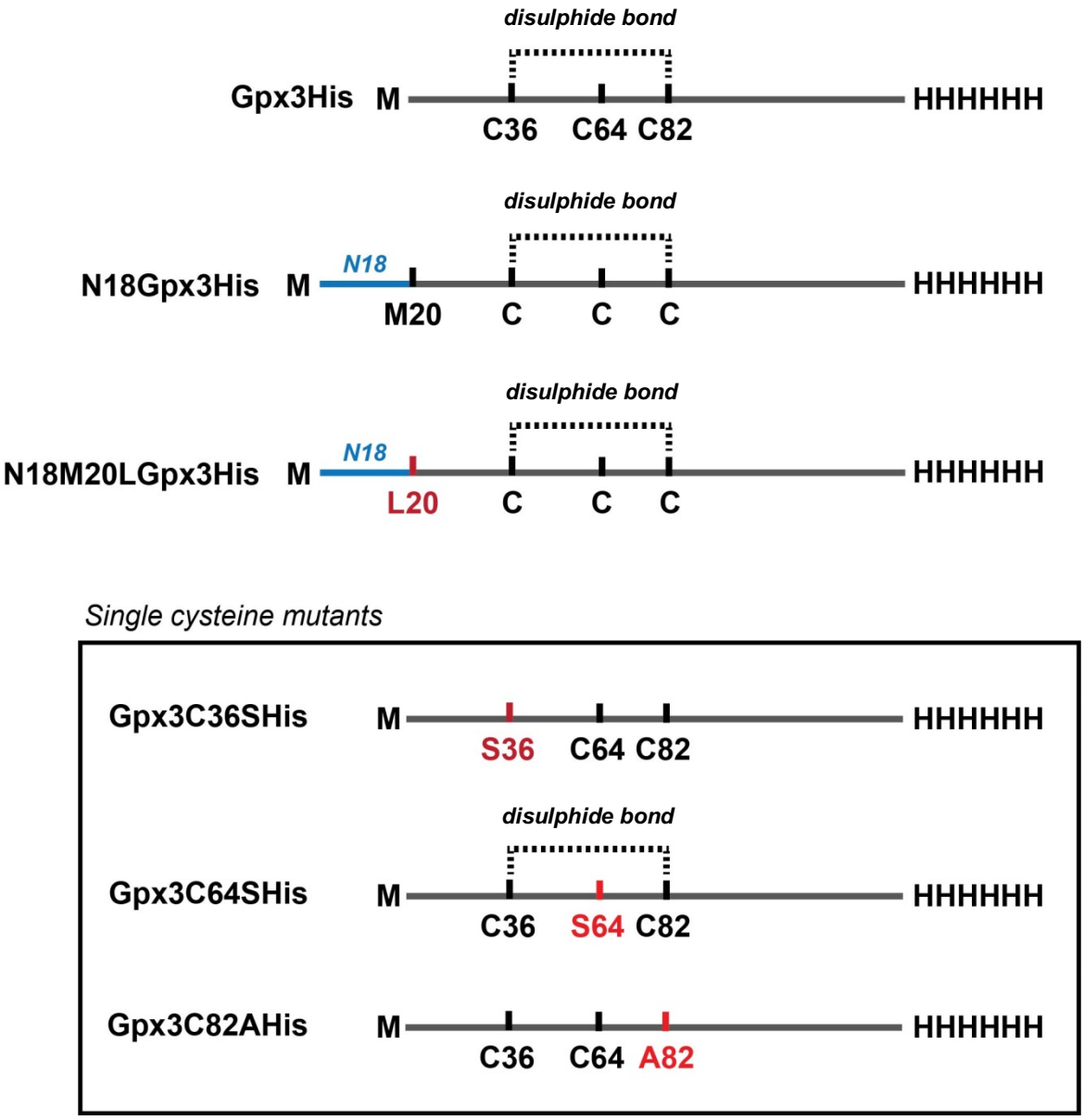

Figure 3.4. Schematic of all Gpx3 proteins purified. M – methionine residue; H- histidine residue; C – cysteine residue; S – serine residue. Red indicates where an amino acid has been mutated. Dotted lines represent disulphide bonds.

3.3.2. Mitochondrial import of Gpx3 and N18Gpx3

Before moving on to pulldown assays it was crucial that the purified proteins, Gpx3His and N18M20LGpx3His, could be imported into wild-type yeast mitochondria following a standard import protocol (**Section 2.2.2.2**, illustrated within **Figure 3.7**). As seen in **Figures 3.5A & 3.5B**, both His-tagged proteins were successfully imported and protease protected.

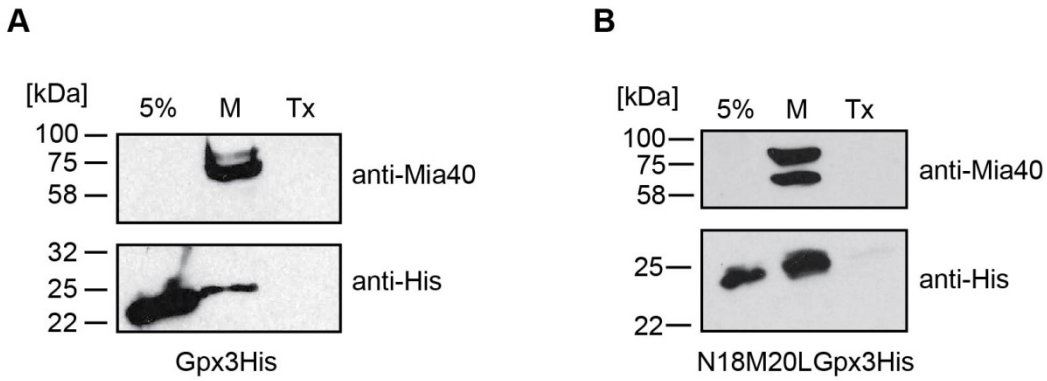

Figure 3.5. Import of purified Gpx3His and N18M20LGpx3His. The purified proteins (**A**) Gpx3His and (**B**) N18M20LGpx3His were treated with DTT & urea and presented to isolated wild-type yeast mitochondria for 20 minutes under standard import conditions, followed by a protease treatment using trypsin to destroy unimported material (M). As a control, samples were also treated with trypsin in combination with a detergent, Triton-X-100, to solubilise the mitochondria and destroy both unimported *and* imported material (Tx). Western blots were used to probe for His-tagged proteins (using anti-His), and for a positive/loading control protein (using anti-Mia40 against mitochondrial intermembrane space assembly protein). 5% corresponds to 5% of the Gpx3His/N18M20LGpx3His used for the import reaction.

Import assays were also performed using radiolabelled versions of both Gpx3 and N18M20LGpx3 to confirm that they could both be imported when produced in this manner (ready for their use in later immunoprecipitation experiments). *GPX3* and *N18M20LGPX3* had been previously cloned into pSP64 vectors by a former lab member which are suitable for use with an *in vitro* coupled transcription and translation kit (Promega) that incorporates ^{35}S-methionine (^{35}S-met) (Chatzi, unpublished obs.). Radioactively-labelled precursors were synthesised on ribosomes shortly before import,

and again both Gpx3 and N18M20LGpx3 were successfully imported into mitochondria and protease protected (**Figure 3.6**). In addition, these experiments show that the import of both proteins happens very quickly, within a matter of seconds, and that pre-treatment of the precursors with DTT and urea results in a more efficient import. In comparison to Gpx3, the N18Gpx3 variant goes in quite substantially in its native state. This could mean that one function of the N18 extension is to draw the protein into mitochondria even when it is folded.

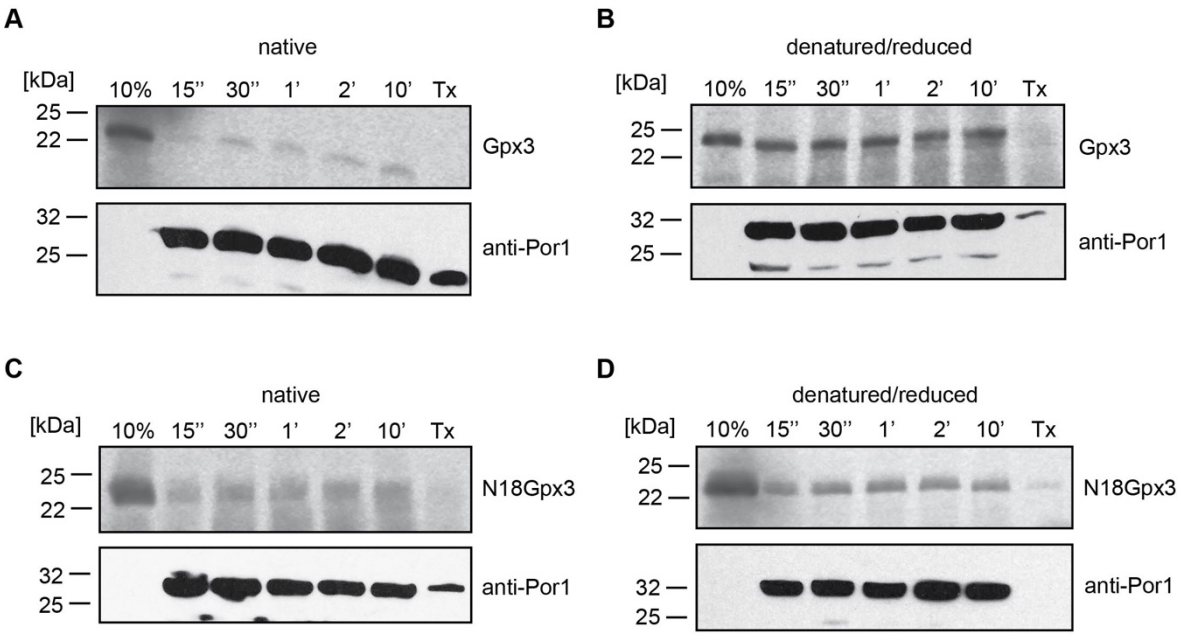

Figure 3.6. Import of radiolabelled Gpx3 and N18M20LGpx3. Gpx3 and N18M20LGpx3 were synthesised as radiolabelled precursors and imported into isolated wild-type yeast mitochondria. Precursors were either imported straight after translation, (**A**) native Gpx3 import and (**C**) native N18M20LGpx3 import, or following treatment with DTT and urea, (**B**) denatured/reduced Gpx3 and (**D**) denatured/reduced N18M20LGpx3. Import reactions were stopped after increasing time points: 15'' – 15 seconds; 30'' – 30 seconds; 1' – one minute; 2' – two minutes; and 10' – ten minutes. All import reactions were treated with trypsin to destroy unimported material, and a combination of Triton-X-100 and trypsin as a negative control (Tx). 10% corresponds to 10% of the precursor used for each import reaction. Radiolabelled precursors were detected by digital autoradiography; western blots were probed for Porin1 (using anti-Por1) as a positive/loading control.

3.3.3. *In organello* affinity pulldown assays to identify Gpx3 interactors

In order to identify interactors of Gpx3 specifically within mitochondria, pulldown assays were performed using mitochondrial isolates rather than whole cells, to minimise the likelihood of detecting cytosolic partners. Pulldown assays were initially carried out using wild-type Gpx3His and the cysteine trap mutant Gpx3C82AHis to allow for optimisation of the assay. The proteins were imported into isolated yeast mitochondria, followed by solubilisation of mitochondria under non-denaturing conditions and pulldown of His-tagged proteins plus interacting partners using Ni-NTA beads. An experimental flowchart is shown in **Figure 3.7** and described in detail in **Section 2.2.2.4**. The detergent n-Dodecyl β-D-maltoside (DDM) was chosen as it had been used in previous lab experiments where it was found to efficiently solubilise mitochondria whilst allowing the isolation of IMS complexes such as the Tim9-Tim10 complex.

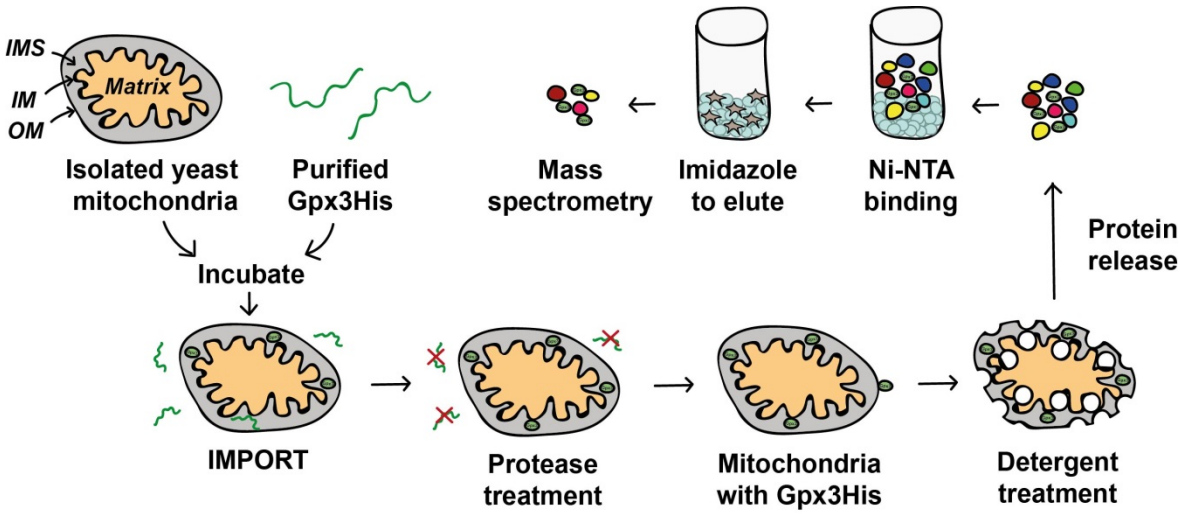

Figure 3.7. Illustration of the pulldown assay. Purified His-tagged proteins are reduced and denatured in DTT and urea, and presented to isolated wild-type yeast mitochondria under standard import conditions. Mitochondria are then treated with the protease trypsin to remove unimported His-tagged proteins before solubilisation with DDM under native conditions to solubilise the mitochondrial membranes without affecting (in theory) protein-protein interactions. Mitochondrial proteins that are released into the supernatant are the ones that have been solubilised and are then collected and passed through Ni-NTA beads. Bound proteins that remain

after subsequent wash steps are eluted using high concentrations of imidazole are putative interactors for Gpx3His and are sent for mass spectrometry analysis.

In theory, the pulldown eluates should contain mitochondrial interacting partners of Gpx3His and Gpx3C82AHis, including the His-tagged proteins themselves. However, Ni-NTA beads are known for having problems of non-specific binding of proteins; thus, the results were analysed with caution and alternative tagging methods were explored (see **Section 3.3.6**). In order to eliminate non-specifically bound proteins from the mass spectrometry data, control pulldowns whereby no His-tagged precursors were imported were performed. Any proteins detected in control eluates were removed from the list of potential interactors.

The cysteine trap mutant Gpx3C82AHis is a very specific and useful tool that was used in parallel to Gpx3 for two reasons: (i) to trap mixed disulphide intermediates which would increase the chance of detecting partners, see **Figure 3.8**; and (ii), to differentiate between partner proteins that interact with Gpx3 via intermolecular disulphide bonds vs other types of interaction that do not rely on covalent bonding, i.e. driven by mainly hydrophobic or electrostatic interactions. Although it is possible, and likely, that a combination of protein-protein interaction types occurs for each partner protein, those that interact in a transient manner may be missed when using the wild-type version of Gpx3.

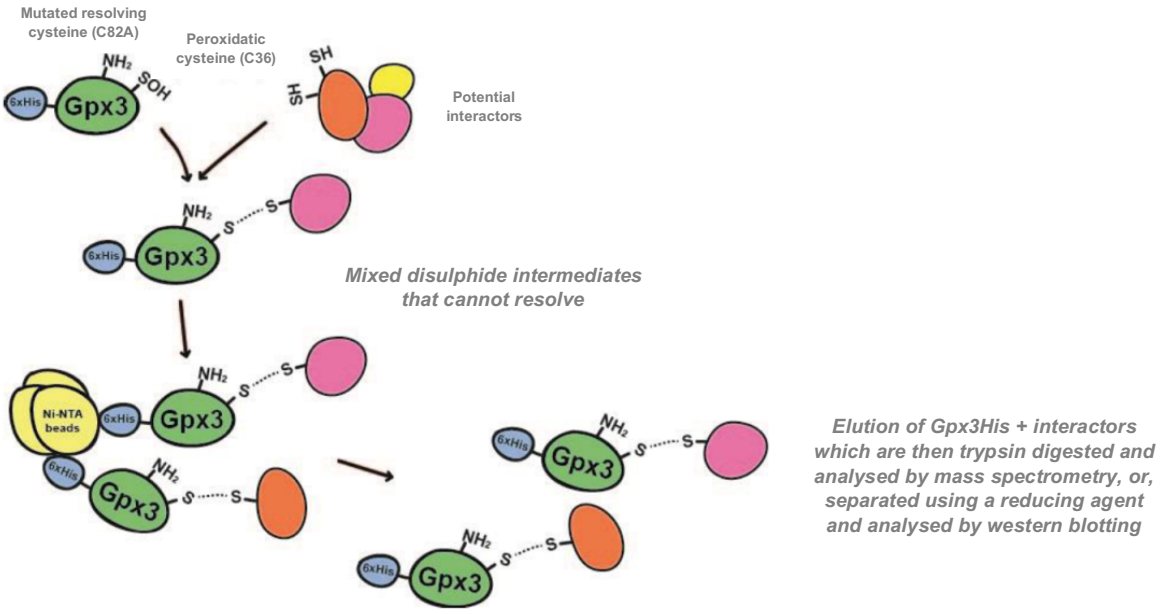

Figure 3.8. Illustration of how Gpx3C82AHis traps mixed disulphide intermediates. Potential partners of Gpx3 that interact via an initial disulphide bond with Gpx3's peroxidatic cysteine (C36) will be unable to resolve when the resolving cysteine of Gpx3 is mutated (C82A), thus they will stay trapped as mixed disulphide intermediates. In this assay, Gpx3C82AHis becomes bound to Ni-NTA beads along with its interactors which are then eluted together and either released by trypsin digestion before mass spectrometry analysis, or, separated using a reducing agent such as DTT before SDS-PAGE and western blot analysis.

Before sending samples for mass spectrometry analysis, the pulldown assay was optimised to reduce the amount of non-specific binding as after the first pulldown attempt it was clear that there was a huge number of proteins in the final eluate (**Figure 3.9**). It was first reasoned that a large proportion of these might not have been successfully removed during the wash step of the assay. Therefore, in proceeding attempts the wash step conditions were altered accordingly, with the ultimate goal to be able to reproduce specific patterns of bands in the elution lanes (detected via silver staining).

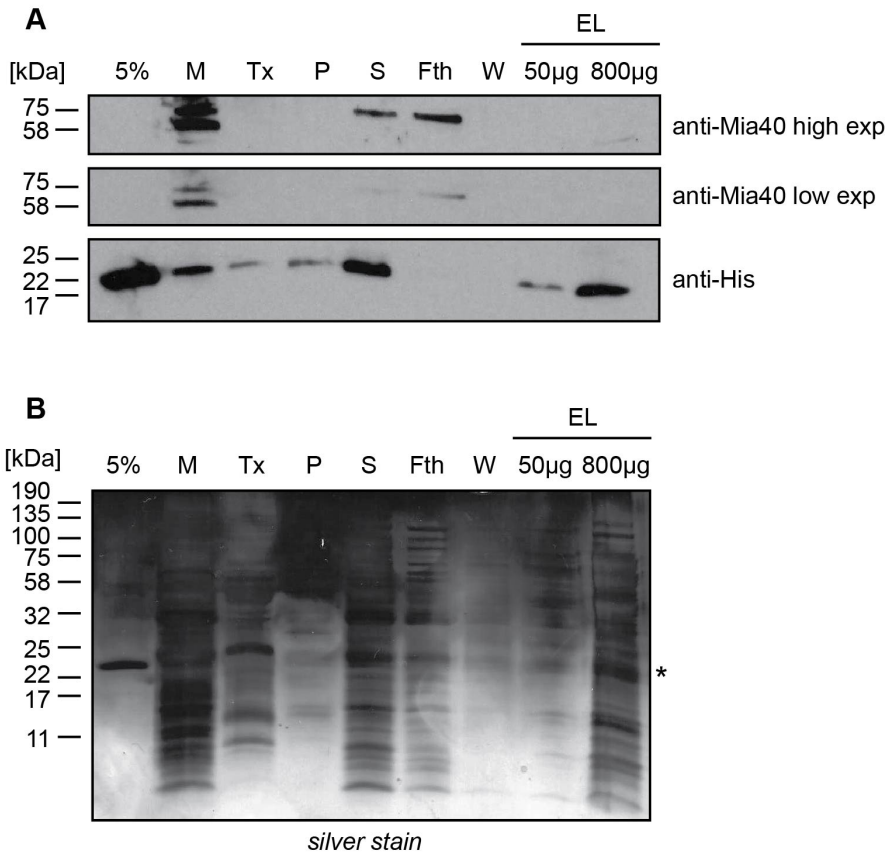

Figure 3.9. Gpx3His pulldown assay – first attempt. Gpx3His was denatured and reduced using DTT and urea before being presented to isolated wild-type yeast mitochondria under standard import conditions, followed by treatment with trypsin to remove unimported material (M) plus a control import treated with trypsin plus Triton-X-100 (Tx). Mitochondria were then solubilised in 1% DDM and separated by centrifugation into the supernatant (S), containing soluble proteins, and the pellet (P), containing membrane fragments. Soluble proteins were passed through Ni-NTA beads and a sample of unbound material from the flow through (Fth) was collected. Ni-NTA beads were washed once (W) and bound material eluted (EL) with 200 mM imidazole. (**A**) Western blot analysis of pulldown samples using anti-His to probe for Gpx3His and anti-Mia40 as a positive IMS control. 5% corresponds to 5% of the Gpx3His used for the import reaction. Each lane is equivalent to 50µg mitochondria except for the final elution lane which is equivalent to 800µg (to increase signal intensity). (**B**) Silver stain analysis of pulldown samples to detect proteins in elution lanes. * - predicated location of eluted Gpx3His.

As there were no problems with the import of the His-tagged proteins, and their binding to the Ni-NTA beads, the conditions changed were solely aimed at reducing the amount of non-specific binding. Many Gpx3His pulldowns were carried out whereby the

conditions detailed in **Table 3.1** were changed, either individually or in combination of two or more (see **Figure 3.10** for some of these attempts). Unfortunately, no matter how many conditions were changed there was still a worryingly large number of proteins detected in the eluates. Furthermore, western blot analysis showed that after only two washes, Gpx3His started to elute along with other potential interactors - in this case, Mia40. However, the fact that Mia40 was detected in both the initial pulldown (**Figure 3.9**) and during optimisation pulldowns (**Figure 3.10**), suggested that the experiment was successful at identifying interactors as it was already suspected at the time that Mia40 was an interactor of Gpx3 in the IMS (now published in Kritsiligkou et al., 2017).

	First attempt	Optimisation
Imidazole in equilibration (mM)	5	5-10
Number of washes	1	2-4
Length of washes (min)	10	10-15
Imidazole in washes (mM)	20	0-40
Imidazole in elution (mM)	200	200-300
Elution with EDTA	no	yes/no

Table 3.1. Pulldown assay optimisation conditions. 'First attempt' lists the initial equilibration, wash and elution conditions tested. 'Optimisation' shows the range of conditions tested. Refer to **Section 2.2.2.4** for full details.

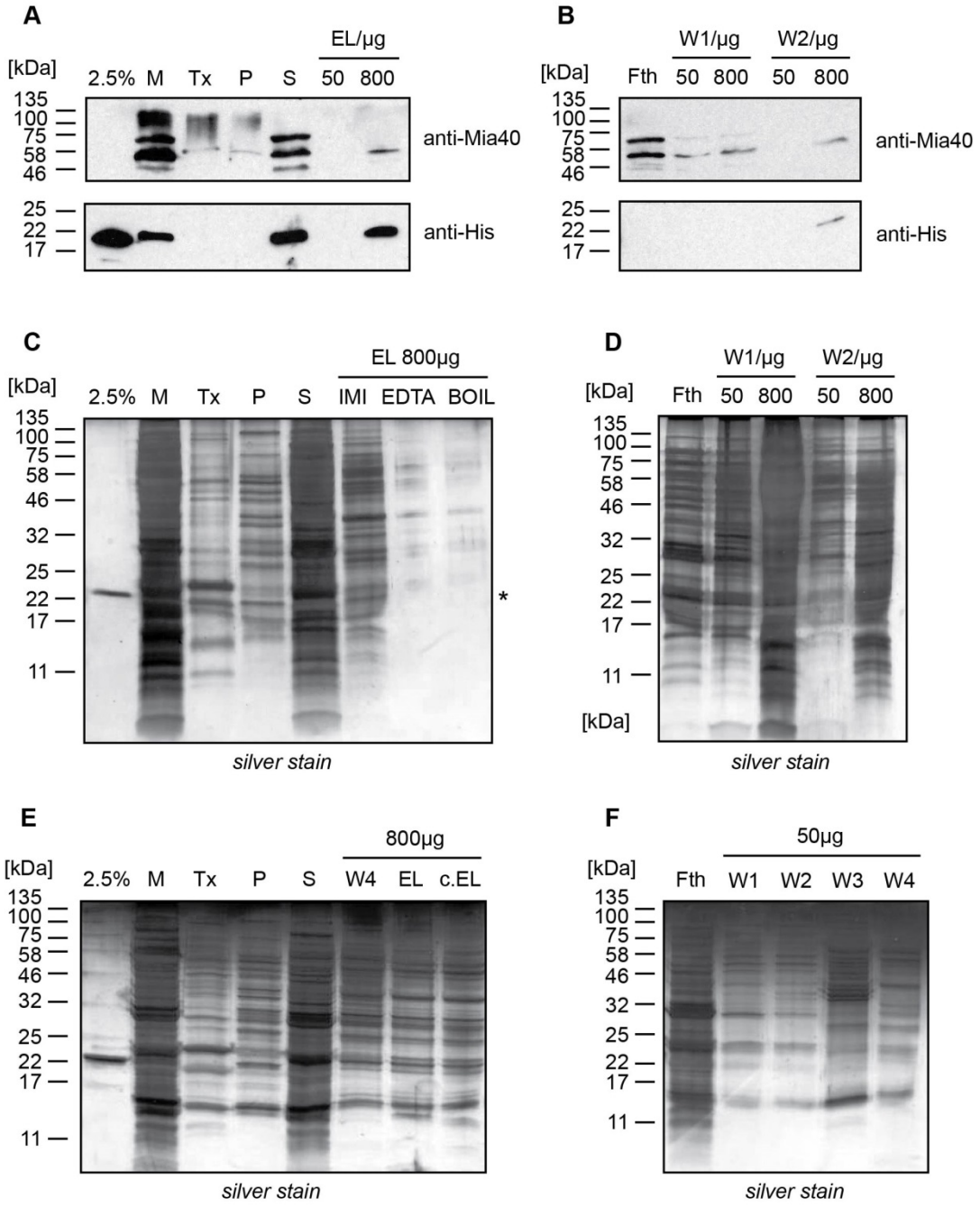

Figure 3.10. Optimisation of Gpx3His pulldown conditions. Gpx3His pulldown as previously described but with the following exceptions: (**A**, **B**, **C**, **& D**) Ni-NTA equilibration with 5 mM imidazole and an additional wash with 40 mM imidazole before an elution with 300 mM imidazole; and (**E & F**) Ni-NTA equilibration with 15 mM imidazole, wash 1 and wash 2 with 0 mM imidazole, wash 3 with 20 mM imidazole, wash 4 with 40 mM imidazole and elution with 10 mM EDTA. **A** & **B** are western blots where anti-His was used to probe for Gpx3His and anti-Mia40 as a positive mitochondrial control; **C** & **D** shows the same experiment analysed by silver staining, and with a trial elution with EDTA or boiling at 95°C. 2.5% - 2.5% of Gpx3His used for import; M – import; Tx – Triton-X-100 control; S – supernatant; P – pellet; Fth – flow through; W1-4 – washes 1-4; EL – eluates; and c.EL – control eluate (no Gpx3His import). Each lane is equivalent to 50µg

mitochondria except for some lanes which are equivalent to 800μg (to increase signal intensity). * - predicted location of eluted Gpx3His.

The final conditions were decided upon based on retaining the maximum amount of His-tagged protein and interactors, whilst removing as much non-specific material as possible (**Table 3.2**). Pulldown experiments were then carried out for both Gpx3His and the trap mutant Gpx3C82AHis, and liquid fractions (collected after the final elution) were sent for mass spectrometry analysis along with a control 'mock' pulldown – no His-tagged protein import. Any proteins detected in the control dataset were removed from the list of potential interactors. Mass spectrometry data from these and subsequent pulldowns are analysed in the next results section.

	Final
Imidazole in equilibration (mM)	5
Number of washes	2
Length of washes (min)	10
Imidazole in washes (mM)	20/40
Imidazole in elution (mM)	300
Elution with EDTA	no

Table 3.2. Final conditions after pulldown optimisation. This table lists the conditions used in pulldowns where liquid eluates were sent for mass spectrometry analysis. Refer to **Section 2.2.2.4** for full details.

3.3.4. Mass spectrometry analysis of Gpx3 pulldown eluates

Initially, two samples were sent for liquid chromatography-mass spectrometry (LC-MS) analysis to check whether proteins could be successfully identified in pulldown elutions. These two samples were from a pulldown using Gpx3C82AHis as bait, and a 'mock' pulldown where no His-tagged protein was imported. Although the hit list was small, the peptides identified were nearly all mitochondrial. Based on this, the pulldown experiments were repeated multiple times: twice using Gpx3His, thrice using Gpx3C82AHis, thrice using N18M20LGpx3His, each time alongside a 'mock' control, and a hit list was generated (**Table 3.3**, see **Section 2.2.5** for analysis criteria).

As expected from the western blot data in **Figures 3.9A and 3.10A**, Mia40 was identified in pulldowns using either Gpx3His or Gpx3C82AHis as bait. However, it was only recognised as a significant hit by the MASCOT search program (refer to analysis criteria) when Gpx3His was used. Gpx3 and Mia40 are known to be transient interaction partners and Gpx3 can re-oxidise Mia40 via its cysteine residues (Kritsiligkou et al., 2017). Interestingly, the IMS electron carrier Cytochrome *c* (Cyt*c*) was also found in nearly all datasets using both Gpx3His, Gpx3C82AHis and N18M20LGpx3His; however, it was present in 2 out of 5 control datasets *but* these datasets also contained hits for the endogenous version of Gpx3. As the mass spectrometry data could not differentiate between Cytochrome *c* isoform 1 (Cyc1) and Cytochrome *c* isoform 2 (Cyc7) due to their sequence similarity as paralogs, the term Cyt*c* is used throughout. Frustratingly, untagged Gpx3 appears to have a slight binding affinity to Ni-NTA beads which could mean that some true partner proteins are being missed as all protein hits present in the controls were removed from the list. The exception to this was Cyt*c* as it also plays a role in the MIA oxidative folding pathway along with Mia40 and Gpx3 in the IMS, and encouragingly it was not found in a control pulldown using mitochondria isolated from a *gpx3Δ* strain. Thus, further work was warranted to confirm whether Cyt*c* could indeed be a true hit. This thesis does not investigate the interaction between Gpx3 and Mia40 as ongoing work was being carried out by other members of the lab (Chatzi, Kritsiligkou and Tokatlidis, unpublished obs.).

Table 3.3. Hits identified by mass spectrometry.

Bait	Systematic name	Standard name	MW	Unique peptides	Total peptides	Total number of hits	Sequence Coverage	Description
Gpx3His	YKL192C	Acp1	13.9	1	1	1	13.6%	Acyl carrier protein (mitochondrial matrix)
Gpx3His/ N18M20Gpx3His	YFL039C	Act1	41.7	1	1	1	3.2%	Structural protein of the cytoskeleton (cytoplasm)
Gpx3His	YGR234W	Yhb1	44.6	1	1	1	4.3%	Nitric oxide oxidoreductase involved in nitrosative and oxidative stress response (cytosol, nucleus and mitochondrial matrix)
Gpx3His/ Gpx3C82AHis	YML054C	Cytb2*	65.5	6	6	6	15.1%	Cytochrome b2 (L-lactate cytochrome-*c* oxidoreductase) (IMS)
Gpx3His/ Gpx3C82AHis	YEL030W	Ecm10*	70.1	1	6	6	12.8%	Heat shock protein (Hsp70 family), localises to mitochondrial nucleoids (mitochondrial matrix)
Gpx3His/ Gpx3C82AHis	YKL195W	Mia40	44.5	1	1	1	4.0%	Component of the mitochondrial intermembrane space MIA oxidative folding pathway (IMS)
Gpx3His/ Gpx3C82AHis/ N18M20LGpx3His	YHR023W	Myo1*	22.4	2	14	31	7.8%	Type II myosin heavy chain involved in cytokinesis and cell separation (cytoplasm)
Gpx3His/ Gpx3C82AHis/ N18M20LGpx3His	YJR048W/ YEL039C	Cyc1/7**	12.2/ 12.5	1	2	2	24.8%	Cytochrome *c* isoforms 1 and 2, both involved in IMS electron transfer (IMS)
Gpx3C82AHis	YOR317W	Faa1	77.9	1	1	1	1.9%	Long chain fatty acyl-CoA synthetase (mitochondrial OM)
Gpx3C82AHis	YDR375C	Bcs1	51.1	1	1	1	3.7%	Protein translocase and chaperone involved in assembly of Complex III (mitochondrial IM)
Gpx3C82AHis/ N18M20LGpx3His	YOR201C	Mrm1	46.4	3	3	4	7.5%	Mitochondrial rRNA methyltransferase (mitochondrial matrix)

N18M20LGpx3His	YAL047C	Spc72	72.1	2	4	8	10.1%	Gamma-tubulin small complex receptor involved in astral microtubule formation and stabilisation (cytoplasm)
N18M20LGpx3His/ Gpx3C82AHis	YIL125W	Kgd1*	114.4	1	1	1	1.6%	Subunit of the mitochondrial alpha-ketoglutarate dehydrogenase complex (mitochondrial matrix)
N18M20LGpx3His/ Gpx3His	YBR244W	Gpx2*	18.4	1	3	15	19.1%	Phospholipid hydroperoxide glutathione peroxidase (cytoplasm, nucleus, mitochondrial OM and IM)
N18M20LGpx3His/ Gpx3C82AHis	YOR127W	Rga1*	112.8	2	4	21	10.1%	GTPase-activating protein (cytoplasm)
N18M20LGpx3His/ Gpx3His	YDR120C	Trm1*	64.1	3	7	8	17.5%	tRNA methyltransferase (nucleus, mitochondrial matrix)

This table includes hits that were identified as significant or *non-significant but present in multiple bait datasets from LC/MS analysis of pulldown eluates as described in **Section 3.3.3**. Mia40 was found to be significant in one dataset (Gpx3His) but non-significant in another (Gpx3C82AHis), thus those that were present in one or more dataset were included despite being deemed non-significant. Refer to **Materials and Methods**, **Section 2.2.5**, for a detailed description of how the mass spectrometry analysis was carried out. ** Cyc1/7 was included in the hit list as even though one of the peptide hits was present in a control dataset (where no His-tagged protein was used), endogenous Gpx3 was also present as it appears to have a slight affinity to bind non-specifically to the Ni-NTA beads. As both Cyc1/7 and Gpx3 are present within the IMS, and both are known to interact with Mia40 (Bien et al., 2010; Kritsiligkou et el., 2017), it is plausible that they are interactors. Where a protein was found in more than one dataset the number of unique hits, total hits and percentage sequence coverage represents the one with the most hits or the largest sequence coverage.

Apart from Mia40 and Cyt*c*, Cytochrome b2 (Cytb2) was the only other IMS protein listed in **Table 3.3**; none of the others are known to localise to the IMS. Some are found in the OM/IM which could in theory have domains that stick out into the IMS, some are cytosolic/cytoplasmic which are likely due to slight contamination in the isolated mitochondrial fractions, and some localise to the mitochondrial matrix. One explanation for matrix proteins is that during the solubilisation process to break the mitochondrial membranes, soluble proteins from the IMS and matrix are 'mixed' together, and therefore free to interact with the His-tagged Gpx3 proteins before their binding to Ni-NTA beads. The only way around this would be to isolate only the mitochondrial IMS during the solubilisation by breaking only the OM. Different concentrations of the detergent Triton-X-100 were tested but unfortunately none were successful even when a very low percentage (0.01%) was used as the matrix protein Hsp70 was present in the soluble fraction (**Figure 3.11**). Other detergents should be tested such as digitonin, DDM and CHAPS, or the OM broken by hyperosmotic shock. However, this approach will only allow partners that bind to the completely soluble Gpx3 (not the pool that associates to the membrane) and those that are soluble themselves as those that are not will not be released into the supernatant.

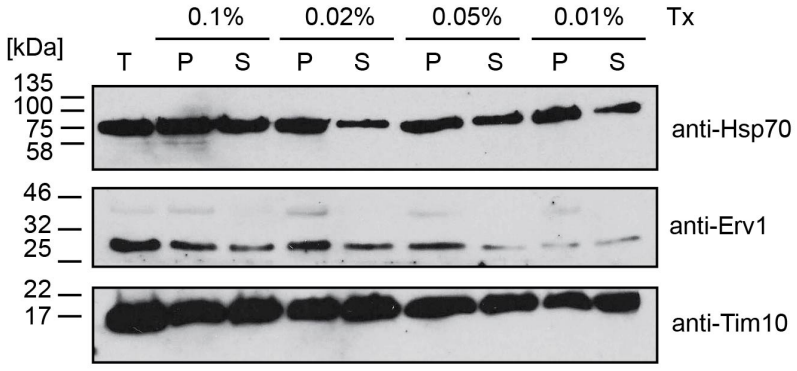

Figure 3.11. Solubilisation of mitochondrial proteins to isolate intermembrane space proteins. Isolated wild-type yeast mitochondria were solubilised in buffers containing increasing amounts of the detergent Triton-x-100: 0.01%, 0.05%, 0.02% and 0.1%. T – total mitochondrial protein before solubilisation; P – pellet fraction; S – soluble fraction. Western blots were used to probe for a soluble matrix protein (using anti-Hsp70 against mitochondrial heat shock 70 protein), and two soluble intermembrane space proteins (Erv1 - sulphydryl oxidase 1, and Tim10 – translocase of the inner membrane 10).

Most importantly though, due to the non-specific binding capacity of the Ni-NTA beads used in these pulldown assays, and the lack of reproducible hits for the majority of putative partners, alternative approaches using different tags were sought and no more samples were sent for mass spectrometry analysis. The data gathered here simply became a collection of potential hits that would act as a rudimentary starting point rather than a conclusive list of mitochondrial Gpx3 interactors, for example, Cyt*c*. Therefore, whilst work was ongoing to create different tagged versions of Gpx3, the putative interaction between Gpx3 and Cyt*c* was investigated using a combination of *in vitro* binding assays, *in vitro* interaction assays and immunoprecipitations (see **Section 3.3.5**).

Separate to the search for Gpx3 interactors, the mass spectrometry data revealed a number of proteins with unknown localisation and unknown function, some of which are very small in molecular weight. In theory, and rather excitingly, these proteins could be previously unidentified mitochondrial proteins. **Section 3.3.7** explores the mitochondrial import of two such proteins.

3.3.5. Investigating the potential interaction between Gpx3 and Cyt*c*

3.3.5.1. *In vitro* binding assays using His-tagged Gpx3 proteins

An alternative attempt to eliminate non-specific binding of non-Gpx3 interactors to Ni-NTA beads was to completely saturate the beads with purified Gpx3His, Gpx3C82AHis, N18M20LGpx3His and N18M20LGpx3C82AHis. Whilst excess His-tagged protein was binding to the beads, mitochondria were solubilised and the soluble proteins then passed over the saturated beads, washed then eluted (**Figure 3.12**). Eluates were analysed by western blotting to probe for the two suspected Gpx3 interactors - Mia40 and Cyt*c*.

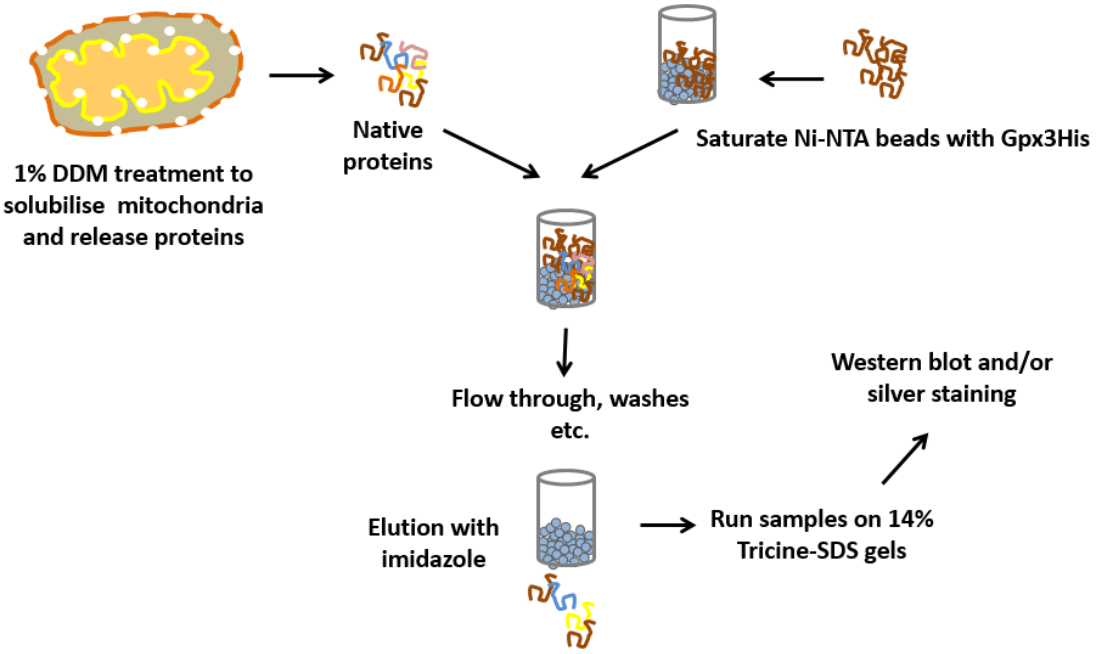

Figure 3.12. Illustration of the *in vitro* binding assay. Purified His-tagged proteins are reduced in a buffer containing DTT, or left native, and presented in excess to Ni-NTA beads. In parallel, mitochondria are solubilised with 1% n-Dodecyl β-D-maltoside (DDM) to break the mitochondrial membranes under native conditions. Mitochondrial proteins that are released into the supernatant are collected and passed through Ni-NTA beads. Bound proteins that remain after subsequent wash steps are eluted using high concentrations of imidazole and analysed by western blotting and/or silver staining.

The results from this assay provide further evidence that Mia40 is an interactor of Gpx3 as Mia40 co-eluted with Gpx3His (**Figure 3.13B**), Gpx3C82AHis (**Figure 3.13G**) and N18M20LGpx3C82AHis (**Figure 3.13G**). However, Mia40 did not always co-elute/the band detected was extremely faint (**Figures 3.13C, 3.13D & 3.13E**) which suggests that its interaction with Gpx3 may be transient. Cyt*c* was very rarely detected (**only Figure 3.13B**) despite a vast abundance of both Gpx3 and Cyt*c* in each assay. It could be that this *in vitro* assay does not represent the physiological conditions required for an interaction between Gpx3-Cyt*c* and/or the interaction is transient, or that they are not true partners. Neither Mia40 nor Cyt*c* were present in 'mock' assays where no His-tagged protein was bound to Ni-NTA beads prior to the addition of soluble mitochondrial proteins. Another possibility is that an interaction between Gpx3 and Cyt*c* might occur when both are associated with the IM of mitochondria, and thus they are unable to interact in this assay as membrane proteins are retained in the insoluble pellet fraction. As can be seen in **Figure 3.13A**, Cyt*c* is found both in the pellet and supernatant fractions after solubilisation.

Interestingly, in the repeat experiment shown in **Figure 3.13G** Thioredoxin 1 (Trx1, a small protein found in both the cytosol and the IMS) co-eluted with the extended cysteine trap mutant, N18M20LGpx3C82AHis. This was a serendipitous finding as the antibody against Trx1 was only used as an extra control. However, it would make sense as Trx1 in the cytosol is important in recycling Gpx3 when Gpx3 becomes disulphide bonded upon stress. This finding could be of importance if it can be confirmed by additional methods, such as by isothermal titration calorimetry (ITC), a method which has previously been used to analyse the interaction between Gpx3 and Mia40 (Chatzi, Kritsiligkou and Tokatlidis, unpublished obs.). This would lend additional support to a functional role of Gpx3 in the IMS. In **Chapter 5**, **Section 5.3.4**, a similar result was found when *in vitro* binding assays were carried out with solubilised peroxisomal proteins.

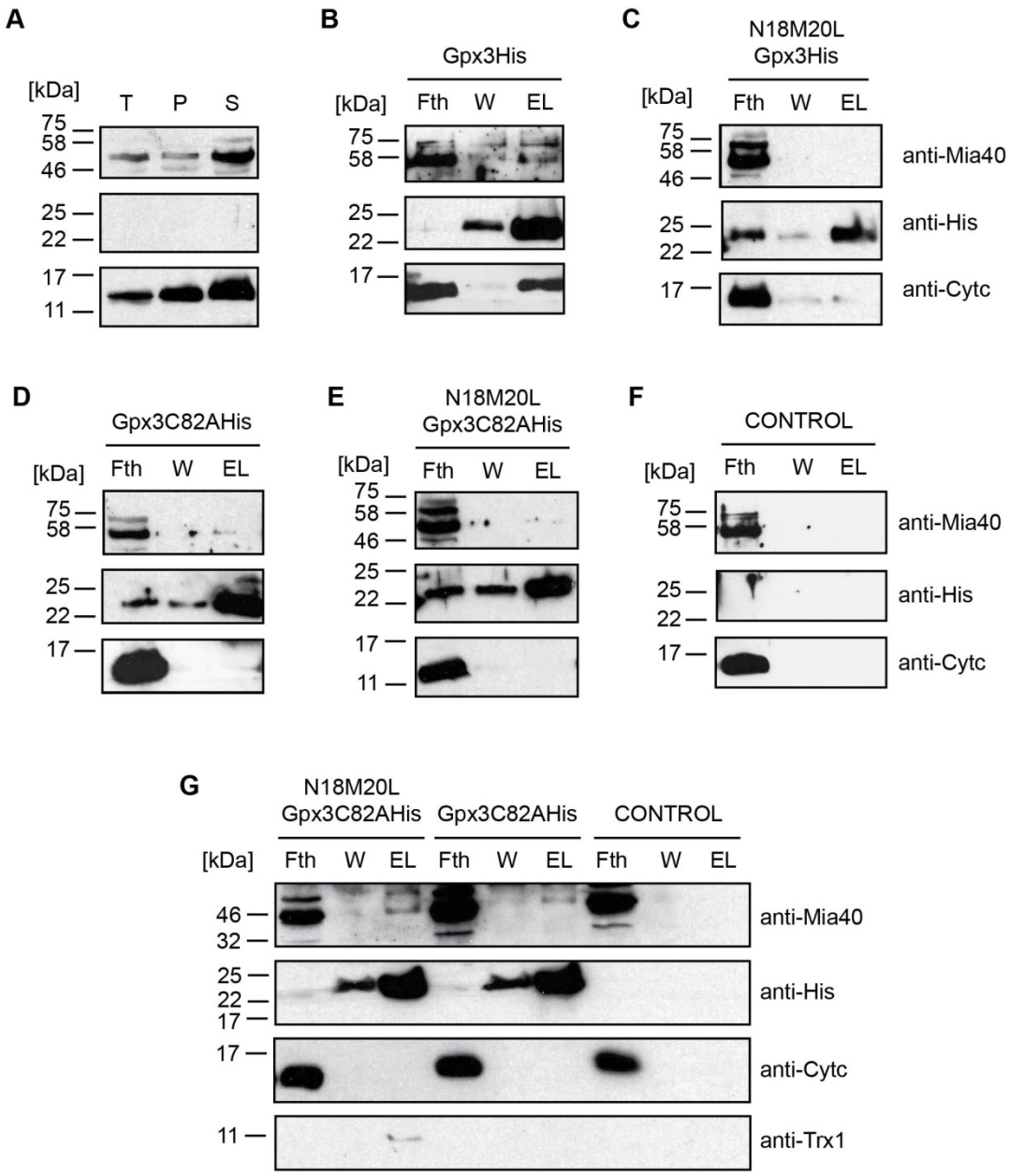

Figure 3.13. *In vitro* binding assays to detect Gpx3 interactors. *In vitro* binding assays using His-tagged versions of Gpx3. (**A**) Solubilisation of isolated wild-type yeast mitochondria using 1% DDM. T – total mitochondrial protein; P – pellet fraction; S – soluble fraction. The purified proteins Gpx3His (**B**), N18M20LGpx3His (**C**), Gpx3C82AHis (**D & G**) and N18M20LGpx3C82AHis (**E & G**), and Gpx3C82AHis (**E & G**), were bound to Ni-NTA beads and mitochondrial proteins from the soluble fraction shown in **A** were passed over. Unbound material can be seen in the flow throughs (Fth) and co-eluted material in the eluates (EL). W – indicates the third and final wash before elution with imidazole. (**F**) CONTROL – control assay where no His-tagged protein was bound to Ni-NTA beads prior to addition of mitochondrial proteins. NOTE: **G** is a repeat of **D**, **E** and **F**. Western blots were probed using anti-His against all His-tagged proteins and anti-Mia40 and anti-Cyt*c* against the putative interactors Mia40 and Cyt*c*. Anti-Trx1 (against Thioredoxin 1) was used as an additional IMS control in **G**.

3.3.5.2. Reciprocal *in vitro* binding assay using Cyt*c*His

CYC1, the gene encoding Cytochrome *c* isoform 1, was cloned into a pET-24 vector which contains a C-terminal sequence for a 6xHis tag. To purify the protein, pET-24/*CYC1* was transformed into DE3 *E. coli*, induced using IPTG, and purified from the soluble fraction using Ni-NTA beads following the same protocol used for Gpx3His (**Figure 3.14A**). A reciprocal *in vitro* binding assay was then carried out using Cyt*c*His bound to Ni-NTA beads instead of Gpx3His, and endogenous Gpx3 was detected in the eluate fraction (**Figure 3.14B**). No Gpx3 was found in the eluate from the control 'mock' assay (**Figure 3.14C**). These data suggest that Gpx3 and Cyt*c* can interact *in vitro* as recombinant proteins.

Unfortunately, attempts to repeat this assay to confirm the result were hindered by the fact that the purified Cyt*c*His protein aggregated within a few days of purification. We concluded that the purification method used was not suitable to obtain a fully folded Cyt*c*His protein as the protein is known to be prone to aggregation when it lacks its heme prosthetic group. Instead, Cyt*c* was obtained from Sigma-Aldrich in a lyophilised form which was resuspended into buffers suitable for performing *in vitro* interaction assays with Gpx3. This version of Cyt*c* lacks a tag and therefore could not be used to repeat the *in vitro* binding assay.

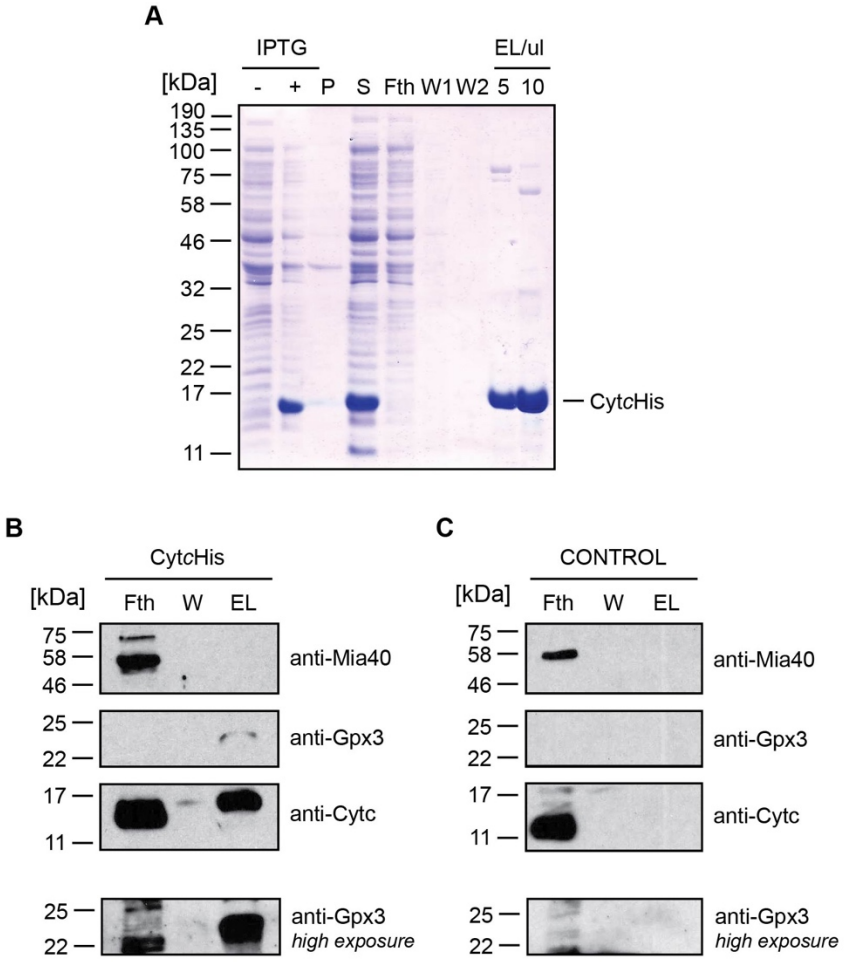

Figure 3.14. Purification of Cyt*c*His and *in vitro* binding assay to detect Cyt*c* interactors. (**A**) Cyt*c*His was purified from the supernatant fraction of IPTG-induced DE3 *E. coli* cells after transformation and expression of a pET-24/*CYC1* plasmid. Cells were induced with 0.4 mM IPTG for 4 hours at 37°C. Coomassie stained SDS-PAGE gel; samples loaded with β-me. –IPTG – no induction; +IPTG – induction/protein expression; P – pellet; S – supernatant; Fth – flow through; W1 – wash 1; W2 – wash 2; EL – eluate. (**B**) *In vitro* interaction assay using Cyt*c*His saturated to Ni-NTA beads. Soluble mitochondrial proteins were passed over and unbound material removed in the flow through (Fth). Beads were washed three times (W – third and final wash) before elution with imidazole (EL). (**C**) CONTROL – control assay where no His-tagged protein was bound to Ni-NTA beads prior to the addition of mitochondrial proteins. Western blots were probed using anti-Cyt*c*, anti-Gpx3 and anti-Mia40 to detect Cyt*c*His (and the endogenous Cyt*c*), Gpx3 and Mia40.

3.3.5.3. *In vitro* interaction assays between Gpx3 and Cyt*c*

To further investigate Cyt*c* as a potential interactor of Gpx3, *in vitro* interaction assays were carried out using purified Gpx3His and Cyt*c* (purchased from Sigma-Aldrich). As nothing was known about the redox state of either protein during their potential interaction, Gpx3His was either oxidised or reduced prior to incubation with Cyt*c* that had been reduced or oxidised respectively (**Figure 3.15**). This assay indicates a strong physical interaction between the two as a suspected mixed intermediate with a molecular weight shift compatible with one Gpx3 monomer and one Cyt*c* monomer was found. Western blotting confirmed a Gpx3-Cyt*c* intermediate as both antibodies (anti-Gpx3 and anti-Cyt*c*) detected the same band of around 32 kDa (**Figure 3.16**). This interaction was independent of whether Gpx3/Cyt*c* was oxidised or reduced prior to their incubation together. This result is interesting but we do not yet have an explanation for this interaction. It is worthwhile pursuing in the future given the importance of Cyt*c* in the oxidative folding pathway and in lipid peroxidation in mitochondria.

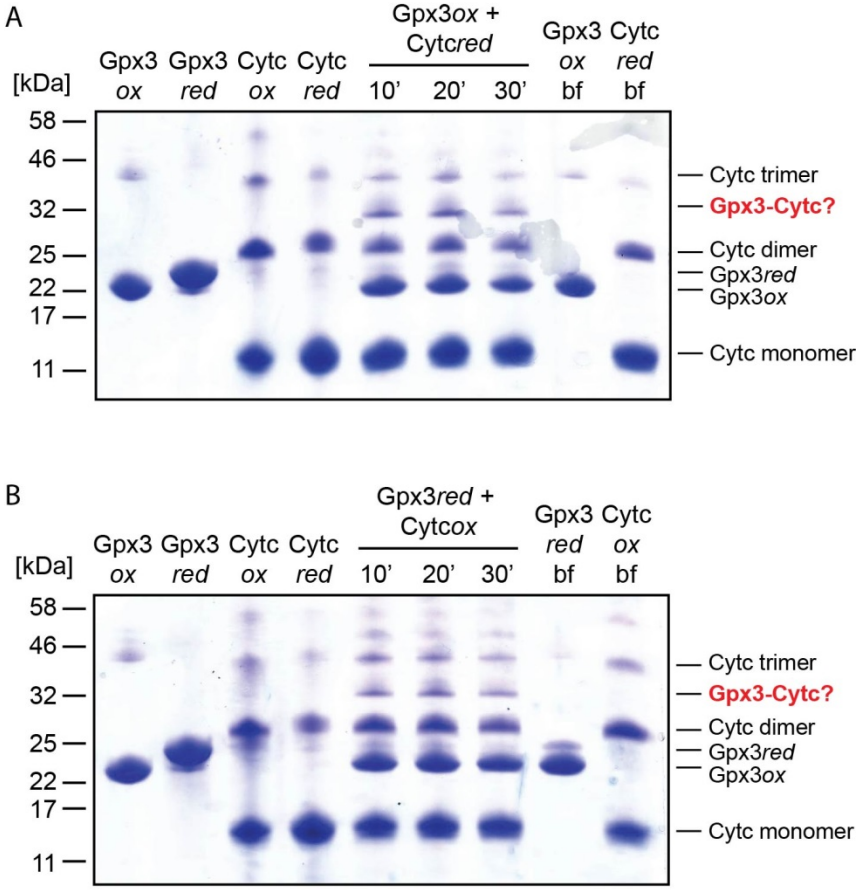

Figure 3.15. Gpx3 interaction with Cyt*c* *in vitro*. (**A**) *In vitro* interaction between Gpx3His oxidised (Gpx3*ox*) and reduced Cyt*c* (Cyt*cred*). (**B**) *In vitro* interaction between Gpx3*red* and Cyt*cox*. Images shown are coomassie stained SDS-PAGE gels. Gpx3/Cyt*c* were oxidised with 10 μM H_2O_2 for 30 mins or reduced with 20 mM DTT for 30 mins. The first four lanes show the oxidised/reduced proteins before their incubation together. bf – controls where the oxidised/reduced proteins were incubated alone in the reaction buffer for 30 mins. Proteins were incubated together and the reactions stopped after 10 mins, 20 mins and 30 mins. AMS was used in all samples to detect shifts in redox state.

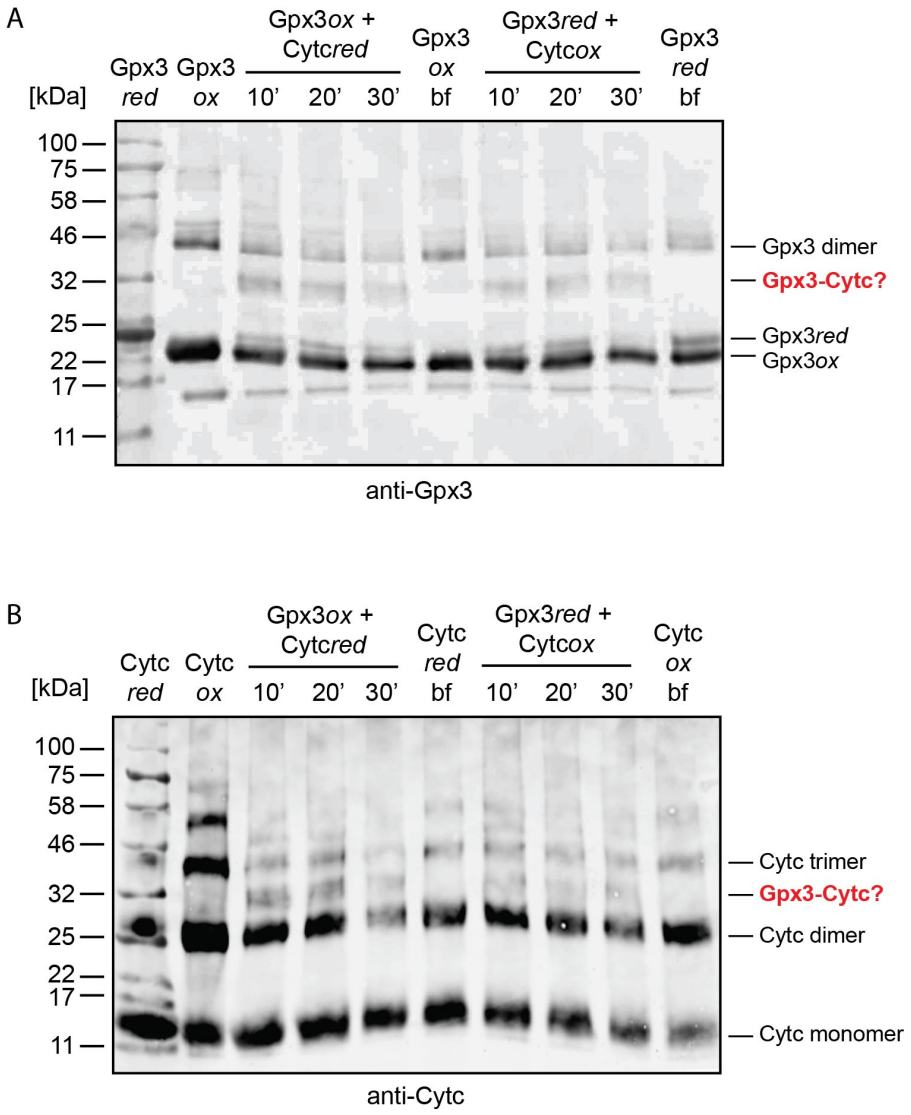

Figure 3.16. Confirmation of a mixed intermediate between Gpx3-Cyt*c* *in vitro*. Western blots using antibodies against Gpx3 (anti-Gpx3) and Cyt*c* (anti-Cyt*c*) to confirm the suspected mixed intermediate between one Gpx3 monomer and one Cyt*c* monomer in both the *in vitro* interaction assays using (**A**) Gpx3*ox* and Cyt*cred* and (**B**) Gpx3*red* and Cyt*cox*. NOTE: Markers were accidentally loaded in the same lane as the first samples which were detected by the secondary antibody.

Rather than observing the presence of a mixed intermediate between Gpx3-Cyt*c* in this assay, it was expected that the results would be interpreted by changes in redox state during incubation. However, this proved challenging in this experiment for two reasons: (i) in **Figure 3.15B**, Gpx3 becomes oxidised in the buffer alone control, and (ii) the difference between oxidised and reduced Cyt*c* is difficult to see as the difference in molecular weight after AMS treatment is minimal. Therefore, it is unknown whether the mixed intermediate is the result of oxidised Gpx3 (that formed during the incubation time) interacting with Cyt*c* (of unknown redox state), rather than the initial reduced Gpx3.

As it could not be determined whether the reduction of Cyt*c* using 20 mM DTT for 30 minutes was enough to reduce the protein, attempts to reduce Cyt*c* were carried out using varying concentrations of DTT or β-mercaptoethanol. The results were not conclusive as shifts were still difficult to detect in each case (**Figure 3.17**).

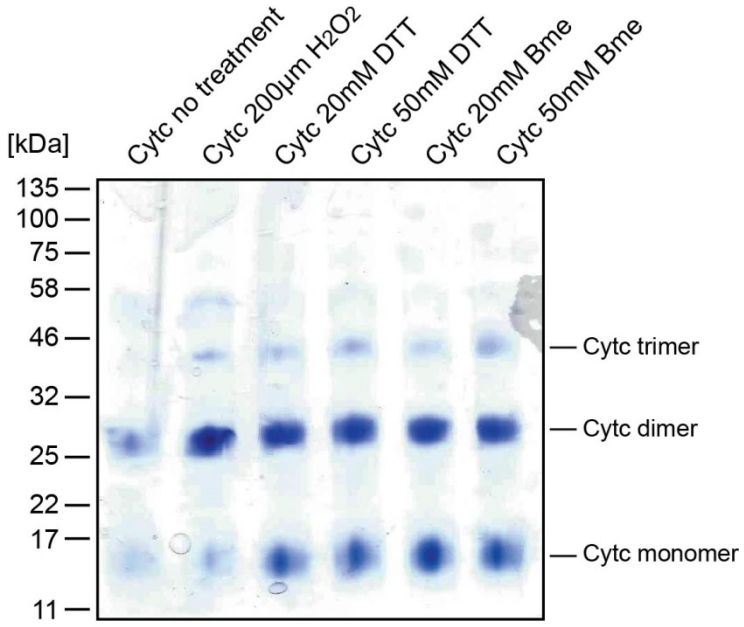

Figure 3.17. Reduction of Cyt*c* *in vitro*. Purified Cyt*c* (Sigma-Aldrich) was subjected to the following treatments: 200 μM H_2O_2, 20 mM DTT, 50 mM DTT, 20 mM β-me, and 50 mM β-me. The first lane shows Cyt*c* in its native form, i.e. after resuspension in 50 mM HEPES-KOH pH 7.4. No differences can be seen between the un-treated, oxidised or reduced samples. Monomers, dimers and trimers are detected in all samples.

Next, to test whether the interaction between Gpx3-Cyt*c* is dependent upon a mixed disulphide bond, single cysteine mutants of Gpx3 (Gpx3C32SHis, Gpx3C64S and Gpx3C82AHis) were incubated with Cyt*c*. Note that the only cysteines known to be involved in Gpx3 disulphide bond formation are its peroxidatic cysteine (C32) and its resolving cysteine (C82); no function for C64 has been reported despite its location within a highly conserved hydrophobic region (**Figure 3.18**). Surprisingly, the only cysteine mutant that had an effect on the Gpx3-Cyt*c* mixed intermediate was C64S (**Figure 3.19**). As this cysteine residue is not known to be involved in disulphide bond formation, we thought that the C64S mutation might be causing a change in protein structure/folding that could be affecting a hydrophobic interaction between Gpx3-Cyt*c*, as the cysteine residue C64 lies within a hydrophobic region.

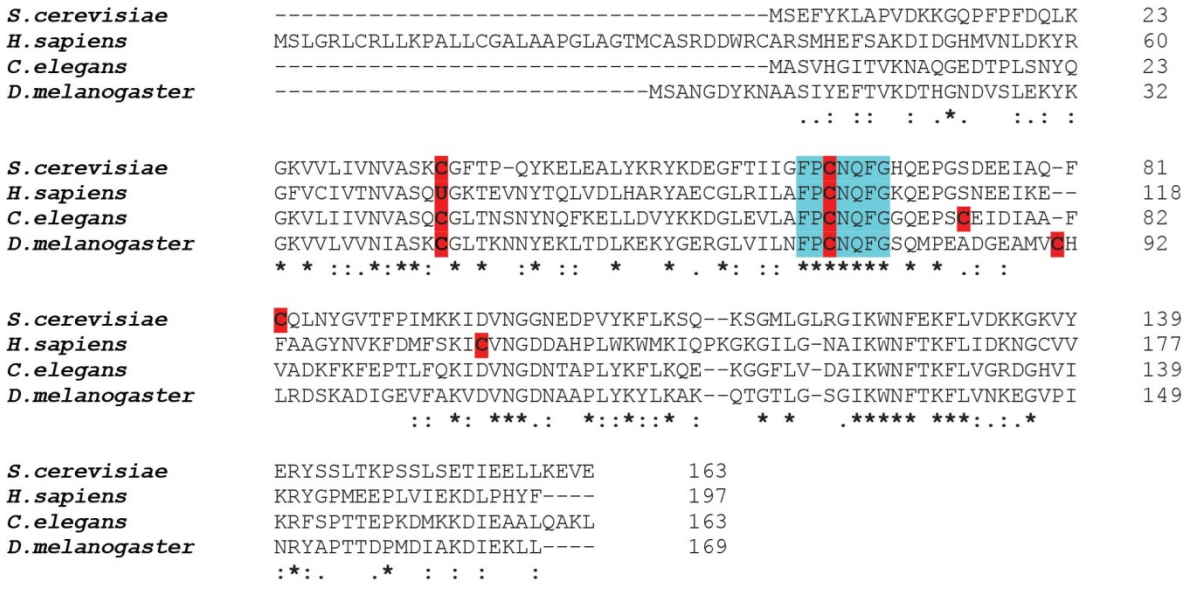

Figure 3.18. *S. cerevisiae* Gpx3 multiple sequence alignment. Clustal Omega (Version 1.2.4) was used to align Gpx3 homologs from *Saccharomyces cerevisiae* (Gpx3), *Caenorhabditis elegans* (Gpx-2), *Drosophila melanogaster* (PHGpx), and *Homo sapiens* (GPX4).* (asterisk) – single, fully conserved residue. : (colon) – conservation between groups of strongly similar properties. . (period) – conservation between groups of weakly similar properties. Red residues include Cysteines (including U for selenocysteine in GPX4). Blue residues show the conserved hydrophobic region in which the C64 of Gpx3 sits.

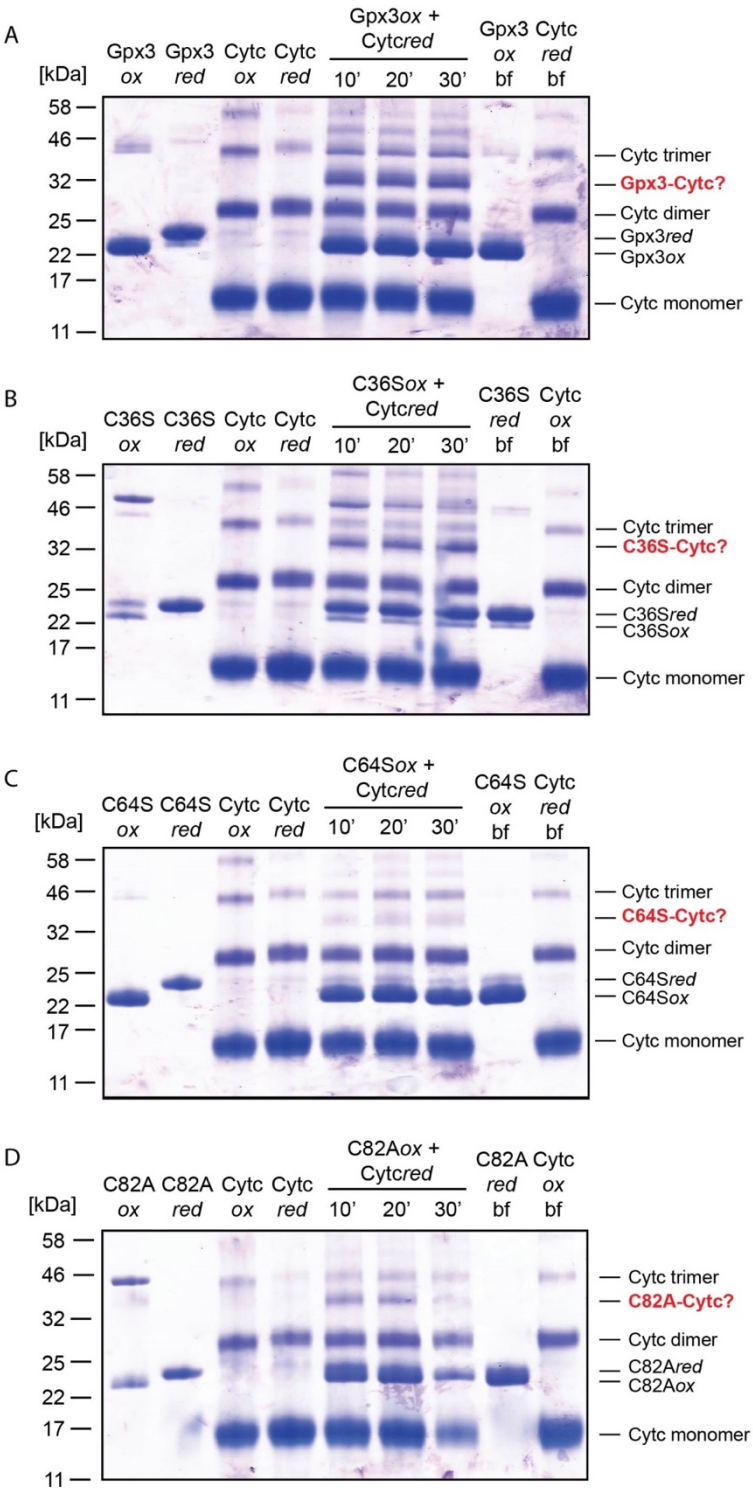

Figure 3.19. Gpx3 single cysteine mutant interactions with Cyt*c* *in vitro*. Coomassie stains showing *in vitro* interaction assays between His-tagged Gpx3 cysteine mutants and Cyt*c* ((**A**) Gpx3ox and Cyt*c*red, (**B**) Gpx3C36Sox and Cyt*c*red, (**C**) Gpx3C64Sox and Cyt*c*red, and (**D**) Gpx3C82A*ox* and Cyt*cred*) for 10 mins, 20 mins and 30 mins. All Gpx3 variants were oxidised with 10 μM H_2O_2 for 30 mins; Cyt*c* was reduced with 20 mM DTT for 30 mins. The first four lanes show the oxidised/reduced proteins before their incubation together. bf – controls where the oxidised/reduced proteins were incubated alone in the reaction buffer for 30 mins. AMS was used in all samples to detect shifts in redox state.

To investigate this idea, circular dichroism (CD) spectroscopy was used to assess the structure of Gpx3His and all three cysteine mutants (**Figure 3.20**). The far UV spectra shown in **Figure 3.20A** indicates that all four proteins contain the expected β-sheet and α-helices of Gpx3, and that their secondary structures do not appear to be hugely affected by any of the single cysteine mutants. However, there are some slight differences as the red and pink lines indicating Gpx3C36SHis and Gpx3C82AHis respectively do not precisely follow those of Gpx3His (blue) and Gpx3C64SHis (green). This is likely attributable to the fact that C36 and C82 are involved in forming the intramolecular disulphide bond in Gpx3 which, when absent, may affect the stability of its secondary structure. The near UV spectra shown in **Figure 3.20B** indicates more subtle differences in their tertiary structures. Based on this data, it remains unclear why the C64S cysteine mutant is the only one that affects the interaction between Gpx3 and Cyt*c*.

Furthermore, the interaction between Gpx3 and Cyt*c* does not appear to be affected by the presence of the reducing agent β-mercaptoethanol, increasing concentrations of NaCl (which generally affect electrostatic interactions) or changes to temperature (which generally affect hydrophobic interactions) (data not shown).

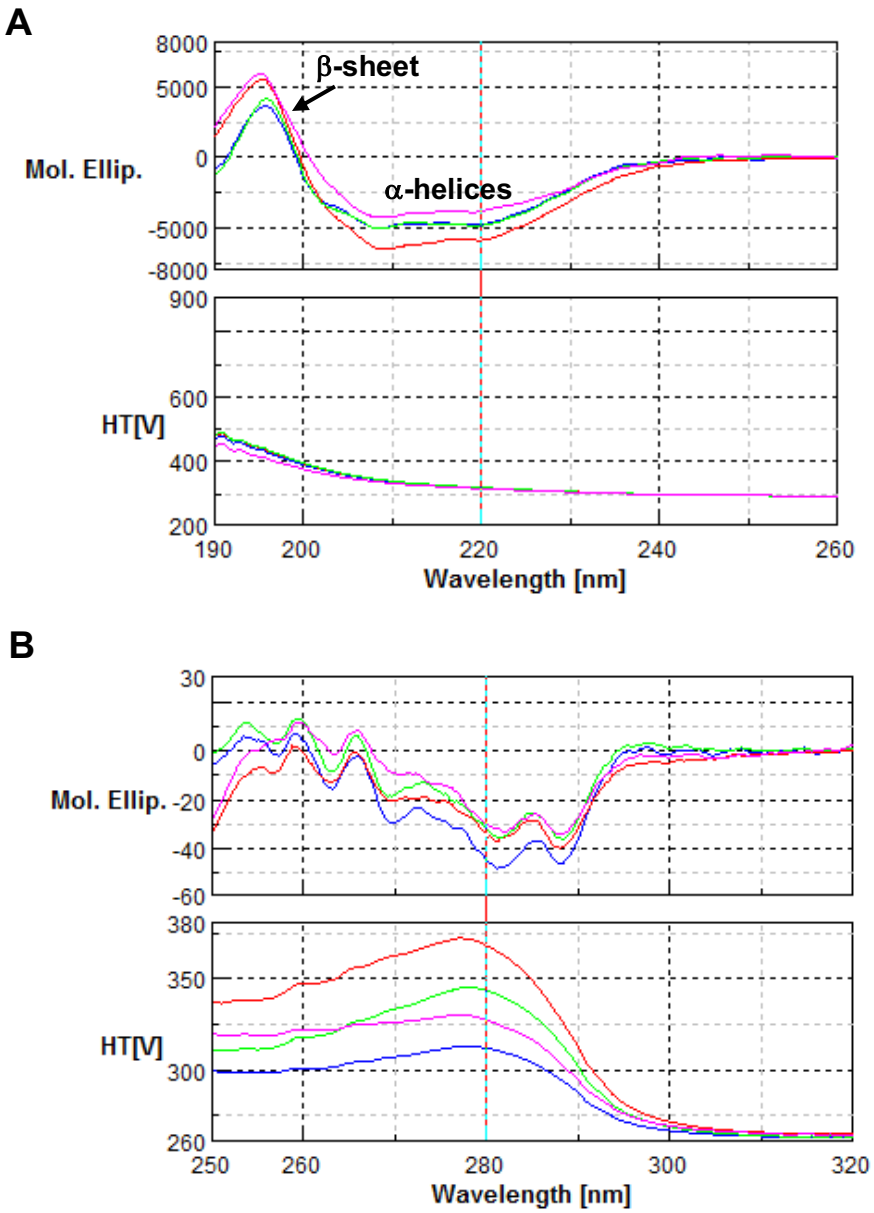

Figure 3.20. CD spectra of Gpx3 cysteine mutants. (**A**) Far UV CD spectra of Gpx3His (blue), Gpx3C36SHis (red), Gpx3C64SHis (green) and Gpx3C82AHis (pink). A 0.02cm pathlength quartz cuvette was used to measure spectra and corrected for concentration. (**B**) Near UV CD spectra of Gpx3His (blue), Gpx3C36SHis (red), Gpx3C64SHis (green) and Gpx3C82AHis (pink). A 0.2cm pathlength quartz cuvette was used to measure spectra. All spectra were corrected for cell pathlength, buffer effect and protein concentration. Mol. Ellip – molar ellipticity; HT – high tension.

3.3.5.4. Immunoprecipitations to detect Gpx3-Cyt*c* *in organello*

The assays in **Sections 3.3.5.1 - 3** were all aimed at characterising the interaction between Gpx3 and Cyt*c* *in vitro*. However, in order to provide convincing evidence that there is a physiological relevance to a Gpx3-Cyt*c* interaction it must be confirmed *in organello*/*in vivo*. Various protein complex immunoprecipitation (Co-IP) protocols were tried using isolated wild-type yeast mitochondria: (i) solubilisation of mitochondria followed by Co-IPs using either anti-Cyt*c* or anti-Gpx3 to detect endogenous protein interactions; and (ii) import of radiolabelled Gpx3 or Cyt*c* followed by solubilisation of mitochondria and Co-IPs using anti-Cyt*c* or anti-Gpx3, respectively.

The first method was unsuccessful due to the strong cross-reactivity of the secondary antibody with the precipitating heavy chain antibodies (from the primaries) – both primary antibodies were raised in rabbits and thus required the same secondary anti-rabbit. Therefore, we could not tell whether there was a signal for either Gpx3 or Cyt*c* in the eluates as any signal would have been masked (data not shown). To circumvent this, the second approach involved importing radioactive Gpx3 or Cyt*c* prior to the Co-IPs so that their signals could instead be visualised by autoradiography thus eliminating antibody cross-reactivity. After import, mitochondria were solubilised in 0.16% DDM followed by the addition of either anti-Gpx3, anti-Cyt*c*, pre-immune serum (PI) or nothing (control). After two hours, pre-equilibrated protein A beads (pA) were added and left to bind for a further hour. Unbound material was then washed off and the remaining proteins eluted using a combination of boiling, vortexing and centrifuging (refer to **Section 2.2.2.5** for detailed methodology). However, neither Gpx3 or Cyt*c* could be detected co-eluting with each other using this method (data not shown). One explanation could be that the amounts of radiolabelled protein interacting with any endogenous proteins are too low to be detected thus a positive control is required. Due to the time limitations of this study, the IP protocol was not successfully optimised and no conclusive results were gathered from these experiments. It was always imperative that a combination of methods was kept in the pipeline which is why different tagging/pulldown methods were also pursued throughout the project – these are discussed in the next section.

3.3.6. Alternative tags

Due to consistently high levels of non-specifically bound proteins when binding His-tagged proteins to Ni-NTA beads, two different approaches were sought: a yeast strain endogenously expressing a Gpx3-TAP fusion protein, and expression of a V5-tagged Gpx3 recombinant protein in yeast from a transformed plasmid. Both of these methods differ from the ones previously described in this chapter as they are *in vivo* techniques that, in addition to hopefully removing unwanted false positive interactors, are much more representative of the physiological conditions within yeast.

3.3.6.1. Gpx3-TAP

The first method is a two-step affinity purification that relies on the binding of the Gpx3-TAP to Immunoglobulin G (IgG) beads, followed by cleavage of the TAP tag with the Tobacco Etch Virus (TEV) protease to release Gpx3 along with protein partners. As the TAP tag also consists of Protein A and a calmodulin-binding peptide (CBP) which is not cleaved by the TEV protease, the cleaved Gpx3-TAP can then re-bound to a Calmodulin resin. After a few wash steps, Gpx3 and its interactors can be eluted using ethylene glycol-bis(β-aminoethyl ether)-N,N,N',N'-tetraacetic acid (EGTA).

One main caveat of this method is that the TAP tag itself is large in size at 21 kDa; Gpx3 is only 19 kDa. Therefore, two problems might exist: (i) the TAP tag interferes with the interaction of partner proteins with Gpx3, and/or (ii) the TAP tag prevents mitochondrial import. Thus, the starting point was to test whether Gpx3-TAP was present within mitochondria isolated from a yeast strain expressing an endogenously C-terminally TAP-tagged version of Gpx3 (strain purchased from GE Healthcare). Unfortunately, only a very small amount of Gpx3-TAP could be detected in isolated mitochondria (**Figure 3.21**) which suggests the TAP tag is affecting the import of Gpx3 into mitochondria. This method was no longer pursued as it is crucial that Gpx3 is within the IMS in a high enough amount in order to identify mitochondrial interactors. Instead, a smaller V5 tag was selected to try to alleviate this problem.

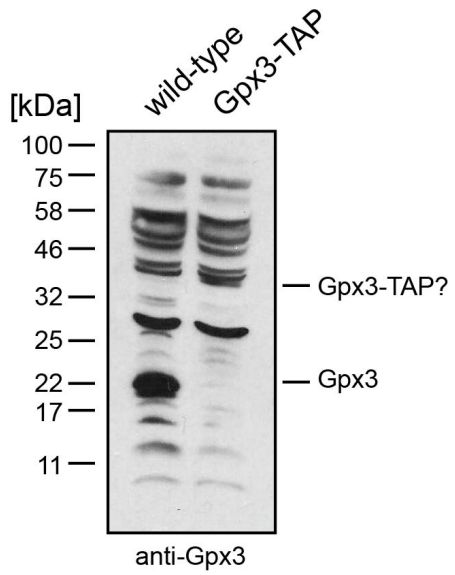

Figure 3.21. Mitochondria isolated from a Gpx3-TAP yeast strain vs wild-type mitochondria. Mitochondria were isolated from both Gpx3-TAP and wild-type BY4741 yeast, and 100μg samples were loaded onto an SDS-PAGE gel followed by western blotting using anti-Gpx3. Endogenous Gpx3 (19 kDa) can be detected in wild-type mitochondria, but it is unclear whether Gpx3-TAP (40 kDa) is found within mitochondria as only one weak band was detected in Gpx3-TAP that was not present in the wild-type lane. NOTE: there are lots of non-specific bands present in the western blot when using anti-Gpx3. Anti-TAP did not detect any differences between the two (data not shown).

3.3.6.2. Gpx3-V5

The V5 tag was chosen next due to its small size of only 14 amino acids, adding roughly 1.4 kDa in molecular weight. This is substantially smaller than the 21 kDa TAP tag previously tried, and only marginally larger than the 6xHis tag at 1 kDa which has been successfully used before. Therefore, the V5 tag is unlikely to interfere with mitochondrial import. Upon successful import of Gpx3-V5, the next step would be to perform a pulldown assay whereby an Anti-V5 Agarose Affinity Gel (Sigma) is used instead of Ni-NTA beads. The gel is made up of agarose beads conjugated to a monoclonal anti-V5 antibody which allows Gpx3-V5 to bind along with its interactors.

As an endogenously expressing Gpx3-V5 yeast strain does not exist, a yeast expression plasmid (pSF-*TEF1*-COOH-V5, Oxford Genetics) was obtained and attempts to insert the *GPX3* gene to the 5' side of the V5 sequence were made. Unfortunately, these clonings were not successful within the timeframe of this thesis and further optimisation of the cloning protocol is required. When successful, the plasmid will be transformed into *gpx3Δ* yeast to allow for constitutive expression of Gpx3-V5 from the strong TEF1 promoter present within the plasmid, without the presence of endogenous un-tagged Gpx3. If Gpx3-V5 is found to localise within the mitochondrial IMS, then pulldowns will be performed using isolated mitochondria and samples sent for mass spectrometry analysis.

3.3.7. Import of Ybr124w and Ypl107w

When searching the mass spectrometry data in **Section 3.3.4**, we uncovered a number of small proteins with unknown functions and localisations which could be of interest to general mitochondrial proteome studies (**Table 3.4**). Although none of these were putative Gpx3 interactors (with the exception of one, Ypl107w), it was still interesting to pursue their potential mitochondrial localisation. Small proteins are often missed during mass spectrometry analysis due to their small fragment sizes and limited cleavage by trypsin, and new proteins are continually being added to the mitochondrial proteome.

Table 3.4. Potential mitochondrial proteins based on mass spectrometry analysis of mitochondria isolated from *S. cerevisiae*.

Standard name	Systematic name*	MW (kDa)	Cysteine motifs	Description	Human homolog
-	Ybr124w	13.2	…CX_3C…CX_9C…	Unknown	No
-	Ydr193w	13.7	None	Unknown	No
-	Ygl024w	12.2	…$CX_5CX_{13}CX_{16}C$…	Unknown	No
-	Yor293c-a	6.1	None	Unknown	No
-	Ypl107w	28.6	…CCX_3CX_2C…	Unknown	hOXLD-1
-	Ypr010c-a	7.9	None	Unknown	No

*Reserved name agreed upon by the yeast community (SGD). Human homologs were searched for using BLASTP (NCBI). No standard names had been given to these proteins when the mass spectrometry data was analysed in 2015. MW – molecular weight in kDa.

Three of these proteins were chosen for further investigation based on the presence of cysteine motifs which could act as mitochondrial targeting signals and/or be important redox motifs: Ybr124w, Ygl024w and Ypl107w. Ybr124w is a 119 amino acid (aa), 13 kDa protein of unknown function which is inviable when knocked out, although this is probably due to its overlap with an essential gene located on the opposite strand. It also contains a potential transmembrane domain (UniProtKB entry - P38269). A MITOPROT

prediction gives a score of 0.07 (7%) probability that it is targeted to mitochondria. Ybr124w is conserved across *Saccharomyces* species. Ygl024w is a non-essential 111aa, 12 kDa protein of unknown function with a MITOPROT score of 0.39 (39%), and is predicted to be a membrane protein based on sequence analysis (UniProtKB entry - P53190). No homologs exist. Ypl107w is a non-essential 248aa, 29 kDa protein with a highly conserved oxidoreductase-like domain (see InterPro entry IPR019180/Pfam entry PF09791), and a MITOPROT score of 0.92 along with a predicted a 26-amino acid N-terminal cleavable presequence. Its human homolog is hOXLD-1, oxidoreductase-like domain-containing protein 1. A C-terminal GFP tagged version of Ypl107w has been found to localise to mitochondria in a high-throughput study (Huh et al., 2003).

YBR124W and *YPL107W* were cloned into pSP64 vectors for subsequent use with an *in vitro* coupled transcription and translation, TNT, kit (Promega) to produce radiolabelled precursors. Unfortunately attempts to clone *YGL024W* into pSP64 failed after multiple attempts. The transcription and translation of Ybr124w and Ypl107w was tested prior to import but no signal was detected for Ybr124w (autoradiography image not shown). This was likely due to the fact that Ybr124w only contains one methionine residue which would not produce a strong enough radioactive signal. Therefore, we re-cloned *YBR124W* with a C-terminal sequence encoding three extra methionines.

The radiolabelled import of Ybr124w-3Met and Ypl107w into isolated wild-type yeast mitochondria was tested under various conditions ('native' precursors vs treatment of precursors with either DTT or DTT and urea). The results show that Ybr124w-3Met cannot be imported into mitochondria in its native state, i.e. immediately after translation (**Figure 3.22A**); its import after reduction with 20 mM DTT (**Figure 3.22D**) or denaturation and reduction with 20 mM DTT and 8 M urea (**Figures 3.22B & 3.22C**) are unclear as the Triton-X-100/protease controls failed to cleave the Ybr124w precursor. This could be due to aggregation of the protein upon import which could result in it being inaccessible to cleavage by the protease. In contrast, the results of Ypl107w indicate that it can be successfully imported into mitochondria, regardless of its precursor pre-treatment, as it is protease-protected upon import (**Figure 3.22E**). **Chapter 5** goes on to investigate Ypl107w.

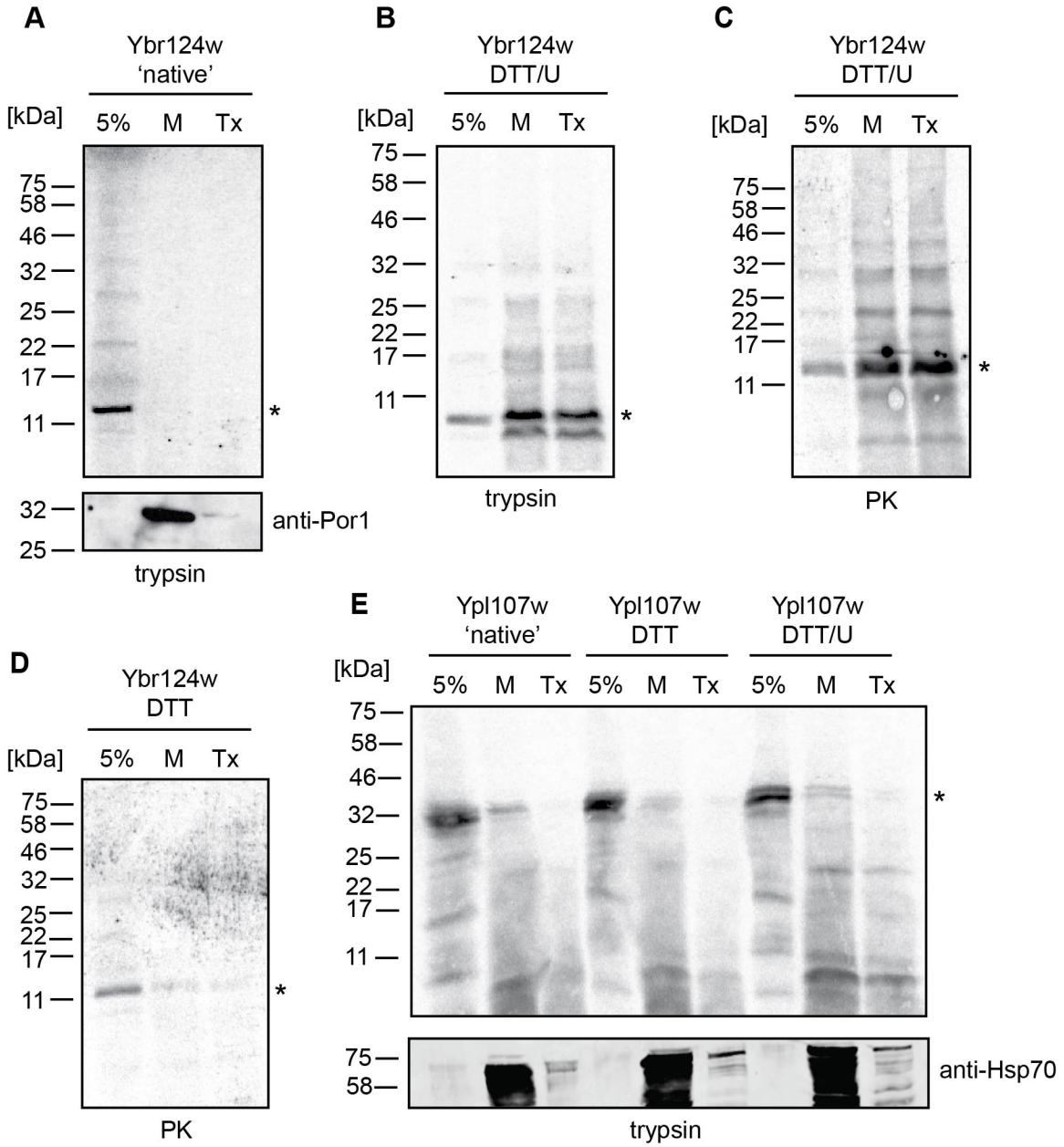

Figure 3.22. Import of radiolabelled Ybr124w and Ypl107w. Ybr124w-3Met and Ypl107w were synthesised as radiolabelled precursors and imported into isolated wild-type yeast mitochondria. (**A**) native Ybr124w import, (**B**) denatured/reduced Ybr124w import, (**C**) repeat denatured/reduced Ybr124w import using PK instead of trypsin, (**D**) reduced Ybr124w import, (**E**) Three Ypl107w imports: native, reduced, and denatured/reduced. All import reactions (M) were stopped after 30 minutes and then treated with trypsin or proteinase k, PK, to destroy unimported material, or a combination of Triton-X-100 and trypsin, or Triton-X-100 and PK, as a negative control (Tx). 5% corresponds to 5% of the precursor used for each import reaction. Radiolabelled precursors were detected by digital autoradiography; western blots were probed for Porin1 (using anti-Por1) or Hsp70 (using anti-Hsp70) as positive loading controls. Note: Three methionines were added to Ybr124w during the cloning process as the endogenous sequence does not encode enough methionines to detect a radioactive signal. * - Ypl107w.

In addition to the small proteins listed in **Table 3.4**, one other was also highlighted as a potential mitochondrial protein: Xrr1. Xrr1/Ymr087w is a 32 kDa protein that has been labelled as a putative ADP-ribose-1"-monophosphatase with a possible role in tRNA splicing (Kumaran et al., 2005). Its localisation is currently unknown but it was found in the majority of mass spectrometry datasets which suggests it could be mitochondrial. A radiolabelled import assay could address this in future.

3.4. Discussion

In this chapter, various Gpx3 and N18Gpx3 recombinant proteins were successfully expressed and purified from *E. coli*, including: Gpx3His, Gpx3C36SHis, Gpx3C64SHis, Gpx3C82AHis, N18Gpx3His, N18M20LGpx3His and N18M20LGpx3C82AHis (**Figures 3.1, 3.2, 3.3 & 3.4**). The purpose of purifying these proteins was to identify putative interactors of both Gpx3 and N18Gpx3 within the mitochondrial IMS in order to help elucidate their function/s. Although prior work has shown that an amino acid N-terminal extension of 18 amino acids can bolster Gpx3's mitochondrial import (Kritsiligkou et al., 2017), it is not yet known whether this extended version has a different interactome. Nor is it known which proteins Gpx3 interacts with outside of the cytosol, apart from Mia40 (Kritsiligkou et al., 2017). To tackle this, we first confirmed that the His-tagged proteins were capable of import into isolated yeast mitochondria (**Figure 3.5**). From there, an *in organello* pulldown assay using Ni-NTA affinity beads was thoroughly optimised in order to minimise the amount of non-specific binding which would later reduce the number of false positives (**Figures 3.7, 3.9 & 3.10, and Tables 3.1 & 3.2**). The success of this assay was determined by the co-elution of its only known mitochondrial interactor, Mia40, with His-tagged Gpx3 (**Figures 3.9 & 3.10**). Based on this, repeat pulldowns were performed and five eluates from pulldowns using either Gpx3His, N18M20LGpx3His, or the cysteine trap mutant Gpx3C82AHis as bait were sent for mass spectrometry analysis. Control 'mock' pulldown eluates where no His-tagged protein was used were also performed to capture non-specifically bound proteins.

Although the pulldown assay and mass spectrometry analysis was fraught with problems despite optimisation (low reproducibility between datasets, high numbers of proteins in control eluates, and the presence of endogenous Gpx3 in some of the control datasets), a putative hit list was generated which would act as a starting point for further investigation (**Table 3.3**). The majority of these hits are not known to localise to the mitochondrial IMS and are therefore unlikely to be true interactors, i.e. mitochondrial matrix proteins and nuclear proteins; however, three IMS proteins were found: Mia40, Cyt*c* (Cyc1/7), and Cytb2. Given that both Mia40 and Cyt*c* play a role in the MIA oxidative folding pathway within the IMS, and that Mia40 is already a known interactor of Gpx3, we decided to focus on characterising the potential interaction between Gpx3 and Cyt*c* – an abundant IMS electron carrier. Alternatively, one possible explanation for Gpx3 interacting with proteins outside the IMS could be that after solubilisation of mitochondria, Gpx3 starts redox relays with proteins in close proximity, like it does with Yap1 in the cytosol (Gutscher et al., 2009). Thus, it may be challenging to identify a reproducible list of proteins.

To investigate Gpx3-Cyt*c*, a combination of *in vitro* and *in vivo* assays was carried out. Firstly, an assay similar to the *in organello* pulldown was performed whereby His-tagged Gpx3 proteins were bound in excess to Ni-NTA beads in an attempt to minimise non-specific binding. Solubilised mitochondrial proteins were then added, washed and eluted along with recombinant Gpx3 (**Figure 3.12**). The assay was reasoned to be successful due to the detection of Mia40, but Cyt*c* was rarely detected (**Figure 3.13**). It could be that Cyt*c* is a very transient interactor of Gpx3, or that the assay does not represent the physiological conditions required for an interaction to occur. Unexpectedly, Trx1 was found to co-elute with Gpx3 which itself warrants a future investigation as Trx1 also localises to the IMS (Vögtle et al., 2012; Manganas, Cárdenas-Rodriquez and Tokatlidis, unpublished obs.). Control pulldowns could be carried out to investigate whether this interaction occurs when galMia40, *cytc*Δ or *trx1*Δ mitochondria are used.

Moving on, Cyt*c*His was purified from *E. coli* for use in a reciprocal *in vitro* binding assay and an initial result suggests that endogenous Gpx3 can interact with Cyt*c*His (**Figure**

3.14). However, this assay could not be repeated due to aggregation of the recombinant Cyt*c*His protein which occurred quickly after its purification. This prompted us to purchase Cyt*c* from Sigma-Aldrich (sourced from *S. cerevisiae*) and continue on with *in vitro* interaction assays using only purified His-tagged Gpx3 proteins and Cyt*c* (no tag available). Interestingly, these assays indicate a strong molecular interaction between Gpx3 and Cyt*c* that results in a mixed intermediate (**Figures 3.15 & 3.16**); this intermediate most likely comprises one Gpx3 monomer and one Cyt*c* monomer based on predicted molecular weight and western blot analysis. These *in vitro* interaction assays were then carried out using the single cysteine mutants of Gpx3 (Gpx3C36SHis, Gpx3C64SHis and Gpx3C82AHis) in order to determine whether any of these cysteine residues are required for its interaction with Cyt*c*. Based on what is known about Gpx3's interaction with Yap1 in the cytosol, we expected that the peroxidatic and resolving cysteine mutants, Gpx3C36SHis and Gpx3C82AHis, would abolish or enhance their interactions with Cyt*c*, respectively. This was not the case. The only cysteine mutant that affected the interaction was Gpx3C64SHis – a cysteine residue which is not known to be involved in disulphide bond formation – as the band detected by Coomassie staining was 'weaker' when compared to that seen for wild-type Gpx3His and the other cysteine mutants (**Figure 3.19**). Although little is known about the function of C64, it is highly conserved across homologs and lies within a hydrophobic region (**Figure 3.18**). We therefore thought that the C64A mutation might be causing a structural change in Gpx3 which might be affecting a potential hydrophobic interaction with Cyt*c*.

To test this theory, we carried out a circular dichroism (CD) analysis on Gpx3His, Gpx3C36SHis, Gpx3C64SHis and Gpx3C82AHis, and also looked at the ÄKTA data generated previously from their purifications (**Figure 3.20 and Appendices Figures 7.1, 7.2, 7.3 & 7.4**). The CD spectroscopy data indicates that all four proteins are folded in terms of their secondary structure; however, there may be some subtle differences between tertiary structures which could be further assessed by nuclear magnetic resonance (NMR). The ÄKTA data does not indicate any substantial differences in oligomeric state between Gpx3His and Gpx3C64SHis as both proteins are largely found as monomers under native conditions. Further analysis on these cysteine mutant proteins is required in order to elucidate how Gpx3 is interacting with Cyt*c* (at least in this *in vitro*

assay). That aside, we cannot be fully certain that this interaction actually exists in yeast until *in vivo*/*in organello* experiments provide 'real-life' evidence.

Confirming a Gpx3-Cyt*c* interaction *in vivo* and *in organello* proved challenging for a number of reasons. Firstly, an endogenously His-tagged Gpx3 yeast strain failed to express the protein at levels sufficient enough to carry out experiments (Chatzi, unpublished obs.), and yeast plasmids expressing Gpx3-myc also failed to express the protein at sufficient levels (Chatzi, unpublished obs.). Due to this, and the low abundance of endogenous Gpx3 in the IMS, it was not possible to carry out *in vivo* assays using whole yeast cells. Instead, we decided to try *in organello* immunoprecipitations via a number of ways including: (i) IPs to detect endogenous mitochondrial Gpx3 and Cyt*c*; and (ii) IPs to detect radiolabelled Gpx3 and Cyt*c* after their import into mitochondria. Frustratingly, neither of these methods proved successful but for different reasons. The former had problems with heavy chain antibody cross-reactivity which would have masked a potential signal. Future Co-IPs could avoid this problem by covalently attaching the primary antibodies to protein A beads or by probing with a light-chain specific antibody. In contrast, the latter method used here likely did not work due to low amounts of radiolabelled protein, much lower than endogenous protein levels, which could have hindered their detection. Future Co-IPs via this method should aim to increase the amount of radiolabelled material present upon import and perhaps optimisation of the binding procedure. On the other hand, it is possible that the reason this method did not show an interaction could simply be because the two proteins do not interact *in organello*, or that their interaction is transient, or that their interaction depends upon specific physiological conditions which were not replicated. Therefore, it is crucial that, alongside continued efforts to optimise these *in organello* Co-IPs, alternative approaches are pursued to express tagged Gpx3 proteins at levels sufficient enough to work with whole yeast cells.

Mitochondria were isolated from a Gpx3-TAP tagged yeast strain in the hopes that enough of the protein would be found inside the mitochondrial IMS in order to carry out pulldown assays with an alternative method. Unfortunately, the TAP tag appears to affect

the mitochondrial import of Gpx3 as only very small amounts of Gpx3-TAP were detected in isolated mitochondria (**Figure 3.21**). Clonings are still ongoing to clone *GPX3* into a pSF-TEF1-COOH-V5 plasmid which will be transformed into yeast cells to express Gpx3-V5; it is hoped that the V5 tag will not affect mitochondria import as it is much smaller in size.

Finally, we identified a list of potential mitochondrial proteins of unknown function from the mass spectrometry data that had previously not been associated with the organelle: Ybr124w, Ydr193w, Ygl024w, Yor293c-a, Ypl107w and Ypr010c-a. Out of the six proteins, three of them have interesting cysteine motifs (**Table 3.4**), of which two are similar to the twin cysteine motifs responsible for mitochondrial IMS targeting via the MIA oxidative folding pathway – Ybr124w and Ygl024w. Ypl107w's cysteine motif, although not resembling any known targeting signals, may have an important functional role. Furthermore, out of these six proteins only one has an identifiable human homolog – Ypl107w (the human homolog is OXLD-1). Therefore, we focused on Ybr124w, Ygl024w and Ypl107w. *YBR124W* and *YPL107W* were successfully cloned into pSP64 vectors (*YGL024W* was not), and mitochondrial import assays were carried out to determine whether they could be imported into isolated mitochondria. Radiolabelled Ybr124w could not be detected in mitochondria, whereas Ypl107w could (**Figure 3.22**). Thus, the next chapter goes on to investigate Ypl107w in more detail.

NOTE: Towards the end of this study, a paper was published by Morgenstern et al. (2017) which identified both Ypl107w and Ypr010c-a in mitochondria as part of a large proteome study; the authors named these proteins Dpc25 and Min8, respectively.

Chapter 4

Ypl107w: a putative oxidoreductase of unknown function

4. Ypl107w: a putative oxidoreductase of unknown function

4.1. Introduction

In *S. cerevisiae*, Ypl107w is a non-essential 29 kDa protein of unknown function (Giaever et al., 2002). It contains a predicted mitochondrial targeting signal at its N-terminus (**Section 3.3.7**) and four cysteine residues which are all located within a highly conserved, oxidoreductase-like, N-terminal domain (see InterPro entry IPR019180/Pfam entry PF09791). The exact function of this domain is not yet known.

Prior to the work presented in this chapter, little literature existed on Ypl107w; most came from the systematic data analysis of null mutants. Large-scale studies have found *ypl107wΔ* cells to be less resistant to oxidative stress induced by H_2O_2 (Brown et al., 2006), less resistant to hyperosmotic stress induced by salt (Yoshikawa et al., 2009), and less competitively fit in minimal media (Breslow et al., 2008). In addition, *ypl107wΔ* cells have also been shown to exhibit a small defect in vacuolar fragmentation (Michaillat and Mayer, 2013), and a decreased resistance to the oncology drug elesclomol which targets the mitochondrial respiratory chain (Blackman et al., 2012; Nagai et al., 2012). Notably though, a C-terminally GFP-tagged version of Ypl107w exhibited mitochondrial localisation during a high-throughput study (Huh et al., 2003), and a paper by Hacioglu et al. (2010) predicted Ypl107w as a thiol oxidoreductase based on the presence of a CXXC redox motif and a predicted helical structure immediately downstream (–CXXC-α).

Like Ypl107w, barely any literature exists on any of its homologs other than some of their associations with mitochondria. The mouse homolog, oxidoreductase-like domain-containing protein 1 (OXLD-1), was identified by mass spectrometry in a mitochondrial proteomics analysis and was found to be expressed in the following tissues: adipose, large intestine and stomach (Pagliarini et al., 2008; Calvo et al., 2016). As a result, OXLD-1 is now listed in both the mouse and human MitoCarta 2.0 databases which each contain

1158 proteins with evidence of mitochondrial localisation. Additionally, the *Schizosaccharomyces pombe* fission yeast homolog, known as P31B10.02, was found to localise to mitochondria when C-terminally tagged with yellow fluorescent protein, YFP (Matsuyama et al., 2006).

Earlier in **Chapter 3**, Ypl107w was identified in one of the mass spectrometry datasets after analysis of an eluate containing putative N18M20LGpx3His interactors (**Section 3.3.4**). An initial import experiment whereby a radiolabelled version of Ypl107w was synthesised and presented to mitochondria indicated that Ypl107w could be successfully imported (**Figure 3.22**). This result prompted further investigation to confirm the localisation of Ypl107w and to start probing its function within mitochondria.

Since starting this work, Ypl107w has been confirmed to reside within yeast mitochondria in a large-scale mitochondrial proteomics study (Morgenstern et al., 2017). The authors renamed the protein Dpc25, for delta-psi dependent mitochondrial import and cleavage protein of ~25 kDa, as they observed a defect in import when membrane potential was abolished and a cleavable sequence upon successful import. Morgenstern et al. (2017) also performed a BN-PAGE analysis on isolated mitochondria after radiolabelled import of Ypl107w/Dpc25 to detect complexes; however, the results were inconclusive. Despite this evidence appearing nearly two years after my work on this protein began, the results shown here add to the literature and provide a more detailed analysis of Ypl107w. The protein will be referred to throughout this chapter as Ypl107w (which is its systematic gene name in the yeast database) and not Dpc25, as this was not known prior to the work.

4.2. Aims

In this chapter, the first aim was to perform a thorough bioinformatics analysis of Ypl107w and its homologs, and confirm its mitochondrial localisation within *S. cerevisiae* which was previously suggested by the mass spectrometry data shown in **Section 3.3.4** using standard import and localisation assays. Given the highly conserved OXLD domain within Ypl107w, it is of importance to unravel the localisation and function of this protein as it may help us understand the role of OXLD domains across many organisms. Once the localisation of Ypl107w was confirmed, the next aim was to perform a BN-PAGE analysis to determine whether Ypl107w is part of any larger complexes within mitochondria, and whether any of the respiratory chain complexes are affected when Ypl107w is absent in a *ypl107wΔ* yeast strain. Furthermore, the predicted N-terminal mitochondrial targeting signal of Ypl107w (N26) was deleted and its effect on import assessed.

A second aim was to carry out a more extensive phenotypic analysis of *ypl107wΔ* cells to determine whether the absence of Ypl107w results in any growth defects that could be attributed to impaired mitochondrial function. In addition, steady-state levels of mitochondrial proteins were compared between mitochondrial isolates from wild-type and *ypl107wΔ* yeast.

Based on the growth defects observed when *ypl107wΔ* cells were grown in non-fermentable carbon sources, a final aim was to assess the import of the human homolog, OXLD-1, with the intention of expressing OXLD-1 in *ypl107wΔ* yeast and determining whether it can rescue these growth defects. If successful, this would provide evidence for the first time as to whether OXLD-1 is a real functional homolog of Ypl107w.

4.3. Results

4.3.1. Bioinformatics analysis of Ypl107w and its homologs

To begin, a multiple sequence alignment between Ypl107w in *S. cerevisiae* and its homologs in various model organisms was performed using Clustal Omega (Sievers et al., 2011). The alignment shown in **Figure 4.1** clearly highlights a conserved domain present in all homologs – '…$PX_2CCX_2GCX_2CVWX_2YX_3L$…'. This domain has been annotated as 'oxidoreductase-like domain, N-terminal' (InterPro - IPR019180), and is present in more than 2000 proteins across 749 species (Pfam - PF09791; Finn et al., 2016). This includes 614 eukaryotic species and 135 bacterial species (**Figure 4.2**). A profile hidden Markov Model, profile HMM, which represents the oxidoreductase-like domain within these proteins is shown in **Figure 4.3**. It is striking to note that although there are so many proteins containing this domain, absolutely nothing is known about the function of any of these proteins.

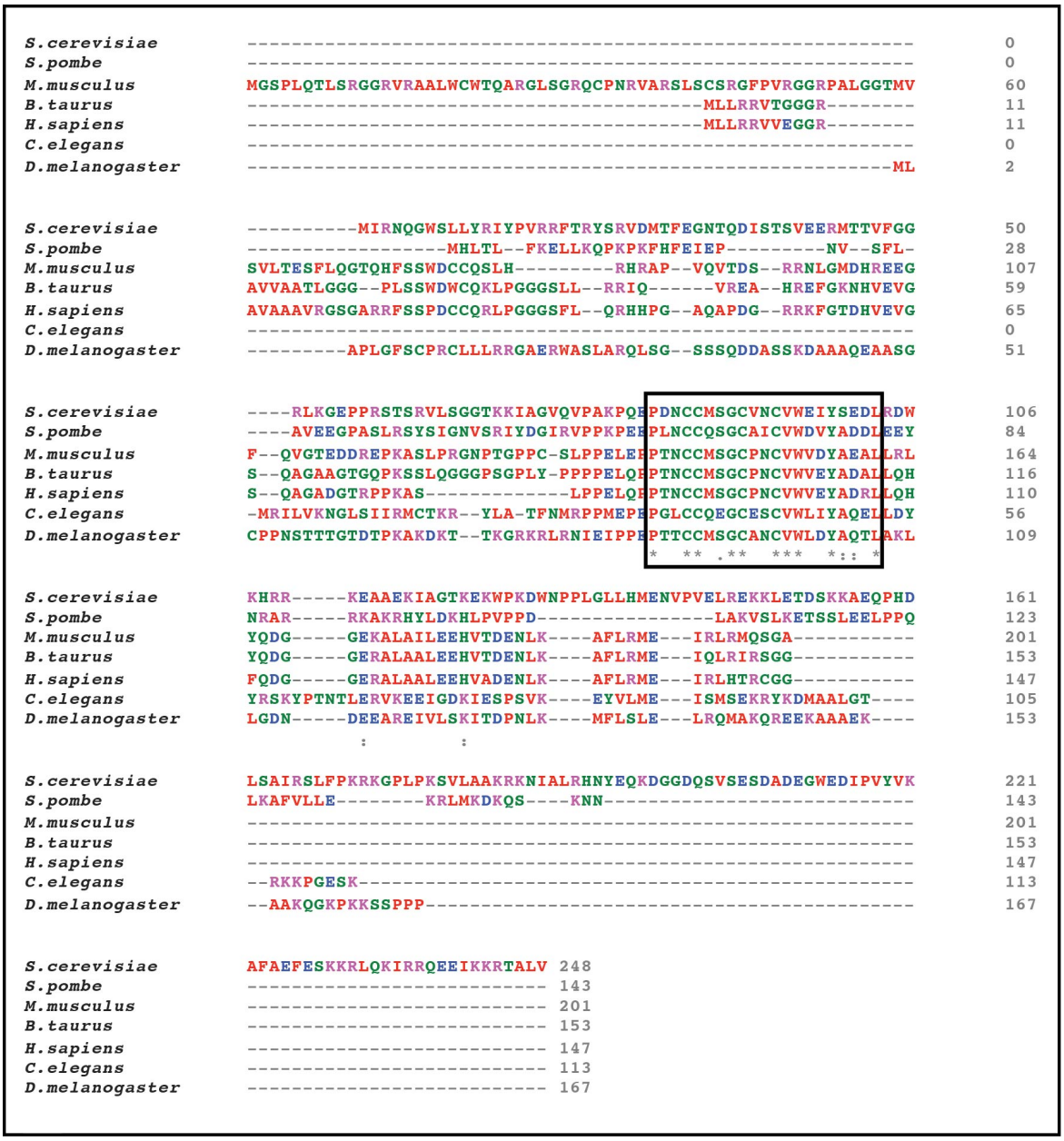

Figure 4.1. *S. cerevisiae* Ypl107w multiple sequence alignment. Clustal Omega (Version 1.2.4) was used to align Ypl107w homologs from *Saccharomyces cerevisiae*, *Schizosaccharomyces pombe*, *Mus musculus*, *Bos Taurus*, *Homo sapiens*, *Caenorhabditis elegans* and *Drosophila melanogaster*. Green – hydroxyl + sulphydryl + amine + G; Red – small (small + hydrophobic, including aromatic – Y); Pink – basic - H; Blue – acidic. * (asterisk) – single, fully conserved residue. : (colon) – conservation between groups of strongly similar properties. . (period) – conservation between groups of weakly similar properties.

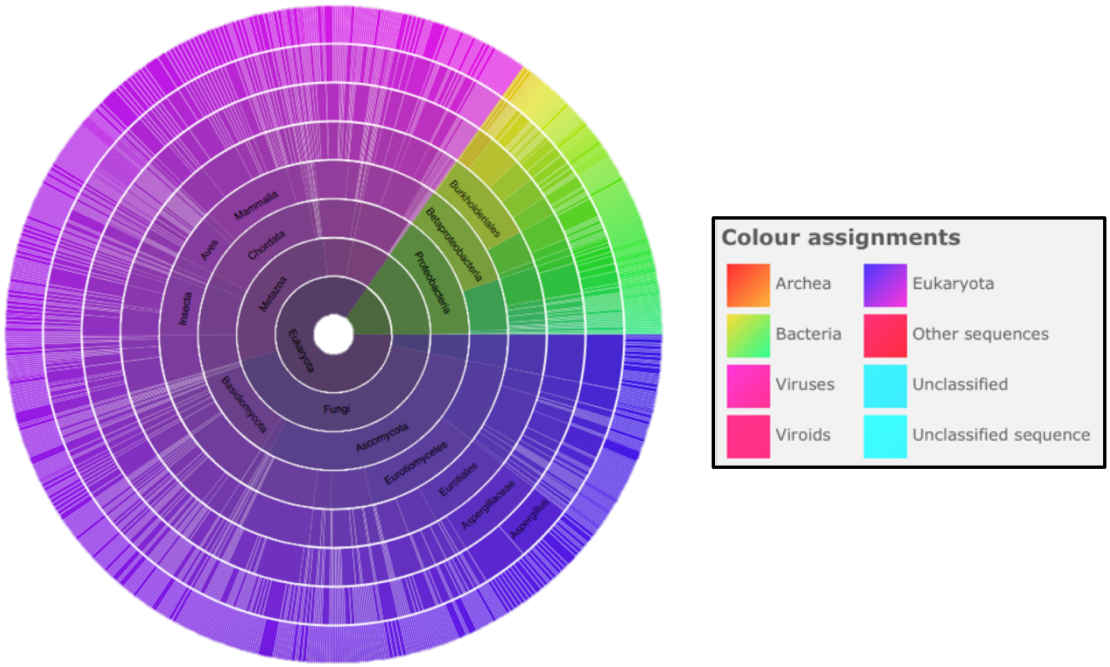

Figure 4.2. Graphical representation of the oxidoreductase-like family across species. Sunburst representation of species containing the oxidoreductase-like, N-terminal domain (Finn et al., 2016). There are 749 species in total; 614 eukaryota and 135 bacteria. The domain is absent from archea, viruses and viroids. (Pfam – PF09791).

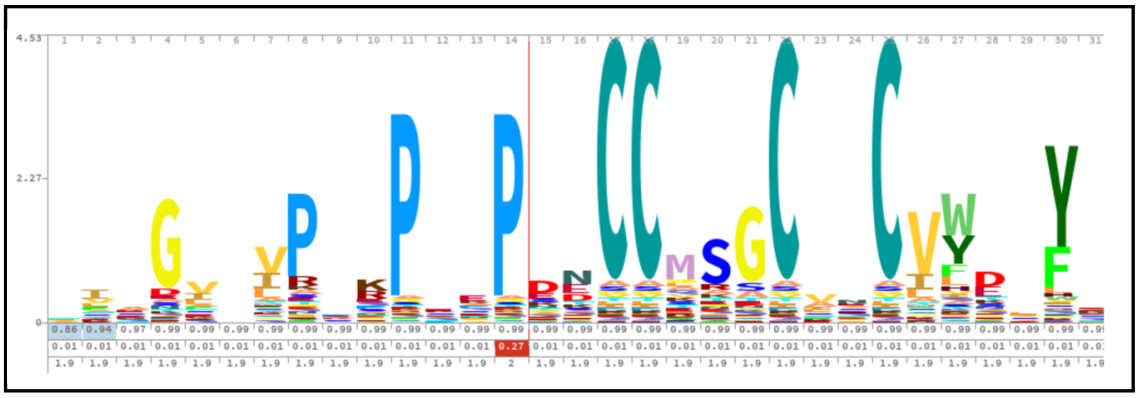

Figure 4.3. Profile HMM for oxidoreductase-like protein family. A graphical representation of the profile hidden Markov model, profile HMM, for the oxidoreductase-like protein family (Pfam – PF09791) (Wheeler et al., 2014). Height of stack – a measure of the invariance of the column; Height of letter – frequency at that position.

As the Mitoprot/targeting analysis of Ypl107w predicted a cleavable N-terminal mitochondrial targeting sequence of around 26 amino acids, a secondary structure prediction was carried out on both Ypl107w and hOXLD-1 (**Figure 4.4**). Ypl107w and hOXLD-1 contain multiple predicted alpha helical structures both with one close to the N-terminus which could act as a potential mitochondrial targeting signal.

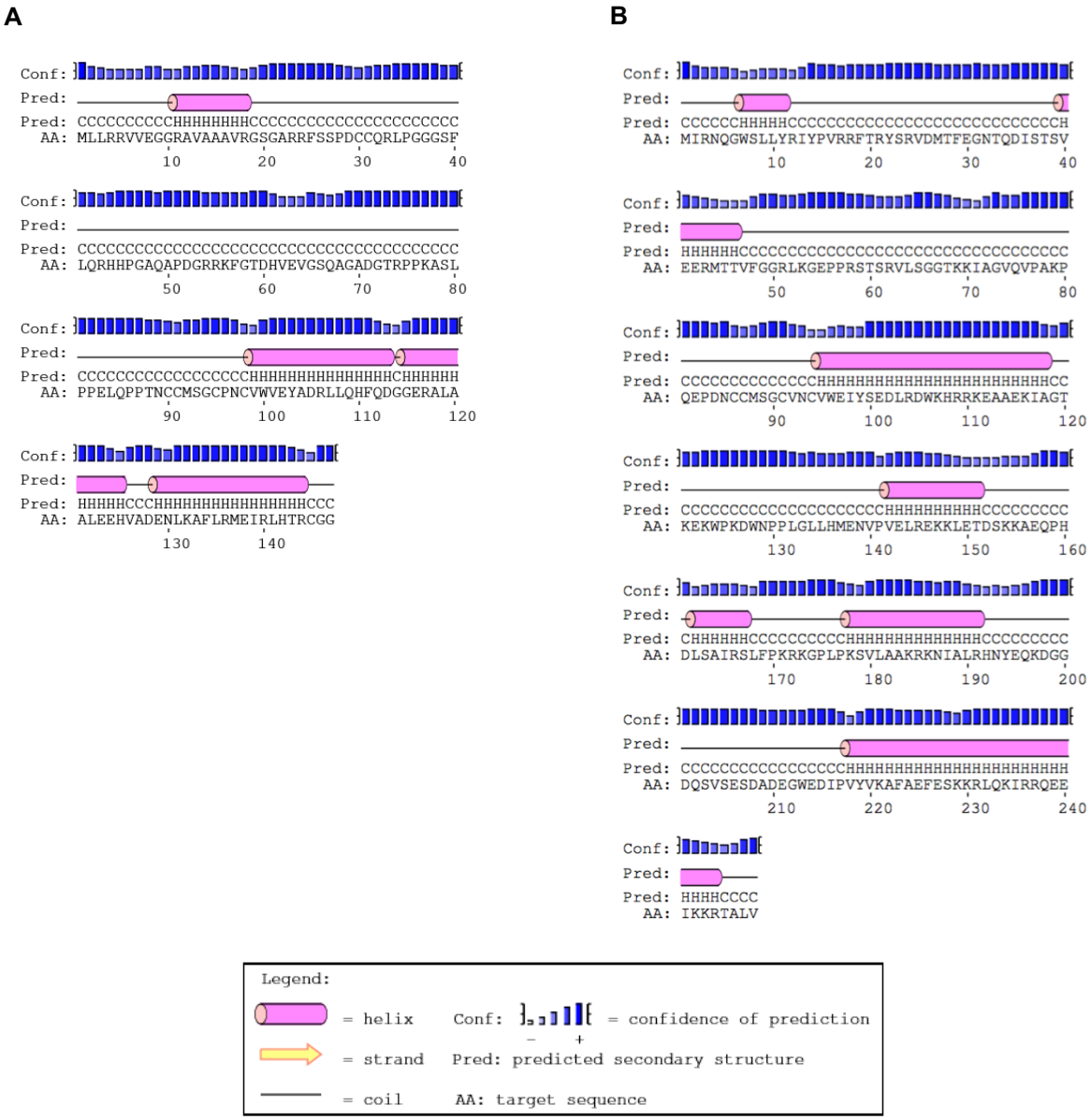

Figure 4.4. Secondary structure prediction for Ypl107w and hOXLD-1. Secondary structure predictions for (**A**) Ypl107w and (**B**) hOXLD-1 were carried out using the online PSIPRED prediction tool (Jones, 1999; Buchan et al., 2013).

In addition to the secondary structure predictions, an ion binding prediction for Ypl107w was carried out using IonCom (Hu et al., 2016). IonCom is a composite binding-site prediction tool that searches for 13 small ligands, including nine metal ions and four acid radical ions: Zn^{2+}, Cu^{2+}, Fe^{2+}, Fe^{3+}, Ca^{2+}, Mg^{2+}, Na^{+}, K^{+}; and CO_3^{2-}, NO_2-, SO_4^{2-} , and PO_4^{3-}, respectively. The tool predicted potential binding sites for Zn^{2+} and Na^{+} - no binding sites were detected for the others (**Figure 4.5**).

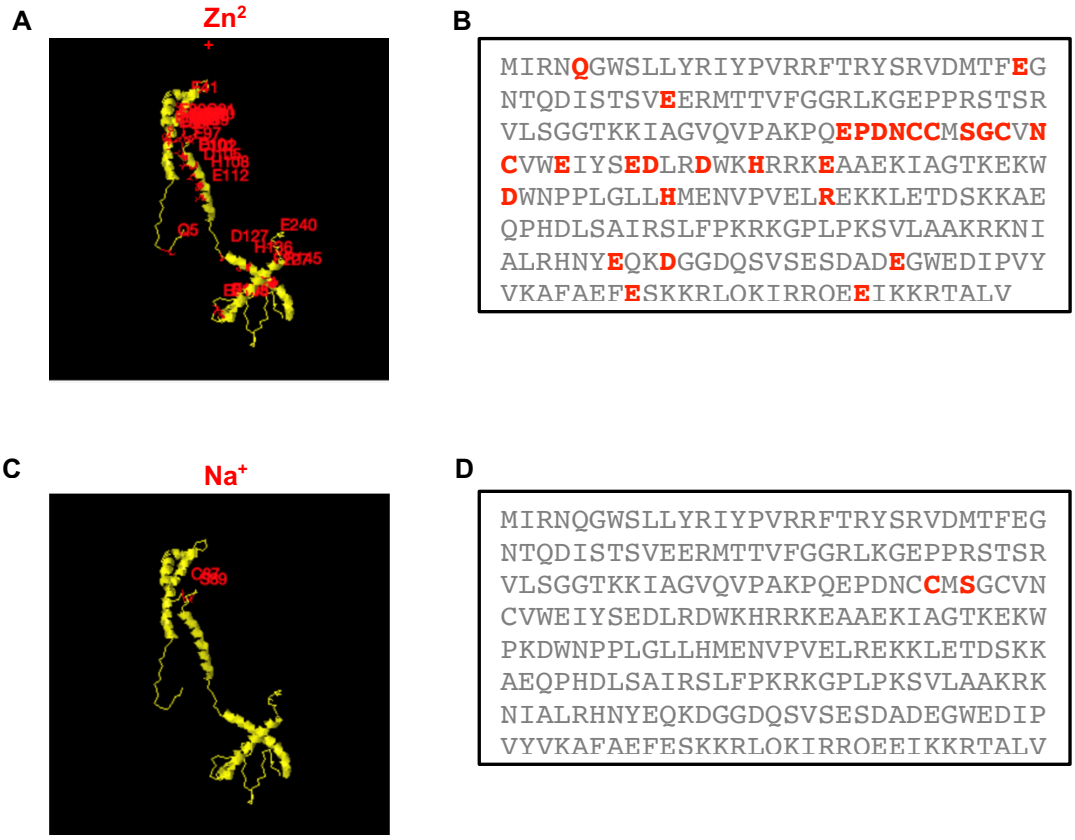

Figure 4.5. Small ligand binding-site prediction for Ypl107w. IonCom results predict putative binding sites for Zn^{2+} (**A & B**) and Na^{+} (**C & D**) (Hu et al., 2016). Predicted residues involved in binding are shown in red. Note that the structures shown in Panels **A** and **C** are also predictions generated by IonCom.

Moving on from sequence and structural analysis, nearly all of the known genetic and physical interactors of Ypl107w and OXLD-1 were compiled together and analysed using Gene Ontology Term Finders. In addition, any literature relating to gene expression and regulation was also analysed.

Although *YPL107W* itself is not an essential gene, there are 75 known genetic interactors of *YPL107W*, of which 23 (31%) are associated with mitochondria either by localisation or function and are listed in **Table 4.1** (Costanzo et al., 2010; Costanzo et al., 2016). Here, genetic interactors are defined when a deletion of *YPL107W* in combination with the deletion of another gene results in either a deleterious or beneficial phenotype, and are classified as either negative or positive. Nearly of all *YPL107W*'s interactors are negative; only two are positive. A Gene Ontology (GO) search for both process and function was carried out by inputting these 23 mitochondrial-associated genetic interactors using the GO Term Finder, Version 0.83, which is available on the yeast genome database website (www.yeastgenome.org). Three processes and two functions were highlighted: processes include mitochondrial tRNA thio-modification, mitochondrial organisation and protein lipoylation; functions include sulphurtransferase and oxidoreductase activity (**Table 4.2**).

Table 4.1. *YPL107W* genetic interactors associated with mitochondria.

Mitochondrial Genetic Interactions with *YPL107W*			
Systematic name	**Standard name**	**Function/Process**	**+/-**
YAL046C	*BOL3*	Mitochondrial Fe/S cluster transfer	-
YDR375C	*BCS1*	Assembly of Complex III	+
YOR125C	*CAT5*	Ubiquinone biosynthesis	-
YNR041C	*COQ2*	Ubiquinone biosynthesis	+
YNL052W	*COX5A*	Subunit of complex IV	-
YOR065W	*CYT1*	Subunit of complex III	-
YMR207C	*HFA1*	Acetyl-coenzyme A carboxylase	-
YOL095C	*HMI1*	ATP-dependent DNA helicase	-
YLR239C	*LIP2*	Lipoyl ligase	-
YOR196C	*LIP5*	Lipoic acid biosynthesis	-
YKL053C-A	*MDM35*	Mitochondrial organisation	-
YOR350C	*MNE1*	Mitochondrial splicing	-
YDR116C	*MRPL1*	Subunit of mitochondrial ribosome	-
YOR354C	*MSC6*	Mitochondrial translation	-
YCL017C	*NFS1*	Fe/S cluster biogenesis & thiol modification of tRNAs	-
YGR231C	*PHB2*	Subunit of prohibitin complex/life span regulation	+
YLL041C	*SDH2*	Fe/S protein subunit of succinate dehydrogenase	-
YDL033C	*SLM3*	tRNA-specific-2-thiouridylase	-
YHR008C	*SOD2*	Manganese superoxide dismutase	-
YKR042W	*UTH1*	Cell wall biogenesis & oxidative stress response	-
YDR049W	*VMS1*	Mitochondrial protein degradation	-
YDL120W	*YFH1*	Mitochondrial Fe/S assembly	-
YMR241W	*YHM2*	Mitochondrial citrate and oxoglutarate carrier	-

Genes that show either a positive or negative genetic interaction when knocked out in combination with *YPL107W* (Costanzo et al., 2010; Costanzo et al., 2016).

Table 4.2. Gene Ontology search for *YPL107W* genetic interactors.

Gene Ontology Term Finder				
Process	**Cluster frequency**	**Background frequency**	**P-value**	**Genes annotated to term**
mitochondrial tRNA thio-modification	2/23, 9%	<0.1%	0.00175	*NFS1*, *SLM3*
mitochondrion organisation	7/23, 30%	3.7%	0.00235	*NFS1*, *SLM3*, *BCS1*, *PHB2*, *MDM35*, *YHM2*, *HMI1*
protein lipoylation	2/23, 9%	0.1%	0.01744	*LIP2*, *LIP5*
Function	**Cluster frequency**	**Background frequency**	**P-value**	**Genes annotated to term**
sulphurtransferase activity	3/23, 13%	0.1%	7.17E-05	*NFS1*, *SLM3*, *LIP5*
oxidoreductase activity	5/23, 22%	4%	0.03764	*YFH1*, *SOD2*, *SDH2*, *COX5A*, *CAT5*

All mitochondrial-associated *YPL107W* genetic interactors were entered into the Gene Ontology Search Finder (available at www.yeastgenome.org). Interactors were searched separately for process or function.

In addition to searching for genetic interactors of Y*PL107W*, genes with similar expression profiles were generated using SPELL, Serial Pattern of Expression Levels Locator (Hibbs et al., 2007). SPELL searches through 11449 microarrays from 386 published studies for genes with similar expression patterns to the query input – in this case *YPL107W*. A list of the top 19 genes similar to *YPL107W* can be seen in the **Appendices**, **Table 7.1**. A GO Term Finder search of these 19 genes for process and function found no significant ontology terms apart from eight of the genes share 'biological process unknown' and 12 share 'molecular function unknown'. Although no genetic interactors are known for any of the *YPL107W* homologs, there are some large-scale studies that identified putative physical interactors of the human homolog, hOXLD-1 (Huttlin et al., 2015 and Huttlin et al., 2017). Those that are localised within mitochondria are listed in **Table 4.3** - 38/49 are mitochondrial. A GO search using these 38 putative interactors brought up a huge list of processes and functions which can be seen in the **Appendices**, **Table 7.2**. Interestingly, in *S. cerevisiae*, although physical partners have not been fully captured, the mitochondrial matrix Hsp70, Ssc1, is listed as a potential protein interactor (Böttinger et al., 2015).

Table 4.3. hOXLD-1 physical interactors associated with mitochondria.

Human hOXLD-1 Mitochondrial Physical Interaction Partners	
Standard name	**Description**
AARS2	Alanine tRNA ligase
ACADVL	Acyl-CoA dehydrogenase
ACOT9	Acyl-CoA thioesterase
ACSF3	Acyl-CoA synthetase
AK4	Adenylate kinase
ALAS1	5-aminolevulinate synthase
ALDH5A1	Succinate-semialdehyde dehydrogenase
ATPAF2	ATP synthase mitochondrial F1 complex assembly
AUH	Methylglutaconyl-CoA hydratase
CARS2	Cysteinyl-tRNA synthetase
CPT2	Carnitine O-palmitoyltransferase
DBT	Lipoamide acyltransferase
FMC1	Assembly/stability of ATP synthase
GLDC	Glycine dehydrogenase
GLS	Glutaminase
GRPEL2	Essential component of PAM complex
HIBCH	3-hydroxyisobutryl-CoA hydrolase
HSD17B8	Estradiol 17-beta-dehydrogenase
IBA57	Putative transferase, maturation of mitochondrial 4Fe-4S proteins
MGME1	Mitochondrial genome maintenance
MMAB	Adenosyltransferase
MRPP3	Catalytic ribonuclease component of mitochondrial ribonuclease P
MTG2	Mitochondrial ribosome-associated GTPase
MTIF2	Mitochondrial translation initiation factor
MUT	Methylmalonyl-CoA mutase
NARS2	Asparaginyl-tRNA synthetase
NDUFAF5	Complex I assembly factor
NDUFAF7	Complex I assembly factor
PDSS2	Decaprenyl-disphophate synthase subunit
POLG	DNA polymerase submit gamma
POLRMT	RNA polymerase
PUS1	tRNA pseudouridine synthase
SIRT3	NAD-dependent protein deacetylase
TRMT2B	tRNA methyltransferase
TRMT61B	tRNA methyltransferase
TSFM	Translation elongation factor
UQCC1	Ubiquinol-cytochrome-*c* reductase complex assembly factor
UQCC2	Ubiquinol-cytochrome-*c* reductase complex assembly factor

All mitochondrial-associated hOXLD-1 putative physical interactors are listed, along with a brief description of their function (Huttlin et al., 2015; Huttlin et al., 2017).

4.3.2. Import and localisation of Ypl107w

The import of Ypl107w was initially tested at the end of Chapter 3, **Section 3.3.7**, where it was found to successfully import into isolated mitochondria (**Figure 3.22**). Further assays were carried out to assess whether Ypl107w import is dependent on membrane potential, along with two extra controls (no mitochondria/no precursor added to reactions). These extra controls were to confirm that the band detected by autoradiography in the import reaction lanes are imported into mitochondria and not protease-resistant aggregates, and that the bands are specific to the radiolabelled precursors. The results shown in **Figures 4.6A & 4.6B** indicate that Ypl107w import requires membrane potential, as no band is detected when membrane potential is abolished by CCCP and valinomycin, and the extra controls confirm its import. Su9-DHFR was used as a control protein that requires membrane potential as it is cleaved after import into the matrix (**Figure 4.6C**). These results suggest that Ypl107w is also targeted to the matrix; however, a localisation assay was required to provide evidence for this.

To investigate the suspected matrix localisation of Ypl107w, a mitochondrial localisation assay was used to detect which subcompartment Ypl107w resides in after import, and whether or not it is soluble (refer to **Chapter 2**, **Section 2.2.2.3** for methodology). The results show that Ypl107w is found within 'mitoplasts', the inner mitochondrial membrane/matrix fraction after osmotic shock, and that it is protease protected (**Figure 4.7**). Carbonate extraction revealed that Ypl107w is a soluble protein. Control antibodies against proteins from various mitochondrial subcompartments and different associations with membranes were used to compare against Ypl107w. The soluble matrix protein Cpn10 showed the same localisation pattern as Ypl107w, providing further evidence that Ypl107w is likely to be a soluble, matrix protein.

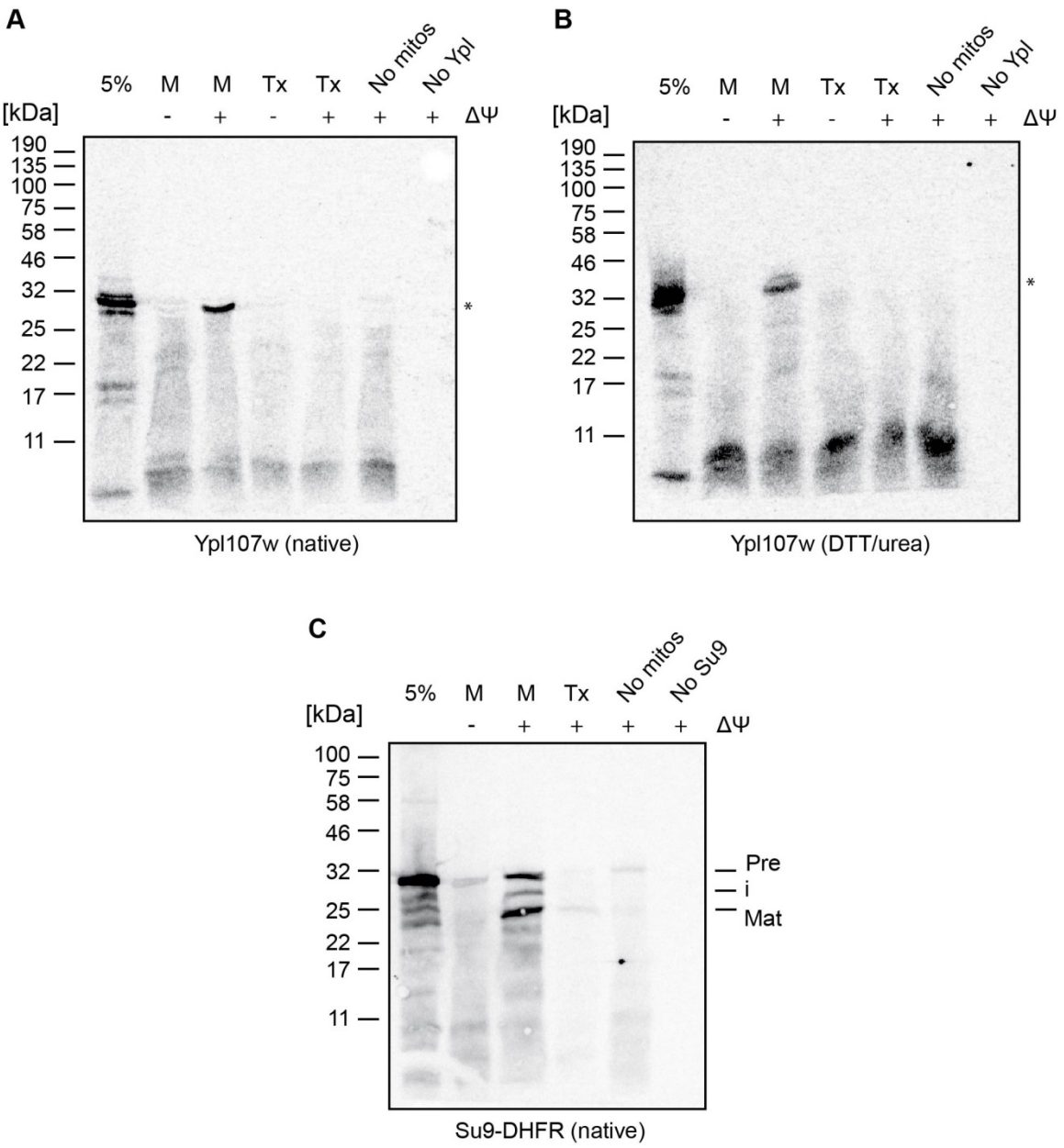

Figure 4.6. Import of radiolabelled Ypl107w and Su9-DHFR. Ypl107w and Su9-DHFR were synthesised as radiolabelled precursors and imported into isolated wild-type yeast mitochondria. (**A**) Ypl107w import straight after translation (native), (**B**) Ypl107w import after treatment with 20 mM DTT and 8 M urea to reduce and denature the precursor, and (**C**) Control Su9-DHFR import (native). Import reactions were stopped after 30 minutes. $\Delta\Psi$ - membrane potential. All import reactions were treated with trypsin to destroy unimported material (M), and a combination of Triton-X-100 and trypsin as a negative control (Tx). Extra controls whereby no mitochondria (No mitos) or no precursor (No Ypl/Su9) were added to the import reaction. 5% corresponds to 5% of the precursor used for each import reaction. Radiolabelled precursors were detected by digital autoradiography. * - Ypl107w. Pre – premature Su9-DHFR, i – IMS stalled Su9-DHR intermediate (incompletely cleaved in transition), Mat – mature Su9-DHFR (cleaved after import into matrix).

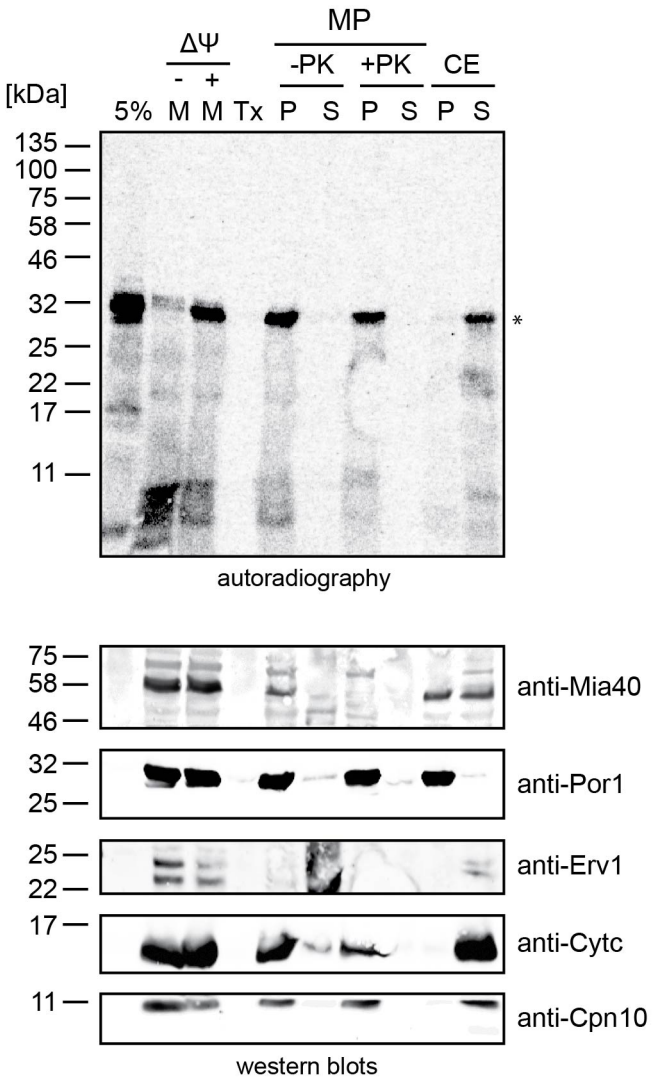

Figure 4.7. Radiolabelled Ypl107w localisation after mitochondrial import. Ypl107w was synthesised as a radiolabelled precursor and imported into isolated wild-type yeast mitochondria straight after translation. The import reaction was stopped after 30 minutes and treated with trypsin to destroy unimported material (M), and a combination of Triton-X-100 and trypsin as a negative control (Tx). Osmotic shock to rupture the OM, mitoplasting (MP), resulted in pellets (P) containing the matrix/IM and supernatants (S) containing IMS proteins, -/+ proteinase K (PK). Carbonate extraction (CE) to separate insoluble from soluble proteins from intact mitochondria after Ypl107w import: (P) – insoluble proteins associated with mitochondrial membranes; and (S) – soluble proteins. Top panel - analysis by autoradiography to detect radiolabelled Ypl107w. Bottom panel - analysis by western blotting to detect mitochondrial proteins from different subcompartments: anti-Mia40 (IMS/IM); anti-Por1 (integral OM); anti-Erv1 (soluble IMS); anti-Cyt*c* (soluble IMS); and anti-Cpn10 (soluble matrix). 5% corresponds to 5% of the precursor used for each import reaction. Radiolabelled precursors were detected by digital autoradiography. * - Ypl107w.

As most matrix proteins contain cleavable sequences at their N-terminus, the next step was to delete the suspected targeting sequence in Ypl107w and test its import capacity. *YPL107W* was subcloned into a pSP64 vector without its first 78 base pairs to create a plasmid which would translate a truncated protein lacking the first 26 amino acids of Ypl107w - *N26Δ*Ypl107w. This vector was then used to produce a ^{35}S-labelled precursor and presented to isolated wild-type yeast mitochondria following the import assay described above (**Figure 4.8**). The results show that Ypl107w cannot be imported without its N26 sequence. Thus, its mitochondrial targeting signal must lie within this region. Altogether, the evidence indicates that Ypl107w is a soluble, mitochondrial matrix protein with an N-terminal mitochondrial targeting signal that requires both its targeting signal and membrane potential for import.

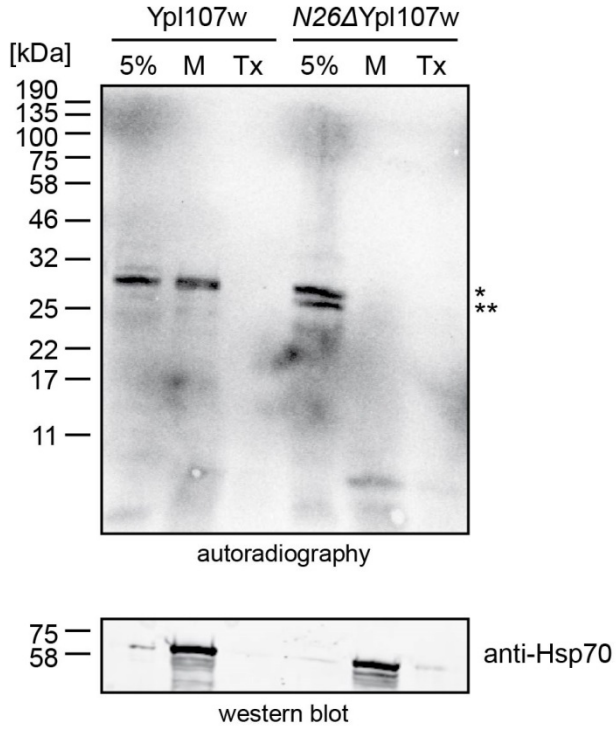

Figure 4.8. Import of radiolabelled *N26Δ*Ypl107w and Ypl107w. *N26Δ*Ypl107w and Ypl107w were synthesised as radiolabelled precursors and imported into isolated wild-type yeast mitochondria. Import reactions were stopped after 20 minutes then treated with trypsin to destroy unimported material (M), and a combination of Triton-X-100 and trypsin as a negative control (Tx). 5% corresponds to 5% of the precursor used for each import reaction. Radiolabelled precursors were detected by digital autoradiography. * - Ypl107w/*N26Δ*Ypl107w (size difference not detectable); ** - Unknown, could be translation from a downstream Met. Anti-Hsp70 was used as a loading control and control for successful Tx/trypsin treatment.

4.3.3. BN-PAGE analysis

As the evidence points strongly in favour of Ypl107w as a true mitochondrial protein, based on mass spectrometry data, import and localisation assays, the next step was to determine whether Ypl107w is part of a complex (or complexes). Blue native PAGE (BN-PAGE) was performed to isolate native protein complexes after radiolabelled import of Ypl107w into isolated wild-type mitochondria. Unfortunately, the results (after multiple tries and using different solubilisation methods) were not clear as no sharp bands could be detected other than one that is assumed to be the monomeric form of Ypl107w (**Figures 4.9A & 4.9B**). However, upon closer inspection there are several 'smears' that *might* indicate the presence of Ypl107w within multiple different complexes of varying molecular weights. These remain to be verified and the BN-PAGE protocol requires further optimisation.

In parallel to the work carried out in **Sections 4.3.2** and **4.3.3**, a phenotypic approach was taken to provide a more detailed analysis of yeast cells lacking Ypl107w (*ypl107wΔ*). Growth assays, drop tests, and H_2O_2 and diamide sensitivity assays were used to gather information that could potentially relate Ypl107w to a role in mitochondrial function.

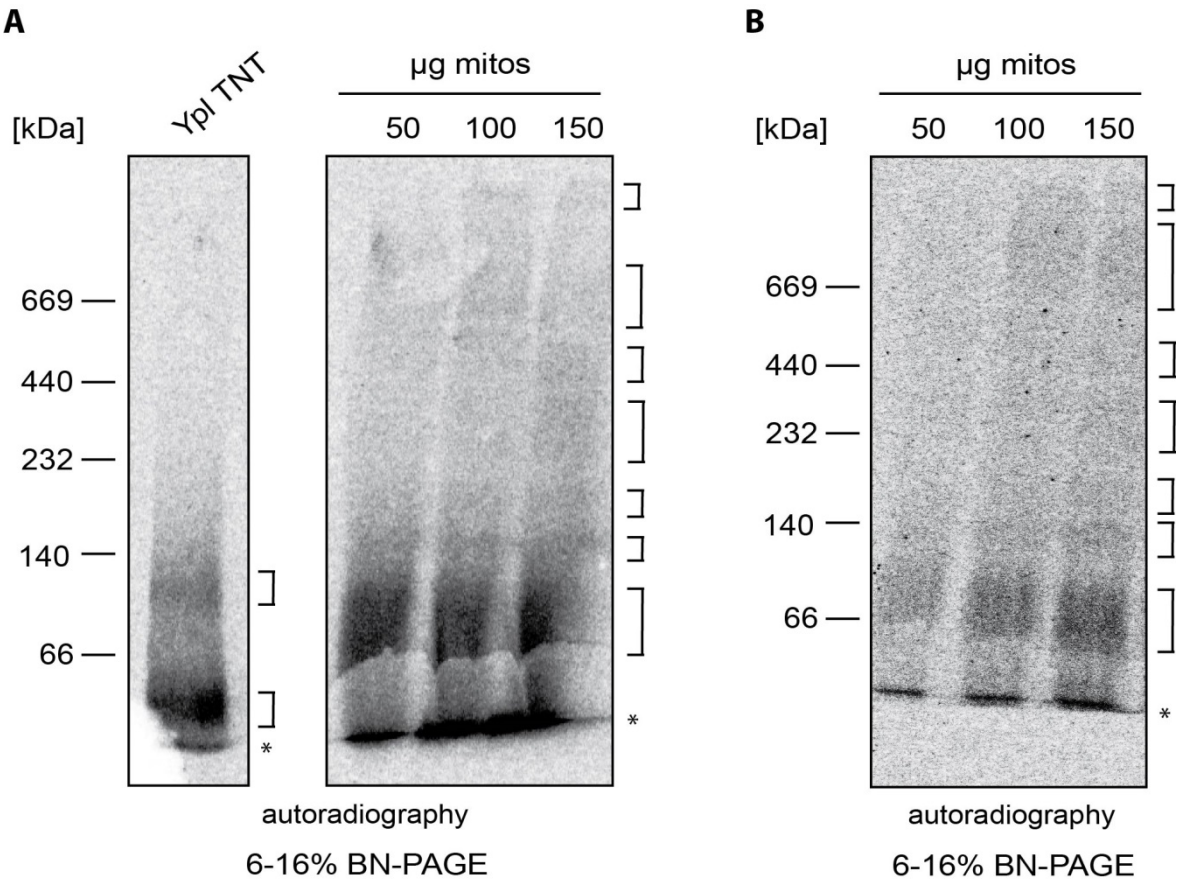

Figure 4.9. BN-PAGE analysis of Ypl107w after radiolabelled import. Ypl107w was synthesised as a ^{35}S-labelled precursor and imported into isolated wild-type yeast mitochondria. The import reaction was stopped after 20 minutes then treated with trypsin to destroy unimported material. Three lanes containing increasing amounts of isolated mitochondria after import were loaded into a 6-16% gel (50 µg, 100 µg and 150 µg) to help detect complexes that might not be apparent in lesser amounts. Ypl107w after transcription and translation was loaded as a control. (**A**) and **(B**) are repeats of the same experiment. * - Ypl107w (monomer?). Brackets indicate potential complexes. Note: Ypl107w is a 29 kDa protein (predicted 25 kDa after cleavage upon import).

4.3.4. Growth assays and drop tests

The first phenotypic analysis that was performed was to check for growth defects between the yeast mutant *ypl107wΔ* which lacks the entire open reading frame (ORF) for Ypl107w and the wild-type BY4741 strain. This *ypl107wΔ* mutant is in the BY4741 genetic background and was obtained from GE Healthcare. These yeasts were grown in fermentable (YPD - glucose) and non-fermentable media (YPLac - lactate; and YPGly - glycerol) over a period of 16 hours. The results indicate that yeast lacking Ypl107w struggle to grow on non-fermentable media which suggests that they have impaired mitochondrial function (**Figure 4.10**). Non-fermentable media is also known as respiration media as they force the cells to use only aerobic respiration to produce ATP.

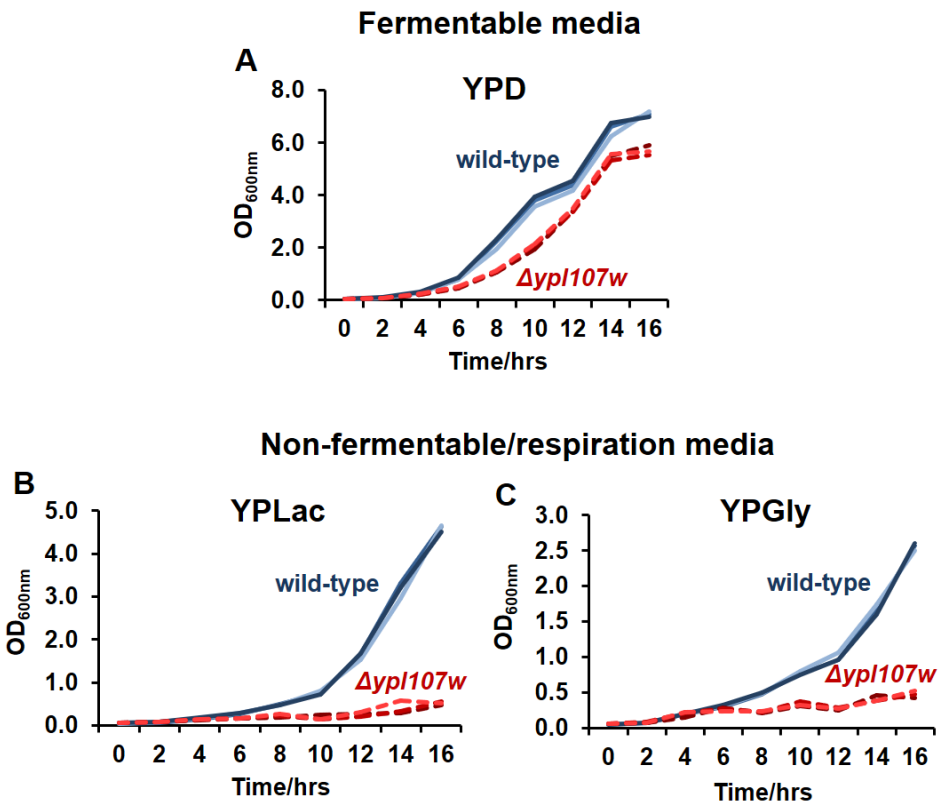

Figure 4.10. Growth of *ypl107wΔ* vs wild-type yeast. Growth curves for *ypl107wΔ* and wild-type BY4741 in (**A**) the fermentable media YPD, and the non-fermentable mediums (**B**) YPLac and (**C**) YPGly. YPD – yeast extract, peptone and glucose. YPLac - yeast extract, peptone and lactic acid. YPGly – yeast extract, peptone and glycerol. Blue lines indicate wild-type yeast; red dashed lines indicate *ypl107wΔ* yeast. Three colonies from each strain were grown to stationary phase in YPD before diluting to OD_{600nm}: 0.05 in each media, and measured every hour for 16 hours.

Drop tests were also performed alongside the growth curves. Agar plates were made containing the same fermentable and non-fermentable carbon sources and *ypl107wΔ* yeast were compared to wild-type, along with various positive and negative controls (**Figure 4.11**). The results of these drop tests indicate that *ypl107wΔ* do not exhibit growth defects on the fermentable media YPD (as expected), but that they were slightly sensitive to growth on the non-fermentable media YPLac (as shown in the growth curves).

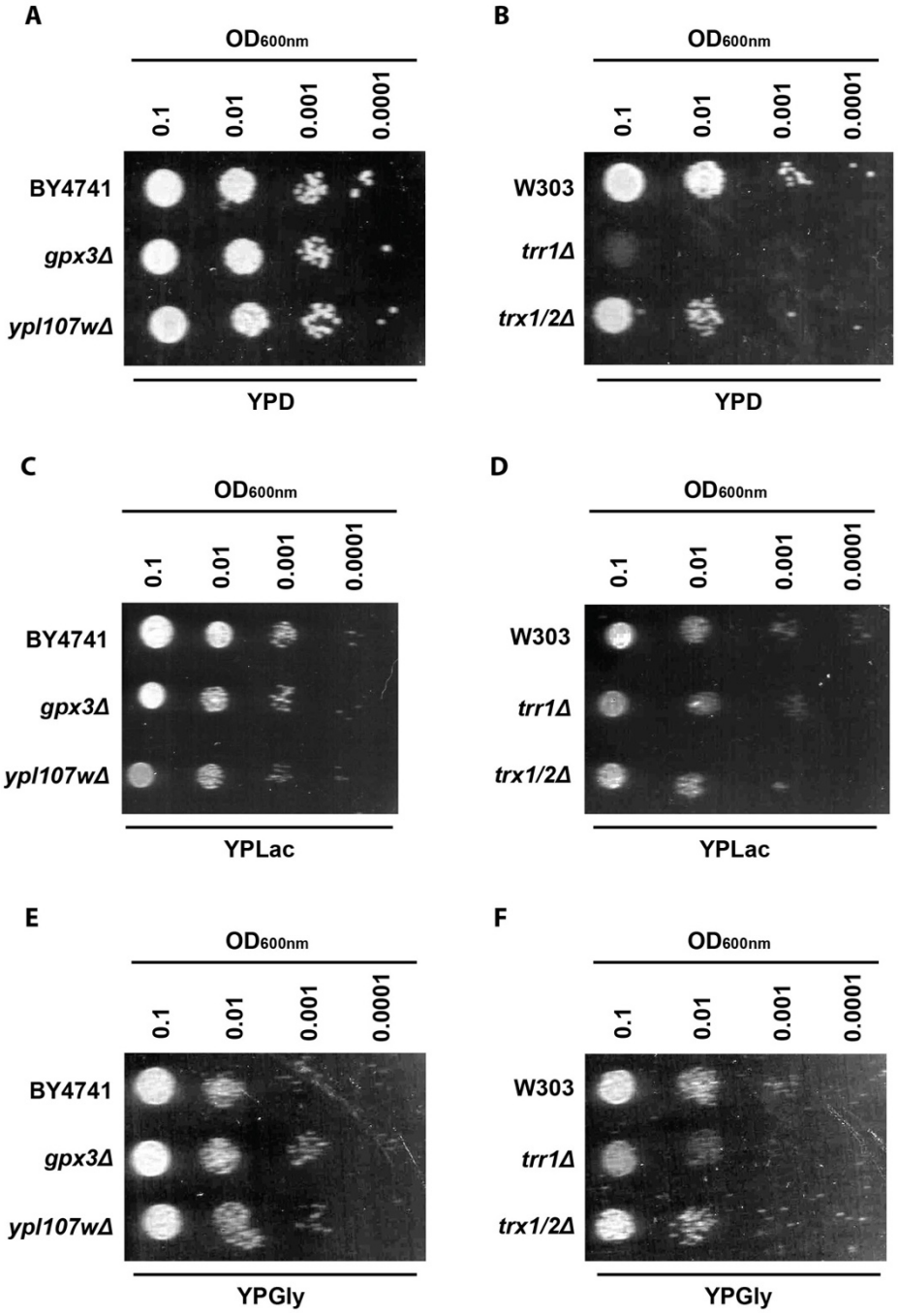

Figure 4.11. Yeast drop tests in fermentable vs non-fermentable media. Yeast were grown to stationary phase in liquid YPD media overnight then serially diluted in the morning and

spotted onto plates containing fermentable media (**A** and **B**) YPD, and non-fermentable media (**C** and **D**) YPLac and (**E** and **F**) YPGly. YPD – yeast extract, peptone and glucose/dextrose. YPLac - yeast extract, peptone and lactic acid. YPGly – yeast extract, peptone and glycerol. Plates were incubated for 48 hours at 30°C. These are representative images from three repeat assays. BY4741 is the representative wild-type background strain for *gpx3Δ* and *ypl107wΔ*. W303 is the representative wild-type background strain for *trr1Δ* and *trx1/2Δ*.

Interestingly, *ypl107wΔ* yeast grown on YPLac plates turned brown in colour, whereas all the other strains stayed their typical white/cream colour (**Figure 4.12**). The reason for this colour change is entirely unknown. This colour change was also observed when the *ypl107wΔ* yeast strain was grown on standard YPD plates but only after storage at 4°C for a few weeks. Thus, it appears that the brown colour phenotype is exacerbated by growth in a non-fermentable carbon source. On observation under a light microscope, *ypl107wΔ* yeast appeared to have a petite phenotype in comparison to BY4741 yeast (data not shown).

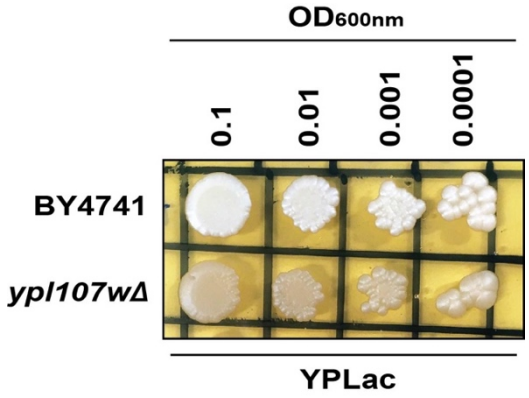

Figure 4.12. Colour of wild-type vs *ypl107wΔ* yeast grown on non-fermentable media. Yeast were grown to stationary phase in liquid YPD media overnight then serially diluted in the morning and spotted onto plates containing the non-fermentable media YPLac (yeast extract, peptone and lactic acid). Plates were incubated for 48 hours at 30°C. BY4741 is the representative wild-type background strain for *ypl107wΔ*. BY4741 yeast cells remained their typical white/cream colour (top row) whereas the mutant *ypl107wΔ* yeast turned brown (bottom row).

4.3.5. Hydrogen peroxide and diamide sensitivity assays

As a high-throughput study found that *ypl107wΔ* yeast have a decreased resistance to oxidative stress when exposed to 3 mM H_2O_2 (Brown et al., 2006), a H_2O_2 sensitivity assay (also known as a halo assay) was performed where H_2O_2 was spotted onto the middle of a YPD agar plate containing yeast cells (refer to **Chapter 2**, **Section 2.2.4**). The results shown in **Figures 4.13 and 4.14** indicate that the *ypl107wΔ* strain obtained from GE Healthcare is more sensitive to H_2O_2 than the wild-type control, along with the positive controls *trr1Δ* and *gpx3Δ*, as they produced larger clear zones in comparison to their wild-type background strains. The *trr1Δ* mutant was chosen as a positive control based on prior evidence by Hacioglu et al (2010) who found that a *trr1Δ* yeast strain exhibited a large halo when grown on plates spotted with H_2O_2. Similarly, yeast lacking Gpx3 are known to be more sensitive to H_2O_2 (Ma et al., 2007).

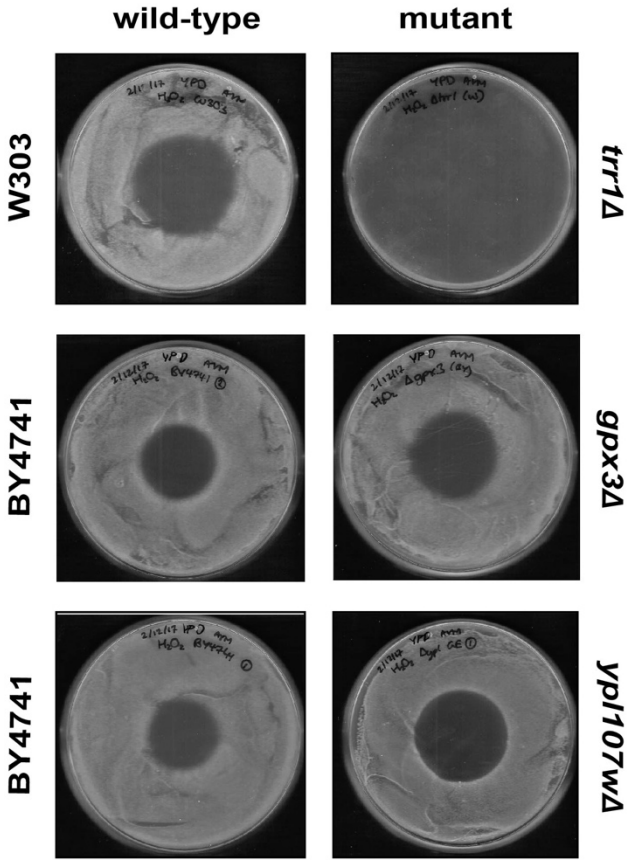

Figure 4.13. H_2O_2 sensitivity assay - plates. Yeast were grown to stationary phase in liquid YPD media, diluted to OD_{600nm}: 0.1 and then spread onto YPD plates. Plates were then spotted with 5µl 8.8 M H_2O_2 in the centre and left to grow for 24 hours at 30°C. Wild-type strains are

shown in the left panels; *trr1Δ* is in the W303 genetic background and *gpx3Δ* and *ypl107wΔ* are in the BY4741 background. Positive controls that are known to be sensitive to H_2O_2 are *trr1Δ* and *gpx3Δ*. These are representative images from four repeat assays. The diameters of the clear zones were measured from four repeats; the results of all four are shown in **Figure 4.14**.

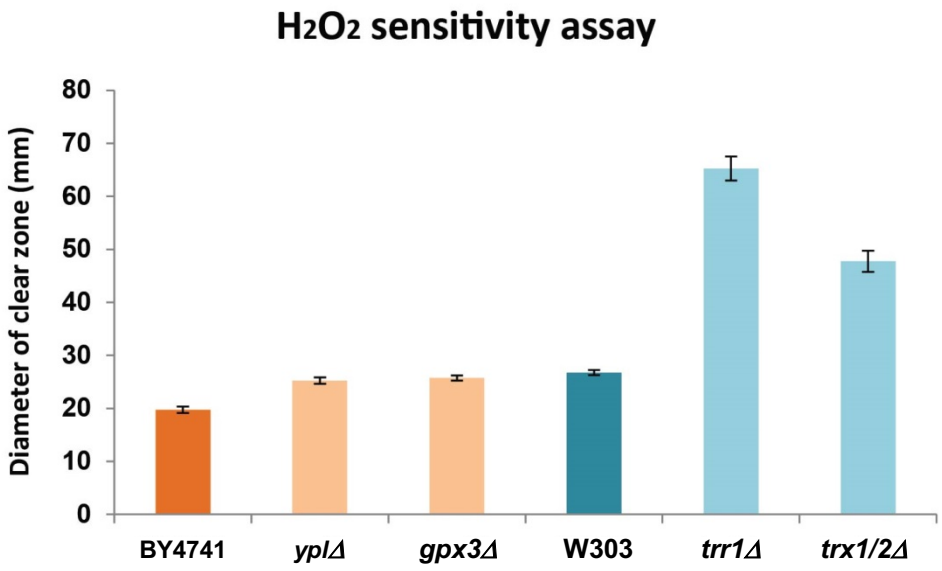

Figure 4.14. H_2O_2 sensitivity assay - diameters. Yeast were grown to stationary phase in liquid YPD media, diluted to OD_{600nm}: 0.1 and then spread onto YPD plates. A 5µl drop of 8.8 M H_2O_2 was placed onto the centre of each plate. Once dried, plates were incubated for 24 hours at 30°C. The diameter of the clear zone, 'halo', was measured. The diameters shown here are the mean of four repeat assays for each yeast strain. Error bars represent standard error of the mean. BY4741 is the representative wild-type background strain for *gpx3Δ* and *ypl107wΔ*. W303 is the representative wild-type background strain for *trr1Δ* and *trx1/2Δ*.

In addition to H_2O_2, the alternative thiol oxidising agent diamide was used to test for oxidant sensitivity in the *ypl107wΔ* strain. Yeast cells were spotted onto YPD plates containing either 0, 2.0 or 2.5 mM diamide and grown for 3 days at 30˚C. The results indicate that *ypl107wΔ* and *gpx3Δ* are slightly more sensitive than wild-type yeast to 2.0 mM diamide; no yeast strains were able to grow with 2.5 mM diamide (**Figure 4.15**). This assay should be repeated using lower concentrations of diamide.

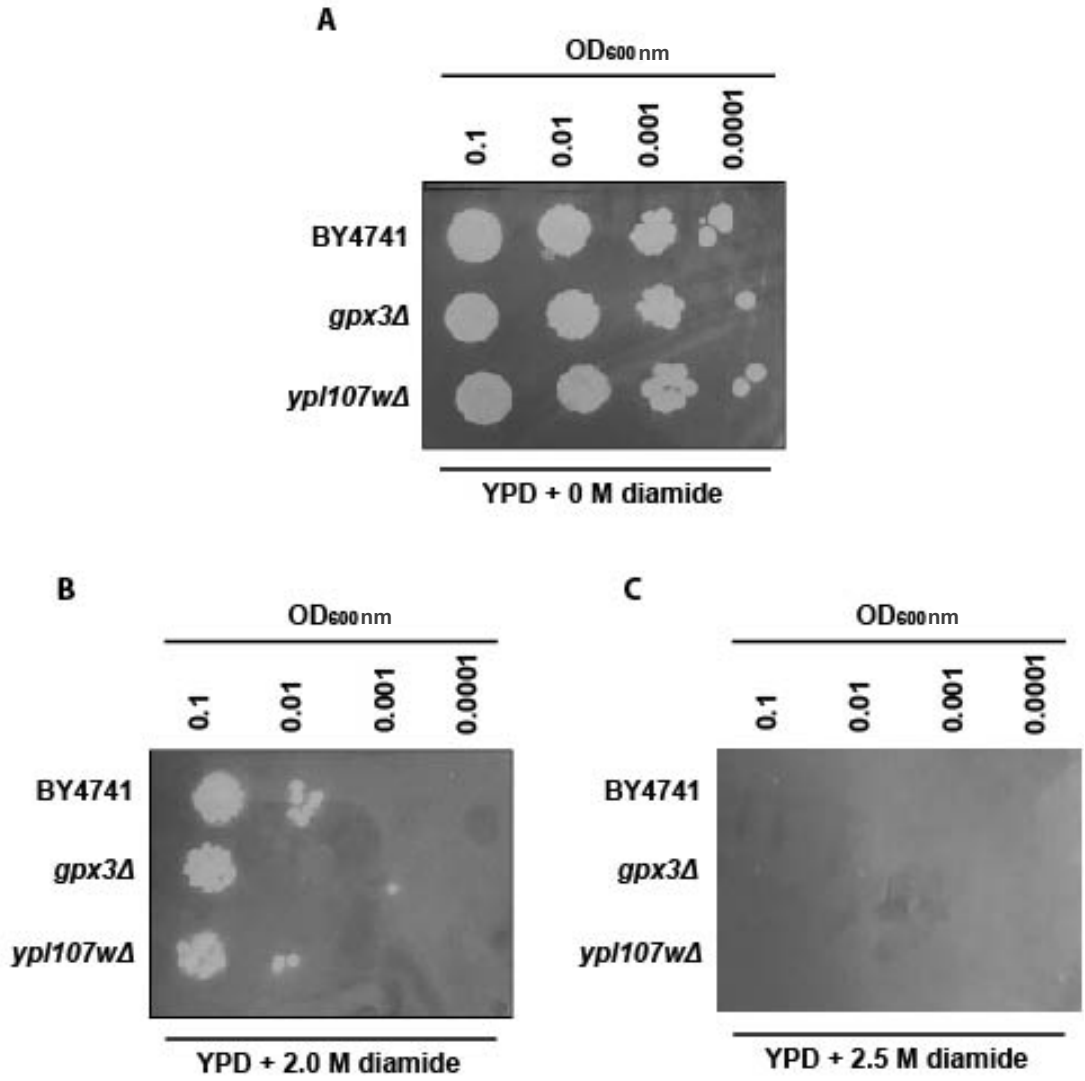

Figure 4.15. Diamide sensitivity assay. Yeast were grown to stationary phase in liquid YPD media overnight before being serially diluted in the morning and spotted onto plates containing either 0, 2.0 or 2.5 mM diamide. Plates were left to grow for 3 days at 30°C. Wild-type BY4741, *gpx3Δ* and *ypl107wΔ* on YPD with (**A**) no diamide, (**B**) 2.0 mM diamide, and (**C**) 2.5 mM diamide. These are representative images from three repeat assays.

4.3.6. Steady-state protein levels in *ypl107wΔ* mitochondria

Mitochondria from *ypl107wΔ* yeast were isolated by density gradient centrifugation and analysed by western blotting. Various mitochondrial proteins were probed and their expression levels were compared to mitochondria from the wild-type BY4741 strain. The results suggest that Gpx3 and Cyt*c* levels are lower in *ypl107wΔ* mitochondria, whilst Erv1 and Tim11 levels are higher (**Figure 4.16**); quantifications are shown in **Figure 4.17** and repeat western blots which indicate the same findings can be seen in the **Appendices**, **Figure 7.5**. It is not known why these levels are different in the mutant strain; however, one could hypothesise that Erv1 is upregulated when the levels of Gpx3 and Cyt*c* are down in order to compensate for their absence in the Mia40 oxidative folding pathway, but this remains to be investigated. Tim11 is a small 11 kDa protein of the IM that is subunit e of the mitochondrial ATP synthase complex (ATPase) (Arnold et al., 1997). Although not essential for ATPase function, it is involved in dimerisation and stability of the complex (Devenish et al., 2000). One hypothesis to explain why Tim11 is upregulated could be that it is compensating for defects in respiratory chain activity (potentially caused by the lack of Ypl107w) by stabilising ATPase in order to maintain adequate ATP production. It would be interesting to determine the individual activities of all the respiratory chain complexes in WT vs *ypl107wΔ* mitochondria.

Intriguingly, an odd band pattern against Tom22 was detected in *ypl107wΔ* mitochondria; although three bands are detected in the wild-type BY4741 and it is unclear which is specifically recognising Tom22, all three are different in the mutant strain. The reason for this is unknown, however, it could be evidence for the loss of Ypl107w function affecting mitochondrial transport.

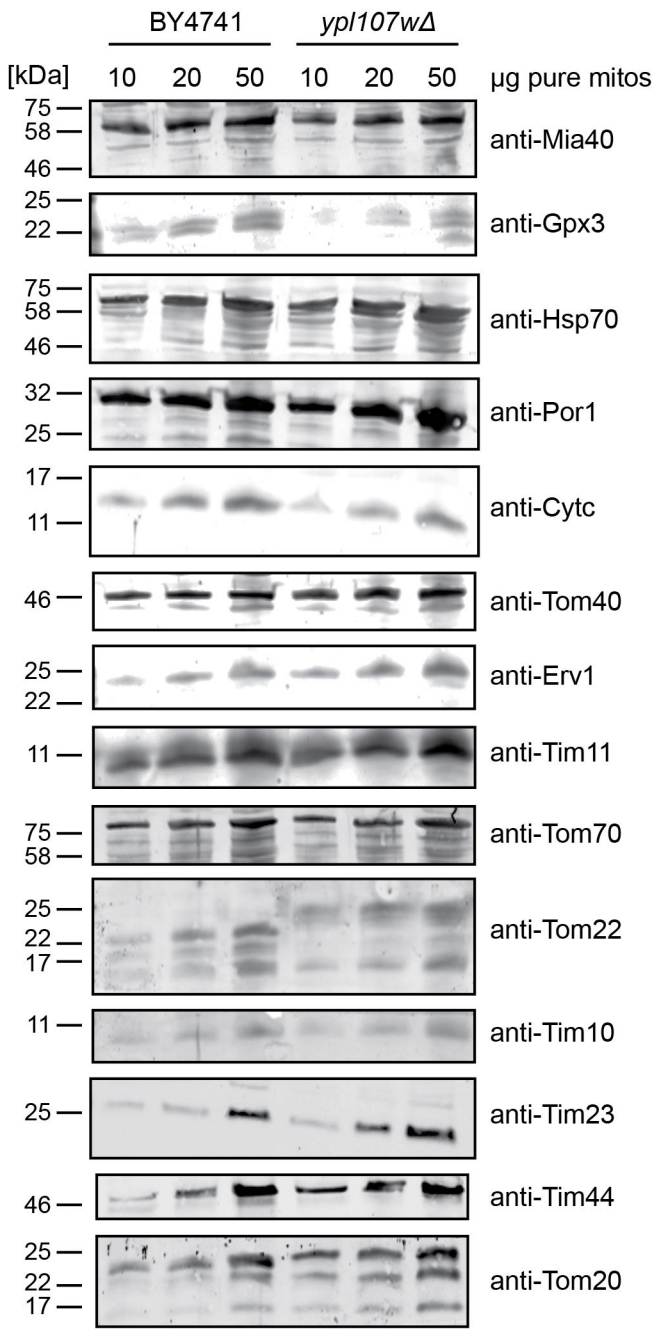

Figure 4.16. Comparison of protein levels in wild-type BY4741 vs *ypl107wΔ* mitochondria. Mitochondria were isolated from yeast grown to mid-log phase in media containing the non-fermentable carbon source lactic acid. After density gradient centrifugation, purified mitochondria (pure mitos) were separated by SDS-PAGE and analysed by western blotting to detect various mitochondrial proteins. Antibodies against OM proteins include: anti-Por1, anti-Tom40, anti-Tom70, anti-Tom22 and anti-Tom20. IMS proteins include: anti-Mia40, anti-Gpx3, anti-Erv1, anti-Cytc and anti-Tim10. IM proteins include: anti-Tim11, anti-Tim23 and anti-Tim44. Anti-Hsp70 was used as a matrix protein marker.

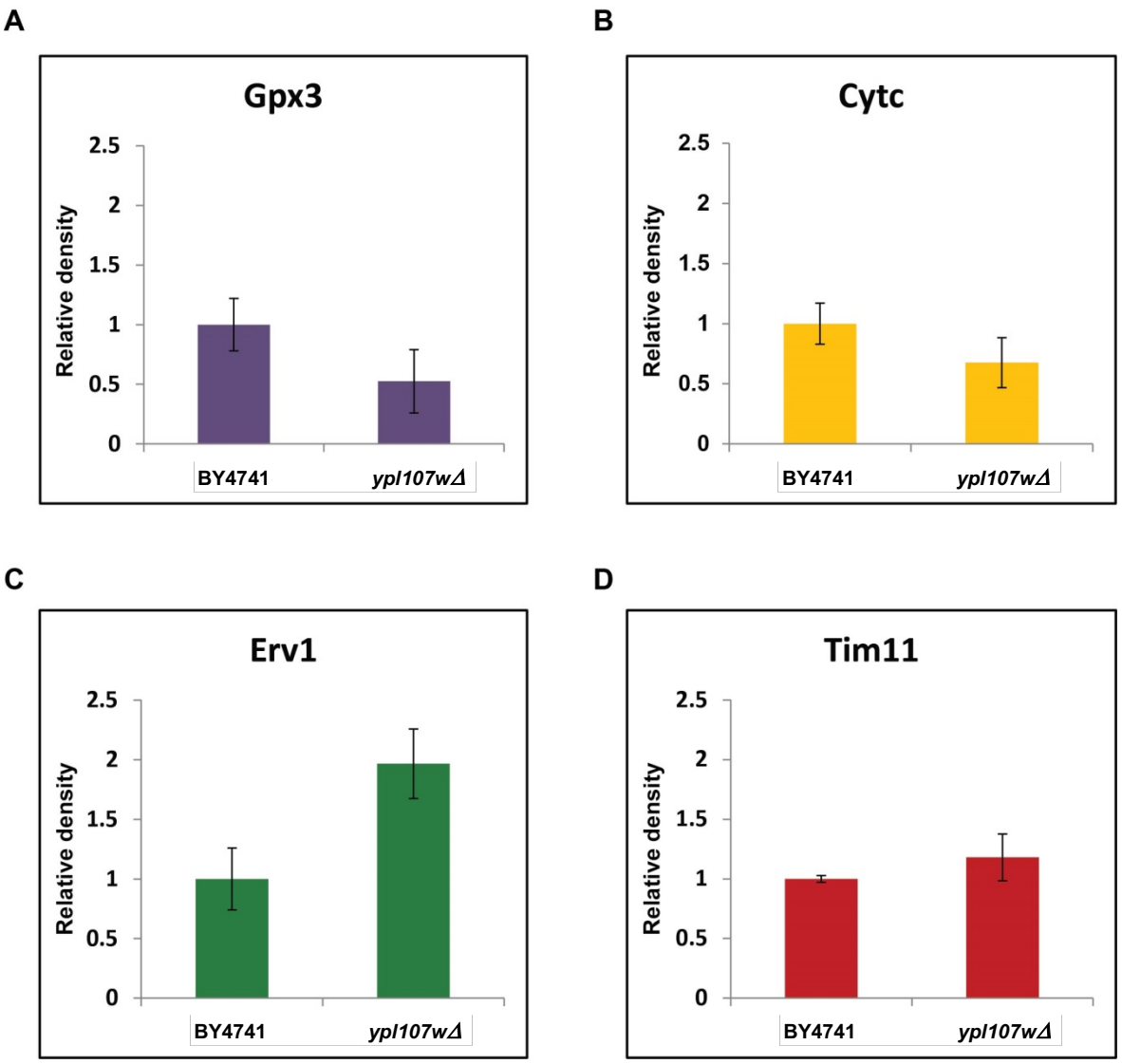

Figure 4.17. Quantification of protein levels in wild-type BY4741 vs *ypl107wΔ* mitochondria. Quantification of western blot band density from **Figure 4.16** was performed using Image J 1.48v. The y-axis represents the relative density of bands when normalised against a control protein which was probed for on the same blot; (**A**) Gpx3 was normalised against Mia40, (**B**) Cyt*c* against Por1, and (**C**) Erv1 and (**D**) Tim11 against Tom40. Error bars show the standard error of the mean.

4.4. Discussion

At the start of this project very little was known about Ypl107w other than its potential mitochondrial localisation based on fluorescent tagging of the protein (Huh et al., 2003) and some phenotypic data on a *ypl107wΔ* yeast strain collected during high-throughput studies (Brown et al., 2006; Yoshikawa et al., 2009; Breslow et al., 2008; Blackman et al., 2012; Michaillat and Mayer, 2013). These studies indicate that *ypl107wΔ* yeast cells are less fit and are less resistant to H_2O_2, salt and the drug elesclomol which targets the respiratory chain, and, have a small defect in vacuolar fragmentation. However, no study to date has exclusively focused on Ypl107w or any of its homologs.

Bioinformatics analysis on Ypl107w revealed that, for every organism checked, a homolog exists; its human homolog is hOXLD-1 (**Figure 4.1**). Furthermore, a highly conserved domain within Ypl107w known as 'oxidoreductase-like domain, N-terminal' is present in over 2000 proteins from 749 species (InterPro – IPR019180; Pfam – PF09791; Finn et al., 2016), but nothing is known about the function of any of these (**Figures 4.2 & 4.3**). A mitochondrial targeting predictor tool, MITOPROT, predicts a cleavable N-terminal targeting sequence comprising the first 26 amino acids of Ypl107w, and a secondary structure prediction of Ypl107w predicts the presence of an alpha-helical structure within this region (**Figure 4.4**). Together, this is suggestive of a classical N-terminal mitochondrial matrix targeting signal that is cleaved upon import. Finally, an ion binding predictor tool predicted Zn^{2+} and Na^{+} binding sites (**Figure 4.5**). In order to test these predictions, Ypl107w would need to purified and structurally characterised using a range of techniques to determine whether it can bind metal ions, and if so, which ones and what its oligomeric state is. Unfortunately, attempts to purify Ypl107w within the duration of this PhD were not successful as the protein was highly prone to aggregation (data not shown). Future work to optimise purification conditions is required. Finally, the potential interaction between Ssc1 and Ypl107w should be explored as this may be of importance to the role of Ypl107w in the mitochondrial matrix. However, as Ssc1 is involved in the refolding import of matrix proteins after entry through the TIM23-PAM complex (Horst et al., 1997), it could be that their interaction is purely to help facilitate the folding of Ypl107w within the matrix.

Switching from biochemistry to genetics, a search revealed that out of 75 known genetic interactions, 23 of these are genes associated with mitochondria; 20 negative and 3 positive (**Table 4.1**). Inputting these 23 genes into a Gene Ontology Term Finder tool highlighted three processes (mitochondrial tRNA thio-modification, mitochondrial organisation and protein lipoylation) and two functions (sulphurtransferase and oxidoreductase activity), see **Table 4.2**. Furthermore, a search for genes with similar expression patterns using SPELL, Serial Pattern of Expression Levels Locator (Hibbs et al., 2017), generated a list of the top 19 genes; however, no significant ontology terms were found other than biological process and molecular function unknown (**Appendices**, **Table 7.1**). Moving back to biochemistry and switching to hOXLD-1, 49 physical interaction partners are listed by Huttlin et al. (2015, 2017), of which 38 are mitochondrial proteins (**Table 4.3**). A GO term finder tool found a vast number of significant ontology terms – mostly related to metabolism but also mitochondrial gene expression, mitochondrial organisation, mitochondrial RNA processing and mitochondrial translation (**Appendices**, **Table 7.2**). Based on these data, could Ypl107w and its homologs be involved in mitochondrial organisation by regulating mitochondrial gene expression and translation, and/or by helping to assemble the respiratory complexes?

To begin our experimental exploration of Ypl107w, its import into mitochondria was confirmed by synthesising a radiolabelled precursor and presenting it to isolated wild-type yeast mitochondria; upon import Ypl107w was protease-protected (**Figure 4.6**). Its import was also dependent on membrane potential. A localisation assay was then carried out to assess which mitochondrial subcompartment the protein resides in, and the results of the assay suggest that Ypl107w is a soluble, matrix protein (**Figure 4.7**). Next, the predicted mitochondrial targeting sequence of Ypl107w was confirmed by checking the import of Ypl107w without its N-terminal 26 amino acids (*N26Δ*Ypl107w) which, as expected, was not successful (**Figure 4.8**). Future import assays using mitochondria isolated from mutant strains defective in different import pathway components could be carried out to establish which pathway Ypl107w follows, for example: *tom40-ts*, *tim23-ts*, *galMia40* and *galErv1* yeast (refer to **Chapter 1** for a description of the various mitochondrial import pathways). If the import of Ypl107w was shown to be dependent on

the presence of the TIM23 complex, this would provide further clarification that Ypl107w resides in the mitochondrial matrix.

Soon after these experiments were completed, a paper was published by Morgenstern et al. (2017) reporting an additional 82 high-confidence mitochondrial proteins, one of which was Ypl107w. After carrying out their own import experiments on a multitude of these new proteins, they gave Ypl107w its standard name, Dpc25, which stands for delta-psi dependent mitochondrial import and cleavage protein of ~25 kDa. Although the timing of their paper was unfortunate, it did provide reassuring evidence in an independent study that is in complete agreement with our own, and it only encouraged us to probe Ypl107w in more detail. Thus, the next aim was to determine whether Ypl107w is part of any complexes.

A BN-PAGE analysis was performed to isolate native protein complexes after radiolabelled import of Ypl107w into wild-type mitochondria. The initial results, although unclear, suggest that Ypl107w may be part of multiple complexes (**Figure 4.9**) but the BN-PAGE analysis requires more extensive optimisation in order to detect clearer, sharper bands. Morgenstern et al. (2017) also attempted BN-PAGE on Ypl107w, however, akin to ours they could not provide any clear evidence of the presence of the protein in distinct complexes. One hypothesis behind the presence of multiple 'smeary' bands in our BN-PAGE could be that Ypl107w is a chaperone/assembly protein and thus might interact with lots of proteins and complex subunits. An additional hypothesis is that it is natively unfolded when produced via the TNT system (or when expressed in bacteria) which leads to aggregation of the protein as it is not tightly folded, thus it can then falsely interact with many other proteins. We also tried to determine whether any of the respiratory chain complexes were affected in *ypl107wΔ* mitochondria by performing BN-PAGE followed by Coomassie staining on wild-type vs *ypl107wΔ* mitochondria. The results were unclear (data not shown) and this assay should be repeated using antibodies against the yeast respiratory chain complexes. Sadly, these were not available in the lab and could not be commercially bought. Another method would be to analyse protein partners of

Ypl107w by carrying out pulldowns and analysing by mass spectrometry or immunoprecipitations with or without the use of crosslinkers.

Parallel phenotypic experiments found that *ypl107wΔ* yeast exhibit growth defects when grown in non-fermentable carbon sources, including lactic acid and glycerol, when compared to glucose (**Figures 4.10 & 4.11**), and, that *ypl107wΔ* yeast colonies turn brown after growth on plates containing lactic acid (**Figure 4.12**). We also confirmed the previous finding that *ypl107wΔ* yeast have a decreased resistance to H_2O_2 (Brown et al., 2006; **Figures 4.13 & 4.14**). As Ypl107w is a bona fide mitochondrial protein (**Figure 4.6**; Morgenstern et al., 2017), it would make sense that a null mutant would display growth defects that are likely attributed to impaired mitochondrial function.

A similar sensitivity assay using diamide instead of H_2O_2 did not yield any conclusive results as the wild-type BY4741 strain was also affected by the concentrations of diamide used (**Figure 4.15**); this assay could be repeated using lower concentrations. However, it is important to note that H_2O_2 and diamide exert very different physiological effects; H_2O_2 and diamide both induce a Yap1-dependent antioxidant response (refer to **Chapter 1**, **Section 1.6**) but diamide drastically alters the cellular balance of GSH and GSSG in a non-specific manner. Thus, it would be interesting to use fluorescent sensors to measure the levels of H_2O_2 in the mitochondrial matrix (and also the cytosol as a control) in both *ypl107wΔ* and wild-type cells.

Mitochondria isolated from wild-type and *ypl107wΔ* yeast by density gradient centrifugation were analysed by western blotting after SDS-PAGE and the levels of various mitochondrial proteins were quantified (**Figures 4.16 & 4.17**). Intriguingly, less Gpx3 and Cyt*c* were found in *ypl107wΔ* mitochondria but the reason for this is currently unknown. Given that Gpx3 and Cyt*c* are putative mitochondrial partners and Ypl107w was a putative hit in the mass spectrometry data when N18M20LGpx3His was used as bait (**Section 3.3.7**), it would be interesting to investigate whether there is a link, direct or

indirect, between all three proteins. *In vitro* interaction assays and immunoprecipitations could be used to help to elucidate which proteins are interacting and under what conditions. It would also be of importance to check whether any other cytochrome proteins are affected in *ypl107w⊿* mitochondria; for this, more antibodies are required. In addition, matrix protein levels need to be assessed due to the localisation of Ypl107w in the mitochondrial matrix but again more antibodies are needed. Another perhaps more suitable method would be to send isolated mitochondria for quantitative mass spectrometry analysis. Furthermore, future work should aim to measure the mitochondrial membrane potential in *ypl107wΔ* mitochondria by using a membrane potential sensitive probe, 3,3'-dipropylthiadicarbocyanine iodide - DiSC(3), and oxygen consumption calculated using a Clarke electrode.

Finally, future work must address the question whether the human homolog hOXLD-1 can be (i) imported into yeast mitochondria, and (ii) rescue any of the phenotypic defects observed in the *ypl107w⊿* yeast strain. This work will be essential in uncovering whether hOXLD-1 is a real functional homolog of Ypl107w, and, together with parallel work in human cells, could provide instrumental information on proteins containing a highly conserved 'oxidoreductase-like domain' of which no literature exists.

Chapter 5

Investigating Gpx3 in peroxisomes

5. Investigating Gpx3 in peroxisomes

5.1. Introduction

Peroxisomes are highly dynamic organelles in respect to their size, shape, protein content and abundance (Smith and Aitchison, 2013). Researchers are still trying to pinpoint exactly which proteins localise to peroxisomes, and under what conditions, but it is clear that the peroxisomal proteome continuously changes in response to the cellular metabolic environment and new proteins are regularly being identified (Yifrach et al., 2016).

In 2012, a study investigating the role of Gpx1 in *S. cerevisiae* peroxisomes also identified Gpx3 in the peroxisomal matrix due to cross-reactivity of anti-Gpx1 with Gpx3 (Ohdate and Inoue, 2012). It was found that Gpx1 exhibits peroxidase activity in peroxisomes, and when absent peroxisome biogenesis and growth in oleic acid media is compromised. Oleic acid induces peroxisome proliferation by inducing the transcription of genes required for fatty acid β-oxidation; a response mediated by the Pip2-Oaf1 transcription factor complex upon binding to the oleate response element (ORE) present within target genes (Rottensteiner et al., 1996; Rottensteiner et al., 1997; and Karpichev et al., 1997). These phenotypes were not rescued by expression of a peroxidatic cysteine mutant, $Gpx1^{C36S}$, whereas expression of resolving cysteine mutants could. This indicates that the function of Gpx1 in peroxisomes relies on the ability of Gpx1 to form disulphide bonds. The authors suggested that Gpx1 might be involved in the redox regulation of Pex11; however, the literature points towards a potential interaction between Gpx3 and Pex11 (Tarassov et al., 2008). No experiments were undertaken to investigate the role of Gpx3 in peroxisomes.

Pex11 is a highly abundant 27 kDa peroxisomal membrane protein required for peroxisomal fission (Erdmann and Blobel, 1995; Marshall et al., 1995), fatty acid oxidation

(van Roermund et al., 2000), establishing mitochondria-peroxisome contact sites via the ERMES complex (Mattiazzi Usaj et al., 2015), and transferring metabolites across the peroxisomal membrane (Mindthoff et al., 2016). The function of Pex11 in peroxisome proliferation depends upon the oligomeric state of the protein; monomeric Pex11 is required for proliferation whilst dimeric Pex11 inhibits organelle division (Marshall et al., 1995). An upstream sequence analysis of Pex11 reveals a possible 17-amino acid N-terminal extension with similarities to the N18 of Gpx3 (see later **Figure 5.12**).

Based on the evidence that Gpx3 and Pex11 are potential interactors (Tarassov et al., 2008) and the localisation of Gpx3 in both organelles (Ohdate and Inoue, 2012), the question as to whether the two are entwined in organelle cross-talk is apparent. Furthermore, the involvement of Pex11 in the ERMES complex (Mattiazzi Usaj et al., 2015) and 'mislocalisation' of Pex11 to mitochondria in the absence of peroxisomes (Mattiazzi Usaj et al., 2015; Wróblewska et al., 2017) are also suggestive of a potential link between the two proteins.

5.2. Aims

The initial aim of this chapter was to confirm the presence of Gpx3 in peroxisomes, and determine whether the N-terminally extended version of Gpx3 (N18Gpx3) is present also in peroxisomes. To do this, peroxisomes and mitochondria were isolated in tandem and steady-state protein levels were assessed by western blotting (**Figures 5.2 & 5.4**). The results were unexpected and suggested that alongside the presence of Gpx3 in both organelles, Trx1, Trx2, Erv1 and Mia40 (albeit a shorter version) may also reside in peroxisomes.

Based on this, four new objectives emerged: (**i**) to look for potential peroxisomal targeting signals in the suspected dually-localised proteins, (**ii**) to confirm the presence of a shorter form of Mia40 in peroxisomes and analyse its targeting signal, (**iii**) to determine peroxisomal interaction partners of Gpx3, (**iv**) to investigate the import of Pex11 and N17Pex11 in mitochondria, and (**v**) to test whether Gpx3 and Pex11 are interactors.

5.3. Results

5.3.1. Isolation of mitochondria and peroxisomes confirms the presence of Gpx3 in both organelles

As it is known that a pool of Gpx3 resides in the mitochondrial IMS, and that an N-terminal extension of 18 amino acids boosts its mitochondrial targeting capacity, it was questioned whether the same targeting signal might be responsible for peroxisomal import. First, the presence of Gpx3 within mitochondria and peroxisomes in yeast was confirmed by isolating both organelles from the same yeast culture. Yeast cells were grown in 0.12% oleic acid to induce peroxisome proliferation, followed by fractionation and separation of organelles by density gradient centrifugation (**Figure 5.1**). Gpx3 was detected in both mitochondria and peroxisomes (**Figure 5.2**).

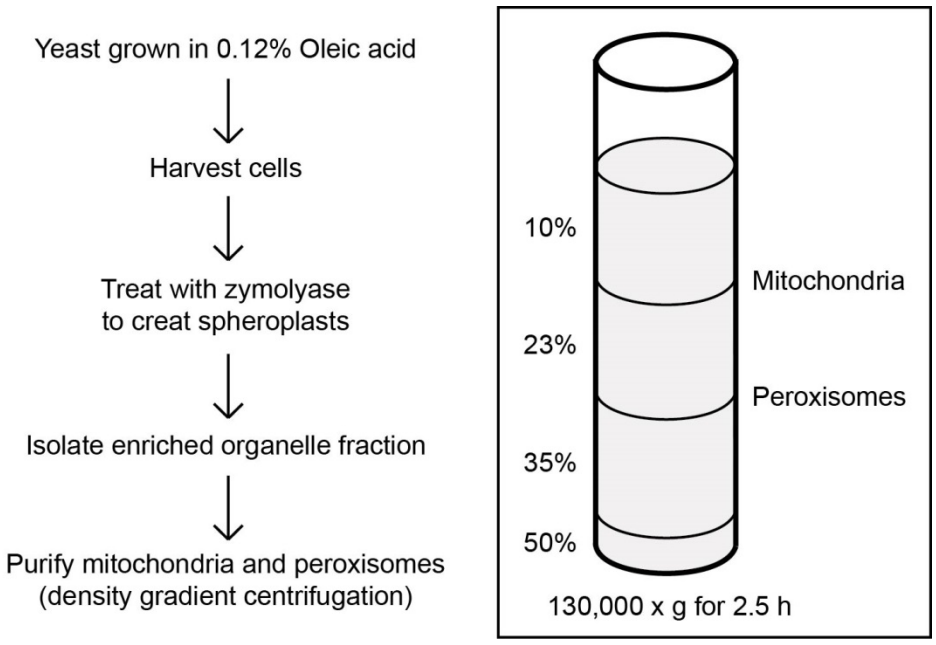

Figure 5.1. Isolation of yeast mitochondria and peroxisomes. Yeast were grown in media containing 0.12% oleic acid for 12-16 hours to induce peroxisome proliferation before purifying both mitochondria and peroxisomes using Nycodenz density gradient centrifugation. Mitochondria were collected from the 10%-23% gradient interface; peroxisomes were collected from the 23%-35% interface. Refer to **Chapter 2**, **Section 2.2.2.1** for detailed methodology.

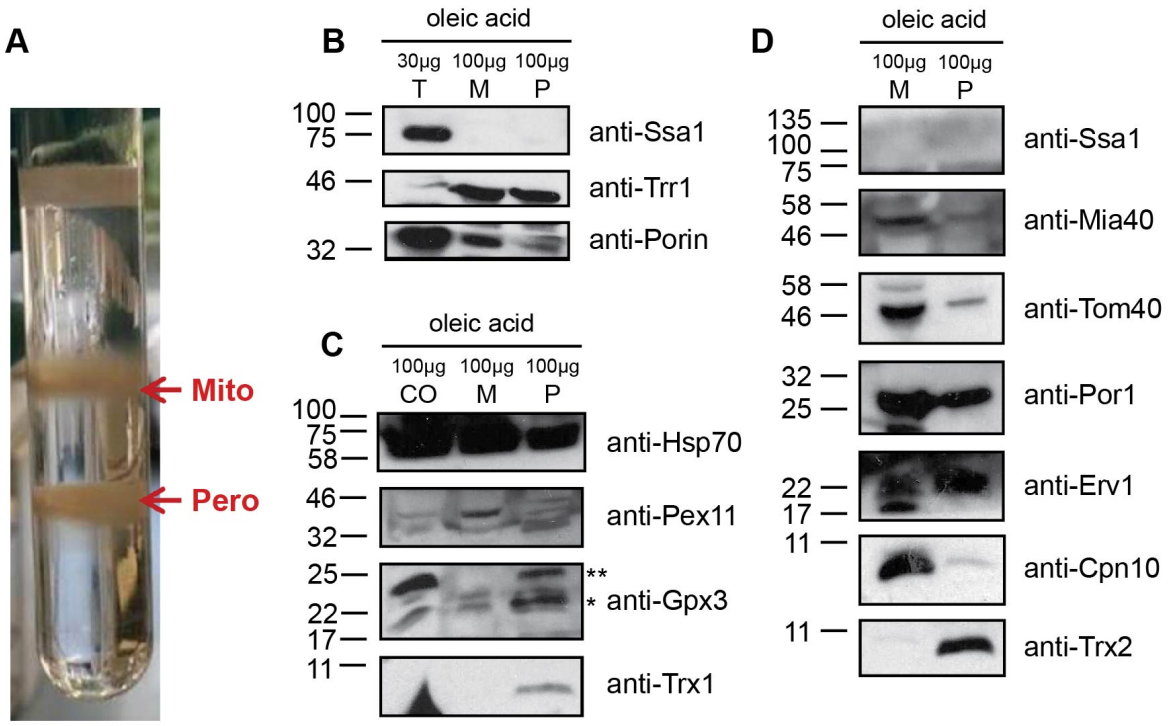

Figure 5.2. Yeast Gpx3 localises to both mitochondria and peroxisomes. (**A**) Nycodenz gradient after density centrifugation to show the separation of mitochondria (Mito) and peroxisomes (Pero) from yeast grown to mid-log phase in 0.12% oleic acid. (**B, C & D**) Western blots to detect cytosolic, peroxisomal or mitochondrial proteins in (T) total yeast cell extract before fractionation, crude organelles before density centrifugation (CO), purified mitochondria (M) and purified peroxisomes (P). Antibodies against the following proteins were used: Ssa1 - cytosolic; Trr1 - cytosol/IMS; Por1 - OM; Hsp70 – matrix; Pex11 – peroxisomal membrane; Gpx3 – cytosol/IMS; Trx1 – cytosol/IMS; Mia40 – IMS; Tom40 – OM; Erv1 - IMS; Cpn10 – matrix; and Trx2 – cytosol. NOTE: Cross-reactivity between anti-Trx1 and anti-Trx2 is likely as the two paralogous proteins are very similar in amino acid sequence (89% similarity). * - Gpx3. ** - possible N18Gpx3.

Under oleic acid growth conditions, a strong band using anti-Gpx3 (denoted with an asterisk) is detected in the peroxisomal fraction, and there appears to be more Gpx3 in peroxisomes than mitochondria, but this would need to be accurately quantified and compared to non-oleic acid conditions (**Figure 5.2C**). Two distinct bands are detected in the mitochondrial fraction; the top band (asterisk) may represent the N18Gpx3 version, although this cannot be confirmed by western blotting alone. The bottom band (double asterisk) is likely to represent the wild-type version which is the more predominant band in the peroxisomal fraction. Although not entirely clear, the western blot suggests that

the N-terminal extension of 18 amino acids which boosts mitochondrial import of Gpx3 is not required for peroxisomal import. Note that there is a band with high intensity that runs higher in molecular weight, at around 25 kDa, when anti-Gpx3 is used. It is not known what this band represents as it is too large to be the N18Gpx3 version of Gpx3, but it is absent in *gpx3Δ* yeast (see later **Figure 5.6**). Saturation of anti-Gpx3 with purified recombinant Gpx3 would also show specificity.

What is also clear from the western blots shown in **Figure 5.2** is that there is a degree of mitochondrial contamination in the isolated peroxisomal fractions as other mitochondrial proteins are detected in peroxisomes. The majority of these are detected to a much lesser extent than in the mitochondrial fraction which suggests they are weak contaminants, for example: Porin1, Tom40 and Cpn10. However, this is a common problem with density gradient centrifugation - 100% pure fractions are extremely unlikely as some organelles may break or stick together during the isolation protocol. The yeast cytosol was successfully removed as the cytosolic protein Ssa1 was only detected in total yeast cell extracts, and never in the organelle fractions (**Figure 5.2B**). Marker antibodies against other cellular components would need to be used to assess the true purity of the fractions but it can be assumed that they are largely enriched for the expected organelles based on organelle density.

An antibody against a peroxisomal membrane protein, anti-Pex11, was sourced from Santa Cruz Biotechnology and used as a control for the enrichment of peroxisomes. Intriguingly, two bands were detected in the crude organelle fraction; one of which appears to be enriched in the mitochondrial fraction and the other in the peroxisomal fraction (**Figure 5.2C**). It could be that Pex11 is dually localised to both peroxisomes and mitochondria via a non-canonical start site resulting in an N-terminal extension akin to Gpx3 that targets Pex11 to mitochondria. **Section 5.3.7** investigates this possibility.

Surprisingly, Erv1 also appears to localise to both mitochondria and peroxisomes as a strong band was detected in the peroxisomal fraction when probing using anti-Erv1 (**Figure 5.2D**). Likewise, Trx1 and Trx2 were detected in peroxisomes (**Figures 5.2C & 5.2D**) but the antibodies against either one may recognise each other due to sequence similarity, so it is difficult to say with certainty which Trx protein is present. To test this, both anti-Trx1 and anti-Trx2 could be saturated with purified recombinant Trx1 and Trx2 prior to their use; however, anti-Trx1 was raised against recombinant Trx1 and so it should be relatively specific. Peroxisomes would also need to be isolated from *trx1Δ*, *trx2Δ*, *trx1Δ*/*trx2Δ* and *galErv1* yeast.

Only the redox-regulated proteins like Gpx3, Trx1, Trx2 and Erv1 are likely to be dually localised to both organelles given that the other mitochondrial proteins analysed by western blotting (Porin1, Cpn10 and Tom40) were mostly enriched in the mitochondrial fraction.

To gather complimentary evidence from a bioinformatics perspective on whether or not the proteins identified could be bona fide peroxisomal proteins, one can look for possible PTS1 or PTS2 motifs in the C- or N-terminal regions, respectively. Sequence analysis, based on what is currently known from the literature, suggests that both Trx1 and Trx2 harbour PTS1 targeting signals (see next **Section 5.3.2**, **Table 5.1**). Although no targeting signals could be detected in the Gpx3, Erv1 and Mia40 proteins, not all bona fide peroxisomal proteins have had their targeting signals identified yet. In addition, based on the potential localisation of Erv1 to peroxisomes, it would make sense that its mitochondrial binding partner, Mia40, would also be present within the organelle. Although the initial western blot data in **Figure 5.2D** only shows a faint band against anti-Mia40, which is more than likely attributed to mitochondrial contamination, the isolated fractions were re-probed using anti-Mia40 across the full-sized membrane. A strong band with a lower molecular weight was detected (see later **Section 5.3.3**, **Figure 5.4**).

5.3.2. Sequence analysis of mitochondrial proteins found in peroxisomal fractions

Peroxisomal targeting signals are somewhat perplexing as different consensus exist for both PTS1 and PTS2 motifs (Brocard and Hartig, 2006). PTS1 motifs are found in the majority of known peroxisomal proteins, but, although they are universal, they can be species specific (Aitchison et al., 1991). To make matters more complicated, some genuine peroxisomal proteins, such as carnitine acetyl transferase (and Catalase A without its –SKL), are still successfully imported into peroxisomes (Elgersma et al., 1995; Kragler et al., 1993). Some are even 'piggy-backed' in under stress conditions, such as Pnc1 by Gpd1 (Kumar et al., 2016). Despite this, an analysis of the putative perixosomal proteins identified in **Section 5.3.1**, along with Mia40, for either PTS1 or PTS2 motifs is shown in **Table 5.1**. Due to the majority of available PTS predictors no longer accessible online due to their web links not working, a 'by eye' analysis was conducted based on the consensus motifs shown in **Figure 5.3**. Genuine peroxisomal proteins were included as controls in this analysis.

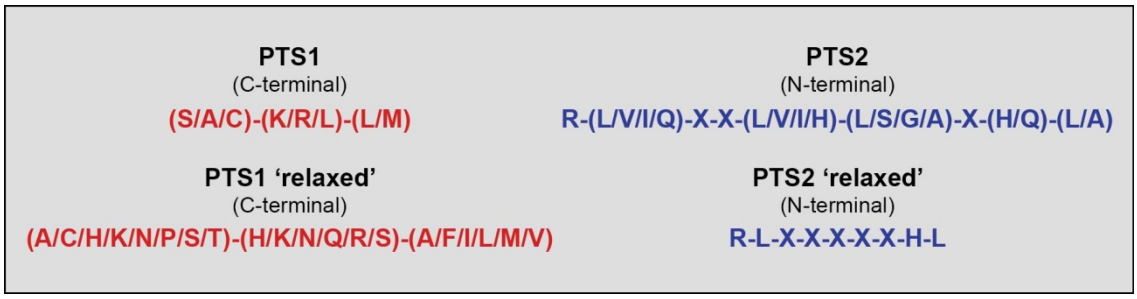

Figure 5.3. PTS1 and PTS2 consensus motifs. Consensus amino acid sequences of peroxisomal targeting signal 1 (PTS1) and peroxisomal targeting signal 2 (PTS2) motifs (Swinkel et al., 1991; Osumi et al., 1992; Dodt et al., 2001; Kiel et al., 2006; Lazarow et al., 2006; Brocard and Hartig, 2006). PTS1 are found at the extreme C-terminus; two versions of this consensus motif are shown in red – PTS1 and PTS1 'relaxed'. PTS2 are found within the N-terminal region; two consensuses are shown in blue – PTS2 and PTS2 'relaxed'. Relaxed motifs are less strict and can be used to identify lesser known targeting signals that might otherwise be missed.

Search for peroxisomal targeting signals					
Protein	**Localisation***	**PTS1**	**PTS1 'relaxed'**	**PTS2**	**PTS2 'relaxed'**
Gpx3	Cytosol/ Peroxisomal matrix/IMS	No	No	No	No
Erv1	IMS	No	No	No	No
Trx1	Cytosol/IMS	No	Yes (**ANA**)	No	No
Trx2	Cytosol	No	Yes (**SNV**)	No	No
Trx3	Mitochondrial matrix	No	No	No	No
Trr1	Cytosol/IMS	No	No	No	No
Trr2	Mitochondrial matrix	No	No	No	No
Mia40	IMS	No	No	No	No
Gpx1	Peroxisomal matrix/IMS	No	No	No	No
Pex11	Peroxisomal membrane/ cytosol	No	No	No**	No
Pex21	Peroxisomal membrane	No	No	No	Yes (**RLNSSRQHL**)
Pot1	Peroxisomal matrix/IMS	No	No	No	Yes (**RLQSIKDHL**)
Cta1	Peroxisomal matrix/ Mitochondrial matrix	No	Yes (**SKF**)	No**	No
Mdh3	Peroxisomal matrix	Yes (**SKL**)	n/a	No	No

Table 5.1. Predicting peroxisomal targeting signals based on consensus PTS1 and PTS2 motifs. The amino acid sequences of various mitochondrial and peroxisomal proteins were analysed for consensus peroxisomal targeting signals (see **Figure 5.3** for motifs). Bona fide peroxisomal proteins were used as controls, whereby for some, but not all, their targeting signals are already known and fit the consensus for either PTS1 or PTS2. These included Gpx1, Pex11, Pex21, Pot1, Cta1 and Mdh3. Gpx3 has also been found in the peroxisomes both in this study and by Ohdate and Inoue (2012). * - Known localisations. ** - A possible 'PTS2-like' signal (see text below). Red indicates PTS1/PTS1-like motifs; blue indicates PTS2/PTS2-like motifs.

Based on these predictions, neither Gpx1 nor Gpx3 contain any identifiable peroxisomal targeting signals. However, no peroxisomal targeting signal could be identified for Pex11 either, which is a genuine peroxisomal membrane protein. Pex11 does appear to contain two 'PTS2-like' motifs which might be responsible for its import: RLXXXLAXXL and RVXXVLXXXXXA (the underlined letters indicate those that do not fit the PTS2 consensuses), although these have never been verified experimentally. In addition, it is known that the SKF C-terminal PTS1 of Cta1 is indispensable for its peroxisomal import; an N-terminal signal near Cta1's FXXXW domain has recently been shown to direct its peroxisomal import (Rymer et al., 2018). Furthermore, a study by Freitag et al. (2012) uncovered cryptic PTS1 motifs in the fungus *Ustilago maydis* that result from either ribosomal read-through or alternative splicing. Cryptic PTS1 motifs by ribosomal read-through were not detected for any of the proteins in **Table 5.1** (ExPASy translate - data not shown).

Interestingly, Trx1 and Trx2 were the only proteins other than the positive controls, Cta1 and Mdh3, found to contain putative PTS1 'relaxed' motifs – ANA and SNV, respectively. The mitochondrial matrix thioredoxin, Trx3, which is made with a typical N-terminal mitochondrial targeting signal, was not found to contain any potential PTS1 or PTS2 motif. Along with the western blot data in **Figure 5.2**, this suggests that both Trx1 and Trx2 may localise within peroxisomes. Future studies could delete their C-terminal tripeptides, or mutagenise them, and test whether this affects their potential peroxisomal import.

Altogether, the analysis here unequivocally suggests that we are far from understanding the true extent of peroxisomal targeting signals. The lack of an identifiable PTS1 or PTS2 does not discount the chance that a protein may be able to import into peroxisomes, whether that is by a 'yet to be confirmed' variation of a PTS1/PTS2 or by an entirely novel signal, or, perhaps even cryptic signals remains to be determined. Therefore, whilst no consensus signals were found for Gpx3, Mia40, or Erv1, further experiments are still warranted in order to validate their localisation.

5.3.3. 'Peroxisomal' Mia40

Mia40, Mitochondrial intermembrane space Import and Assembly 40, is a 44 kDa protein well known for its crucial role in the mitochondrial IMS oxidative folding pathway (Mordas and Tokatlidis, 2015). Erv1, an essential IMS sulphydryl oxidase, interacts with and re-oxidises Mia40 in order to maintain the oxidation state of Mia40 required for introducing disulphide bonds to incoming proteins. As both proteins co-localise in the IMS and are heavily involved in this pathway, and our detection of Erv1 in a peroxisomal fraction (**Figure 5.2**), we wondered whether Mia40 was also present. Although western blots using anti-Mia40 only detected a very weak band in the peroxisomal fraction which was likely due to mitochondrial contamination (**Figure 5.2D**), a lower band running between the 17-22 kDa marker was detected when anti-Mia40 was probed across the full membrane after transfer from SDS-PAGE (**Figure 5.4**).

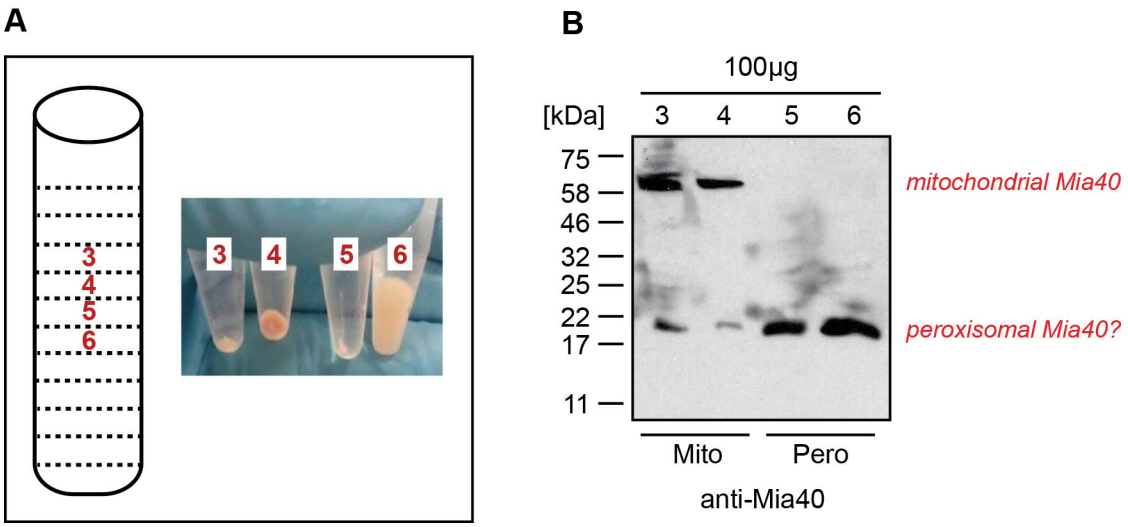

Figure 5.4. Detection of yeast Mia40 in mitochondria vs peroxisomes. (**A**) Diagram to show fractions 3-6 from Nycodenz gradient centrifugation (final step of isolation protocol, refer to **Figure 5.1** and **Chapter 2**, **Section 2.2.2.1**). Mitochondria are enriched in fractions 3 & 4; peroxisomes are enriched in fractions 5 & 6. (**B**) Western blot to detect Mia40 (using anti-Mia40) in fractions 3-6. NOTE: Full length mitochondrial Mia40 is 44 kDa but always runs higher on SDS-PAGE, at ~60 kDa, due to its low isoelectric point (pI: 4.2).

Whilst it is possible that anti-Mia40 is non-specifically binding to a lower molecular weight species in the peroxisomal fractions 5 and 6 (**Figure 5.4B**), or a degradation product of full length Mia40, it is interesting to speculate that there is a shorter, alternatively translated version of Mia40. This shorter product may start translation at Met272 within the Mia40 amino acid sequence which would remove the N-terminal mitochondrial targeting signal (**Figure 5.5**). In *Arabidopsis*, Mia40 (AtMia40) is a shorter soluble protein that is found in both mitochondria and peroxisomes (**Figure 5.5**). AtMia40 is known to be involved in the import of proteins to both organelles (Carrie et al., 2010). No other Mia40 homolog has been found in peroxisomes in other organisms to date.

Saccharomyces cerevisiae Mia40

MLRNLVVRNA**C**RNRPSIQVARGL**C**RHQTRRLMASSPQFGRNSNQEKTAGFIMGILSMAGALYFI
APNRKPLFASRKVESDKTAEEELSSGGEQSPENEDDNNSKSDENGDDNDSKNDETEAGPQLGGD
KIGASKVAEDGELVVLAEEDNKSSEDKDTDESKVSTKDDEQSNEDNATANNQKDENISSENSEE
NTSDKTLDNNAGSSEKKDPEHSDDEKSQQGQSDDKTTTEDNNGEEESSKKTVSDSENSAKQSES
SDEEKEELRKQEEKQMGPTEEEVQHEGAYNPDTGEINWD**C**P**C**LGGMAHGP**C**GEEFKSAFS**C**FVY
SEAEPKGID**C**VEKFQHMQD**C**FRKYPEHYAEQLKETSDDEEPQDKVKVNTIESAPNVSSAKENAA
KKAEQSDVKKEPLNEE**SKP**

Arabidopsis thaliana Mia40

MGQAQSDENSIPTTTTTNTPPPSANSPRDSEDTSSPSMDSLLAEAAAYGEDDNENESLEAKAQR
ALD**C**P**C**IADLRNGS**C**GSQFSEAFL**C**FLKSTAEEKGSD**C**VNPFVALQS**C**INANPDAFSKSVTGDE
KETEKKEEQPPVQDHRIIPPLWAKDPPRSGN**SKL**

Figure 5.5. Mia40 amino acid sequence in *S. cerevisiae* vs *A. thaliana*. ScMia40 is 403aa in length and has eight cysteine residues (red) including those that make up its redox active CPC and …CX_9C…CX_9C… motifs. The light/dark grey shading together indicates the full-length ScMia40 protein; the dark grey highlights the potential shorter version. AtMia40 is 162aa containing six cysteine residues which also include its redox active CPC and …CX_9C…CX_9C… motifs. AtMia40 has a C-terminal peroxisomal targeting tripeptide, SKL (yellow). Yeast Mia40 has a C-terminal SKP tripeptide (green).

The C-terminal tripeptide SKL of AtMia40 is responsible for its targeting and import into *Arabidopsis* peroxisomes. Could the yeast C-terminal tripeptide SKP of yeast Mia40 be a weak peroxisome targeting sequence that acts when the N-terminal mitochondrial targeting signal is absent?

Although SKP does not fit any current PTS1 consensus, evidence from a study over two decades ago would suggest otherwise. A study conducted by Elgersma et al. (1996) investigated whether various tripeptide combinations fused to the peroxisomal malate dehydrogenase, Mdh3, without its canonical SKL found that SKP still resulted in import, albeit at a much lesser amount of around 5-20% in comparison to SKL. Thus, a SKP tripeptide might in theory be enough to direct the import of proteins to peroxisomes in the absence of other targeting signals.

To investigate whether any other proteins within the *S. cerevisiae* genome database contain SKP tripeptides at their extreme C-terminus, a yeast genome pattern matching search was carried out using PatMatch at www.yeastgenome.org. Four proteins were detected using SKP> as the search parameter: Mia40 (as expected), Bud27, Ybr209w and Ynl162w-a. Bud27 is an unconventional prefoldin which is involved in promoting translation initiation, especially under nutrient stress conditions (Gstaiger et al., 2003; Deplazes et al., 2009). Ybr209w is a 12 kDa protein of unknown function with a …CX_3C… motif but no detectable human homolog (Fisk et al. 2006). Ynl162w-a is an 8 kDa protein of unknown function with a …$CX_2CX_7CX_{11}CX_4C$… motif but also no human homolog (Blandin et al., 2000). It should be noted that this motif is different from the OXLD domain described in **Chapter 4**.

In order to elucidate whether a shorter version of Mia40 exists in yeast peroxisomes, the first approach taken was to repeat the isolation of mitochondria and peroxisomes from *galMia40* yeast. Mia40 is an essential protein so a yeast strain whereby Mia40 is under a galactose controlled promoter was used to reduce, but not entirely eliminate, Mia40 production. Cells were first grown in galactose before a switch to oleic acid to induce peroxisome proliferation and reduce Mia40 levels. The results suggest that the lower molecular weight band detected by anti-Mia40 is specific to Mia40 as it is not detected in *galMia40* peroxisomes and only very weakly in the crude organelle fraction before density gradient centrifugation (**Figure 5.6**). However, the signal seen in this fraction is most likely because Mia40 is never completely absent in *galMia40* yeast. Organelles were also isolated from yeast lacking the *GPX3* gene sequence (*gpx3Δ*) to verify the specificity

of anti-Gpx3 in detecting Gpx3 in peroxisomes from wild-type yeast. No Gpx3 was detected in *gpx3Δ* yeast (**Figure 5.6**).

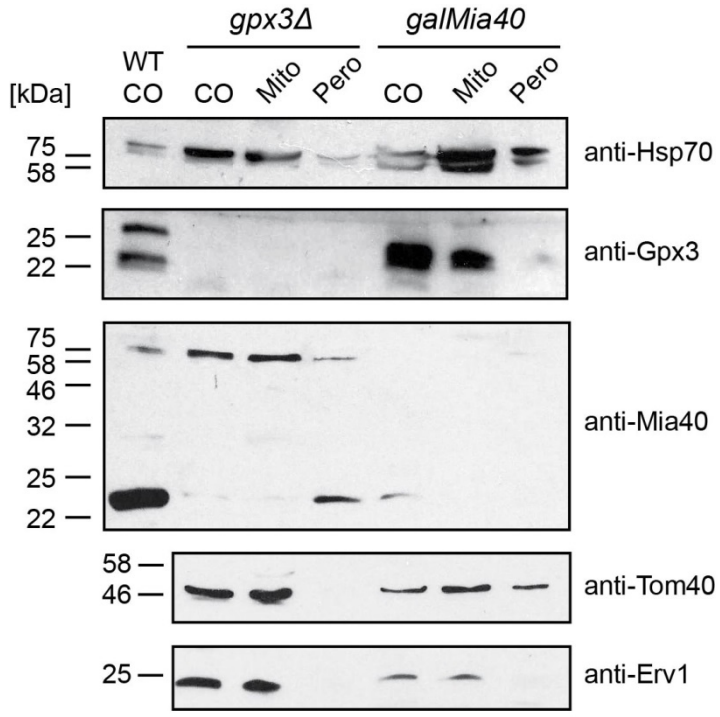

Figure 5.6. Isolation of mitochondria and peroxisomes from *gpx3Δ* and *galMia40* yeast. Western blots to analyse crude organelle (CO), mitochondrial (Mito), and peroxisomal (Pero) fractions from *gpx3Δ* and *galMia40* yeast grown in 0.12% oleic acid. WT CO – wild-type crude organelle fraction. Antibodies against the following proteins were used: Hsp70 – matrix; Gpx3 – cytosol/IMS/peroxisomal matrix; Mia40 – IMS; Tom40 – OM; and Erv1 – IMS. NOTE: The control peroxisomal antibody against the peroxisomal membrane protein Pex11 (anti-Pex11) did not work during this analysis. Thus, it can only be assumed that the Pero fraction is enriched for peroxisomes based on the use of an established protocol that is commonly used within the field, and the presence of the putative peroxisomal Mia40 detected in only CO and Pero (but not in Pero from *galMia40*).

Other observations from **Figure 5.6** suggest that the import of Gpx3 to peroxisomes may require the presence of Mia40, as only a very faint band was detected by anti-Gpx3 in peroxisomes isolated from *galMia40* yeast. This faint band is probably due to a slight mitochondrial contamination within the peroxisomal fraction. By contrast, the signal for Gpx3 was stronger in the peroxisomal fraction compared to the mitochondrial fraction in

wild-type yeast (**Figure 5.2**). Previous experiments by Kritsiligkou et al. (2017) have shown that Mia40 is not required for the import of Gpx3 into the mitochondrial IMS, but perhaps it is needed for Gpx3 to be imported into the peroxisomal matrix. An *in organello* peroxisomal vs mitochondrial import assay, akin to the standard import assay used throughout this thesis, would need to be established in order to investigate this possibility. It would also be useful in elucidating whether a truncated version of Mia40, starting at amino acid residue 272, could be imported into either organelle.

Intriguingly, Erv1 was absent from *galMia40* and *gpx3Δ* peroxisomes which either suggests that the band detected in **Figure 5.2D** was an artefact or that the import of Erv1 into peroxisomes requires Gpx3 and/or Mia40. However, it cannot be ruled out in this instance that the isolation of these peroxisomes was not successful given that the antibody against Pex11 did not recognise anything in this western blot. Therefore, these fractions remain to be verified as peroxisomal. In repeat western blots using the fractions previously obtained from wild-type cells, anti-Pex11 could no longer detect Pex11. Thus, the conclusion was that the anti-Pex11 obtained from Santa Cruz Biotechnology was in no way reliable at detecting Pex11. It is extremely important for the validity of these data that these isolations are repeated with antibodies that work against one or more peroxisomal proteins. Unfortunately, attempts to obtain peroxisomal antibodies through requests from three other labs did not come to fruition during the course of this thesis.

Whilst antibodies were being sought, work on this chapter temporarily continued with the material already collected in the hope that verification would happen at a later date, and the next section began to explore potential interactors of peroxisomal Gpx3.

5.3.4. *In vitro* binding assays to investigate peroxisomal Gpx3 interactors

Akin to the *in vitro* binding assays to investigate mitochondrial interactors of Gpx3 (**Section 3.3.5**), the same was carried out for peroxisomal interactors. Peroxisomes were solubilised whilst His-tagged versions of Gpx3 were bound in excess to Ni-NTA beads. The solubilised proteins were then passed over the saturated beads which were then washed before bound material was eluted (refer to **Section 2.2.3.1** for methodology). Initially, the cysteine trap mutants of both Gpx3 and N18Gpx3 (Gpx3C82AHis and N18M20LGpx3C82AHis) were used as bait. Elutions were analysed by western blotting, first to check whether the His-tagged protein was present in the elutions (using anti-His) and then with anti-Mia40, anti-Trx1 and anti-Trr1 (**Figure 5.7**). These mitochondrial proteins were chosen due to the suspected presence of Mia40 and Trx within peroxisomes; anti-Trr1 was used as Trr1 is the reductase partner of Trx1.

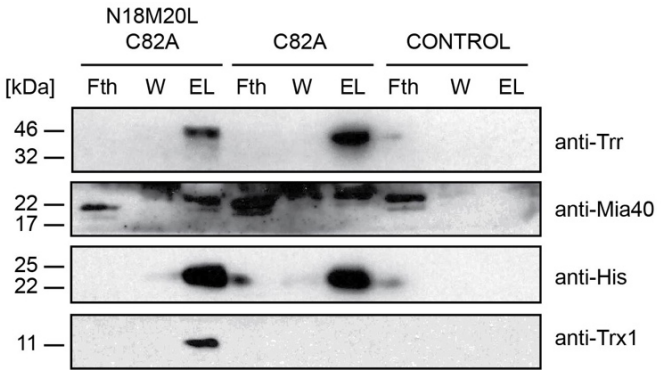

Figure 5.7. *In vitro* binding assays to detect peroxisomal interactors of Gpx3 cysteine mutants. N18M20LGpx3C82AHis and Gpx3C82AHis were bound to Ni-NTA beads and solubilised peroxisomal proteins were passed over. Unbound material can be seen in the flow throughs (Fth) and co-eluted material detected in the elutions (EL). W – indicates the third and final wash before elution with imidazole. CONTROL – control assay where no His-tagged protein was bound to Ni-NTA beads prior to addition of peroxisomal proteins. Western blots were used to probe for His-tagged proteins (using anti-His) and putative peroxisomal Mia40 (using anti-Mia40). Anti-Trx1 and anti-Trr1 were used as additional markers due to their potential localisation within peroxisomes. No peroxisomal antibodies were used as anti-Pex11 could not detect Pex11 even in total cell extracts, and no other antibodies were available.

The results suggest that both cysteine trap mutants may interact with peroxisomal 'putative Mia40' and Trr1, whilst the N18 extended cysteine trap mutant may also interact with Trx1 (**Figure 5.7**). However, these results should be analysed with caution because of the slight mitochondrial contamination within the isolated peroxisomal fractions. It is possible that Trr1 and Trx1 co-eluting in this assay came from solubilised mitochondria. Nevertheless, as the putative shorter version of Mia40 is only found within the peroxisomal fractions (refer back to **Figure 5.5**), and it is known that full-length Mia40 interacts with Gpx3 in the mitochondrial IMS (**Sections 3.3.3 – 3.3.5** and Kritsiligkou et al., 2017), it is plausible that peroxisomal Gpx3 can interact with a peroxisomal Mia40. The *in vitro* binding assays were repeated to include Gpx3His and N18M20LGpx3His with no cysteine mutations (**Figure 5.8**).

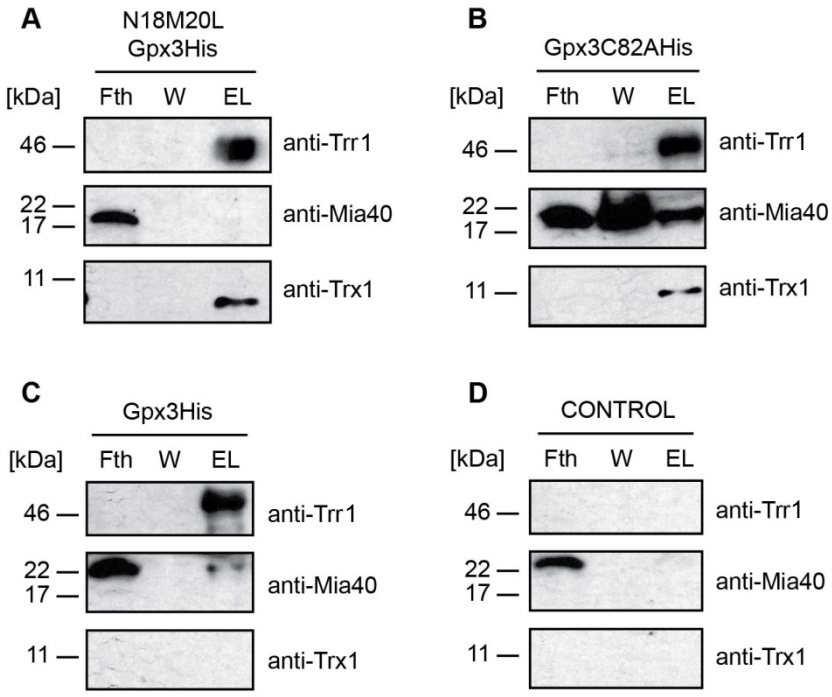

Figure 5.8. Further *in vitro* binding assays to detect peroxisomal interactors of Gpx3. (**A**) N18M20LGpx3His, (**B**) Gpx3C82AHis and (**C**) Gpx3His were bound to Ni-NTA beads and solubilised peroxisomal proteins were passed over. Unbound material can be seen in the flow throughs (Fth) and co-eluted material detected in the elutions (EL). W – indicates the third and final wash before elution with imidazole. (**D**) CONTROL – control assay where no His-tagged protein was bound to Ni-NTA beads prior to addition of peroxisomal proteins. Western blots were used to probe for putative peroxisomal Mia40 (using anti-Mia40), Trx1 (using anti-Trx1) and Trr1 (using anti-Trr1). No peroxisomal antibodies were used as anti-Pex11 could not detect Pex11 even in total cell extracts, and no other antibodies were available.

This time no 'peroxisomal' Mia40 was detected in the co-elution with N18M20LGpx3His (**Figure 5.8A**) and only a weak band in the co-elution with Gpx3His (**Figure 5.8C**). The cysteine trap mutant, Gpx3C82AHis, again co-eluted with Mia40 (**Figure 5.8B**). This indicates that the resolving cysteine of Gpx3 (C82) is required for its interaction with 'peroxisomal' Mia40. Trx1 was found co-eluting with N18M20LGpx3His and Gpx3C82AHis (**Figure 5.8A and 5.8B**). However, as noted previously the antibody against Trx1 may also recognise Trx2 due to sequence similarity, therefore it may be that Trx1 and/or Trx2 co-eluted with N18M20LGpx3His and Gpx3C82AHis. Strikingly, anti-Trr1 detected a band in all three *in vitro* binding assays in **Figure 5.8** and in the previous assay using N18M20LGpx3C82AHis (**Figure 5.7**). The relevance of this is unknown as the well-established binding partner of Trr1 is Trx1.

No further experiments were carried out on the isolated peroxisomal fractions due to not having any reliable peroxisomal antibodies. Instead, attempts to visualise *S. cerevisiae* organelles by electron microscopy were made in the hope of being able to detect both mitochondria and peroxisomes.

5.3.5. Electron microscopy to visualise *S. cerevisiae* organelles

Rather than analysing mitochondrial and peroxisomal fractions for the presence of proteins, an alternative approach was sought – electron microscopy. The idea behind optimising an electron microscopy protocol was to be able to visualise yeast organelles (including mitochondria and peroxisomes) in wild-type vs mutant yeast strains. For example, the morphology of peroxisomes could be assessed in *galMia40* and *gpx3Δ* yeast. A protocol by Bauer et al. (2001) claiming to have found an improved electron microscopy technique for visualising yeast membrane structures was used. This protocol was followed (see **Section 2.2.7** for detailed methodology) and the images from wild-type yeast cells, using a transmission electron microscope (TEM), are shown in **Figure 5.9**.

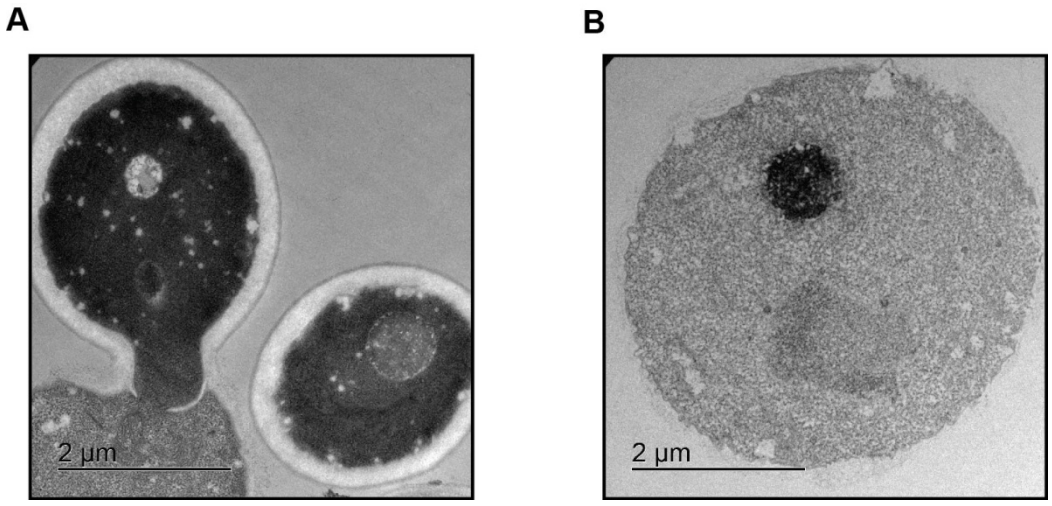

Figure 5.9. Wild-type yeast cells visualised by transmission electron microscopy. Wild-type D273-10B yeast cells were grown to stationary phase in liquid YPD overnight at 30°C and then diluted the next morning to OD_{600nm}: 0.05 in fresh YPD. Cells were then grown at 30°C until they reached OD_{600nm}: 0.7-1.0 before being harvested and prepared for TEM (see **Section 2.2.7** for detailed methodology). TEM was carried out by Margaret Mullen at the Electron Microscopy Facility (University of Glasgow). (**A**) and (**B**) are TEM images from two identical yeast cell preparations.

Unfortunately, our attempts to visualise *S. cerevisiae* organelles (**Figure 5.9**) did not yield clear images. The yeast cell shown on the left-hand side of **Figure 5.9A** appears to have burst and its cytosolic contents released; whereas the yeast cell shown in **Figure 5.9B** does not appear to have an intact cell wall. The reason behind both these outcomes is unknown; however, it could be that the Zymolyase treatment used to 'punch' tiny holes into the yeast cell walls to allow the fixatives to enter was too harsh. Future optimisation of this stage of the protocol is thus required.

The following sections delve into the possibility of Pex11 as a potential dually-localised mitochondrial protein which was based on the results shown in **Section 5.3.1**.

5.3.6. Import and localisation of Pex11 in mitochondria

Given that Pex11 'mislocalises' to mitochondria in *pex3Δ* yeast that lack peroxisomes (Mattiazzi Usaj et al., 2015; Wróblewska et al., 2017), and Pex11 was initially detected in both mitochondrial and peroxisomal fractions, the import of Pex11 in mitochondria was investigated. *PEX11* was cloned into a pSP64 vector for production of a ^{35}S-labelled precursor that was then presented to isolated wild-type yeast mitochondria following a standard import assay protocol. Pex11 was indeed imported into a protease-protected compartment and, interestingly, its import was independent from the membrane potential (**Figure 5.10**).

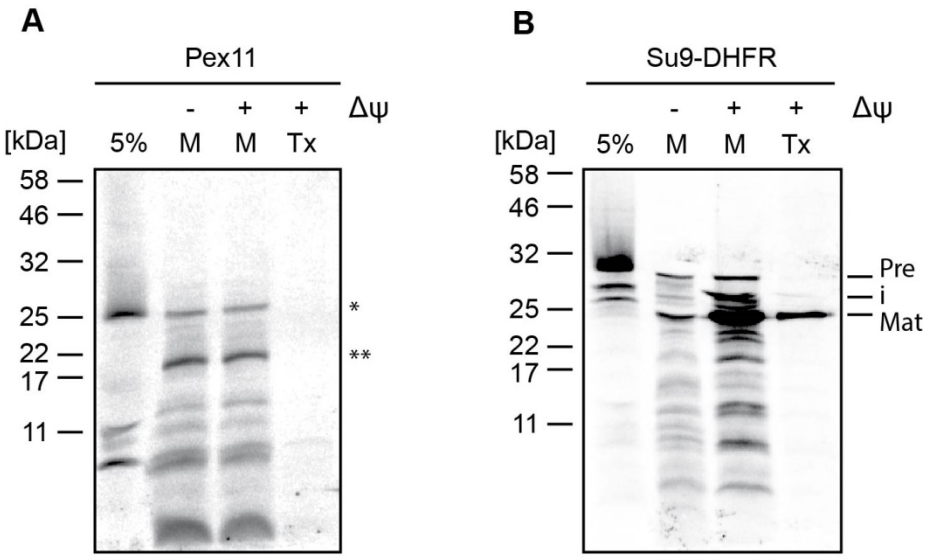

Figure 5.10. Import of radiolabelled Pex11 and Su9-DHFR. Pex11 and Su9-DHFR were synthesised as ^{35}S-labelled precursors and imported into isolated wild-type yeast mitochondria. Precursors were imported straight after translation: (**A**) Pex11 import and (**B**) Su9-DHFR import. Import reactions were stopped after 30 minutes. $\Delta\Psi$ - membrane potential. All import reactions were treated with trypsin to destroy unimported material (M), and a combination of Triton-X-100 and trypsin as a negative control (Tx). 5% corresponds to 5% of the precursor used for each import reaction. Radiolabelled precursors were detected by digital autoradiography. * - full length Pex11, ** - Cleaved Pex11, Pre – Su9-DHFR precursor, i – IMS stalled Su9-DHFR intermediate (incompletely cleaved in transition), Mat – mature Su9-DHFR (cleaved after import into matrix). The lower molecular weight bands seen in both gels are likely degradation products resulting from incomplete inactivation of trypsin, or incomplete cleavage by trypsin.

Although there is a possibility that the radiolabelled Pex11 is 'mislocalising' to mitochondria in this import assay (due to the unlikelihood of other organelles being present), it was still of interest to determine which mitochondrial subcompartment Pex11 resides in upon import, and whether it is a soluble, peripheral or integral membrane protein. First, a localisation assay was carried out after import to determine if (i) Pex11 is protease protected after mitoplasting – a process where the OM is broken by osmotic shock – leaving soluble IMS proteins susceptible to protease degradation, (ii) whether Pex11 is extracted from mitoplasts by urea and (iii) whether Pex11 is soluble after carbonate extraction.

The results show that radiolabelled Pex11 remains in the pellet fraction after mitoplasting which rules out the possibility that it is a soluble IMS protein (**Figure 5.11**). However, it appears that some of Pex11 is cleaved when Proteinase K is added to the mitoplast buffer which suggests that it might have a domain that is exposed on the IMS side of either the IM or OM. For some reason the signal for Pex11 is largely lost during the urea extraction from mitoplasts but this also occurred for the control Tim44, a peripheral IM protein. The reason for this is unknown. Finally, the carbonate extraction reveals that Pex11 is mostly found in the pellet fraction and is therefore mostly membrane bound. Overall, when compared to the control proteins, the assay points towards Pex11 as an integral membrane protein of either the IM or OM that has a region exposed to the IMS.

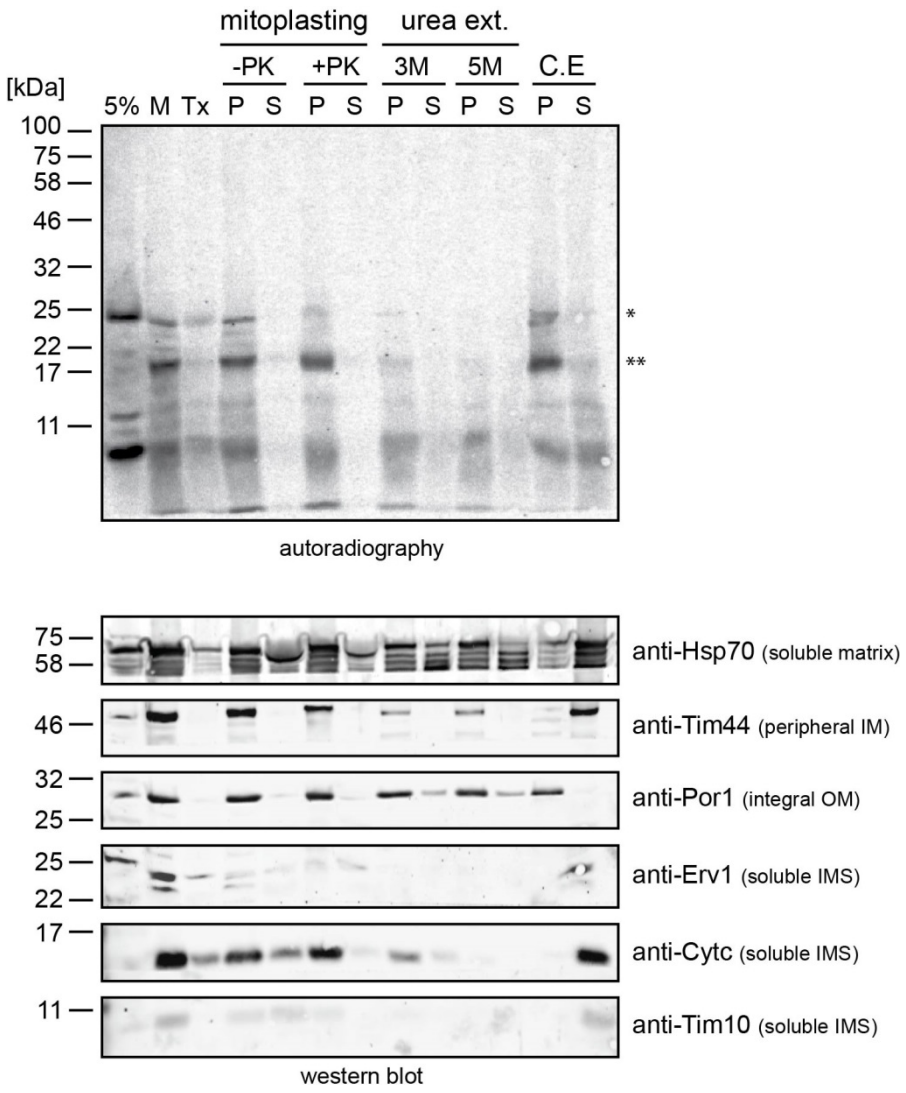

Figure 5.11. Radiolabelled Pex11 localisation after mitochondrial import. Pex11 was synthesised as a radiolabelled precursor and imported into isolated wild-type yeast mitochondria straight after translation. The import reaction was stopped after 30 minutes and treated with trypsin to destroy unimported material (M), and a combination of Triton-X-100 and trypsin as a negative control (Tx). Osmotic shock to rupture the OM, mitoplasting, resulted in pellets (P) containing the matrix/IM and supernatants (S) containing IMS proteins, -/+ proteinase K (PK). Urea extraction from mitoplasts using 3 M and 5 M urea to disrupt hydrophobic interactions and release peripheral membrane proteins. Carbonate extraction (C.E) to separate insoluble from soluble proteins from intact mitochondria after Pex11 import: (P) – insoluble proteins associated with mitochondrial membranes; and (S) – soluble proteins. (**A**) Analysis by autoradiography to detect radiolabelled Pex11. (**B**) Analysis by western blotting to detect mitochondrial proteins from different subcompartments: anti-Hsp70 (soluble matrix); anti-Tim44 (peripheral IM); anti-Por1 (integral OM); anti-Erv1 (soluble IMS); anti-Cyt*c* (soluble IMS); and anti-Tim10 (soluble IMS). 5% corresponds to 5% of the precursor used for each import reaction. Radiolabelled precursors were detected by digital autoradiography. * - full length Pex11, ** - Cleaved Pex11?

5.3.7. Import of N17Pex11 – does an N17 extension exist?

As the western blot data from the isolation of mitochondria and peroxisomes (**Figure 5.2**) detected two bands using anti-Pex11, one with a slightly larger molecular weight in the mitochondrial fraction, it was suggested that perhaps Pex11 might have an N-terminal extension that targets it to mitochondria, akin to Gpx3. A putative upstream translation read reveals a sequence of ~17 amino acids with similarities to the N18 of Gpx3 (**Figure 5.12**). Whilst this is purely hypothetical and there is no data to support that upstream translation of Pex11 occurs from a non-canonical start site, it was interesting to pursue this possibility given the evidence for association of Pex11 with mitochondria (Mattiazzi Usaj et al., 2015).

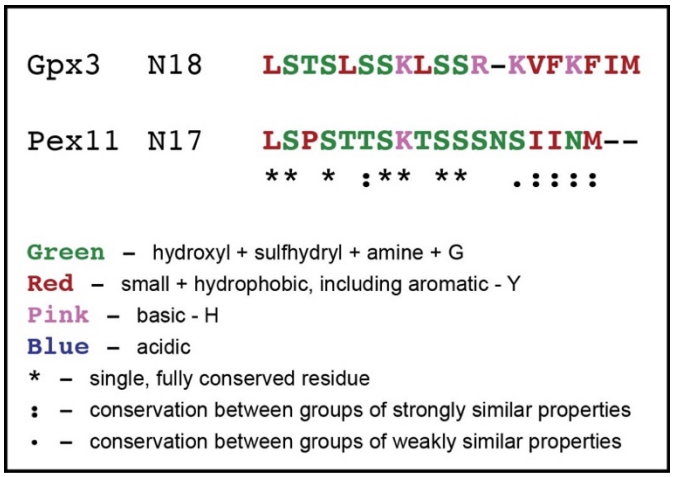

Figure 5.12. Alignment of the N18 upstream of Gpx3 with the putative N17 upstream of Pex11. Alignment performed using Clustal Omega at EMBL-EBI (McWilliam et al., 2013). Seven out of 17 residues within the putative N17 of Pex11 are fully conserved, five are conserved between groups of strongly similar properties, and one is conserved between groups of weakly similar properties.

To compare the import of Pex11 with the putative N17Pex11, *N17PEX11* was cloned into a pSP64 vector, and both Pex11 and N17Pex11 were produced as ^{35}S-labelled precursors that were then presented in parallel to isolated wild-type yeast mitochondria for various time points. The results show that both the wild-type Pex11 and the N17Pex11 are successfully imported into mitochondria; however, there does not appear to be any advantage of the N17 to Pex11 import as kinetics show a similar import efficiency across multiple time points (**Figure 5.13**). Thus, it was concluded that the putative N17 extension does not provide a more efficient mitochondrial import when presented to isolated mitochondria.

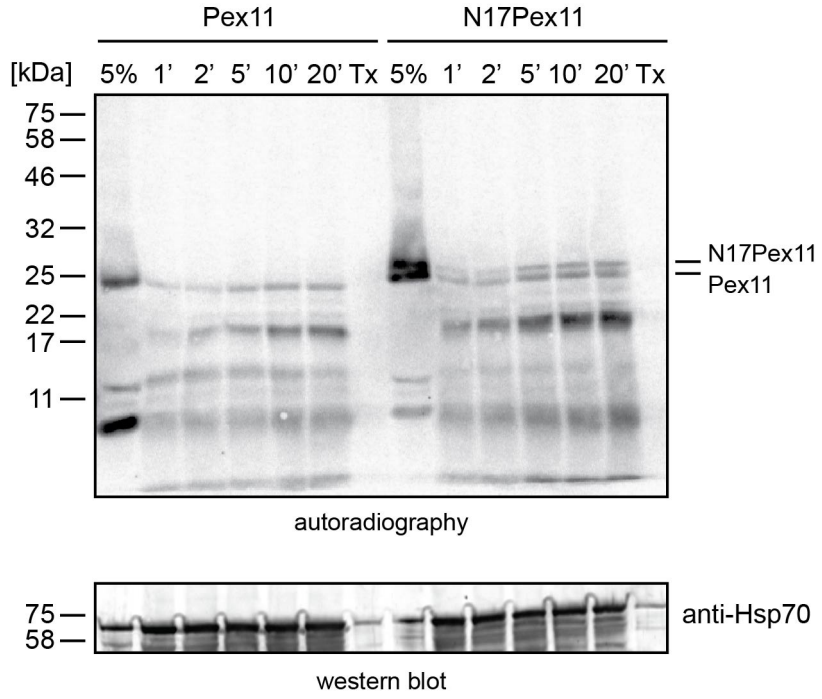

Figure 5.13. Radiolabelled import of Pex11 vs N17Pex11 in mitochondria. Pex11 and N17Pex11 were synthesised as ^{35}S-labelled precursors and imported into isolated wild-type yeast mitochondria. Precursors were imported straight after translation. Import reactions were stopped after 1 minute (1'), 2 minutes (2'), 5 minutes (5'), 10 minutes (10') and 20 minutes (20'). All import reactions were treated with trypsin to destroy unimported material, and a combination of Triton-X-100 and trypsin as a negative control (Tx). 5% corresponds to 5% of the precursor used for each import reaction. Radiolabelled precursors were detected by digital autoradiography (top panel). A western blot using anti-Hsp70 against the matrix heat shock protein 70 was performed as a loading control (bottom panel).

5.4. Discussion

Over the past decade and since work on this thesis began, evidence has continued to mount on how mitochondria and peroxisomes may be intricately linked, both in terms of physical contact and metabolism (Mattiazzi Ušaj et al., 2015; Wanders et al., 2016; Luis and Michael, 2018; Shai et al., 2018). Increasing data supports the existence of a 'redox triangle' comprising of mitochondria, peroxisomes and the ER - otherwise known as a redoxosome (Cohen et al., 2014; Mattiazzi Usaj et al., 2015). The peroxisomal redox state is known to influence the mitochondrial redox state (Baumgart et al., 2001; Ivashchenko et al., 2011), and it known that ROS can readily cross amongst organelle membranes (Boveris et al., 1972; Biernet and Chaumont, 2014). But how exactly do peroxisomes and mitochondria co-ordinate such a fine-tuned interplay with ROS, and what controls their contact sites? The results presented in this chapter add to this ever-confounding but intriguing puzzle.

The first aim was to isolate both mitochondria and peroxisomes from wild-type yeast and detect which fractions Gpx3 resided in. Western blots confirmed the localisation of Gpx3 to both organelles (**Figure 5.2**) and also indicated the presence of Trx1/Trx2 and Erv1. Although the results should be analysed with caution as there was very slight mitochondrial contamination within the peroxisomal fraction, and the control peroxisomal antibody against Pex11 was unreliable, it is more than likely that Gpx3 and Trx1/Trx2 are bona fide peroxisomal proteins given the identification of Gpx3 and Trx (unknown which paralog) in a previous study by Ohdate and Inoue (2012). Future studies should aim to repeat these isolations under different conditions, i.e. H_2O_2 stress, glucose vs oleic acid, and decipher under what conditions these proteins localise to either organelle, whilst making sure to use trustworthy control antibodies. Also of importance is how are these proteins targeted to peroxisomes, and how do the cells regulate when and where each protein will go?

Sequence analysis was performed to try to identify potential peroxisomal targeting signals within these putative peroxisomal proteins which could be responsible for their

import. PTS1, PTS1 'relaxed', PTS2 and PTS2 'relaxed' consensus motifs were searched for within various proteins, including genuine peroxisomal proteins (**Figure 5.3**, **Table 5.1**). Though it is clear that there is a lot still to be understood about how some proteins are targeted to peroxisomes (no signals were identified for Pex11, Gpx1 or Gpx3), surprisingly PTS1 'relaxed' motifs were identified at the extreme C-terminus of both Trx1 and Trx2. Future work to confirm this would require mutating or deleting these tripeptides and testing their import capacity. It would also be interesting to determine through which peroxisomal import pore/mechanism these proteins enter, which receptors they interact with, and whether any chaperone proteins are required to 'piggy-back' them in.

Intriguingly, anti-Mia40 recognised a smaller protein running between the 17 – 22 kDa protein marker only in peroxisomal fractions (**Figure 5.4**); this protein disappeared when organelles were obtained from *galMia40* yeast (**Figure 5.6**). But why would a shorter, soluble version of Mia40 be present within peroxisomes, and how is it targeted there? In *A. thaliana*, Mia40 is a shorter soluble protein which localises to mitochondria and peroxisomes, playing a role in protein import in both organelles (**Figure 5.5**; Carrie et al., 2010). Different methods are needed to confirm whether Mia40 truly does exist in *S. cerevisiae* peroxisomes, such as: confocal microscopy using fluorescently tagged versions, immunoprecipitations using anti-Mia40 and solubilised peroxisomes, and import assays to name a few. In *A. thaliana*, a PTS1 SKL motif is responsible for its peroxisomal import; can the SKP of 'peroxisomal' Mia40 in yeast target it to peroxisomes in the absence of an N-terminal mitochondrial targeting signal? Akin to Trx1/Trx2, its tripeptide SKP could be mutated or deleted and any effects on import assessed.

In addition, 'peroxisomal' Mia40 was found to interact with Gpx3 when *in vitro* interaction assays were carried out using solubilised peroxisomal proteins and His-tagged versions of Gpx3 bound to Ni-NTA beads (**Figures 5.7 & 5.8**). This interaction was more apparent when the cysteine trap mutants Gpx3C82AHis and N18M20LGpx3C82AHis were used which suggests that 'peroxisomal' Mia40 might interact with Gpx3 via disulphide bonds (**Figure 5.8**). Of course, this interaction with Gpx3 would need to be checked *in vivo*, for example by immunoprecipitation, and further characterised. Could Gpx3 be involved

in re-oxidising Mia40 in peroxisomes like it does with full-length Mia40 in the mitochondrial IMS (Kritsiligkou et al., 2017)?

The final part of this chapter was aimed at tackling the import and localisation of Pex11 in mitochondria as the literature has thus far suggested that Pex11 is mistargeted to mitochondria in the absence of peroxisomes (Mattiazzi Usaj et al., 2015; Wróblewska et al., 2017). Radiolabelled Pex11 could be imported into mitochondria in a protease-protected manner and was independent of membrane potential (**Figure 5.10**). Import kinetics was then performed to compare the radiolabelled import of Pex11 against a hypothetical N17Pex11 but the results show no advantage of a N-terminal extension (**Figure 5.13**). Whilst it remains to be elucidated whether an N17 extension of Pex11 could actually exist *in vivo*, if it does exist then one hypothesis would be that it may be required for mitochondrial import when peroxisomes are also present. A dual import assay with both organelles could be set up in the future to assess this, but only if an N17Pex11 is found to be translated *in vivo*. Yeast would need to be grown under various conditions, i.e. -/+ H_2O_2, -/+ oleic acid, and combinations thereof, to determine whether an extension similar to the N18 of Gpx3 occurs.

The localisation assays carried out here point towards Pex11 as an integral membrane protein of either the IM or OM with a domain exposed to the IMS (**Figure 5.11**). In peroxisomes, there has been conflicting evidence on where Pex11 resides – the first paper in 1996 suggested it to be a peripheral membrane protein facing the inner side (Marshall et al., 1996), whereas a later paper in 2016 indicates it to be an integral membrane protein with pore-forming capabilities, acting as a non-selective channel (Mindthoff et al., 2016). Could Pex11 act as a similar pore-forming channel in mitochondria? Finally, it remains to be tested whether Gpx3 and Pex11 are interactors, either within mitochondria, peroxisomes or both. Attempts to express and purify a recombinant His-tagged version of Pex11 from *E. coli* were unsuccessful (data not shown) during this thesis. Further optimisation of the protein purification protocol is required in order to purify Pex11 and carry out *in vitro* interaction assays.

Chapter 6

General discussion

6. General discussion

6.1. Mitochondrial interactors of Gpx3

In *S. cerevisiae*, Gpx3 is an atypical 2-Cys peroxiredoxin that acts as a H_2O_2 sensor within the yeast cytosol where it has generally been well-characterised. However, in 2012 it was discovered within a mitochondrial IMS proteomics study (Vögtle et al., 2012). Another study published in the same year suggested that Gpx3 could be translated from an upstream non-AUG codon after exposure to H_2O_2 (Gerashchenko et al., 2012), thus producing an N-terminal extension that might act as a targeting signal. Work carried out by our lab in collaboration with the lab of Prof. Chris Grant (University of Manchester) confirmed the IMS localisation of Gpx3 both under physiological and H_2O_2 stress conditions, and revealed that an N-terminal extension of around 18 amino acids produced under H_2O_2 stress resulted in more efficient targeting to the IMS; although it was not necessary for import (Kritsiligkou et al., 2017). As previous studies only focused on the role of cytosolic Gpx3, namely its activation of the transcription factor Yap1, the role of both Gpx3 and N18Gpx3 in the IMS was yet to be determined.

Whilst the paper by Kritsiligkou et al. (2017) highlighted an interaction between Gpx3 and the IMS oxidoreductase Mia40, the work presented in this thesis aimed to define in an unbiased manner the potential mitochondrial-specific interactors of Gpx3/N18Gpx3, and went on to investigate one that may be of importance – the IMS electron carrier Cyt*c* (**Chapter 3**). Future work is required to validate an *in vivo* interaction between Gpx3 and Cyt*c* and to determine its physiological relevance. As both Mia40 and Cyt*c* are involved in oxidative protein folding in the IMS (following the MIA import pathway) (see Mordas and Tokatlidis, 2015), it is possible that Gpx3 also plays a role in oxidative folding and could act to regulate (or ensure the proper function of) the MIA pathway under oxidative stress. However, in mammals Cyt*c* is a multi-functional protein that plays roles outside of respiration and oxidative folding, such as its ability to interact with cardiolipin to attain peroxidase activity and trigger apoptosis (Schweitzer-Stenner, 2018). Interestingly,

questions remain as to how structural changes in Cyt*c* determine its function; perhaps Gpx3 helps Cyt*c* associate with cardiolipin at the IM by influencing its protein structure. Here, the only cysteine residue in Gpx3 that we found affected its *in vitro* interaction with Cyt*c* was Cys64. This cysteine is not involved in the interaction cycle with Yap1, and its function is not yet known although it is a highly conserved residue. Therefore, further investigation into the role of Cys64 of Gpx3 and its putative effect on a potential interaction with Cyt*c* will be of interest.

Another putative interactor of mitochondrial Gpx3 that warrants validation is the IMS protein Cytb2, a L-lactate cytochrome *c* oxidoreductase that is required for utilising lactate as a carbon source (Guiard, 1985). Other than this, its function is uncertain. Aside from confirming the IMS interactors identified in this study, future work should also aim to determine whether there are differences between Gpx3 and N18Gpx3 interactors, and whether specific physiological conditions such as oxidative stress are required for those interactions to occur.

6.2. Missing mitochondrial proteins?

Amongst the mass spectrometry data that was collected in **Chapter 3**, we identified six small proteins that had not been previously characterised or associated with mitochondria: Ybr124w, Ydr193w, Ygl024w, Yor293c-a, Ypl107w and Ypr010c-a. Out of these, three have interesting cysteine motifs, some of which are similar to the targeting signals found in substrate proteins of Mia40 (Ybr124w and Ygl024w). However, the only protein that we could identify a human homolog for was Ypl107w which also contains a highly conserved oxidoreductase-like domain, but so far the function of this protein (in any organism) is completely unknown. We focused on testing whether Ybr124w, Ygl024w and Ypl107w could be imported into mitochondria by producing radiolabelled proteins and following a standard import assay. Unfortunately, we were unable to clone *YGL024W* into a suitable plasmid for translation during this thesis. Upon successful production of radiolabelled Ybr124w and Ypl107w, only Ypl107w could be imported into mitochondria. Based on this, Ypl107w became the focus of the next results chapter as we aimed to

uncover some of its characteristics (**Chapter 4**). Nearing the end of my work, a large mitochondrial proteomics study was published that identified Ypl107w and Ypr010c-a as bona fide mitochondrial proteins and they were named Dpc25 and Min8, respectively (Morgenstern et al., 2017). Ypl107w was named Dpc25 for delta-psi dependent mitochondrial import and cleavage protein of ~25 kDa, as the protein exhibited defects in import when membrane potential was abolished and had a cleavable sequence upon successful import. Ypr010c-a was named Min8 for mitochondrial-MINi protein of 8 kDa. This provided reassurance that our methodology was successful in detecting previously unidentified mitochondrial proteins. Therefore, it would be of interest to confirm whether any of the other proteins identified in our list indeed reside in mitochondria as this would continue to add to our current understanding of the yeast mitochondrial proteome.

6.3. A new mitochondrial matrix protein – Ypl107w

Before we began our work, not much was known about Ypl107w apart from some large-scale phenotypic studies indicating that *ypl107wΔ* cells have a decreased resistance to H_2O_2, salt, and elesclomol (a drug that targets the mitochondrial respiratory chain), and a defect in fragmentation of vacuoles (Brown et al., 2006; Yoshikawa et al., 2009; Breslow et al., 2008; Blackman et al., 2012; Michaillat and Mayer, 2013). Another study had also suggested its localisation within mitochondria based on GFP-tagging of Ypl107w as part of a large genome screen (Huh et al., 2003). No study had solely focused on Ypl107w or its human homolog, hOXLD1, despite the presence of a highly conserved oxidoreductase-like domain (OXLD). This domain is present in more than 2000 proteins across 749 species (Pfam - PF09791; Finn et al., 2016), yet nothing is known about the function of OXLD.

In this study, we found that the *ypl107wΔ* null mutant exhibits growth defects only when grown on non-fermentable carbon sources such as lactic acid and glycerol (but not when grown on glucose), and confirmed the previous finding that *ypl107wΔ* null yeast mutant cells are less resistant to H_2O_2; these phenotypes are most probably attributed to an

impaired mitochondrial function. Our bioinformatics analysis on Ypl107w also heavily pointed towards its association with mitochondria through a number of findings: (i) a predicted cleavable N-terminal targeting sequence with an alpha-helical structure resembling that of a mitochondrial targeting signal; (ii) 23/75 predicted genetic interactors of *YPL107W* were genes encoding mitochondrial proteins; and (iii) inputting these proteins into a GO term finder revealed three common processes (mitochondrial tRNA thio-modification, mitochondrial organisation and protein lipoylation) and two functions (sulphurtransferase and oxidoreductase activity). Furthermore, an analysis of hOXLD-1 revealed that 38/49 physical interaction partners are mitochondrial proteins, and a GO term finder came up with a large number of significant ontology terms relating to mitochondrial functions including metabolism, gene expression, organisation, RNA processing and translation. Based on this information, our hypothesis is that Ypl107w and hOXLD-1 are involved in mitochondrial assembly, for example through helping to assemble some respiratory complexes and/or regulating mitochondrial gene expression and translation. Alternatively, Ypl107w may help assist in protein transport into the matrix by interacting with Ssc1.

Next, we confirmed the import of Ypl107w into mitochondria and found that its import was dependent on the inner membrane potential and its N-terminal 26 amino acid sequence. We also determined its localisation within the mitochondrial matrix where it remains as a soluble protein after import and maturation. Future import experiments should examine which import pathway Ypl107w follows by using mitochondria from different mutant strains such as *tom40-ts*, *tim23-ts*, *galMia40* and *galErv1*. We predict that Ypl107w import would be dependent on the presence of the TIM23 complex as this is the default pathway for proteins containing presequences which are destined for the mitochondrial matrix. This prediction is also based on the potential interaction between Ypl107w and a catalytic component of the TIM23-PAM complex, Ssc1.

We then began to investigate whether Ypl107w was part of any protein complexes with other mitochondrial proteins after import to the organelle. Although our BN-PAGE results were unclear, they were suggestive that Ypl107w likely participates in multiple complexes

due to the presence of many 'smeary' bands. One hypothesis is that Ypl107w may transiently interact with multiple proteins/complex subunits as it could be acting as a chaperone or assembly protein. Future BN-PAGE experiments should be performed using either a recombinant Ypl107w protein purified from *E. coli*, or by detecting the endogenous protein using antibodies against Ypl107w, or generating a tagged version of the protein in yeast. At present, none of these tools exist and attempts to purify Ypl107w from bacteria during the course of this thesis were unsuccessful. It would also be interesting to determine whether respiratory complexes are affected in *ypl107wΔ* yeast. This could be done by performing BN-PAGE and detecting the respiratory complexes using antibodies against individual subunits from each. In addition, pulldowns could be performed (akin to those done for Gpx3) to detect Ypl107w interactors.

Mitochondria from wild-type and *ypl107wΔ* cells were isolated and the levels of several mitochondrial proteins were quantified (those which we had antibodies against). We detected less Gpx3 and Cyt*c* when Ypl107w was absent. As Gpx3 and Cyt*c* are potential interactors, and Ypl107w was also a putative hit in the mass spectrometry data shown in **Chapter 3**, it is intriguing to speculate whether there is a link between all three. Future work should address this by carrying out a combination of *in vitro* interaction assays, reciprocal pulldowns, and immunoprecipitations to help determine whether Ypl107w interacts with Gpx3 and/or Cyt*c*. Furthermore, it would be interesting to determine whether the levels of other cytochrome proteins (or matrix proteins) are affected in *ypl107wΔ* yeast. However, this would require access to antibodies against numerous proteins which are not commercially available; therefore, quantitative mass spectrometry using isolated mitochondria could be a suitable alternative approach. Future work should also test whether the inner membrane potential is affected in *ypl107wΔ* mitochondria given its hypothesised role. Finally, an important question to address is whether hOXLD-1 acts in a similar manner to Ypl107w and is a true functional homolog. Parallel work using human cells would help elucidate the roles of proteins containing this elusive OXLD domain.

6.4. Does the MIA pathway exist in peroxisomes?

In recent years, there has been significant growth in the number of papers exploring the intricate links between mitochondria and peroxisomes, especially given that the redox state of peroxisomes has been shown to influence that of mitochondria (Baumgart et al., 2001; Ivashchenko et al., 2011; Wanders et al., 2016) and the increasing number of known membrane-membrane contact sites between both organelles (Mattiazzi Ušaj et al., 2015; Shai et al., 2018). However, there is still much to be understood about how these two organelles co-ordinate their interplay with ROS. Furthermore, researchers are still trying to identify the full extent of the peroxisomal proteome, especially as it is known to change in response to the metabolic environment (Yifrach et al., 2016). The work presented in **Chapter 5** adds to the literature regarding the peroxisomal proteome and may help to understand the complex mitochondria-peroxisome relationship.

When confirming the presence of Gpx3 within peroxisomes, we serendipitously stumbled upon the presence of a putative version of Mia40 in peroxisomes (which is a shorter, soluble form compared to the full length protein present in mitochondria), as well as Trx1 and/or Trx2 – three proteins that had not previously been associated with peroxisomes. As mentioned earlier, due to the sequence similarity between Trx1 and Trx2, it is not currently possible to tell which, or both, Thioredoxin(s) were detected. Whilst future work must validate the presence of these, for example by mass spectrometry analysis, confocal microscopy and import assays, our analysis is certainly suggestive of their localisation to both organelles. Our hypothesis is that the extreme C-terminal SKP tripeptide of Mia40, which is similar to the classical C-terminal SKL PTS1 signal, is enough to target Mia40 to peroxisomes in the absence of its N-terminal mitochondrial targeting signal which could result from alternative translation starting at a downstream methionine (although we have not looked specifically for such an alternative protein translation mechanism for Mia40). Whereas we found that both Trx1 and Trx2 contain PTS1 ‘relaxed’ motifs, ANA and SNV, respectively that could result in their dual-targeting as full-length proteins. It is imperative that future work investigates these ideas further by mutating or deleting these tripeptides and testing their ability to import into both organelles. It should also be determined precisely which physiological conditions dictate any dual localisations.

Although the import of peroxisomal proteins is largely known to occur via a considerably different machinery compared to those for mitochondrial proteins, in *A. thaliana* the Mia40 pathway is present and operates in both organelles (Carrie et al., 2010). Furthermore, whilst attempting to identify interactors of peroxisomal Gpx3 we found a putative interaction between Gpx3 and 'peroxisomal' Mia40; an interaction which was more apparent when the cysteine trap mutant of Gpx3 (Gpx3C82A) was used as bait. Thus, although a peroxisomal Gpx3-Mia40 interaction must first be validated, we can hypothesise that Gpx3 may be involved in re-oxidising Mia40 in peroxisomes, akin to its known ability to re-oxidise Mia40 in the mitochondrial IMS (Kritsiligkou et al., 2017). In this respect, it is notable that the default oxidant protein for Mia40 (which is Erv1) is not known to reside in peroxisomes. This opens the possibility that Gpx3 may functionally replace the Erv1 action in peroxisomes, whereas in mitochondria it may serve a more backup role to Erv1. However, there is some evidence presented here that suggests Erv1 may also be present in peroxisomes. Thioredoxin (Trx1 and/or Trx2) were also identified as potential interactors of peroxisomal Gpx3, and as Trx1 in the IMS can affect Mia40 oxidation (Mauricio Cárdenas-Rodriquez, 2019, PhD Thesis, University of Glasgow), and Trx1 reduces Gpx3 in the cytosol, it is plausible that Gpx3, Mia40 and Trx1 (and/or Trx2) are also interconnected in peroxisomes. Perhaps the MIA pathway regulates the import of proteins in both organelles which helps maintain their close redox relationship?

6.5. Conclusion

The work presented in this thesis has added to our knowledge of Gpx3 in two organelles, mainly the mitochondrion but also, to a lesser extent, the peroxisome. No previous literature existed on the role of Gpx3 outside of the cytosol, other than the publication on the targeting of Gpx3 to the IMS and its interaction with Mia40 reported by our lab during the course of this thesis (Kritsiligkou et al., 2017). Here, two new putative IMS interactors of Gpx3 were identified: Cyt*c* and Cytb2. We also uncovered six small proteins in our mass spectrometry analysis, none of which had been previously associated with mitochondria, and we went on to investigate one in more detail – Ypl107w. We also discovered components of the MIA pathway in yeast peroxisomes and hypothesise that this pathway may operate in both organelles, under the regulation of Gpx3 and Trx1 (and/or Trx2).

Chapter 7

Appendices

7. Appendices

7.1. Appendix 1 – Gpx3 purifications

Gpx3His

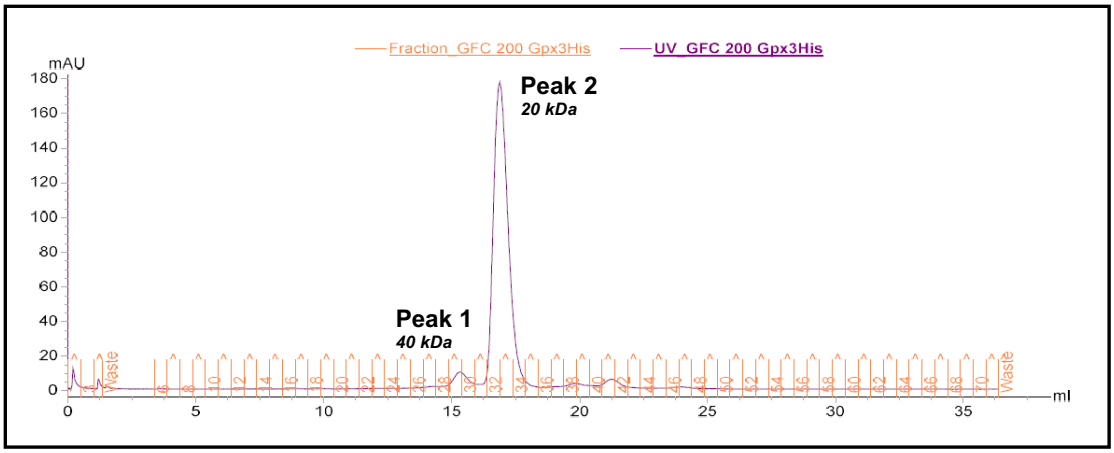

Figure 7.1. Purification of Gpx3His – ÄKTA peaks. Purified recombinant Gpx3His was analysed on an ÄKTA Pure FPLC system using a Superdex 200 10/30 GL column in its native state. The most abundant peak is peak 2 which eluted at a retention volume of 16.9 ml with an estimated molecular weight of 20 kDa. A weak peak, peak 1, eluted at a retention volume of 15.4 ml with an estimated molecular weight of 40 kDa. These estimations were calculated based on the standard curve shown in **Section 2.2.1.7**, **Figure 2.1**. Under these conditions, Gpx3His native is largely in its monomeric state (peak 2) with a small fraction of it in its dimeric state (peak 1). A third even weaker peak is likely to be a degradation product as its molecular weight is less than 6.5 kDa.

Gpx3C36SHis

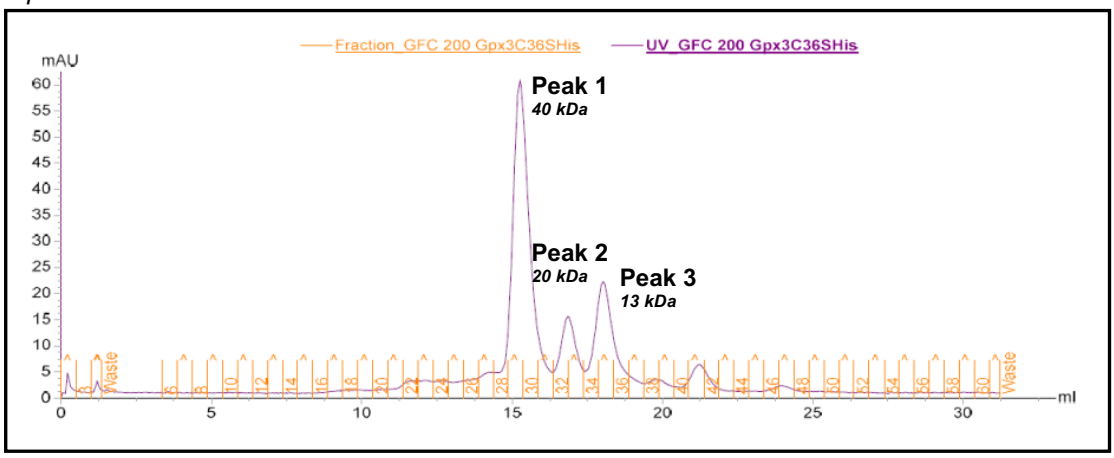

Figure 7.2. Purification of Gpx3C36SHis – ÄKTA peaks. Purified recombinant Gpx3C36SHis, a peroxidatic cysteine mutant, was analysed on an ÄKTA Pure FPLC system using Superdex 200 10/30 GL column in its native state. The majority of Gpx3C36SHis (peak 1) eluted at a retention volume of 15.4 ml, with an estimated molecular weight of 40 kDa. A second peak eluted at a retention volume of 16.9 ml with an estimated molecular weight of 20 kDa. A third peak eluted at a retention volume of 17.9 ml with an estimated molecular weight of 13 kDa. These estimations are calculated based on the standard curve shown in **Section 2.2.1.7**, **Figure 2.1**. Under these conditions, Gpx3C36SHis is mostly in its dimeric state, with a small fraction remaining as monomeric. The third peak is likely to be a degradation product.

Gpx3C64SHis

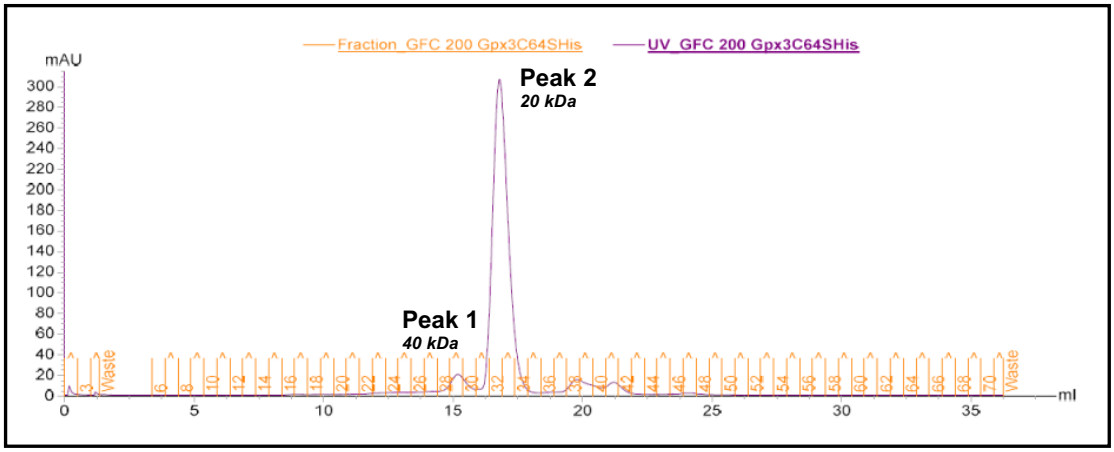

Figure 7.3. Purification of Gpx3C64SHis – ÄKTA peaks. Purified recombinant Gpx3C64SHis was analysed on an ÄKTA Pure FPLC system using Superdex 200 10/30 GL column in its native state. The majority of Gpx3C64SHis (peak 2) eluted at a retention volume of 16.9 ml with an estimated molecular weight of 20 kDa. A smaller peak (peak 1) eluted at a retention volume of 15.4 ml with an estimated molecular weight of 40 kDa. These estimations are calculated based on the standard curve shown in **Section 2.2.1.7**, **Figure 2.1**. Under these conditions, Gpx3C64SHis is mostly in its monomeric state, with a small fraction being dimeric.

Gpx3C82AHis native

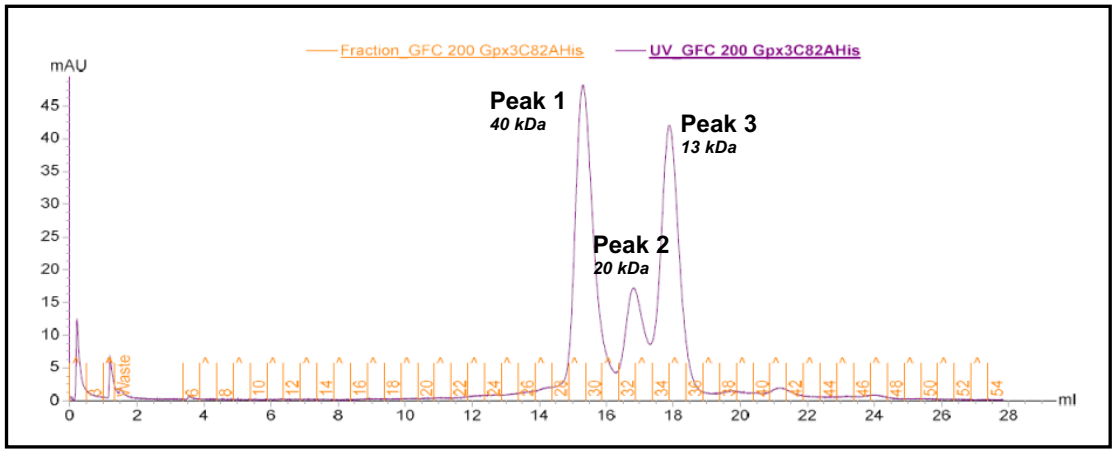

Figure 7.4. Purification of Gpx3C82AHis – ÄKTA peaks. Purified recombinant Gpx3C82AHis, a resolving cysteine mutant, was analysed on an ÄKTA Pure FPLC system using Superdex 200 10/30 GL column in its native state. The most abundant peak (peak 1) eluted at a retention volume of 15.4 ml with an estimated molecular weight of 40 kDa. A second peak eluted at a retention volume of 16.9 ml with an estimated molecular weight of 20 kDa. A third peak eluted at a retention volume of 17.9 ml with an estimated molecular weight of 13 kDa. These estimations are calculated based on the standard curve shown in **Section 2.2.1.7**, **Figure 2.1**. Under these conditions, Gpx3C82AHis is mostly in its dimeric state, with a small fraction remaining as monomeric. The third peak is likely to be a degradation product which indicates that Gpx3C82AHis is more prone to degradation than the other Gpx3His recombinant proteins.

7.2. Appendix 2 – Ypl107w and hOXLD-1 bioinformatics

Table 7.1. Genes with similar expression patterns to *YPL107W*.

Gene	Protein Localisation	Description
SPS22	Cytosol, plasma membrane	Ascospore spore wall assembly and cell wall organisation
PET20	Mitochondrion	Stability of mitochondrial genome
PEP12	Endosome, golgi apparatus, vacuole membrane	SNAP receptor activity, golgi to vacuole transport, macroautophagy, protein localisation, vacuole inheritance
DGA1	Lipid droplet, ER	Diacylglycerol acyltransferase
JID1	Mitochondrion	Unknown function but suspected Hsp40 co-chaperone involved in ER-associated degradation of misfolded proteins
CUB1	Cytoplasm, nucleus	Unknown function
AIM41	Mitochondrion	Unknown function but possible mitochondrial genome maintenance
ISU1	Mitochondrial matrix	Iron sulphur cluster scaffold protein
FYV6	Nucleus	Unknown function
CWC15	Nucleus	mRNA splicing
YOR062C	Cytoplasm, nucleus	Unknown function

HRT3	SCF-ubiquitin ligase complex	SCF-ubiquitin ligase F-box protein
NSG2	ER	Regulation of sterol biosynthesis
CMG1	Cytoplasm, nucleus	Unknown function
ATG19	Cytosol	Cytoplasm-vacuole targeting receptor
PEX15	Peroxisomal membrane	Peroxisome biogenesis
YNL115C	Mitochondrion, vacuole	Unknown function
GLC8	Cytoplasm, nucleus	Glycogen metabolism and chromosome segregation
GTF1	Mitochondrion	Glutaminyl-tRNA synthase activity

Genes with similar expression profiles to *YPL107W* were generated using SPELL, Serial Pattern of Expression Levels Locator (Hibbs et al., 2007). A list of the top 19 genes similar to *YPL107W* going from the most to least similar in descending order. ER – endoplasmic reticulum.

Table 7.2. GO Term Finder search of 38 mitochondrial hOXLD-1 interactors.

Gene Ontology Term Finder				
GO term	**Cluster frequency**	**Background frequency**	**P-value**	**Genes annotated to term**
Mitochondrial gene expression	10/38, 26%	0.8%	1.29E-10	TSFM, MTG2, TRMT61B, POLRMT, PUS1, AARS2, UQCC2, UQCC1, MRPP3, MTIF2
Mitochondrion organisation	12/38, 32%	2.6%	4.47E-8	ALAS1, GRPEL2, POLRMT, SIRT3, NDUFAF5, AARS2, UQCC1, UQCC2, NDUFAF7, MGME1, POLG
Small molecule metabolic process	19/38, 50%	10.2%	2.32E-7	CARS2, ACADVL, GLS, ACOT9, HSD17B8, AARS2, UQCC2, CPT2, MUT, NARS2, AK4, ACSF3, GLDC, ALDH5A1, MMAB, DBT, HIBCH, PDSS2, AUH
Cellular amino acid metabolic process	9/38, 24%	1.7%	3.46E-6	CARS2, GLS, GLDC, AARS2, ALDH5A1, HIBCH, NARS2, AUH, MUT
Mitochondrial RNA metabolic process	5/38, 13%	0.2%	4.20E-6	TRMT61B, POLRMT, PUS1, MRPP3, AARS2
Carboxylic acid metabolic process	13/38, 34%	5.0%	6.51E-6	CARS2, ACSF3, ACADVL, GLS, HSD17B8, GLDC, AARS2, ALDH5A1, CPT2, HIBCH, NARS2, AUH, MUT
Organic acid catabolic process	8/38, 21%	1.4%	1.35E-5	ACSF3, ACADVL, GLS, GLDC, ALDH5A1, CPT2, HIBCH, AUH
Carboxylic acid catabolic process	8/38, 21%	1.4%	1.35E-5	ACSF3, ACADVL, GLS, GLDC, ALDH5A1, CPT2, HIBCH, AUH
Oxoacid metabolic process	13/38, 34%	5.5%	1.80E-5	CARS2, ACSF3, ACADVL, GLS, HSD17B8, GLDC, AARS2, ALDH5A1, CPT2, HIBCH, NARS2, AUH, MUT
tRNA metabolic process	7/38, 18%	1.0%	2.25E-5	CARS2, TRMT61B, NARS2, TRMT2B, PUS1, MRPP3, AARS2
Organic acid metabolic process	13/38, 34%	5.6%	2.38E-5	CARS2, ACSF3, ACADVL, GLS, HSD17B8, GLDC, AARS2, ALDH5A1, CPT2, HIBCH, NARS2, AUH
Organic substance metabolic process	36/38, 95%	56.2%	4.61E-5	TSFM, MTG2, CARS2, ACADVL, GLS, TRMT61B, HSD17B8, SIRT3, AARS2, UQCC2, CPT2, AK4, POLG, ALAS1, IBA57, NDUFAF5, NDUFAF7, DBT, HIBCH, AUH, ACOT9, PUS1, UQCC1, NARS2, TRMT2B, MGME1, ACSF3, GLDC, POLRMT, ALDH5A1, MMAB, PDSS2, MRPP3, MTIF2, MUT

Regulation of mitochondrial translation	4/38, 11%	0.1%	4.76E-5	UQCC2, UQCC1, TSFM, MTG2
Mitochondrial translation	6/38, 16%	0.7%	7.70E-5	UQCC2, UQCC1, TSFM, MTG2, AARS2, MTIF2
Cellular amide metabolic process	12/38, 32%	5.4%	0.00012	TSFM, MTG2, CARS2, ACSF3, ACOT9, AARS2, ALDH5A1, UQCC2, UQCC1, DBT, NARS2, MTIF2
Cellular metabolic process	35/38, 92%	54.3%	0.00014	TSFM, MTG2, CARS2, ACADVL, GLS, TRMT61B, HSD17B8, SIRT3, AARS2, UQCC2, CPT2, AK4, POLG, ALAS1, IBA57, NDUFAF5, NDUFAF7, DBT, HIBCH, AUH, ACOT9, PUS1, UQCC1, NARS2, TRMT2B, MGME1, ACSF3, GLDC, POLRMT, ALDH5A1, MMAB, PDSS2, MRPP3, MTIF2, MUT
Metabolic process	36/38, 95%	58.8%	0.0002	TSFM, MTG2, CARS2, ACADVL, GLS, TRMT61B, HSD17B8, SIRT3, AARS2, UQCC2, CPT2, AK4, POLG, ALAS1, IBA57, NDUFAF5, NDUFAF7, DBT, HIBCH, AUH, ACOT9, PUS1, UQCC1, NARS2, TRMT2B, MGME1, ACSF3, GLDC, POLRMT, ALDH5A1, MMAB, PDSS2, MRPP3, MTIF2, MUT, C7ORF55
Cofactor metabolic process	9/38, 24%	2.8%	0.00023	DBT, ALAS1, ACSF3, IBA57, ACOT9, PDSS2, MMAB, ALDH5A1, MUT
Mitochondrial tRNA processing	3/38, 8%	0.1%	0.00035	TRMT61B, PUS1, MRPP3
Mitochondrial respiratory chain complex assembly	5/38, 13%	0.5%	0.00036	UQCC2, UQCC1, NDUFAF7, NDUFAF5, AARS2
Small molecule catabolic process	8/38, 21%	2.2%	0.00048	ACSF3, ACADVL, GLS, GLDC, ALDH5A1, CPT2, HIBCH, AUH
Mitochondrial RNA processing	3/38, 8%	0.1%	0.00097	TRMT61B, PUS1, MRPP3
tRNA processing	5/38, 13%	0.6%	0.00113	TRMT61B, TRMT2B, PUS1, MRPP3, AARS2
Cellular amino acid catabolic process	5/38, 13%	0.6%	0.00113	HIBCH, GLS, GLDC, AUH, ALDH5A1
Primary metabolic process	34/38, 90%	54.4%	0.00118	TSFM, MTG2, CARS2, ACADVL, GLS, TRMT61B, HSD17B8, SIRT3, AARS2, UQCC2, CPT2, AK4, POLG, ALAS1, NDUFAF5, NDUFAF7, DBT, HIBCH, AUH, ACOT9, PUS1, UQCC1, NARS2, TRMT2B, MGM1, ACSF3, GLDC, POLRMT, ALDH5A1, PDSS2, MRPP3, MTIF2, MUT, C7ORF55
Alpha-amino metabolic process	6/38, 16%	1.1%	0.00139	HIBCH, GLS, GLDC, MUT, AUH, ALDH5A1
Tetrapyrrole metabolic process	4/38, 11%	0.3%	0.00142	ALAS1, IBA57, MUT, MMAB

Monocarboxylic acid catabolic process	5/38%, 13%	0.7%	0.00149	CPT2, ACADVL, HIBCH, AUH, ALDH5A1
Fatty acid metabolic process	7/38, 18%	1.8%	0.00167	CPT2, ACSF3, ACADVL, HIBCH, HSD17B8, AUH, ALDH5A1
Fatty acid beta-oxidation	4/38, 11%	0.4%	0.00343	CPT2, ACADVL, HIBCH, AUH
Amide biosynthetic process	9/38, 24%	4.0%	0.00486	TSFM, MTG2, CARS2, ACSF3, AARS2, UQCC2, UQCC1, NARS2, MTIF2
Peptide metabolic process	9/38, 24%	4.1%	0.00527	TSFM, MTG2, CARS2, AARS2, ALDH5A1, UQCC2, UQCC1, NARS2, MTIF2
Tetrapyrrole biosynthetic process	3/38, 8%	0.1%	0.00549	ALAS1, IBA57, MMAB
Organonitrogen compound biosynthetic	13/38, 34%	9.2%	0.00646	TSFM, MTG2, ALAS1, CARS2, ACSF3, IBA57, GLS, AARS2, MMAB, UQCC2, UQCC1, NARS2, MTIF2
Translation	8/38, 21%	3.2%	0.00742	TSFM, MTG2, CARS2, AARS2, UQCC1, UQCC2, NARS2, MTIF2

All mitochondrial-associated hOXLD-1 physical interactors were entered into a Gene Ontology Term Finder tool (available at www.go.princeton.edu). P-value cut-off at 0.01.

7.3. Appendix 3 – *ypl107wΔ* mitochondria

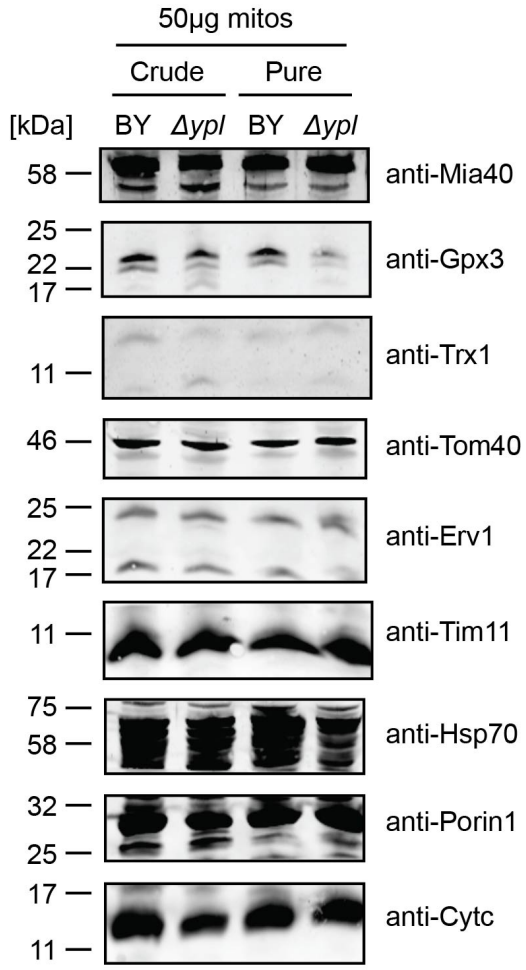

Figure 7.5. Steady-state protein levels in wild-type BY4741 vs *ypl107wΔ* mitochondria. BY4741 and *ypl107wΔ* yeast cells were grown in liquid YPLac media and their mitochondria were isolated by cell fractionation (crude) followed by density gradient centrifugation to yield highly purified mitochondria (pure) - refer to **Materials and Methods**, **Section 2.2.2.1** for detailed protocol. Samples were separated by SDS-PAGE and analysed by western blotting to detect various mitochondrial proteins; each lane represents 50µg protein. Antibodies against OM proteins include: anti-Por1 and anti-Tom40. IMS proteins include: anti-Mia40, anti-Gpx3, anti-Trx1, anti-Erv1 and anti-Cyt*c*. Anti-Tim11 was used as an IM protein marker and anti-Hsp70 as a matrix protein marker.

7.4. Appendix 4 – Supplementary materials and methods

7.4.1. Primers

Table 7.3. List of primers.

Primers		
Primers for cloning	**Primer sequence 5' -3'**	**Description/use**
His-tag REV EcoRI	CCGGAATTCTCAGTGGTGGTGGTGGTG	Reverse primer designed to amplify genes from pET24 and sublcone into pSP64 or other plasmids, incorporating the His-tag.
Frw_+18Gpx3 NdeI	CGCCATATGCTTTCCACGTCTCTCTCTTC	Forward primer to subclone +18Gpx3 from pSP64 into pET24
Rev_+18Gpx3 XhoI	CCGCTCGAGTTCCACCTCTTTCAAAAG	Reverse primer to subclone +18Gpx3 from pSP64 into pET24
Frw_Atp23 XbaI	CGCTCTAGAATGACGATGCGAACAAATAA	Forward Atp23 primer for cloning in pSP64
Rev_Atp23 XmaI	CCCCCCGGGTCATCTGTAAATCTCATCAA	Reverse Atp23 primer for cloning in pSP64
Frw_Atp23 NdeI	CGCCATATGACGATGCGAACAAATAAGAA	Forward Atp23 primer for cloning in pET24
Rev_Atp23 NotI	ATTTGCGGCCGCTCTGTAAATCTCATCAA	Reverse Atp23 primer for cloning in pET24
Frw_Cyc1 NdeI	CGCCATATGACTGAATTCAAGGCCGGTTC	Forward Cyc1 primer for cloning in pET24
Rev_Cyc1 XhoI	CCGCTCGAGCTCACAGGCTTTTTTCAAGT	Reverse Cyc1 primer for cloning in pET24
Frw_Cyc1 XbaI	CGCTCTAGAATGACTGAATTCAAGGCCGG	Forward Cyc1 primer for cloning in pSP64
Rev_Cyc1 XmaI	CCCCCCGGGTTACTCACAGGCTTTTTTCA	Reverse Cyc1 primer for cloning in pSP64
Frw_Pex11 BamHI/NdeI	CGCGGATCCCATATGGTCTGTGATACACT	Forward primer to clone Pex11 in pET24 and pSP64
Rev_Pex11 EcoRI	CCGGAATTCCTATGTAGCTTTCCACATGT	Reverse primer to clone Pex11 in pSP64
Rev_Pex11 XhoI (no stop, pET24)	CCGCTCGAGTGTAGCTTTCCACATGTCTT	Reverse primer to clone Pex11 in pET24
Frw_N17Pex11 BamHI/NdeI	CGCGGATCCCATATGTTGTCTCCATCTACTAC	Forward primer to clone N17Pex11 in pET24 and pSP64
Frw_YBR124W XbaI	CGCTCTAGAATGCCCCCACACATTTTTAT	Forward Ybr124w primer for cloning in pSP64
Rev_YBR124W XmaI	CCGCCCGGGTTAGTACAGAGAAGTCCTCT	Reverse Ybr124w primer for cloning in pSP64
Frw_YGL024W XbaI	CCGCGCTCTAGAATGTTTGCCATTATCTGTAT	Forward Ygl024w primer for cloning in pSP64
Rev_YGL024W XmaI	CCGCCGCCCGGGTTAATATAATATGATATAAT	Reverse Ygl024w primer for cloning in pSP64
Rev_YBR124W 3Met	CCGCCCGGGTTACATCATCATGTACAGAGAAGTCC	For adding three methionines to the end of YBR124W for radiolabelled expression

Frw_N18GPX3 HindIII	GCCAAGCTTATGCTTTCCACGTCTCTC	Forward primer for cloning N18Gpx3 in pSF-COOH-TEV-V5
Frw_PEX11 HindIII	GCCAAGCTTATGGTCTGTGATACACTG	Forward primer for cloning Pex11 in pSF-COOH-TEV-V5
Frw_N17Pex11 HindIII	GCCAAGCTTTTGTCTCCATCTACTAC	Forward primer for cloning N17Pex11 in pSF-COOH-TEV-V5
Fwd_YPL107W PstI/NheI	GGGCTGCAGGCTAGCATGATAAGAAATCAG	Forward primer to clone Ypl107w in pET24 and pSP64
Rev_YPL107W NotI (no stop)	AGTGCGGCCGCAACCAAAGCTGTCCTC	Reverse primer to clone Ypl107w in pET24
Rev_YPL107W XmaI	TCGCCCGGGTCAAACCAAAGCTGTCCT	Reverse primer to clone Ypl107w in pSP64
Primers for mutagenesis	**Primer sequence 5' -3'**	**Description/use**
Frw_C36S**_Gpx3**	GTTAATGTTGCCTCCAAATCTGGATTCACTCCTCAATAC	Forward primer for the mutagenesis of Cys36 to Ser in Gpx3/N18Gpx3
Rev_C36S**_Gpx3**	GTATTGAGGAGTGAATCCAGATTTGGAGGCAACATTAAC	Reverse primer for the mutagenesis of Cys36 to Ser in Gpx3/N18Gpx3
Frw_Gpx3 C64S	ATCATCGGGTTCCCATCCAACCAGTTTGGCCAC	Forward primer for the mutagenesis of Cys64 to Ser in Gpx3/N18Gpx3
Rev_Gpx3 C64S	GTGGCCAAACTGGTTGGATGGGAACCCGATGAT	Reverse primer for the mutagenesis of Cys64 to Ser in Gpx3/N18Gpx3
Frw_+18Gpx3 M20L	GTATTCAAGTTTATCCTGTCAGAATTCTATAAG	Forward primer for the mutagenesis of Methionine to Leucine in N18Gpx3/pET24 plasmid
Rev_+18Gpx3 M20L	CTTATAGAATTCTGACAGGATAAACTTGAATAC	Reverse primer for the mutagenesis of Methionine to Leucine in N18Gpx3/pET24 plasmid

All primers were designed in the lab and sent to Sigma Aldrich for synthesis; primers were kept as 100 µM stocks at -20°C.

7.4.2. Antibodies

Table 7.4. List of antibodies. All antibodies used in this study.

Antibodies				
Antibody	**Company**	**Origin**	**Conditions**	**Source**
anti-Cpn10	Davids Biotechnologie	Rabbit polyclonal	1:1000 in 1% milk	Tokatlidis lab
anti-Cyt*c*	Davids Biotechnologie	Rabbit polyclonal	1:2000 in 5% milk	Gifted by Prof. N. Pfanner
anti-Erv1	Davids Biotechnologie	Rabbit polyclonal	1:1000 in 1% milk	(Lionaki et al., 2010)
anti-Gpx3	Davids Biotechnologie	Rabbit polyclonal	1:1000 in 1% milk	(Kritsiligkou et al., 2017)
anti-His	AbD Serotec (Bio-Rad)	Mouse monoclonal	1:2000 in 1% milk	Obtained from Bio-Rad
anti-Mia40	Davids Biotechnologie	Rabbit polyclonal	1:1000 in 1% milk	(Sideris et al., 2009)
anti-mtHsp70	Davids Biotechnologie	Rabbit polyclonal	1:2000 in 5% milk	Gifted by Prof. N. Pfanner
anti-Pex11	Santa Cruz Biotechnology	Goat	1:500 in 1% milk	Obtained from Santa Cruz Biotech
anti-Porin1	Davids Biotechnologie	Rabbit polyclonal	1:2000 in 5% milk	Gifted by Prof. N. Pfanner
anti-TAP	CusAb (Flarebio)	Mouse	1:5000 in 1% milk	Obtained from Flarebio
anti-Tim10	Davids Biotechnologie	Rabbit polyclonal	1:1000 in 1% milk	Tokatlidis lab
anti-Tim11	Davids Biotechnologie	Rabbit polyclonal	1:1000 in 1% milk	Tokatlidis lab
anti-Tim23	Davids Biotechnologie	Rabbit polyclonal	1:1000 in 1% milk	Gifted by Prof. N. Pfanner
anti-Tim44	Davids Biotechnologie	Rabbit polyclonal	1:1000 in 1% milk	Gifted by Prof. G. Schatz
anti-Tim9	Davids Biotechnologie	Rabbit polyclonal	1:1000 in 1% milk	Tokatlidis lab
anti-Tom22	Davids Biotechnologie	Rabbit polyclonal	1:1000 in 1% milk	Gifted by Prof. N. Pfanner
anti-Tom5	Davids Biotechnologie	Rabbit polyclonal	1:1000 in 1% milk	Gifted by Prof. N. Pfanner
anti-Tom70	Davids Biotechnologie	Rabbit polyclonal	1:1000 in 1% milk	Tokatlidis lab
anti-Trr1	Davids Biotechnologie	Rabbit polyclonal	1:1000 in 1% milk	Tokatlidis lab
anti-Trx1	Davids Biotechnologie	Rabbit polyclonal	1:1000 in 5% milk	Tokatlidis lab
anti-rabbit IgG HRP	Sigma Aldrich or Elabscience	Goat	1:10000 in 1% milk	Sigma Aldrich or Elabscience
anti-mouse IgG HRP	Elabscience or CALIBIOCHEM	Goat	1:10000 in 1% milk	Elabscience or CALIBIOCHEM
anti-goat IgG HRP	Sigma Aldrich	Rabbit	1:10000 in 1% milk	Sigma Aldrich
anti-rabbit IRDye 680RD	LI-COR	Goat	1:10000 in dH_2O	LI-COR
anti-mouse IRDye 800CW	LI-COR	Goat	1:10000 in dH_2O	LI-COR
anti-mouse IgG DyLight 680	Invitrogen	Goat	1:500 in blocking buffer	Obtained from Thermo Fisher
anti-mouse IgG DyLight 488	Invitrogen	Goat	1:500 in blocking buffer	Obtained from Thermo Fisher

7.5. Appendix 5 – Characterisation of *T. gondii* Erv3

7.5.1. Localisation of TgErv3

To investigate the potential mitochondrial localisation of the TgErv homologs, *TgERV* gene sequences were cloned into a plasmid suitable for transfection and expression in *T. gondii* parasites (i.e. pTUB8/*MYC-TgERV3*). An N-terminal *MYC* gene sequence was also inserted to produce myc-tagged recombinant TgErv proteins. The *S. cerevisiae ERV1* gene along with an N-terminal *MYC* was also cloned into the pTUB8 plasmid to determine whether ScErv1 can be imported into *T. gondii* mitochondria. These plasmids were created by a previous lab member, *E. Kallergi*. In this project, the plasmids were transfected into *T. gondii* parasites expressing an endogenously GFP-tagged mitochondrial protein (Mys) and visualised using fluorescent microscopy. The only TgErv homolog to successfully express was Myc-TgErv3 which co-localised with Mys, indicating its mitochondrial localisation (**Figure 7.6A**). Myc-ScErv1 expression was observed in some parasites, however its mitochondrial localisation was uncertain as it appeared to express throughout (**Figure 7.6B**). It is possible that some Myc-ScErv1 was imported into mitochondria but that some remained in the cytosol. Unfortunately, the results were inconclusive from Myc-TgErv1 and Myc-TgErv2 as the proteins could not be detected. Attempts to clone TgErv1 and TgErv2 into alternative plasmids suitable for parasite expression, and with C-terminal myc tags, are ongoing.

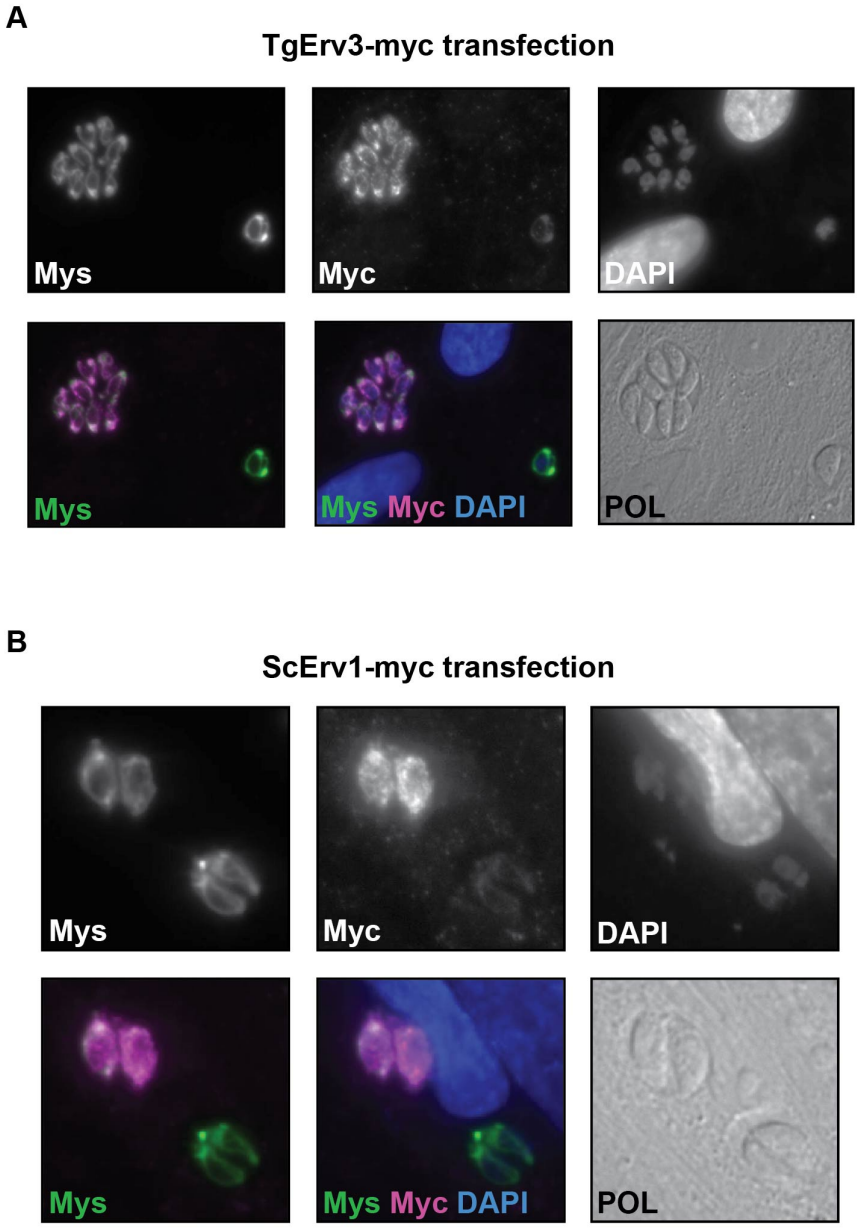

Figure 7.6. Fluorescent microscopy to detect localisation of TgErv3 and ScErv1 in *T. gondii* mitochondria. Plasmids containing the gene sequences for either TgErv3-myc or ScErv1-myc were transfected into *T. gondii* parasites that express an endogenously GFP-tagged Mys protein (green) that localises to mitochondria. Parasites were grown within human fibroblast foreskin cells. Primary antibodies against myc (anti-myc) and a red fluorescently-labelled secondary antibody was used to visualise myc-tagged proteins. DAPI staining (blue) was used to visualise the nucleus. Fluorescent microscopy was performed with the help of Jana Ovciarikova (Sheiner lab) who then analysed and created these images. Refer to **Section 2.2.4.2** for detailed methodology. Top panels – monochrome fluorescence images; bottom two left panels – multi-channel fluorescence images; bottom right panel, POL – polarised light only.

7.5.2. Purification of GST-TgErv3 and GST

The purification of recombinant GST-TgErv3 was first attempted from insoluble inclusion bodies (IB) (**Figure 7.7A**) as the majority of GST-TgErv3 expressed in all strains of *E. coli* tested remained in the pellet fraction after cell disruption (data not shown). The yield of GST-TgErv3 obtained from inclusion bodies after purification with Glutathione Sepharose 4B beads was very low – this was due to a large amount of protein being lost to aggregation. Attempts to optimise the purification protocol from inclusion bodies were not successful in either preventing or limiting aggregation, therefore we endeavoured to purify the very small amount of GST-TgErv3 that was found in the initial soluble fraction after protein expression and cell disruption (**Figure 7.7B**). It was hoped that by using the already soluble GST-TgErv3, the amount of protein lost to aggregation would be minimal. Unfortunately, the yield of GST-TgErv3 was still low; however, a higher molecular weight band appeared that corresponds to that of a potential GST-TgErv3 dimer.

Intriguingly, the purification eluates from both the inclusion bodies and soluble fraction contained a large amount of protein running at molecular weights that do not correspond with GST-TgErv3, or TgErv3 or GST alone – *especially* in the latter soluble purification (**Figures 7.7A & 7.7B**, **E1-3 lanes**). One possibility is that they are degradation products due to an unstable GST-TgErv3 protein that has fragmented at multiple regions. Despite this, eluates from both purifications were analysed using an ÄKTA Pure FPLC system. GST alone was purified as a control to assess whether the fusion of GST to TgErv3 could be affecting the results as GST itself is known to be dimeric (**Figure 7.8**). As GST is a soluble protein, it was purified from the soluble fraction after cell disruption. The yield obtained was high and corresponded to the correct molecular weight of GST at ~26 kDa.

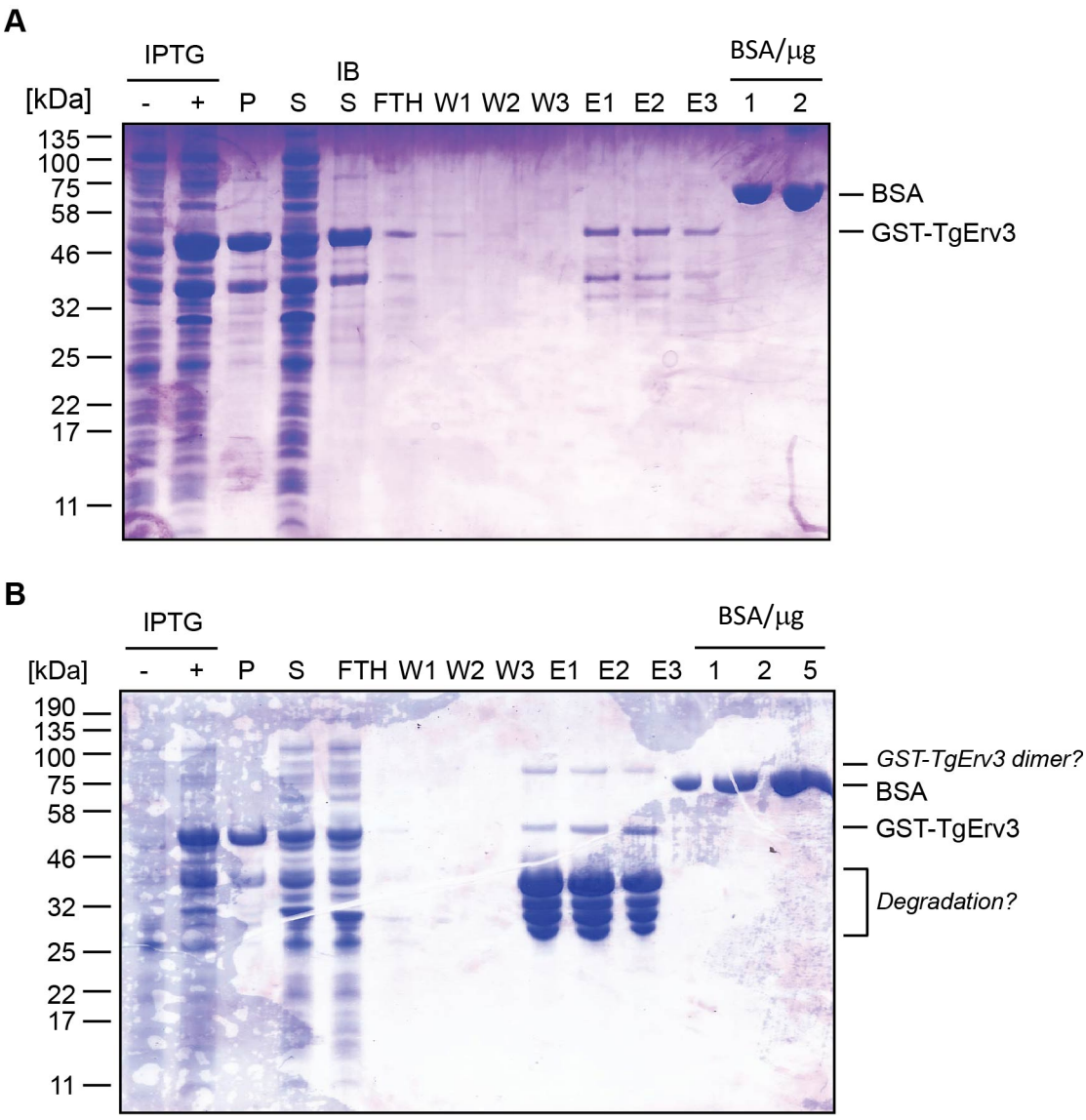

Figure 7.7. Purification of GST-TgErv3. GST-TgErv3 purifications from C+ (DE3) *E. coli* after induction with 0.4 mM IPTG (-/+) and 10 µM FAD for 4 hours at 37°C. Cells were fractionated using a French Press (P – pellet fraction containing insoluble proteins/inclusion bodies; S – supernatant fraction containing soluble proteins). Purification of GST-TgErv3 was attempted from both the pellet fraction containing GST-TgErv3 in inclusion bodies (**A**) and the soluble fraction **(B)** using Glutathione Sepharose 4B beads. Inclusion bodies were solubilised in urea to release GST-TgErv3 (IB S) which was then renatured. Supernatants, IB S from (**A**) after renaturation and S from (**B**), were incubated with pre-equilibrated beads and the flow throughs (FTH) collected. Beads were then washed three times (W1, W2 and W3) followed by three elutions with reduced glutathione (E1, E2 and E3). Image shown is a Coomassie stained SDS-PAGE gel loaded with β-me. BSA was loaded as a control for protein concentration (BSA/µg).

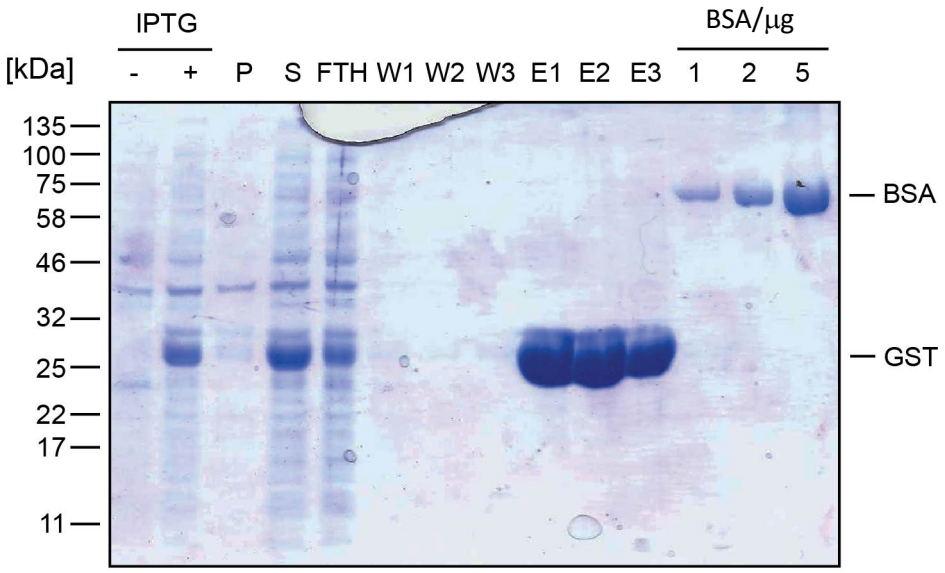

Figure 7.8. Purification of GST. GST purification from DE3 *E. coli* after induction with 0.4 mM IPTG (-/+) for 4 hours at 37°C. Cells were fractionated using a French Press (P – pellet fraction containing insoluble proteins/inclusion bodies; S – supernatant fraction containing soluble proteins). GST from the supernatant (S) was purified using Glutathione Sepharose 4B beads. Soluble material was incubated with pre-equilibrated beads and the flow through (FTH) collected. Beads were then washed three times (W1, W2 and W3) followed by three elutions with reduced glutathione (E1, E2 and E3). Image shown is a Coomassie stained SDS-PAGE gel loaded with β-me. BSA was loaded as a control for protein concentration (BSA/μg).

An ÄKTA Pure FPLC system was used to check the purity of the GST-TgErv3 recombinant proteins obtained from both purifications and to estimate their molecular weights; however, the results were puzzling (**Figures 7.9 & 7.10**). When the GST-TgErv3 eluate from the IB purification shown in **Figure 7.7A** was run through the system using a GFC 200 column, four distinct peaks appeared with estimated molecular weights of ≥2000 kDa (peak 1), 179 kDa (peak 2), 50 kDa (peak 3), and <6.5 kDa (peak 4) (**Figure 7.9**, top panel). Pre-treatment of GST-TgErv3 with 10 mM DTT prior to its run through the column did not seem to affect the size of these peaks, although it did produce an extra two peaks both estimated at <6.5 kDa (**Figure 7.9**, bottom panel). Samples from all of these peaks were analysed by SDS-PAGE (**Figure 7.10**). Despite the ÄKTA estimating a molecular weight of ≥2000 kDa for peak 1, the corresponding SDS-PAGE peak ran at ~50 kDa which equals that of one GST-TgErv3 monomer. It is possible that the denaturing SDS-PAGE conditions were enough to break a much larger oligomeric species but this is yet to be determined.

GST-TgErv3 from IBs (no DTT)

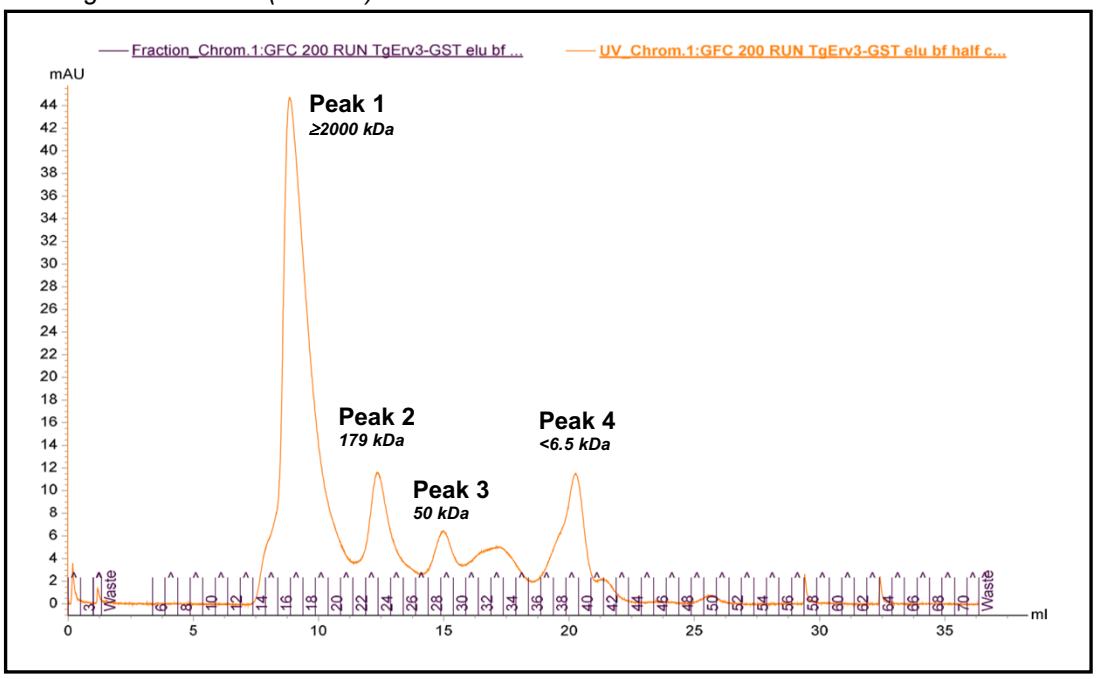

GST-TgErv3 from IBs (10 mM DTT)

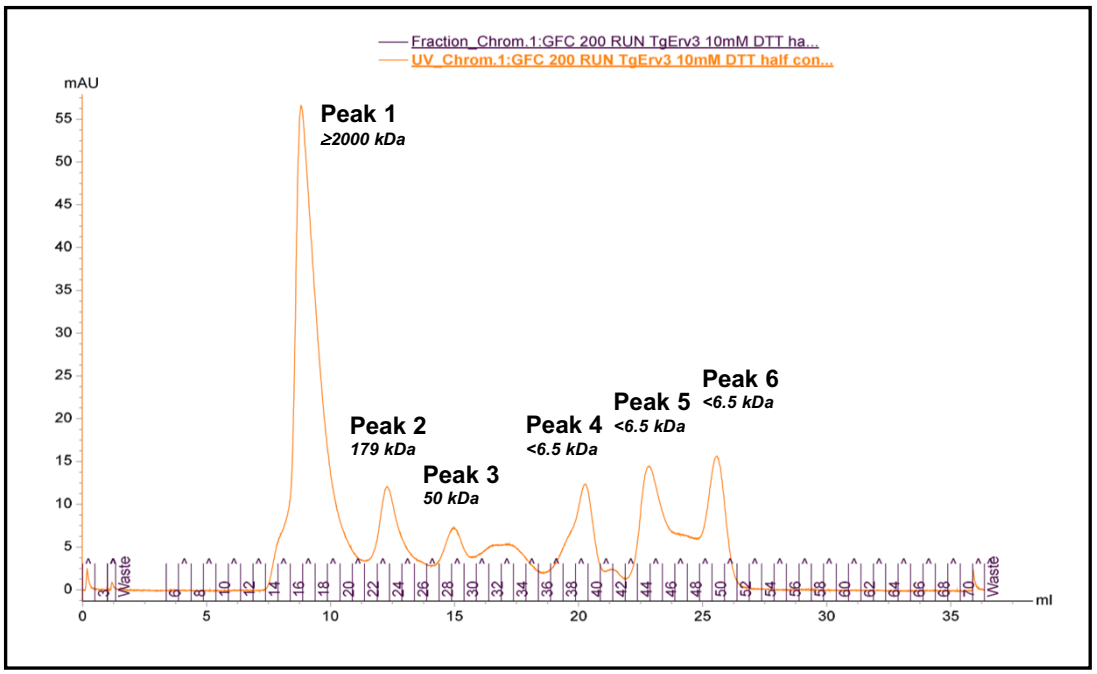

Figure 7.9. Purification of GST-TgErv3 from inclusion bodies – ÄKTA peaks. Purified recombinant GST-TgErv3 from inclusion bodies (IBs) was analysed on an ÄKTA Pure FPLC system using a GFC 200 column in both its native (top panel) vs reduced state (bottom panel). In the latter, GST-TgErv3 was pre-treated with 10 mM DTT for 30 minutes on ice to reduce disulphide bonds. X axis – retention volume; y axis – absorbance (mAU); purple – collection fractions; orange – UV chromatogram. Peak molecular weight estimations are calculated based on the standard curve shown in **Section 2.2.1.7**, **Figure 2.1**. Peaks represent fractions to be analysed by SDS-PAGE.

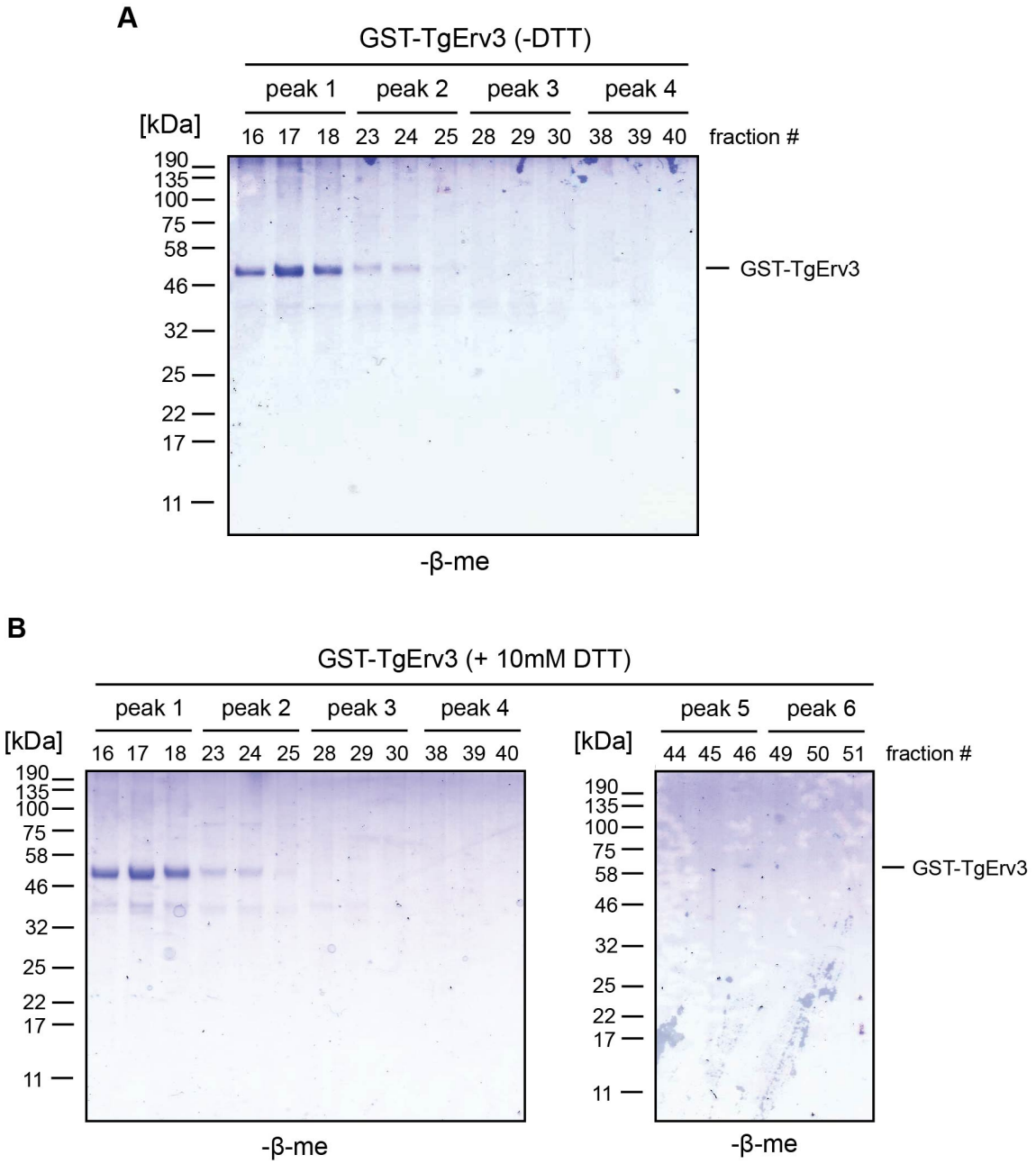

Figure 7.10. Purification of GST-TgErv3 from inclusion bodies – Fractions from ÄKTA peaks. Purified recombinant GST-TgErv3 from inclusion bodies (IBs) was analysed on an ÄKTA Pure FPLC system using a GFC 200 column, without pre-treatment with DTT (**A**) vs with pre-treatment with 10 mM DTT (**B**). Fractions containing peaks (as seen in **Figure 7.9**) were collected and loaded onto SDS-PAGE gels without β-me. Fractions were also loaded onto SDS-PAGE gels with the addition of β-me but the data is not shown as the results were the same.

ÄKTA analysis of GST-TgErv3 purified from the soluble fraction using the same GFC 200 column showed different results to that from the IBs. Three peaks were detected when soluble GST-TgErv3 was run through the column natively (without DTT pre-treatment) with estimated molecular weights of ≥2000 kDa (peak 1), 60 kDa (peak 2), and <6.5 kDa (peak 3) (**Figure 7.11**, top panel). Pre-treatment of soluble GST-TgErv3 with 10 mM DTT again produced an extra two peaks with estimated molecular weights of <6.5 kDa (**Figure 7.11**, bottom panel). However, the major species detected in **Figure 7.11** is peak 2 which corresponds to roughly the expected molecular weight of one GST-TgErv3 monomer; whereas the most abundant species in **Figure 7.10** is estimated at a staggering ≥2000 kDa. The logical explanation for the differences in the two purifications (IB vs soluble fraction) is that the former produced a very large oligomeric species which is likely attributed to incorrect refolding/aggregation of the protein during renaturation; the exact molecular weight of which could not be accurately determined using the GFC 200 column due to its molecular weight cut off point at 2000 kDa. Whereas the latter purification produced a species which is most likely to be correctly folded.

Samples from all peaks seen in **Figure 7.11** were analysed by SDS-PAGE but only those from the top panel whereby GST-TgErv3 was loaded to the column in its native state are shown (**Figure 7.12**). When the samples were loaded without the addition of β-me in the sample buffer, multiple bands were detected from peaks 2 and 3 that ran between 48-190 kDa and 25-35 kDa (**Figure 7.12A**). When samples were loaded *with* β-me, multiple bands were detected but only between 25-35 kDa (**Figure 7.12B**). Explanations for these findings may be that the GST-TgErv3 protein can form dimeric/higher oligomeric species but is also highly sensitive to degradation. GST alone was analysed by the ÄKTA using the same parameters (**Figure 7.13**) but it eluted as expected with an estimated molecular weight of ~52 kDa, indicating a GST dimer. Thus, it was unlikely that the fusion of GST to TgErv3 was affecting our analysis of GST-TgErv3. Even so, we attempted to cleave GST from the fusion protein using Thrombin, but the results were inconclusive as TgErv3 appears to be a very unstable protein upon purification (data not shown). Different purification protocols are warranted, i.e. using different tags, optimising the renaturation steps, use of different elution/storage buffers etc. to try to improve the yield and stability of soluble GST-TgErv3 so that it can be properly structurally analysed.

GST-TgErv3 from soluble fraction (no DTT)

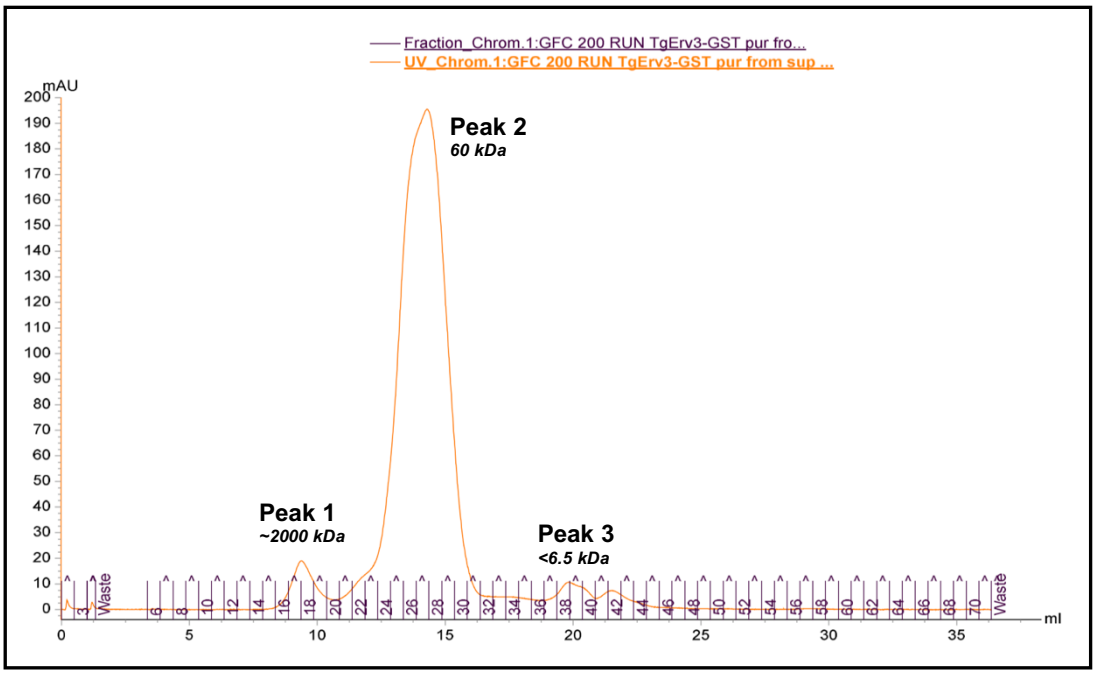

GST-TgErv3 from soluble fraction (10 mM DTT)

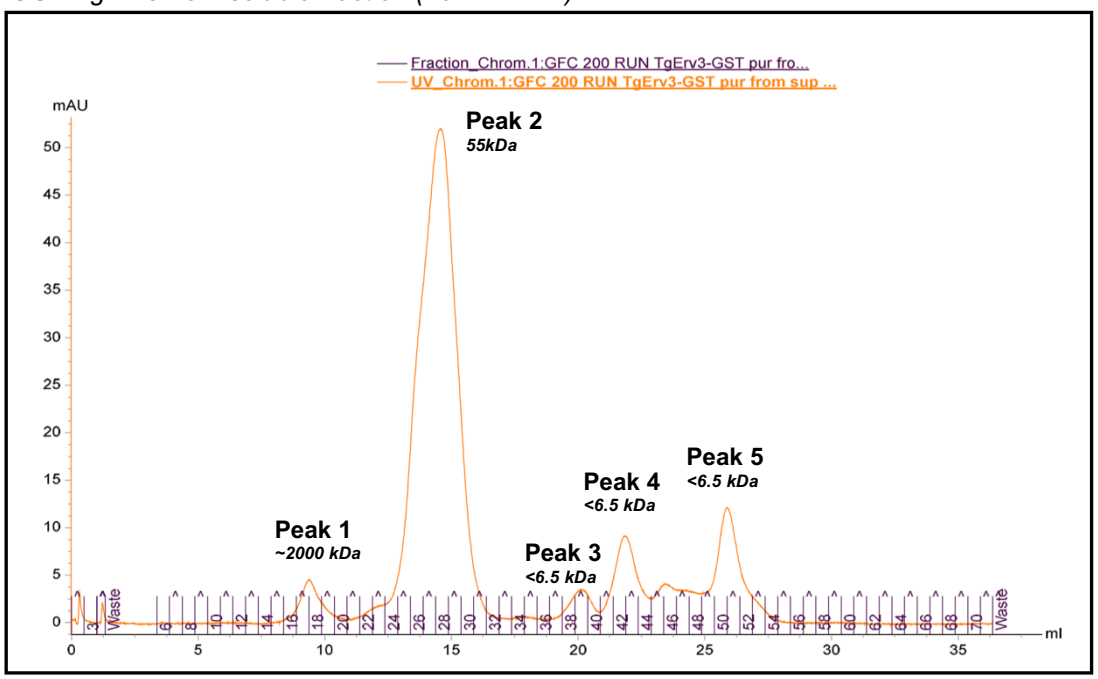

Figure 7.11. Purification of GST-TgErv3 from the soluble fraction – ÄKTA peaks. Purified recombinant GST-TgErv3 was analysed on an ÄKTA Pure FPLC system using a GFC 200 column in both its native (top panel) vs reduced state (bottom panel). In the latter, GST-TgErv3 was pre-treated with 10 mM DTT for 30 minutes on ice to reduce disulphide bonds. X axis – retention volume; y axis – absorbance (mAU); purple – collection fractions; orange – UV chromatogram. Peak molecular weight estimations are calculated based on the standard curve shown in **Section 2.2.1.7**, **Figure 2.1**. Peaks represent fractions to be analysed by SDS-PAGE.

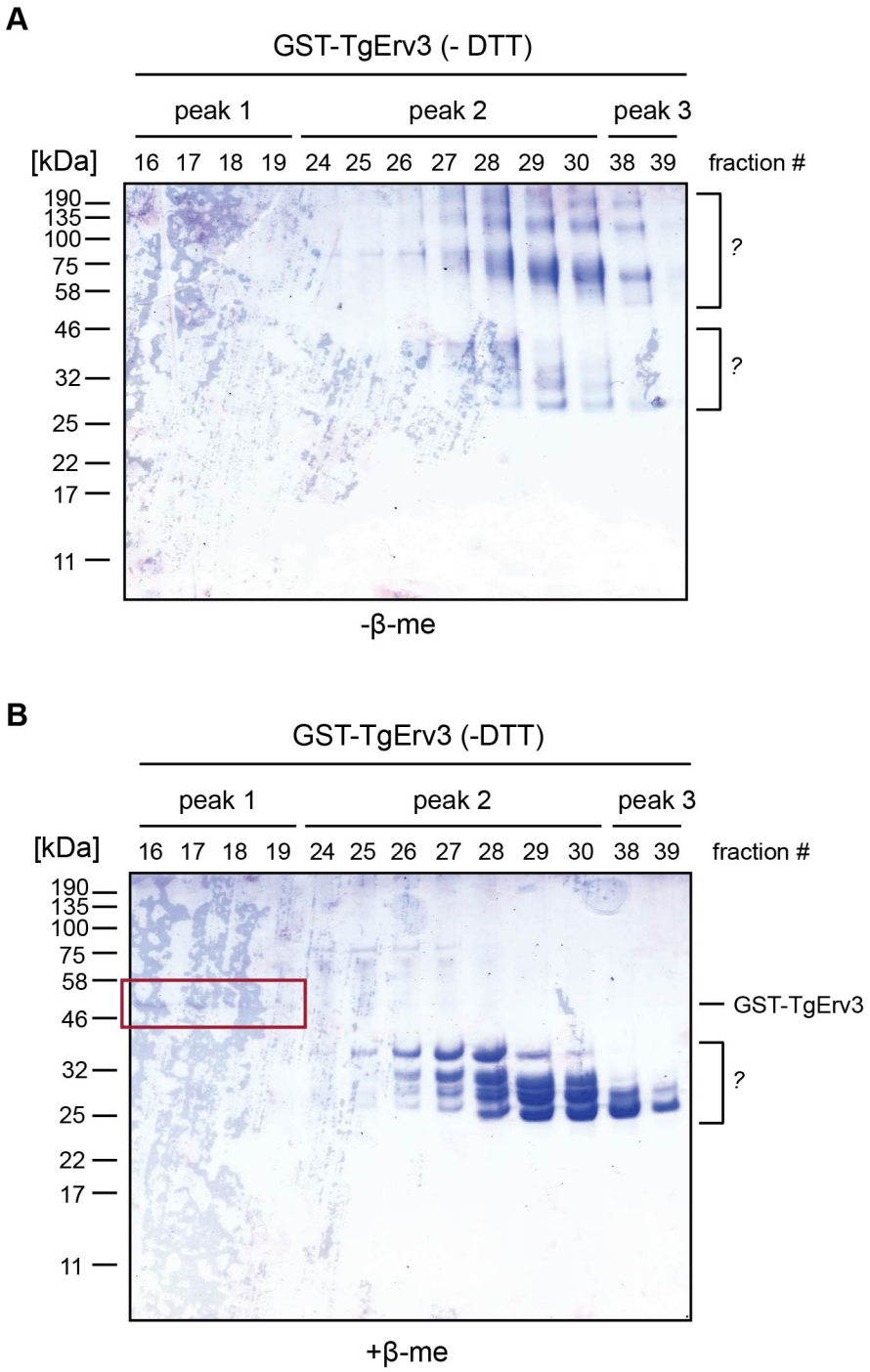

Figure 7.12. Purification of GST-TgErv3 from the soluble fraction – Fractions from ÄKTA peaks (-DTT). Purified recombinant GST-TgErv3 from the soluble fraction was analysed on an ÄKTA Pure FPLC system using a GFC 200 column. Fractions containing peaks (as seen in **Figure 7.11**, **top panel**) were collected and loaded onto SDS-PAGE gels either without β-me (**A**) or with β-me (**B**). The red box highlights where a faint band corresponding to the molecular weight of GST-TgErv3 can be seen in peak 1.

GST alone (-DTT)

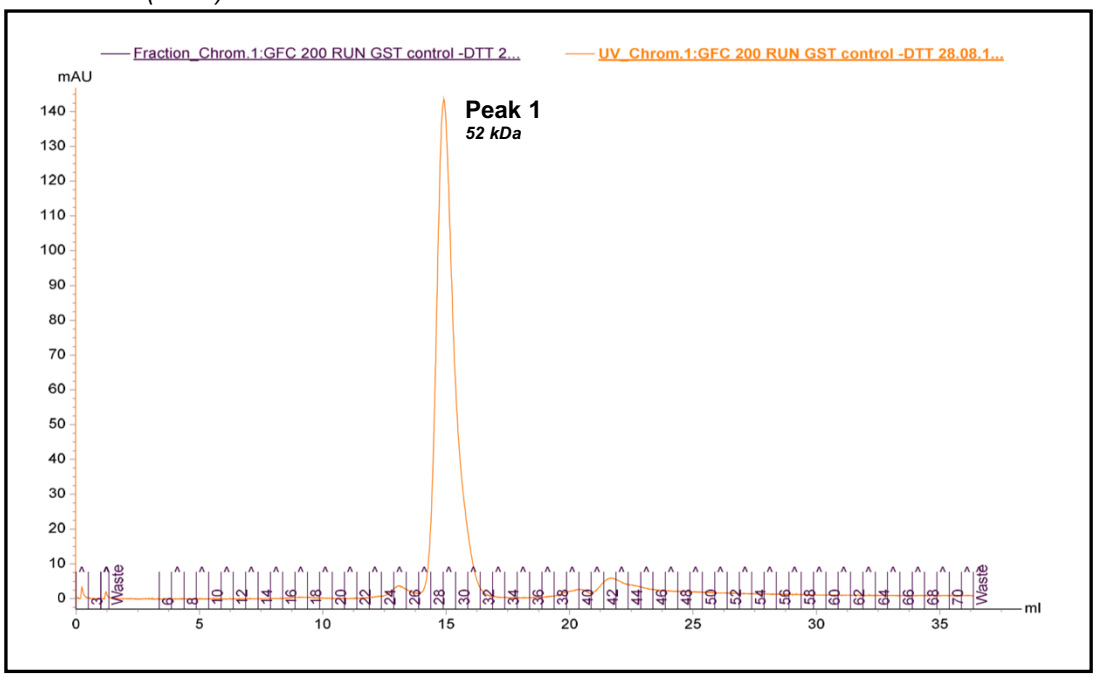

Figure 7.13. GST alone – ÄKTA peaks. Purified recombinant GST was analysed on an ÄKTA Pure FPLC system using a GFC 200 column in its native state. X axis – retention volume; y axis – absorbance (mAU); purple – collection fractions; orange – UV chromatogram. GST native eluted at a retention volume of ~15 ml with an estimated molecular weight of 52 kDa, equalling that of the expected GST in its dimeric state. This estimation was calculated based on the standard curve shown in **Section 2.2.1.7**, **Figure 2.1**.

References

Abe, Y., Shodai, T., Muto, T., Mihara, K., Torii, H., Nishikawa, S. ichi, … Kohda, D. (2000). Structural basis of presequence recognition by the mitochondrial protein import receptor Tom20. Cell, 100(5), 551–560. https://doi.org/10.1016/S0092-8674(00)80691-1

Adl, S. M., Simpson, A. G. B., Farmer, M. A., Andersen, R. A., Anderson, O. R., Barta, J. R., … Taylor, M. F. J. R. (2005). The new higher level classification of eukaryotes with emphasis on the taxonomy of protists. Journal of Eukaryotic Microbiology, 52(5), 399–451. https://doi.org/10.1111/j.1550-7408.2005.00053.x

Aitchison, J. D., Murray, W. W., & Rachubinski, R. A. (1991). The carboxyl-terminal tripeptide Ala-Lys-Ile is essential for targeting Candida tropicalis trifunctional enzyme to yeast peroxisomes. Journal of Biological Chemistry, 266(34), 23197–23203.

Allen, J. W. A., Ferguson, S. J., & Ginger, M. L. (2008). Distinctive biochemistry in the trypanosome mitochondrial intermembrane space suggests a model for stepwise evolution of the MIA pathway for import of cysteine-rich proteins. FEBS Letters, 582(19), 2817–2825. https://doi.org/10.1016/j.febslet.2008.07.015

Allen, S., Balabanidou, V., Sideris, D. P., Lisowsky, T., & Tokatlidis, K. (2005). Erv1 mediates the Mia40-dependent protein import pathway and provides a functional link to the respiratory chain by shuttling electrons to cytochrome c. Journal of Molecular Biology, 353(5), 937–944. https://doi.org/10.1016/j.jmb.2005.08.049

Altmann, R. (1890). Die Elementarorganismem Und Ihre Beziehungen Zu Den Zellen. Leipzig.

Ang, S. K., & Lu, H. (2009). Deciphering structural and functional roles of individual disulfide bonds of the mitochondrial sulfhydryl oxidase Erv1p. Journal of Biological Chemistry, 284, 28754–28761. https://doi.org/10.1074/jbc.M109.021113

Appenzeller-Herzog, C., & Ellgaard, L. (2008). The human PDI family: Versatility packed into a single fold. Biochimica et Biophysica Acta - Molecular Cell Research, 1783(4), 535–548. https://doi.org/10.1016/j.bbamcr.2007.11.010

Arnold, I., Bauer, M. F., Brunner, M., Neupert, W., & Stuart, R. A. (1997). Yeast mitochondrial F1F0-ATPase: The novel subunit e is identical to tim11. FEBS Letters, 411(2–3), 195–200. https://doi.org/10.1016/S0014-5793(97)00691-1

Avery, A. M., & Avery, S. V. (2001). Saccharomyces cerevisiae Expresses Three Phospholipid Hydroperoxide Glutathione Peroxidases. Journal of Biological Chemistry, 276(36), 33730–33735. https://doi.org/10.1074/jbc.M105672200

Backes, S., & Herrmann, J. M. (2017). Protein Translocation into the Intermembrane Space and Matrix of Mitochondria: Mechanisms and Driving Forces. Frontiers in Molecular Biosciences, 4(December), 1–11. https://doi.org/10.3389/fmolb.2017.00083

Bajaj, R., Jaremko, Ł., Jaremko, M., Becker, S., & Zweckstetter, M. (2014). Molecular basis of the dynamic structure of the TIM23 complex in the mitochondrial intermembrane space. Structure, 22(10), 1501–1511. https://doi.org/10.1016/j.str.2014.07.015

Baker, A., Hogg, T. L., & Warriner, S. L. (2016). Peroxisome protein import: a complex journey. Biochemical Society Transactions, 44(3), 783–789. https://doi.org/10.1042/BST20160036

Baker, K. M., Chakravarthi, S., Langton, K. P., Sheppard, A. M., Lu, H., & Bulleid, N. J. (2008). Low reduction potential of Ero1α regulatory disulphides ensures tight control of substrate oxidation. EMBO Journal, 27(22), 2988–2997. https://doi.org/10.1038/emboj.2008.230

Baker, M. J., Mooga, V. P., Guiard, B., Langer, T., Ryan, M. T., & Stojanovski, D. (2012). Impaired folding of the mitochondrial small TIM chaperones induces clearance by the i-AAA protease. Journal of Molecular Biology, 424(5), 227–239. https://doi.org/10.1016/j.jmb.2012.09.019

Banci, L., Bertini, I., Calderone, V., Cefaro, C., Ciofi-Baffoni, S., Gallo, A., … Tokatlidis, K. (2011). Molecular recognition and substrate mimicry drive the electron-transfer process between MIA40 and ALR. Proceedings of the National Academy of Sciences, 108(12), 4811–4816. https://doi.org/10.1073/pnas.1014542108

Banci, L., Bertini, I., Cefaro, C., Cenacchi, L., Ciofi-Baffoni, S., Felli, I. C., … Tokatlidis, K. (2010). Molecular chaperone function of Mia40 triggers consecutive induced folding steps of the substrate in mitochondrial protein import. Proceedings of the National Academy of Sciences, 107(17067), 20190–20195. https://doi.org/10.1073/pnas.1010095107

Banci, L., Bertini, I., Ciofi-Baffoni, S., Boscaro, F., Chatzi, A., Mikolajczyk, M., … Winkelmann, J. (2011). Anamorsin Is a [2Fe-2S] cluster-containing substrate of the Mia40-dependent mitochondrial protein trapping machinery. Chemistry and Biology, 18(6), 794–804. https://doi.org/10.1016/j.chembiol.2011.03.015

Basu, S., Leonard, J. C., Desai, N., Mavridou, D. A. I., Tang, K. H., Goddard, A. D., … Allen, J. W. A. (2013). Divergence of Erv1-associated mitochondrial import and export pathways in trypanosomes and anaerobic protists. Eukaryotic Cell, 12(2), 343–355. https://doi.org/10.1128/EC.00304-12

Bauer, M. F., Sirrenberg, C., Neupert, W., & Brunner, M. (1996). Role of Tim23 as voltage sensor and presequence receptor in protein import into mitochondria. Cell, 87(1), 33–41. https://doi.org/10.1016/S0092-8674(00)81320-3

Bauer et al., 2001

Becker, T., Pfannschmidt, S., Guiard, B., Stojanovski, D., Milenkovic, D., Kutik, S., … Wiedemann, N. (2008). Biogenesis of the mitochondrial TOM complex: Mim1 promotes insertion and assembly of signal-anchored receptors. Journal of Biological Chemistry, 283(1), 120–127. https://doi.org/10.1074/jbc.M706997200

Becker, T., Wenz, L. S., Krüger, V., Lehmann, W., Müller, J. M., Goroncy, L., … Pfanner, N. (2011). The mitochondrial import protein Mim1 promotes biogenesis of multispanning outer membrane proteins. Journal of Cell Biology, 194(3), 387–395. https://doi.org/10.1083/jcb.201102044

Becker, T., & Wagner, R. (2018). Mitochondrial Outer Membrane Channels: Emerging Diversity in Transport Processes. BioEssays, 40(7), 1–8. https://doi.org/10.1002/bies.201800013

Benda, C. (1898). Weitere mitteilungen über die mitochondria. Verh Dtsch Physiol Ges, 376-383.

Bersweiler, A., D'Autréaux, B., Mazon, H., Kriznik, A., Belli, G., Delaunay-Moisan, A., … Rahuel-Clermont, S. (2017). A scaffold protein that chaperones a cysteine-sulfenic acid in H_2O_2 signaling. Nature Chemical Biology, 13(8), 909–915. https://doi.org/10.1038/nchembio.2412

Bien, M., Longen, S., Wagener, N., Chwalla, I., Herrmann, J. M., & Riemer, J. (2010). Mitochondrial Disulfide Bond Formation Is Driven by Intersubunit Electron Transfer in Erv1 and Proofread by Glutathione. Molecular Cell, 37(4), 516–528. https://doi.org/10.1016/j.molcel.2010.01.017

Bienert, G. P., & Chaumont, F. (2014). Aquaporin-facilitated transmembrane diffusion of hydrogen peroxide. Biochimica et Biophysica Acta - General Subjects, 1840(5), 1596–1604. https://doi.org/10.1016/j.bbagen.2013.09.017

Bihlmaier, K., Mesecke, N., Terziyska, N., Bien, M., Hell, K., & Herrmann, J. M. (2007). The disulfide relay system of mitochondria is connected to the respiratory chain. Journal of Cell Biology, 179(3), 389–395. https://doi.org/10.1083/jcb.200707123

Blackman, R. K., Cheung-Ong, K., Gebbia, M., Proia, D. A., He, S., Kepros, J., … Nislow, C. (2012). Mitochondrial electron transport is the cellular target of the oncology drug Elesclomol. PLoS ONE, 7(1). https://doi.org/10.1371/journal.pone.0029798

Blandin, G., Durrens, P., Tekaia, F., Aigle, M., Bolotin-Fukuhara, M., Bon, E., … Dujon, B. (2000). Genomic Exploration of the Hemiascomycetous Yeasts: 4. The genome of Saccharomyces cerevisiae revisited. FEBS Letters, 487(1), 31–36. https://doi.org/10.1016/S0014-5793(00)02275-4

Bottinger, L., Gornicka, A., Czerwik, T., Bragoszewski, P., Loniewska-Lwowska, a., Schulze-Specking, a., … Chacinska, a. (2012). In vivo evidence for cooperation of Mia40 and Erv1 in the oxidation of mitochondrial proteins. Molecular Biology of the Cell, 23(20), 3957–3969. https://doi.org/10.1091/mbc.E12-05-0358

Böttinger et al., 2015

Boveris, A., Oshino, N., and Chance, B. (1972). The cellular production of hydrogen peroxide. Biochemical Journal, 128, 617-630.

Brandt, T., Mourier, A., Tain, L. S., Partridge, L., Larsson, N. G., & Kühlbrandt, W. (2017). Changes of mitochondrial ultrastructure and function during ageing in mice and Drosophila. ELife, 6, 1–19. https://doi.org/10.7554/eLife.24662

Breslow, D. K., Cameron, D. M., Collins, S. R., Schuldiner, M., Stewart-Ornstein, J., Newman, H. W., … Weissman, J. S. (2008). A comprehensive strategy enabling high-resolution functional analysis of the yeast genome. Nature Methods, 5(8), 711–718. https://doi.org/10.1038/nmeth.1234

Brocard, C., & Hartig, A. (2006). Peroxisome targeting signal 1: Is it really a simple tripeptide? Biochimica et Biophysica Acta - Molecular Cell Research, 1763(12), 1565–1573. https://doi.org/10.1016/j.bbamcr.2006.08.022

Brown, A. I., Kim, P. K., & Rutenberg, A. D. (2014). PEX5 and Ubiquitin Dynamics on Mammalian Peroxisome Membranes. PLoS Computational Biology, 10(1). https://doi.org/10.1371/journal.pcbi.1003426

Brown, J. A., Sherlock, G., Myers, C. L., Burrows, N. M., Deng, C., Wu, H. I., … Brown, J. M. (2006). Global analysis of gene function in yeast by quantitative phenotypic profiling. Molecular Systems Biology, 2. https://doi.org/10.1038/msb4100043

Callegari, S., Richter, F., Chojnacka, K., Jans, D. C., Lorenzi, I., Pacheu-Grau, D., … Rehling, P. (2016). TIM29 is a subunit of the human carrier translocase required for protein transport. FEBS Letters, 590(23), 4147–4158. https://doi.org/10.1002/1873-3468.12450

Calvo, S. E., Julien, O., Clauser, K. R., Shen, H., Kamer, K. J., Wells, J. A., & Mootha, V. K. (2017). Comparative Analysis of Mitochondrial N-Termini from Mouse, Human, and Yeast. Molecular & Cellular Proteomics, 16(4), 512–523. https://doi.org/10.1074/mcp.M116.063818

Carrie, C., Giraud, E., Duncan, O., Xu, L., Wang, Y., Huang, S., … Whelan, J. (2010). Conserved and novel functions for Arabidopsis thaliana MIA40 in assembly of proteins in mitochondria and peroxisomes. Journal of Biological Chemistry, 285(46), 36138–36148. https://doi.org/10.1074/jbc.M110.121202

Chacinska, A., & Rehling, P. (2004). Moving proteins from the cytosol into mitochondria. Biochemical Society Transactions, 32(5), 774–776. https://doi.org/10.1042/BST0320774

Chacinska, A., Lind, M., Frazier, A. E., Dudek, J., Meisinger, C., Geissler, A., … Rehling, P. (2005). Mitochondrial presequence translocase: Switching between TOM tethering and motor recruitment involves Tim21 and Tim17. Cell, 120(6), 817–829. https://doi.org/10.1016/j.cell.2005.01.011

Chacinska, A., Koehler, C. M., Milenkovic, D., Lithgow, T., & Pfanner, N. (2009). Importing Mitochondrial Proteins: Machineries and Mechanisms. Cell, 138(4), 628–644. https://doi.org/10.1016/j.cell.2009.08.005

Chacinska, A., Pfannschmidt, S., Wiedemann, N., Kozjak, V., Sanjuán Szklarz, L. K., Schulze-Specking, A., … Pfanner, N. (2004). Essential role of Mia40 in import and assembly of mitochondrial intermembrane space proteins. EMBO Journal, 23(19), 3735–3746. https://doi.org/10.1038/sj.emboj.7600389

Chakravarthi, S., Jessop, C. E., & Bulleid, N. J. (2006). The role of glutathione in disulphide bond formation and endoplasmic-reticulum-generated oxidative stress. EMBO Reports, 7(3), 271–275. https://doi.org/10.1038/sj.embor.7400645

Chan, N. C., and Lithgow, T. (2008). The Peripheral Membrane Subunits of the SAM Complex Function Codependently in Mitochondrial Outer Membrane Biogenesis. Molecular Biology of the Cell, 19, 126–136. https://doi.org/10.1091/mbc.e07-08-0796

Chan, N.C., Likić, V.A., and Waller, R.F. (2006). The C-terminal TPR Domain of Tom70 Defines a Family of Mitochondrial Protein Import Receptors Found only in Animals and Fungi. Journal of Molecular Biology, 358, 1010–1022. https://doi.org/10.1016/j.jmb.2006.02.062

Chatzi, A., Sideris, D. P., Katrakili, N., Pozidis, C., & Tokatlidis, K. (2013). Biogenesis of yeast Mia40 - Uncoupling folding from import and atypical recognition features. FEBS Journal, 280(20), 4960–4969. https://doi.org/10.1111/febs.12482

Checchetto, V., & Szabo, I. (2018). Novel Channels of the Outer Membrane of Mitochondria: Recent Discoveries Change Our View. BioEssays, 40(6), 1–7. https://doi.org/10.1002/bies.201700232

Clayton, D.A., & Vinograd, J. (1967). Circular Dimer and Catenate Forms of Mitochondrial DNA in Human Leukaemic Leucocytes. Nature, 216, 652-657.

Cohen, Y., Klug, Y. A., Dimitrov, L., Erez, Z., Chuartzman, S. G., Elinger, D., … Schuldiner, M. (2014). Peroxisomes are juxtaposed to strategic sites on mitochondria. Molecular BioSystems, 10(7), 1742–1748. https://doi.org/10.1039/c4mb00001c

Collet, J. F., Riemer, J., Bader, M. W., & Bardwell, J. C. A. (2002). Reconstitution of a disulfide isomerization system. Journal of Biological Chemistry, 277(30), 26886–26892. https://doi.org/10.1074/jbc.M203028200

Constanzo, M. Baryshnikova, A., Bellay, J., Kim, Y., Spear, E.D., Sevier, C., … Boone, C. (2010). The Genetic Landscape of a Cell. Science, 327(5964), 425–431. https://doi.org/10.1126/science.1180823

Constanzo, M., VanderSluis, B., Koch, E.N., Baryshnikova, A., Pons, C., Tan, G., … Boone, C. (2016). A global interaction network maps a wiring diagram of cellular function. Science, 23; 353(6306). https://doi.org/10.1126/science.aaf1420

Craig, E. A. (2018). Hsp70 at the membrane: Driving protein translocation. BMC Biology, 16(1), 1–11. https://doi.org/10.1186/s12915-017-0474-3

Dabir, D. V., Leverich, E. P., Kim, S. K., Tsai, F. D., Hirasawa, M., Knaff, D. B., & Koehler, C. M. (2007). A role for cytochrome c and cytochrome c peroxidase in electron shuttling from Erv1. EMBO Journal, 26(23), 4801–4811. https://doi.org/10.1038/sj.emboj.7601909

Darshi, M., Trinh, K. N., Murphy, A. N., & Taylor, S. S. (2012). Targeting and import mechanism of coiled-coil helix coiled-coil helix domain-containing protein 3 (ChChd3) into the mitochondrial intermembrane space. Journal of Biological Chemistry, 287(47), 39480–39491. https://doi.org/10.1074/jbc.M112.387696

De Duve, C., & Baudhuin, P. (1966). Peroxisomes (microbodies and related particles). Physiological Reviews, 46, 323–353. https://doi.org/10.1152/physrev.1966.46.2.323

Demishtein-Zohary, K., Günsel, U., Marom, M., Banerjee, R., Neupert, W., Azem, A., & Mokranjac, D. (2017). Role of Tim17 in coupling the import motor to the translocation channel of the mitochondrial presequence translocase. ELife, 6, 1–11. https://doi.org/10.7554/eLife.22696

Deplazes, A., Möckli, N., Luke, B., Auerbach, D., & Peter, M. (2009). Yeast Uri1p promotes translation initiation and may provide a link to cotranslational quality control. EMBO Journal, 28(10), 1429–1441. https://doi.org/10.1038/emboj.2009.98

Devenish, R. J., Prescott, M., Roucou, X., & Nagley, P. (2000). Insights into ATP synthase assembly and function through the molecular genetic manipulation of subunits of the yeast mitochondrial enzyme complex. Biochimica et Biophysica Acta - Bioenergetics, 1458(2–3), 428–442. https://doi.org/10.1016/S0005-2728(00)00092-X

Diekert, K., Kispal, G., Guiard, B., & Lill, R. (1999). An internal targeting signal directing proteins into the mitochondrial intermembrane space. Proceedings of the National Academy of Sciences, 96(21), 11752–11757. https://doi.org/10.1073/pnas.96.21.11752

Diekert, K., De Kroon, A. I. P. M., Ahting, U., Niggemeyer, B., Neupert, W., De Kruijff, B., & Lill, R. (2001). Apocytochrome c requires the TOM complex for translocation across the mitochondrial outer membrane. EMBO Journal, 20(20), 5626–5635. https://doi.org/10.1093/emboj/20.20.5626

Dietmeier, K., Hönlinger, A., Bömer, U., Dekker, P. J. T., Eckerskorn, C., Lottspeicht, F., … Pfanner, N. (1997). Tom5 functionally links mitochondrial preprotein receptors to the general import pore. Nature, 388(6638), 195–200. https://doi.org/10.1038/40663

Dimmer, K. S., Papic, D., Schumann, B., Sperl, D., Krumpe, K., Walther, D. M., & Rapaport, D. (2012). A crucial role for Mim2 in the biogenesis of mitochondrial outer membrane proteins. Journal of Cell Science, 125(14), 3464–3473. https://doi.org/10.1242/jcs.103804

Dodt, G., Warren, D., Becker, E., Rehling, P., & Gould, S. J. (2001). Domain Mapping of Human PEX5 Reveals Functional and Structural Similarities to Saccharomyces cerevisiae Pex18p and Pex21p. Journal of Biological Chemistry, 276(45), 41769–41781. https://doi.org/10.1074/jbc.M106932200

Donzeau, N., Káldi, K., Adam, A., Paschen, S., Wanner, G., Guiard, B., … Brunner, M. (2000). Tim23 Links the Inner and Outer Mitochondrial Membranes. Cell, 101, 401–412. https://doi.org/10.1016/S0092-8674(00)80850-8

Dudek, J., Rehling, P., & van der Laan, M. (2013). Mitochondrial protein import: Common principles and physiological networks. Biochimica et Biophysica Acta - Molecular Cell Research, 1833(2), 274–285. https://doi.org/10.1016/j.bbamcr.2012.05.028

Dyall, S. D., Agius, S. C., De Marcos Lousa, C., Trézéguet, V., & Tokatlidis, K. (2003). The dynamic dimerization of the yeast ADP/ATP carrier in the inner mitochondrial membrane is affected by conserved cysteine residues. Journal of Biological Chemistry, 278(29), 26757–26764. https://doi.org/10.1074/jbc.M302700200

Eckers, E., Cyrklaff, M., Simpson, L., & Deponte, M. (2012). Mitochondrial protein import pathways are functionally conserved among eukaryotes despite compositional diversity of the import machineries. Biological Chemistry, 393(6), 513–524. https://doi.org/10.1515/hsz-2011-0255

Eckers, E., Petrungaro, C., Gross, D., Riemer, J., Hell, K., & Deponte, M. (2013). Divergent molecular evolution of the mitochondrial sulfhydryl: Cytochrome c oxidoreductase Erv in opisthokonts and parasitic protists. Journal of Biological Chemistry, 288(4), 2676–2688. https://doi.org/10.1074/jbc.M112.420745

Elgersma, Y., van Roermund, C. W., Wanders, R. J., & Tabak, H. F. (1995). Peroxisomal and mitochondrial carnitine acetyltransferases of Saccharomyces cerevisiae are encoded by a single gene. EMBO Journal, 14(14), 3472–3479. https://doi.org/10.1002/j.1460-2075.1995.tb07353.x

Elgersma, Y., Vos, A., Van den Berg, M., Van Roermund, C. W. T., Van der Sluijs, P., Distel, B., & Tabak, H. F. (1996). Analysis of the carboxyl-terminal peroxisomal targeting signal 1 in a homologous context in Saccharomyces cerevisiae. Journal of Biological Chemistry, 271(42), 26375–26382. https://doi.org/10.1074/jbc.271.42.26375

Erdmann, R. (2016). Assembly, maintenance and dynamics of peroxisomes. Biochimica et Biophysica Acta - Molecular Cell Research, 1863(5), 787–789. https://doi.org/10.1016/j.bbamcr.2016.01.020

Erdmann, R., & Blobel, G. (1995). Giant peroxisomes in oleic acid-induced Saccharomyces cerevisiae lacking the peroxisomal membrane protein Pmp27p. Journal of Cell Biology, 128(4), 509–523. https://doi.org/10.1083/jcb.128.4.509

Farrell, S. R., & Thorpe, C. (2005). Augmenter of liver regeneration: A flavin-dependent sulfhydryl oxidase with cytochrome c reductase activity. Biochemistry, 44(5), 1532–1541. https://doi.org/10.1021/bi0479555

Finkel, T. (2012). Signal transduction by mitochondrial oxidants. Journal of Biological Chemistry, 287(7), 4434–4440. https://doi.org/10.1074/jbc.R111.271999

Finn, R. D., Coggill, P., Eberhardt, R. Y., Eddy, S. R., Mistry, J., Mitchell, A. L., … Bateman, A. (2016). The Pfam protein families database: Towards a more sustainable future. Nucleic Acids Research, 44(D1), D279–D285. https://doi.org/10.1093/nar/gkv1344

Fisk, D. G., Ball, C. A., Dolinski, K., Engel, S. R., Hong, E. L., Issel-tarver, L., … Michael, J. (2011). Saccharomyces cerevisiae S288C genome annotation: a working hypothesis. Yeast, 23(12), 857–865. https://doi.org/10.1002/yea.1400.Saccharomyces

Fraga, H., Bech-Serra, J. J., Canals, F., Ortega, G., Millet, O., & Ventura, S. (2014). The mitochondrial intermembrane space oxireductase mia40 funnels the oxidative folding pathway of the cytochrome c oxidase assembly protein cox19. Journal of Biological Chemistry, 289(14), 9852–9864. https://doi.org/10.1074/jbc.M114.553479

Freitag, J., Ast, J., & Bölker, M. (2012). Cryptic peroxisomal targeting via alternative splicing and stop codon read-through in fungi. Nature, 485(7399), 522–525. https://doi.org/10.1038/nature11051

Geissler, A., Chacinska, A., Truscott, K. N., Wiedemann, N., Brandner, K., Sickmann, A., … Rehling, P. (2002). The mitochondrial presequence translocase: An essential role of Tim50 in directing preproteins to the import channel. Cell, 111(4), 507–518. https://doi.org/10.1016/S0092-8674(02)01073-5

Gentle, I. E., Perry, A. J., Alcock, F. H., Likić, V. A., Dolezal, P., Ng, E. T., … Lithgow, T. (2007). Conserved motifs reveal details of ancestry and structure in the small TIM chaperones of the mitochondrial intermembrane space. Molecular Biology and Evolution, 24(5), 1149–1160. https://doi.org/10.1093/molbev/msm031

Gerashchenko, M. V., Lobanov, A. V., & Gladyshev, V. N. (2012). Genome-wide ribosome profiling reveals complex translational regulation in response to oxidative stress. Proceedings of the National Academy of Sciences, 109(43), 17394–17399. https://doi.org/10.1073/pnas.1120799109

Giaever, G., Chu, A.M., Ni, L., Connelly, C., Riles, L., Véronneau, S., … Johnston, M. (2002). Functional profiling of the Saccharomyces cerevisiae genome. Nature, 418, 387-391.

Glick, B.S. (1991). Protein import into isolated yeast mitochondria. Methods Cell Biology. 34, 389-399.

Glover, J. R., Andrews, D. W., Subramani, S., & Rachubinski, R. A. (1994). Mutagenesis of the amino targeting signal of Saccharomyces cerevisiae 3-ketoacyl-CoA thiolase reveals conserved amino acids required for import into peroxisomes in vivo. Journal of Biological Chemistry, 269(10), 7558–7563.

Goldstone, D., Haebel, P. W., Katzen, F., Bader, M. W., Bardwell, J. C., Beckwith, J., & Metcalf, P. (2001). DsbC activation by the N-terminal domain of DsbD. Proceedings of the National Academy of Sciences, 98(17), 9551–9556. https://doi.org/10.1073/pnas.171315498

Gross, E., Sevier, C. S., Heldman, N., Vitu, E., Bentzur, M., Kaiser, C. A., … Fass, D. (2006). Generating disulfides enzymatically: Reaction products and electron acceptors of the endoplasmic reticulum thiol oxidase Ero1p. Proceedings of the National Academy of Sciences, 103(2), 299–304. https://doi.org/10.1073/pnas.0506448103

Gstaiger, M., Luke, B., Hess, D., Oakeley, E.J., Wirbelauer, C., Blondel, M., … Krek, W. (2003). Control of Nutrient-Sensitive Transcription Programs by the Unconventional Prefoldin URI. Science, 302(5648), 1208-1212. https://doi.org/10.1126/science.1088401

Guiard, B. (1985). Structure, expression and regulation of a nuclear gene encoding a mitochondrial protein: the yeast L(+)-lactate cytochrome c oxidoreductase (cytochrome b2). EMBO Journal, 4(12), 3265-3272.

Gulshan, K., Lee, S. S., & Moye-Rowley, W. S. (2011). Differential oxidant tolerance determined by the key transcription factor Yap1 is controlled by levels of the Yap1-binding protein, Ybp1. Journal of Biological Chemistry, 286(39), 34071–34081. https://doi.org/10.1074/jbc.M111.251298

Habich, M., Salscheider, S. L., & Riemer, J. (2018). Cysteine residues in mitochondrial intermembrane space proteins: more than just import. British Journal of Pharmacology. https://doi.org/10.1111/bph.14480

Hacioglu, E., Esmer, I., Fomenko, D.E., Gladyshev, V.N., & Koc, A. (2012). Regulation of yeast replicative life span by thiol oxidoreductases. Mechanisms of Ageing and Development, 131, 692–699. https://doi.org/10.1016/j.mad.2010.09.006.

Haindrich, A. C., Boudová, M., Vancová, M., Diaz, P. P., Horáková, E., & Lukeš, J. (2017). The intermembrane space protein Erv1 of Trypanosoma brucei is essential for mitochondrial Fe-S cluster assembly and operates alone. Molecular and Biochemical Parasitology, 214, 47–51. https://doi.org/10.1016/j.molbiopara.2017.03.009

Hangen, E., Féraud, O., Lachkar, S., Mou, H., Doti, N., Fimia, G. M., … Modjtahedi, N. (2015). Interaction between AIF and CHCHD4 Regulates Respiratory Chain Biogenesis. Molecular Cell, 58(6), 1001–1014. https://doi.org/10.1016/j.molcel.2015.04.020

Haque, S. J., Majumdar, T., & Barik, S. (2012). Redox-Assisted Protein Folding Systems in Eukaryotic Parasites. Antioxidants & Redox Signaling, 17(4), 674–683. https://doi.org/10.1089/ars.2011.4433

Hibbs, M. A., Hess, D. C., Myers, C. L., Huttenhower, C., Li, K., & Troyanskaya, O. G. (2007). Exploring the functional landscape of gene expression: Directed search of large microarray compendia. Bioinformatics, 23(20), 2692–2699. https://doi.org/10.1093/bioinformatics/btm403

Hill, K., Model, K., Ryan, M. T., Dietmeier, K., Martin, F., Wagner, R., & Pfanner, N. (1998). Tom40 forms the hydrophilic channel of the mitochondrial import pore for preproteins. Nature, 395(6701), 516–521. https://doi.org/10.1038/26780

Hofmann, S., Rothbauer, U., Mühlenbein, N., Baiker, K., Hell, K., & Bauer, M. F. (2005). Functional and mutational characterization of human MIA40 acting during import into the mitochondrial intermembrane space. Journal of Molecular Biology, 353(3), 517–528. https://doi.org/10.1016/j.jmb.2005.08.064

Höhr, A. I. C., Straub, S. P., Warscheid, B., Becker, T., & Wiedemann, N. (2015). Assembly of β-barrel proteins in the mitochondrial outer membrane. Biochimica et Biophysica Acta - Molecular Cell Research, 1853(1), 74–88. https://doi.org/10.1016/j.bbamcr.2014.10.006

Horst, M., Oppliger, W., Rospert, S., Schönfeld, H.J., Schatz, G., & Azem, A. (1997). Sequential action of two hsp70 complexes during protein import into mitochondria. EMBO Journal, 16(8), 1842–1849. https://doi.org/10.1093/emboj/16.8.1842

Horvath, S. E., Rampelt, H., Oeljeklaus, S., Warscheid, B., Van Der Laan, M., & Pfanner, N. (2015). Role of membrane contact sites in protein import into mitochondria. Protein Science, 24(3), 277–297. https://doi.org/10.1002/pro.2625

Houtkooper, R. H., & Vaz, F. M. (2008). Cardiolipin, the heart of mitochondrial metabolism. Cellular and Molecular Life Sciences, 65(16), 2493–2506. https://doi.org/10.1007/s00018-008-8030-5

Hu, X., Wang, K., & Dong, Q. (2016). Protein ligand-specific binding residue predictions by an ensemble classifier. BMC Bioinformatics, 17(1), 1–12. https://doi.org/10.1186/s12859-016-1348-3

Huh, W., Falvo, J. V, Gerke, L. C., Carroll, A. S., Howson, R. W., Weissman, J. S., & Shea, E. K. O. (2003). Global analysis of protein localization in budding yeast. Nature, 425, 686-691. https://doi.org/10.1038/nature02026

Huttlin, E. L., Bruckner, R. J., Paulo, J. A., Cannon, J. R., Ting, L., Colby, G., … Wade, J. (2017). Communities and Disease Networks, 545(7655), 505–509. https://doi.org/10.1038/nature22366.Architecture

Huttlin, E. L., Ting, L., Bruckner, R. J., Gebreab, F., Gygi, M. P., Szpyt, J., … Gygi, S. P. (2015). The BioPlex Network of Human Protein Interactions. Cell, 162(2), 425–440. https://doi.org/10.1016/j.cell.2015.06.043.The

Inoue, Y., Matsuda, T., Sugiyama, K. I., Izawa, S., & Kimura, A. (1999). Genetic analysis of glutathione peroxidase in oxidative stress response of Saccharomyces cerevisiae. Journal of Biological Chemistry, 274(38), 27002–27009. https://doi.org/10.1074/jbc.274.38.27002

Ivashchenko, O., Van Veldhoven, P. P., Brees, C., Ho, Y.-S., Terlecky, S. R., & Fransen, M. (2011). Intraperoxisomal redox balance in mammalian cells: oxidative stress and interorganellar cross-talk. Molecular Biology of the Cell, 22(9), 1440–1451. https://doi.org/10.1091/mbc.E10-11-0919

Jores, T., Klinger, A., Groß, L. E., Kawano, S., Flinner, N., Duchardt-Ferner, E., … Rapaport, D. (2016). Characterization of the targeting signal in mitochondrial β-barrel proteins. Nature Communications, 7(May). https://doi.org/10.1038/ncomms12036

Josyula, R., Jin, Z., Fu, Z., & Sha, B. (2006). Crystal Structure of Yeast Mitochondrial Peripheral Membrane Protein Tim44p C-terminal Domain. Journal of Molecular Biology, 359(3), 798–804. https://doi.org/10.1016/j.jmb.2006.04.020

Joza, N., Susin, S.A., Daugas, E., Stanford, W.L., Cho, S.K., Li, C.Y.J., … Penninger, J.M. (2001). Essential role of the mitochondrial apoptosis-inducing factor in programmed cell death. Nature, 410(6828), 549-534. https://doi.org/10.1038/35069004

Kallergi, E., Andreadaki, M., Kritsiligkou, P., Katrakili, N., Pozidis, C., Tokatlidis, K., … Peruzzini, R. (2012). Targeting and maturation of Erv1/ALR in the mitochondrial intermembrane space. ACS Chemical Biology, 7(4), 707–714. https://doi.org/10.1021/cb200485b

Kallergi, E., Kalef-Ezra, E., Karagouni-Dalakoura, K., & Tokatlidis, K. (2014). Common players in mitochondria biogenesis and neuronal protection against stress-induced apoptosis. Neurochemical Research, 39(3), 546–555. https://doi.org/10.1007/s11064-013-1109-x

Kang, P.J., Ostermann, J., Shilling, J., Neupert, W., Craig, E.A., & Pfanner, N. (1990). Requirement for hsp70 in the mitochondrial matrix for translocation and folding of precursor protein. Nature, 348(6297), 137-143. https://doi.org/10.1038/348137a0

Kang, Y., Baker, M. J., Liem, M., Louber, J., McKenzie, M., Atukorala, I., … Stojanovski, D. (2016). Tim29 is a novel subunit of the human TIM22 translocase and is involved in complex assembly and stability. ELife, 5(AUGUST), 1–23. https://doi.org/10.7554/eLife.17463

Karpichev, I. V., Durand-Heredia, J. M., Luo, Y., & Small, G. M. (2008). Binding characteristics and regulatory mechanisms of the transcription factors controlling oleate-responsive genes in Saccharomyces cerevisiae. Journal of Biological Chemistry, 283(16), 10264–10275. https://doi.org/10.1074/jbc.M708215200

Kaurov, I., Vancová, M., Schimanski, B., Cadena, L. R., Heller, J., Bílý, T., … Hashimi, H. (2018). The Diverged Trypanosome MICOS Complex as a Hub for Mitochondrial Cristae Shaping and Protein Import. Current Biology, 28(21), 3393–3407. https://doi.org/10.1016/j.cub.2018.09.008

Kennedy, E.P., & Lehninger, A.L. (1947). Intracellular structures and the fatty acid oxidase system of rat liver. Journal of Biological Chemistry, 172, 847-848.

Kenney, W. C., Edmondson, D. E., Singer, T. P., Nishikimi, M., Noguchi, E., & Yagi, K. (1979). Identification of the Covalently-Bound Flavin of L-Galactonolactone Oxidase From Yeast. FEBS Letters, 97(1), 6–8.

Kerscher, O., Holder, J., Srinivasan, M., Leung, R. S., & Jensen, R. E. (1997). The Tim54p-Tim22p complex mediates insertion of proteins into the mitochondrial inner membrane. Journal of Cell Biology, 139(7), 1663–1675. https://doi.org/10.1083/jcb.139.7.1663

Kho, C. W., Lee, P. Y., Bae, K. H., Cho, S., Lee, Z. W., Park, B. C., … Park, S. G. (2006). Glutathione peroxidase 3 of Saccharomyces cerevisiae regulates the activity of methionine sulfoxide reductase in a redox state-dependent way. Biochemical and Biophysical Research Communications, 348(1), 25–35. https://doi.org/10.1016/j.bbrc.2006.06.067

Kho, C. W., Lee, P. Y., Bae, K. H., Kang, S., Cho, S., Lee, D. H., … Park, S. G. (2008). Gpx3-dependent responses against oxidative stress in Saccharomyces cerevisiae. Journal of Microbiology and Biotechnology, 18(2), 270–282. https://doi.org/7144 [pii]

Kiel, J. A. K. W., Veenhuis, M., & van der Klei, I. J. (2006). PEX genes in fungal genomes: Common, rare or redundant. Traffic, 7(10), 1291–1303. https://doi.org/10.1111/j.1600-0854.2006.00479.x

Koch, J. R., & Schmid, F. X. (2014a). Mia40 Is Optimized for Function in Mitochondrial Oxidative Protein Folding and Import. ACS Chemical Biology, 9(9), 2049-2057. https://doi.org/10.1021/cb500408n

Koch, J. R., & Schmid, F. X. (2014b). Mia40 Combines Thiol Oxidase and Disulfide Isomerase Activity to Efficiently Catalyze Oxidative Folding in Mitochondria. Journal of Molecular Biology, 426(24), 4087–4098. https://doi.org/10.1016/j.jmb.2014.10.022

Koehler, C. M. (2004). The small Tim proteins and the twin Cx3C motif. Trends in Biochemical Sciences, 29(1), 1–4. https://doi.org/10.1016/j.tibs.2003.11.003

Kojer, K., Peleh, V., Calabrese, G., Herrmann, J. M., & Riemer, J. (2015). Kinetic control by limiting glutaredoxin amounts enables thiol oxidation in the reducing mitochondrial intermembrane space. Molecular Biology of the Cell, 26(2), 195–204. https://doi.org/10.1091/mbc.E14-10-1422

Kojer, K., Bien, M., Gangel, H., Morgan, B., Dick, T. P., & Riemer, J. (2012). Glutathione redox potential in the mitochondrial intermembrane space is linked to the cytosol and impacts the Mia40 redox state. EMBO Journal, 31(14), 3169–3182. https://doi.org/10.1038/emboj.2012.165

Kojer, K., & Riemer, J. (2014). Balancing oxidative protein folding: The influences of reducing pathways on disulfide bond formation. Biochimica et Biophysica Acta - Proteins and Proteomics, 1844(8), 1383–1390. https://doi.org/10.1016/j.bbapap.2014.02.004

Komiya, T., Rospert, S., Schatz, G., & Mihara, K. (1997). Binding of mitochondrial precursor proteins to the cytoplasmic domains of the import receptors Tom70 and Tom20 is determined by cytoplasmic chaperones. EMBO Journal, 16(14), 4267–4275. https://doi.org/10.1093/emboj/16.14.4267

Kovermann, P., Truscott, K. N., Guiard, B., Rehling, P., Sepuri, N. B., Müller, H., … Pfanner, N. (2002). Tim22, the essential core of the mitochondrial protein insertion complex, forms a voltage-activated and signal-gated channel. Molecular Cell, 9(2), 363–373. https://doi.org/10.1016/S1097-2765(02)00446-X

Kragler, F., Langeder, A., Raupachova, J., Binder, M., & Hartig, A. (1993). Two independent peroxisomal targeting signals in catalase A of Saccharomyces cerevisiae. Journal of Cell Biology, 120(3), 665–673. https://doi.org/10.1083/jcb.120.3.665

Kritsiligkou, P., Chatzi, A., Charalampous, G., Mironov, A., Grant, C. M., & Tokatlidis, K. (2017). Unconventional Targeting of a Thiol Peroxidase to the Mitochondrial Intermembrane Space Facilitates Oxidative Protein Folding. Cell Reports, 18(11), 2729–2741. https://doi.org/10.1016/j.celrep.2017.02.053

Krüger, V., Becker, T., Becker, L., Montilla-Martinez, M., Ellenrieder, L., Vögtle, F. N., … Meisinger, C. (2017). Identification of new channels by systematic analysis of the mitochondrial outer membrane. Journal of Cell Biology, 216(11), 3485–3495. https://doi.org/10.1083/jcb.201706043

Kumar, S., Singh, R., Williams, C. P., & van der Klei, I. J. (2016). Stress exposure results in increased peroxisomal levels of yeast Pnc1 and Gpd1, which are imported via a piggy-backing mechanism. Biochimica et Biophysica Acta - Molecular Cell Research, 1863(1), 148–156. https://doi.org/10.1016/j.bbamcr.2015.10.017

Künkele, K. P., Heins, S., Dembowski, M., Nargang, F. E., Benz, R., Thieffry, M., … Neupert, W. (1998). The preprotein translocation channel of the outer membrane of mitochondria. Cell, 93(6), 1009–1019. https://doi.org/10.1016/S0092-8674(00)81206-4

Kunze, M., & Berger, J. (2015). The similarity between N-terminal targeting signals for protein import into different organelles and its evolutionary relevance. Frontiers in Physiology, 6(SEP), 1–27. https://doi.org/10.3389/fphys.2015.00259

Kunze, M., Neuberger, G., Maurer-Stroh, S., Ma, J., Eck, T., Braverman, N., … Berger, J. (2011). Structural requirements for interaction of peroxisomal targeting signal 2 and its receptor PEX7. Journal of Biological Chemistry, 286(52), 45048–45062. https://doi.org/10.1074/jbc.M111.301853

Kutik, S., Stroud, D. A., Wiedemann, N., & Pfanner, N. (2009). Evolution of mitochondrial protein biogenesis. Biochimica et Biophysica Acta - General Subjects, 1790(6), 409–415. https://doi.org/10.1016/j.bbagen.2009.04.004

Lang, B.F., Gray, M.W., & Burger, G. (1999). Mitochondrial Genome Evolution and the Origin of Eukaryotes. Annual Review of Genetics. 33, 351-397. https://doi.org/10.1146/annurev.genet.33.1.351

Lazarow, P. B. (2006). The import receptor Pex7p and the PTS2 targeting sequence. Biochimica et Biophysica Acta - Molecular Cell Research, 1763(12), 1599–1604. https://doi.org/10.1016/j.bbamcr.2006.08.011

Lee, P. Y., Kho, C. W., Lee, D. H., Kang, S., Kang, S., Lee, S. C., … Park, S. G. (2007). Glutathione peroxidase 3 of Saccharomyces cerevisiae suppresses non-enzymatic proteolysis of glutamine synthetase in an activity-independent manner. Biochemical and Biophysical Research Communications, 362(2), 405–409. https://doi.org/10.1016/j.bbrc.2007.08.035

Lee, P.Y., Bae, K.H., Kho, C.W., Kang, S., Lee, D.H., … Park, S.G. (2008). Interactome Analysis of Yeast Glutathione Peroxidase 3. Journal of Microbiology and Biotechnology. 18(8), 1364–1367.

Lee, H., Chi, S. W., Lee, P. Y., Kang, S., Cho, S., Lee, C. K., … Park, S. G. (2009). Reduced formation of advanced glycation endproducts via interactions between glutathione peroxidase 3 and dihydroxyacetone kinase 1. Biochemical and Biophysical Research Communications, 389(1), 177–180. https://doi.org/10.1016/j.bbrc.2009.08.116

Lee, P. Y., Bae, K. H., Jeong, D. G., Chi, S. W., Moon, J. H., Kang, S., … Park, S. G. (2011). The S-nitrosylation of glyceraldehyde-3-phosphate dehydrogenase 2 is reduced by interaction with glutathione peroxidase 3 in *Saccharomyces cerevisiae*. Molecules and Cells, 31(3), 255–259. https://doi.org/10.1007/s10059-011-0029-3

Lill, R., Srinivasan, V., & Mühlenhoff, U. (2014). The role of mitochondria in cytosolic-nuclear iron-sulfur protein biogenesis and in cellular iron regulation. Current Opinion in Microbiology, 22, 111–119. https://doi.org/10.1016/j.mib.2014.09.015

Liu, Q., Krzewska, J., Liberek, K., & Craig, E.A. (2001). Mitochondrial Hsp70 Ssc1: Role in Protein Folding. Journal of Biological Chemistry, 276(9), 6112-6118. https://doi.org/ 10.1074/jbc.M009519200

Longen, S., Woellhaf, M., Petrungaro, C., Riemer, J., & Herrmann, J. (2014). The Disulfide Relay of the Intermembrane Space Oxidizes the Ribosomal Subunit Mrp10 on Its Transit into the Mitochondrial Matrix. Developmental Cell, 28(1), 30–42. https://doi.org/10.1016/j.devcel.2013.11.007

Lu, H., Allen, S., Wardleworth, L., Savory, P., & Tokatlidis, K. (2004). Functional TIM10 Chaperone Assembly Is Redox-regulated in Vivo. Journal of Biological Chemistry, 279(18), 18952–18958. https://doi.org/10.1074/jbc.M313045200

Luis, A., & Michael, R. (2018). Proteomics of Peroxisomes (Vol. 89). https://doi.org/10.1007/978-981-13-2233-4

Ma, L. H., Takanishi, C. L., & Wood, M. J. (2007). Molecular mechanism of oxidative stress perception by the Orp1 protein. Journal of Biological Chemistry, 282(43), 31429–31436. https://doi.org/10.1074/jbc.M705953200

Maiorino, M., Ursini, F., Bosello, V., Toppo, S., Tosatto, S. C. E., Mauri, P., … Flohé, L. (2007). The Thioredoxin Specificity of Drosophila GPx: A Paradigm for a Peroxiredoxin-like Mechanism of many Glutathione Peroxidases. Journal of Molecular Biology, 365(4), 1033–1046. https://doi.org/10.1016/j.jmb.2006.10.033

Manganas, P. (2017). Oxidative Regulation Mechanisms in the Mitochondrial Intermembrane Space. University of Glasgow.

Manganas, P., MacPherson, L., & Tokatlidis, K. (2017). Oxidative protein biogenesis and redox regulation in the mitochondrial intermembrane space. Cell and Tissue Research, 367(1), 43–57. https://doi.org/10.1007/s00441-016-2488-5

Mani, J., Meisinger, C., & Schneider, A. (2016). Peeping at TOMs - Diverse entry gates to mitochondria provide insights into the evolution of eukaryotes. Molecular Biology and Evolution, 33(2), 337–351. https://doi.org/10.1093/molbev/msv219

Marshall, P. A., Krimkevich, Y. I., Lark, R. H., Dyer, J. M., Veenhuis, M., & Goodman, J. M. (1995). Pmp27 promotes peroxisomal proliferation. Journal of Cell Biology, 129(2), 345–355. https://doi.org/10.1083/jcb.129.2.345

Marshall, P. A., Dyer, J. M., Quick, M. E., & Goodman, J. M. (1996). Redox-sensitive homodimerization of Pex11p: A proposed mechanism to regulate peroxisomal division. Journal of Cell Biology, 135(1), 123–137. https://doi.org/10.1083/jcb.135.1.123

Martinez-Caballero, S., Grigoriev, S. M., Herrmann, J. M., Campo, M. L., & Kinnally, K. W. (2007). Tim17p regulates the twin pore structure and voltage gating of the mitochondrial protein import complex TIM23. Journal of Biological Chemistry, 282(6), 3584–3593. https://doi.org/10.1074/jbc.M607551200

Matsuyama, A., Arai, R., Yashiroda, Y., Shirai, A., Kamata, A., Sekido, S., … Yoshida, M. (2006). ORFeome cloning and global analysis of protein localization in the fission yeast Schizosaccharomyces pombe. Nature Biotechnology, 24(7), 841–847. https://doi.org/10.1038/nbt1222

Mattiazzi Ušaj, M., Brložnik, M., Kaferle, P., Žitnik, M., Wolinski, H., Leitner, F., … Petrovič, U. (2015). Genome-wide localization study of yeast pex11 identifies peroxisome-mitochondria interactions through the ERMES complex. Journal of Molecular Biology, 427(11), 2072–2087. https://doi.org/10.1016/j.jmb.2015.03.004

Mayer, A., Nargang, F. E., Neupert, W., & Lill, R. (1995). MOM22 is a receptor for mitochondrial targeting sequences and cooperates with MOM19. EMBO Journal, 14(17), 4204–4211

McNew, J. A., & Goodman, J. M. (1994). An oligomeric protein is imported into peroxisomes in vivo. Journal of Cell Biology, 127(5), 1245–1257. https://doi.org/10.1083/jcb.127.5.1245

McQuibban, G.A., Saurya, S., & Freeman, M. (2003). Mitochondrial membrane remodelling regulated by a conserved rhomboid protease. Nature, 423(6939), 537-541. https://doi.org/10.1038/nature01633

McWilliam, H., Li, W., Uludag, M., Squizzato, S., Park, Y. M., Buso, N., … Lopez, R. (2013). Analysis Tool Web Services from the EMBL-EBI. Nucleic Acids Research, 41(Web Server issue), 597–600. https://doi.org/10.1093/nar/gkt376

Meier, S., Neupert, W., & Herrmann, J. M. (2005). Conserved N-terminal negative charges in the Tim17 subunit of the TIM23 translocase play a critical role in the import of preproteins into mitochondria. Journal of Biological Chemistry, 280(9), 7777–7785. https://doi.org/10.1074/jbc.M412158200

Melin, J., Schulz, C., Wrobel, L., Bernhard, O., Chacinska, A., Jahn, O., … Rehling, P. (2014). Presequence Recognition by the Tom40 Channel Contributes to Precursor Translocation into the Mitochondrial Matrix. Molecular and Cellular Biology, 34(18), 3473–3485. https://doi.org/10.1128/MCB.00433-14

Mesecke, N., Terziyska, N., Kozany, C., Baumann, F., Neupert, W., Hell, K., & Herrmann, J. M. (2005). A disulfide relay system in the intermembrane space of mitochondria that mediates protein import. Cell, 121(7), 1059–1069. https://doi.org/10.1016/j.cell.2005.04.011

Michaillat, L., & Mayer, A. (2013). Identification of Genes Affecting Vacuole Membrane Fragmentation in Saccharomyces cerevisiae. PLoS ONE, 8(2). https://doi.org/10.1371/journal.pone.0054160

Milenkovic, D., Ramming, T., Muller, J. M., Wenz, L.-S., Gebert, N., Schulze-Specking, A., … Chacinska, A. (2009). Identification of the Signal Directing Tim9 and Tim10 into the Intermembrane Space of Mitochondria. Molecular Biology of the Cell, 20(10), 2530–2539. https://doi.org/10.1091/mbc.E08-11-1108

Mindthoff, S., Grunau, S., Steinfort, L. L., Girzalsky, W., Hiltunen, J. K., Erdmann, R., & Antonenkov, V. D. (2016). Peroxisomal Pex11 is a pore-forming protein homologous to TRPM channels. Biochimica et Biophysica Acta - Molecular Cell Research, 1863(2), 271–283. https://doi.org/10.1016/j.bbamcr.2015.11.013

Missiakas, D., Schwager, F., & Raina, S. (1995). Identification and characterization of a new disulfide isomerase-like protein (DsbD) in Escherichia coli. EMBO Journal, 14(14), 3415–3424. https://doi.org/10.1002/j.1460-2075.1995.tb07347.x

Mokranjac, D., Popov-Čeleketić, D., Hell, K., & Neupert, W. (2005). Role of Tim21 in mitochondrial translocation contact sites. Journal of Biological Chemistry, 280(25), 23437–23440. https://doi.org/10.1074/jbc.C500135200

Mokranjac, D., Sichting, M., Popov-Cělektić, D., Mapa, K., Gevorkyan-Airapetov, L., Zohary, K., … Azem, A. (2009). Role of Tim50 in the Transfer of Precursor Proteins from the Outer to the Inner Membrane of Mitochondria. Molecular Biology of the Cell, 20, 1400–1407. https://doi.org/10.1091/mbc.E08–09–0934

Morano, K. A., Grant, C. M., & Moye-Rowley, W. S. (2012). The response to heat shock and oxidative stress in *Saccharomyces cerevisiae*. Genetics, 190(4), 1157–1195. https://doi.org/10.1534/genetics.111.128033

Mordas, A., & Tokatlidis, K. (2015). The MIA Pathway: A Key Regulator of Mitochondrial Oxidative Protein Folding and Biogenesis. Accounts of Chemical Research, 48(8), 2191–2199. https://doi.org/10.1021/acs.accounts.5b00150 ***(Personal publication during PhD)***

Morgenstern, M., Stiller, S. B., Lübbert, P., Peikert, C. D., Dannenmaier, S., Drepper, F., … Warscheid, B. (2017). Definition of a High-Confidence Mitochondrial Proteome at Quantitative Scale. Cell Reports, 19(13), 2836–2852. https://doi.org/10.1016/j.celrep.2017.06.014

Mossmann, D., Meisinger, C., & Vögtle, F. N. (2012). Processing of mitochondrial presequences. Biochimica et Biophysica Acta - Gene Regulatory Mechanisms, 1819(9–10), 1098–1106. https://doi.org/10.1016/j.bbagrm.2011.11.007

Muratsubaki, H., & Enomoto, K. (1998). One of the fumarate reductase isoenzymes from *Saccharomyces cerevisiae* is encoded by the OSM1 gene. Archives of Biochemistry and Biophysics, 352(2), 175–181. https://doi.org/10.1006/abbi.1998.0583

Murcha, M. W., Elhafez, D., Lister, R., Tonti-Filippini, J., Baumgartner, M., Philippar, K., … Whelan, J. (2006). Characterization of the Preprotein and Amino Acid Transporter Gene Family in Arabidopsis. Plant Physiology, 143(1), 199–212. https://doi.org/10.1104/pp.106.090688

Murphy, M. P. (2009). How mitochondria produce reactive oxygen species. Biochemical Journal, 417(1), 1–13. https://doi.org/10.1042/BJ20081386

Nagai, M., Vo, N. H., Ogawa, L. S., Chimmanamada, D., Inoue, T., Chu, J., … Wada, Y. (2012). The oncology drug elesclomol selectively transports copper to the mitochondria to induce oxidative stress in cancer cells. Free Radical Biology and Medicine, 52(10), 2142–2150. https://doi.org/10.1016/j.freeradbiomed.2012.03.017

Nass, & Nass. (1963). FIBERS WITH DNA CHARACTERISTICS I . Fixation and Electron Staining Reactions. https://doi.org/10.1083/jcb.19.3.593

Neal, S. E., Dabir, D. V., Tienson, H. L., Horn, D. M., Glaeser, K., Ogozalek Loo, R. R., … Koehler, C. M. (2015). Mia40 protein serves as an electron sink in the Mia40-Erv1 import pathway. Journal of Biological Chemistry, 290(34), 20804–20814. https://doi.org/10.1074/jbc.M115.669440

Neal, S. E., Dabir, D. V., Wijaya, J., Boon, C., & Koehler, C. M. (2017). Osm1 facilitates the transfer of electrons from Erv1 to fumarate in the redox-regulated import pathway in the mitochondrial intermembrane space. Molecular Biology of the Cell, 28(21), 2773–2785. https://doi.org/10.1091/mbc.E16-10-0712

Neupert, W., & Herrmann, J.M. (2007). Translocation of proteins into mitochondria. Annual Review of Biochemistry, 76, 723-749. https://doi.org/10.1146/annurev.biochem.76.052705.163409

Nunnari, J., Fox, T. D., & Walter, P. (1993). A mitochondrial protease with two catalytic subunits of nonoverlapping specificities. Science, 262(5142), 1997–2004. https://doi.org/10.1126/science.8266095

Ohdate, T., Kita, K., & Inoue, Y. (2010). Kinetics and redox regulation of Gpx1, an atypical 2-Cys peroxiredoxin, in Saccharomyces cerevisiae. FEMS Yeast Research, 10(6), 787–790. https://doi.org/10.1111/j.1567-1364.2010.00651.x

Ohdate, T., & Inoue, Y. (2012). Involvement of glutathione peroxidase 1 in growth and peroxisome formation in Saccharomyces cerevisiae in oleic acid medium. Biochimica et Biophysica Acta - Molecular and Cell Biology of Lipids, 1821(9), 1295–1305. https://doi.org/10.1016/j.bbalip.2012.05.004

Oka, O. B. V, & Bulleid, N. J. (2013). Forming disulfides in the endoplasmic reticulum. Biochimica et Biophysica Acta - Molecular Cell Research, 1833(11), 2425–2429. https://doi.org/10.1016/j.bbamcr.2013.02.007

Okazaki, S., Tachibana, T., Naganuma, A., Mano, N., & Kuge, S. (2007). Multistep Disulfide Bond Formation in Yap1 Is Required for Sensing and Transduction of H2O2 Stress Signal. Molecular Cell, 27(4), 675–688. https://doi.org/10.1016/j.molcel.2007.06.035

Osumi, T., Tsukamoto, T., & Hata, S. (1992). Signal Peptide For Peroxisomal Targeting:Replacement Of An Essential Histidine Residue By Certain Amino Acids Converts The Amino-Terminal Presequence Of Peroxisomal 3-Ketoacyl-Coa Thiolase To A Mitochondrial Signal Peptide. Biochemical and Biophysical Research Communications, 186(2), 811-818

Ouyang, X., Tran, Q. T., Goodwin, S., Wible, R. S., Sutter, C. H., & Sutter, T. R. (2011). Yap1 activation by H2O2 or thiol-reactive chemicals elicits distinct adaptive gene responses. Free Radical Biology and Medicine, 50(1), 1–13. https://doi.org/10.1016/j.freeradbiomed.2010.10.697

Pagliarini, D. J., Calvo, S. E., Chang, B., Sheth, S. A., Vafai, S. B., Ong, S. E., … Mootha, V. K. (2008). A Mitochondrial Protein Compendium Elucidates Complex I Disease Biology. Cell, 134(1), 112–123. https://doi.org/10.1016/j.cell.2008.06.016

Palay, S. L., & Palade, G. E. (1955). The fine structure of neurons. Journal of Biophysical and Biochemical Cytology, 1(1), 69–88. https://doi.org/10.1083/jcb.1.1.69

Pan, D., Nakatsu, T., & Kato, H. (2013). Crystal structure of peroxisomal targeting signal-2 bound to its receptor complex Pex7p-Pex21p. Nature Structural and Molecular Biology, 20(8), 987–993. https://doi.org/10.1038/nsmb.2618

Papić, D., Krumpe, K., Dukanovic, J., Dimmer, K. S., & Rapaport, D. (2011). Multispan mitochondrial outer membrane protein Ugo1 follows a unique Mim1-dependent import pathway. Journal of Cell Biology, 194(3), 397–405. https://doi.org/10.1083/jcb.201102041

Pathak, T., & Trebak, M. (2018). Mitochondrial Ca2+signaling. Pharmacology and Therapeutics, 192, 112-123. https://doi.org/10.1016/j.pharmthera.2018.07.001

Patterson, M. J., McKenzie, C. G., Smith, D. A., da Silva Dantas, A., Sherston, S., Veal, E. A., … Quinn, J. (2013). Ybp1 and Gpx3 Signaling in Candida albicans Govern Hydrogen Peroxide-Induced Oxidation of the Cap1

Transcription Factor and Macrophage Escape. Antioxidants & Redox Signaling, 19(18), 2244–2260. https://doi.org/10.1002/asna.19061720603

Peikert, C. D., Mani, J., Morgenstern, M., Käser, S., Knapp, B., Wenger, C., … Warscheid, B. (2017). Charting organellar importomes by quantitative mass spectrometry. Nature Communications, 8(May). https://doi.org/10.1038/ncomms15272

Peleh, V., Cordat, E., & Herrmann, J. M. (2016). Mia40 is a trans-site receptor that drives protein import into the mitochondrial intermembrane space by hydrophobic substrate binding. Journal of Chemical Information and Modeling, 53(9), 1689–1699. https://doi.org/10.1017/CBO9781107415324.004

Peleh, V., Zannini, F., Backes, S., Rouhier, N., & Herrmann, J. M. (2017). Erv1 of Arabidopsis thaliana can directly oxidize mitochondrial intermembrane space proteins in the absence of redox-active Mia40. BMC Biology, 15(1), 1–14. https://doi.org/10.1186/s12915-017-0445-8

Picard, M., McManus, M. J., Gray, J. D., Nasca, C., Moffat, C., Kopinski, P. K., … Wallace, D. C. (2015). Mitochondrial functions modulate neuroendocrine, metabolic, inflammatory, and transcriptional responses to acute psychological stress. Proceedings of the National Academy of Sciences, 112(48), E6614–E6623. https://doi.org/10.1073/pnas.1515733112

Popov-Čeleketić, J., Waizenegger, T., & Rapaport, D. (2008). Mim1 Functions in an Oligomeric Form to Facilitate the Integration of Tom20 into the Mitochondrial Outer Membrane. Journal of Molecular Biology, 376(3), 671–680. https://doi.org/10.1016/j.jmb.2007.12.006

Ramesh, A., Peleh, V., Martinez-Caballero, S., Wollweber, F., Sommer, F., van der Laan, M., … Herrmann, J. M. (2016). A disulfide bond in the TIM23 complex is crucial for voltage gating and mitochondrial protein import. Journal of Cell Biology, 214(4), 417–431. https://doi.org/10.1083/jcb.201602074

Reddehase, S., Grumbt, B., Neupert, W., & Hell, K. (2009). The Disulfide Relay System of Mitochondria Is Required for the Biogenesis of Mitochondrial Ccs1 and Sod1. Journal of Molecular Biology, 385(2), 331–338. https://doi.org/10.1016/j.jmb.2008.10.088

Rietsch, A., Belin, D., Martin, N., & Beckwith, J. (1996). An in vivo pathway for disulfide bond isomerization in Escherichia coli. Proceedings of the National Academy of Sciences, 93(23), 13048–13053. https://doi.org/10.1073/pnas.93.23.13048

Rissler, M., Wiedemann, N., Pfannschmidt, S., Gabriel, K., Guiard, B., Pfanner, N., & Chacinska, A. (2005). The essential mitochondrial protein Erv1 cooperates with Mia40 in biogenesis of intermembrane space proteins. Journal of Molecular Biology, 353(3), 485–492. https://doi.org/10.1016/j.jmb.2005.08.051

Roger, A.J., Munoz-Gomez, S.A., and Kamikawa, R. (2017). The origin and diversification of mitochondria. Current Biology, 27, 1177–1192. https://doi.org/10.1016/j.cub.2017.09.015

Rottensteiner, H., Kal, A. J., Filipits, M., Binder, M., Hamilton, B., Tabak, H. F., & Ruis, H. (1996). Pip2p: a transcriptional regulator of peroxisome proliferation in the yeast Saccharomyces cerevisiae. EMBO Journal, 15(12), 2924–2934. https://doi.org/10.1002/j.1460-2075.1996.tb00655.x

Rottensteiner, H., Kal, A. J., Hamilton, B., Ruis, H., & Tabak, H. F. (1997). A heterodimer of the Zn2Cys6transcription factors pip2p and oaf1p controls induction of genes encoding peroxisomal proteins in Saccharomyces cerevisiae. European Journal of Biochemistry, 247(3), 776–783. https://doi.org/10.1111/j.1432-1033.1997.00776.x

Rozhkova, A., & Glockshuber, R. (2008). Thermodynamic Aspects of DsbD-Mediated Electron Transport. Journal of Molecular Biology, 380(5), 783–788. https://doi.org/10.1016/j.jmb.2008.05.050

Rymer, Ł., Kempiński, B., Chełstowska, A., & Skoneczny, M. (2018). The budding yeast Pex5p receptor directs Fox2p and Cta1p into peroxisomes via its N-terminal part near the FxxxW domain. Journal of Cell Science, 131, 1-11. https://doi.org/10.1242/jcs.216986

Schneider, W.C. (1948). Intracellular Distribution Of Enzymes. Journal of Biological Chemistry, 176, 259-266.

Schulz, C., Lytovchenko, O., Melin, J., Chacinska, A., Guiard, B., Neumann, P., … Rehling, P. (2011). Tim50's presequence receptor domain is essential for signal driven transport across the TIM23 complex. Journal of Cell Biology, 195(4), 643–656. https://doi.org/10.1083/jcb.201105098

Schweitzer-Stenner, R. (2018). Relating the multi-functionality of cytochrome c to membrane binding and structural conversion. Biophysical Reviews, 10(4), 1151–1185. https://doi.org/10.1007/s12551-018-0409-4

Schwerter, D. P., Grimm, I., Platta, H. W., & Erdmann, R. (2017). ATP-driven processes of peroxisomal matrix protein import. Biological Chemistry, 398(5–6), 607–624. https://doi.org/10.1515/hsz-2016-0293

Shai, N., Yifrach, E., Van Roermund, C. W. T., Cohen, N., Bibi, C., Ijlst, L., … Zalckvar, E. (2018). Systematic mapping of contact sites reveals tethers and a function for the peroxisome-mitochondria contact. Nature Communications, 9(1). https://doi.org/10.1038/s41467-018-03957-8

Sherman, E.L., Go, N.E., & Nargang, F.E. (2005). Functions of the Small Proteins in the TOM Complex of *Neurospora crassa*. Molecular Biology of the Cell, 16, 4172–4182. https://doi.org/10.1091/mbc.E05–03–0187)

Shiota, T., Imai, K., Qui, J., Hewitt, V.L., Tan, K., Shen, H., … & Endo, T. (2015). Molecular architecture of the active mitochondrial protein gate, 349(6255), 1544-1548. https://doi.org/10.1126/science.aac6428.

Sibirny, A. A. (2016). Yeast peroxisomes: Structure, functions and biotechnological opportunities. FEMS Yeast Research, 16(4), 1–14. https://doi.org/10.1093/femsyr/fow038

Sideris, D. P., Petrakis, N., Katrakili, N., Mikropoulou, D., Gallo, A., Ciofi-Baffoni, S., … Tokatlidis, K. (2009). A novel intermembrane space-targeting signal docks cysteines onto Mia40 during mitochondrial oxidative folding. Journal of Cell Biology, 187(7), 1007–1022. https://doi.org/10.1083/jcb.200905134

Sideris, D. P., & Tokatlidis, K. (2007). Oxidative folding of small Tims is mediated by site-specific docking onto Mia40 in the mitochondrial intermembrane space. Molecular Microbiology, 65(August), 1360–1373. https://doi.org/10.1111/j.1365-2958.2007.05880.x

Sies, H., Berndt, C., & Jones, D.P. (2017). Oxidative Stress. Annual Review of Biochemistry, 86, 717-748. https://doi.org/10.1146/annurev-biochem-061516-045037

Sirrenberg, C., Bauer, M. F., Guiard, B., Neupert, W., & Brunner, M. (1996). Import of carrier proteins into the mitochondrial inner membrane mediated by Tim22. Nature, 384(6609), 582–585. https://doi.org/10.1038/384582a0

Sjöstrand, F.S. (1953). Electron Microscopy of Mitochondria and Cytoplasmic Double Membranes. Nature, 171, 30-31

Smeitink, J., van den Heuvel, L., & DiMauro, S. (2001). The genetics and pathology of oxidative phosphorylation. Nature Reviews Genetics, 2(5), 342–352. https://doi.org/10.1038/35072063

Smith, J. J., & Aitchison, J. D. (2014). Peroxisomes take shape. Nature Reviews Molecular Cellular Biology, 14(12), 803–817. https://doi.org/10.1038/nrm3700

Song, J., Tamura, Y., Yoshihisa, T., & Endo, T. (2014). A novel import route for an N-anchor mitochondrial outer membrane protein aided by the TIM23 complex. EMBO Reports, 15(6), 670–677. https://doi.org/10.1002/embr.201338142

Specht, S., Liedgens, L., Duarte, M., Stiegler, A., Wirth, U., Eberhardt, M., … Deponte, M. (2018). A single-cysteine mutant and chimeras of essential Leishmania Erv can complement the loss of Erv1 but not of Mia40 in yeast. Redox Biology, 15(December 2017), 363–374. https://doi.org/10.1016/j.redox.2017.12.010

Spinelli, J. B., & Haigis, M. C. (2018). The multifaceted contributions of mitochondria to cellular metabolism. Nature Cell Biology, 20(7), 745–754. https://doi.org/10.1038/s41556-018-0124-1

Steiner, H., Zollner, A., Haid, A., Neupert, W., & Lill, R. (1995). Biogenesis of mitochondrial heme lyases in yeast. Import and folding in the intermembrane space. Journal of Biological Chemistry, 270(39), 22842–22849. https://doi.org/10.1074/jbc.270.39.22842

Stewart, E. J., Katzen, F., & Beckwith, J. (1999). Six conserved cysteines of the membrane protein DsbD are required for the transfer of electrons from the cytoplasm to the periplasm of Escherichia coli. EMBO Journal, 18(21), 5963–5971. https://doi.org/10.1093/emboj/18.21.5963

Stiller, S. B., Höpker, J., Oeljeklaus, S., Schütze, C., Schrempp, S. G., Vent-Schmidt, J., … Wiedemann, N. (2016). Mitochondrial OXA Translocase Plays a Major Role in Biogenesis of Inner-Membrane Proteins. Cell Metabolism, 23(5), 901–908. https://doi.org/10.1016/j.cmet.2016.04.005

Stojanovski, D., Milenkovic, D., Müller, J. M., Gabriel, K., Schulze-Specking, A., Baker, M. J., … Chacinska, A. (2008). Mitochondrial protein import: precursor oxidation in a ternary complex with disulfide carrier and sulfhydryl oxidase. Journal of Cell Biology, 183(2), 195–202. https://doi.org/10.1083/jcb.200804095

Swinkels, B. W., Gould, S. J., Bodnar, A. G., Rachubinski, R. A., & Subramani, S. (1992). A novel, cleavable peroxisomal targeting signal at the amino-terminus of the rat 3-ketoacyl-coA thiolase. Trends in Cell Biology, 2(2), 38. https://doi.org/10.1016/0962-8924(92)90153-E

Tarassov, K., Messier, V., Landry, C.R., Radinovic, S., Serna Molina, M.M., Shames, I., … Michnick, S. (2008). An in Vivo Map of the Yeast Protein Interactome. Nature, 320(5882), 1465-1470. https://doi.org/10.1126/science.1153878

Tavender, T. J., Springate, J. J., & Bulleid, N. J. (2010). Recycling of peroxiredoxin IV provides a novel pathway for disulphide formation in the endoplasmic reticulum. EMBO Journal, 29(24), 4185–4197. https://doi.org/10.1038/emboj.2010.273

Terziyska, N., Grumbt, B., Bien, M., Neupert, W., Herrmann, J. M., & Hell, K. (2007). The sulfhydryl oxidase Erv1 is a substrate of the Mia40-dependent protein translocation pathway. FEBS Letters, 581(6), 1098–1102. https://doi.org/10.1016/j.febslet.2007.02.014

Truscott, K.N., Wiedemann, N., Rehling, P., Müller, H., Meisinger, C., Pfanner, N., & Guiard, B. (2002). Mitochondrial Import of the ADP/ATP Carrier: the Essential TIM Complex of the Intermembrane Space Is Required for Precursor Release from the TOM Complex. Molecular and Cellular Biology, 22(22), 7780-7789. https://doi.org/10.1128/mcb.22.22.7780–7789.2002

Turcotte, B., Liang, X. B., Robert, F., & Soontorngun, N. (2010). Transcriptional regulation of nonfermentable carbon utilization in budding yeast. FEMS Yeast Research, 10(1), 2–13. https://doi.org/10.1111/j.1567-1364.2009.00555.x

Ukai, Y., Kishimoto, T., Ohdate, T., Izawa, S., & Inoue, Y. (2011). Glutathione peroxidase 2 in Saccharomyces cerevisiae is distributed in mitochondria and involved in sporulation. Biochemical and Biophysical Research Communications, 411(3), 580–585. https://doi.org/10.1016/j.bbrc.2011.06.189

Van Wilpe, S., Ryan, M. T., Hill, K., Maarse, A. C., Meisinger, C., Brix, J., … Pfanner, N. (1999). Tom22 is a multifunctional organizer of the mitochondrial preprotein translocase. Nature, 401(6752), 485–489. https://doi.org/10.1038/46802

Veal, E., & Day, A. (2011). Hydrogen Peroxide as a Signaling Molecule. Antioxidants & Redox Signaling, 15(1), 147–151. https://doi.org/10.1089/ars.2011.3968

Veal, E. A., Ross, S. J., Malakasi, P., Peacock, E., & Morgan, B. A. (2003). Ybp1 is required for the hydrogen peroxide-induced oxidation of the Yap1 transcription factor. Journal of Biological Chemistry, 278(33), 30896–30904. https://doi.org/10.1074/jbc.M303542200

Vergnolle, M. A. S., Baud, C., Golovanov, A. P., Alcock, F., Luciano, P., Lian, L. Y., & Tokatlidis, K. (2005). Distinct domains of small Tims involved in subunit interaction and substrate recognition. Journal of Molecular Biology, 351(4), 839–849. https://doi.org/10.1016/j.jmb.2005.06.010

Vögtle, F.-N., Burkhart, J. M., Rao, S., Gerbeth, C., Hinrichs, J., Martinou, J.-C., … Meisinger, C. (2012). Intermembrane space proteome of yeast mitochondria. Molecular & Cellular Proteomics, 11(12), 1840–1852. https://doi.org/10.1074/mcp.M112.021105

Vögtle, F. N., Wortelkamp, S., Zahedi, R. P., Becker, D., Leidhold, C., Gevaert, K., … Meisinger, C. (2009). Global Analysis of the Mitochondrial N-Proteome Identifies a Processing Peptidase Critical for Protein Stability. Cell, 139(2), 428–439. https://doi.org/10.1016/j.cell.2009.07.045

Voos, W., Gambill, B.D., Guiard, B., Pfanner, N., & Craig, E.A. (1993). Presequence and mature part of preproteins strongly influence the dependence of mitochondrial protein import on heat shock protein 70 in the matrix. Journal of Cell Biology, 123(1), 119–126. https://doi.org/10.1083/jcb.123.1.119

Wanders, R. J. A., Waterham, H. R., & Ferdinandusse, S. (2016). Metabolic Interplay between Peroxisomes and Other Subcellular Organelles Including Mitochondria and the Endoplasmic Reticulum. Frontiers in Cell and Developmental Biology, 3, 1–15. https://doi.org/10.3389/fcell.2015.00083

Waterham, H. R., Ferdinandusse, S., & Wanders, R. J. A. (2016). Human disorders of peroxisome metabolism and biogenesis. Biochimica et Biophysica Acta - Molecular Cell Research, 1863(5), 922–933. https://doi.org/10.1016/j.bbamcr.2015.11.015

Webb, C. T., Gorman, M. A., Lazarou, M., Ryan, M. T., & Gulbis, J. M. (2006). Crystal structure of the mitochondrial chaperone TIM9•10 reveals a six-bladed α-propeller. Molecular Cell, 21(1), 123–133. https://doi.org/10.1016/j.molcel.2005.11.010

Weckbecker, D., Longen, S., Riemer, J., & Herrmann, J. M. (2012). Atp23 biogenesis reveals a chaperone-like folding activity of Mia40 in the IMS of mitochondria. EMBO Journal, 31(22), 4348–4358. https://doi.org/10.1038/emboj.2012.263

Wenz, L. S., Opaliński, Ł., Schuler, M. H., Ellenrieder, L., Ieva, R., Böttinger, L., … Becker, T. (2014). The presequence pathway is involved in protein sorting to the mitochondrial outer membrane. EMBO Reports, 15(6), 678–685. https://doi.org/10.1002/embr.201338144

Wheeler, T. J., Clements, J., & Finn, R. D. (2014). Skylign: A tool for creating informative, interactive logos representing sequence alignments and profile hidden Markov models. BMC Bioinformatics, 15(1), 1–9. https://doi.org/10.1186/1471-2105-15-7

Wiedemann, N., Kozjak, V., Prinz, T., Ryan, M. T., Meisinger, C., Pfanner, N., & Truscott, K. N. (2003). Biogenesis of yeast mitochondrial cytochrome c: A unique relationship to the TOM machinery. Journal of Molecular Biology, 327(2), 465–474. https://doi.org/10.1016/S0022-2836(03)00118-9

Wiedemann, N., & Pfanner, N. (2017). Mitochondrial Machineries for Protein Import and Assembly. Annual Review of Biochemistry, 86(1), 685–714. https://doi.org/10.1146/annurev-biochem-060815-014352

Wood, M. J., Storz, G., & Tjandra, N. (2004). Structural basis for redox regulation of Yap1 transcription factor localization. Nature, 430(7002), 917–921. https://doi.org/10.1038/nature02790

Wrobel, L., Trojanowska, A., Sztolsztener, M. E., & Chacinska, A. (2013). Mitochondrial protein import: Mia40 facilitates Tim22 translocation into the inner membrane of mitochondria. Molecular Biology of the Cell, 24(5), 543–554. https://doi.org/10.1091/mbc.E12-09-0649

Wróblewska, J. P., Cruz-Zaragoza, L. D., Yuan, W., Schummer, A., Chuartzman, S. G., de Boer, R., … van der Klei, I. J. (2017). Saccharomyces cerevisiae cells lacking Pex3 contain membrane vesicles that harbor a subset of peroxisomal membrane proteins. Biochimica et Biophysica Acta - Molecular Cell Research, 1864(10), 1656–1667. https://doi.org/10.1016/j.bbamcr.2017.05.021

Yamamoto, H., Esaki, M., Kanamori, T., Tamura, Y., Nishikawa, S. ichi, & Endo, T. (2002). Tim50 is a subunit of the TIM23 complex that links protein translocation across the outer and inner mitochondrial membranes. Cell, 111(4), 519–528. https://doi.org/10.1016/S0092-8674(02)01053-X

Yifrach, E., Chuartzman, S. G., Dahan, N., Maskit, S., Zada, L., Weill, U., … Zalckvar, E. (2016). Characterization of proteome dynamics in oleate reveals a novel peroxisome targeting receptor. Journal of Cell Science, 129, 4067-4075. https://doi.org/10.1242/jcs.195255

Yoshikawa, K., Tanaka, T., Furusawa, C., Nagahisa, K., Hirasawa, T., & Shimizu, H. (2009). Comprehensive phenotypic analysis for identification of genes affecting growth under ethanol stress in Saccharomyces cerevisiae. FEMS Yeast Research, 9(1), 32–44. https://doi.org/10.1111/j.1567-1364.2008.00456.x

Zito, E., Melo, E. P., Yang, Y., Wahlander, Å., Neubert, T. A., & Ron, D. (2010). Oxidative Protein Folding by an Endoplasmic Reticulum-Localized Peroxiredoxin. Molecular Cell, 40(5), 787–797. https://doi.org/10.1016/j.molcel.20

Schapira, A. H. Mitochondrial diseases. Lancet 379, 1825–1834 (2012).

Mossmann, D. et al. Amyloid-β peptide induces mitochondrial dysfunction by inhibition of preprotein maturation. Cell Metab. 20, 662–669 (2014)

Klootwijk, E. D. et al. Mistargeting of peroxisomal EHHADH and inherited renal Fanconi's syndrome. N. Engl. J. Med. 370, 129–138 (2014).